Methods in Molecular Biology 2076

Springer Protocols

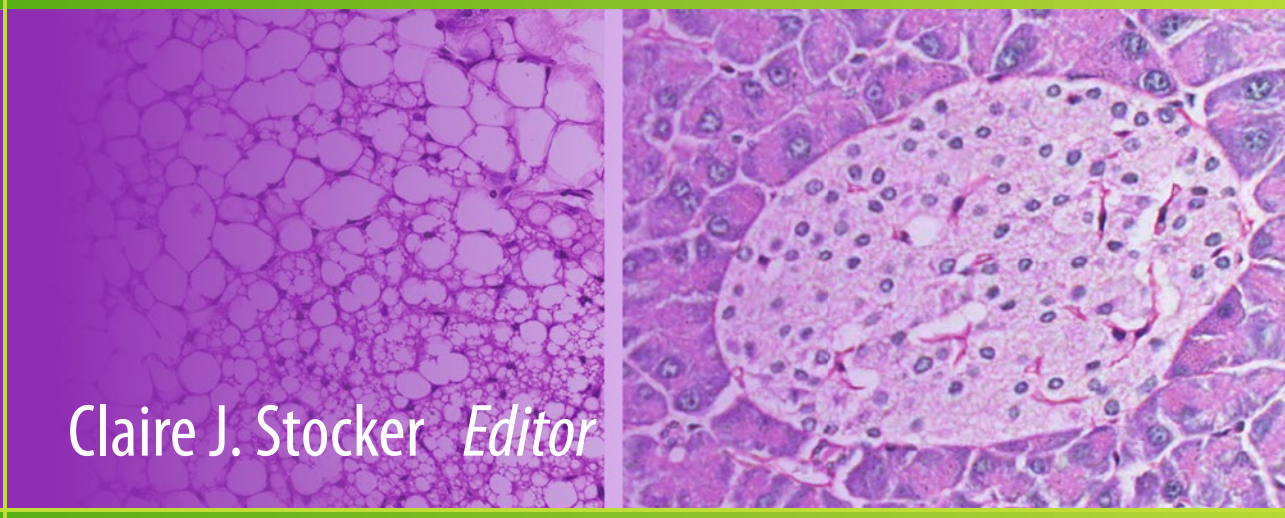

Claire J. Stocker *Editor*

# Type 2 Diabetes

## Methods and Protocols

*Second Edition*

Humana Press

# METHODS IN MOLECULAR BIOLOGY

*Series Editor*
**John M. Walker**
**School of Life and Medical Sciences**
**University of Hertfordshire**
**Hatfield, Hertfordshire, UK**

For further volumes:
http://www.springer.com/series/7651

For over 35 years, biological scientists have come to rely on the research protocols and methodologies in the critically acclaimed *Methods in Molecular Biology* series. The series was the first to introduce the step-by-step protocols approach that has become the standard in all biomedical protocol publishing. Each protocol is provided in readily-reproducible step-by-step fashion, opening with an introductory overview, a list of the materials and reagents needed to complete the experiment, and followed by a detailed procedure that is supported with a helpful notes section offering tips and tricks of the trade as well as troubleshooting advice. These hallmark features were introduced by series editor Dr. John Walker and constitute the key ingredient in each and every volume of the *Methods in Molecular Biology* series. Tested and trusted, comprehensive and reliable, all protocols from the series are indexed in PubMed.

# Type 2 Diabetes

## Methods and Protocols

### Second Edition

Edited by

**Claire J. Stocker**

*Medical School, University of Buckingham, Buckingham, Buckinghamshire, UK*

Humana Press

*Editor*
Claire J. Stocker
Medical School
University of Buckingham
Buckingham, Buckinghamshire, UK

ISSN 1064-3745 ISSN 1940-6029 (electronic)
ISBN 978-1-4939-9880-7 ISBN 978-1-4939-9882-1 (eBook)
https://doi.org/10.1007/978-1-4939-9882-1



This Humana imprint is published by the registered company Springer Science+Business Media, LLC, part of Springer Nature.
The registered company address is: 233 Spring Street, New York, NY 10013, U.S.A.

# Preface

Diabetes is now reaching pandemic proportions, and the associated complications are often life-threatening and disabling. Diabetes and its comorbidities are considered among the biggest killers of UK society and by many estimate a worse threat than cancer. Over the last decade, both clinical and basic researchers have increased our understanding of the physiological and molecular mechanisms involved in the progression of diabetes and importantly the relative roles played by both environmental and genetic factors.

The primary purpose of this edition is to provide up-to-date and relevant explanations of commonly used protocols and analyses used in diabetes research. Specifically, the chapters start with a series of overarching reviews and will provide its readers with simple explanations of practical techniques or models in a short succinct format, thus allowing research scientist and early career clinicians with quick and easy practical information to address a particular question. There are key practical notes at the end of each chapter, as well as numerous helpful figures and tables.

*Buckingham, UK* *Claire J. Stocker*

# Contents

# Contributors


Matthew J. Butcher • *Department of Microbiology and Molecular Cell Biology, Eastern Virginia Medical School, Norfolk, VA, USA*

Rodrigo Carlessi • *School of Pharmacy and Biomedical Sciences, Curtin Health Innovation Research Institute, Perth, WA, Australia*

Younan Chen • *Key Laboratory of Transplant Engineering and Immunology, NHFPC, Regenerative Medicine Research Center, West China Hospital, Sichuan University, Chengdu, PR China*

John C. Clapham • *Medical School, University of Buckingham, Buckingham, UK*

Vinicius Cruzat • *Faculty of Health, Torrens University Australia, Melbourne, Victoria, Australia*

Donald R. Dunbar • *Edinburgh Genomics, University of Edinburgh, Edinburgh, UK*

Paul W. Finn • *School of Computing, University of Buckingham, Buckingham, UK*

Elena V. Galkina • *Department of Microbiology and Molecular Cell Biology, Eastern Virginia Medical School, Norfolk, VA, USA*

Sheridan Gentili • *Sansom Institute for Health Research, School of Pharmacy and Medical Sciences, University of South Australia, Adelaide, SA, Australia*

Parvathy E. Harikumar • *National Institute for Biological Standards and Control (NIBSC) and Buckingham Institute of Translational Medicine, University of Buckingham, Buckingham, UK*

Jayne A. L. Houghton • *Royal Devon and Exeter Foundation Trust, Exeter, UK*

Maysson Ibrahim • *Clinical Trial Service Unit and Epidemiological Studies Unit, Nuffield Department of Population Health, University of Oxford, Oxford, UK*

Yumi Imai • *Department of Internal Medicine, Strelitz Diabetes Center, Eastern Virginia Medical School, Norfolk, VA, USA*

Aileen J. F. King • *Diabetes Research Group, School of Life Course Sciences, King's College London, London, UK*

Milind C. Mahajan • *Sema4, a Mount Sinai venture, Stamford, CT, USA*

Andrew S. McLellan • *Sema4, a Mount Sinai venture, Stamford, CT, USA*

Beverly Sara Mühlhäusler • *Food and Nutrition Research Group, Department of Food and Wine Sciences, School of Agriculture, Food and Wine, The University of Adelaide, Adelaide, SA, Australia; FOODplus Research Centre, School of Agriculture, Food and Wine, The University of Adelaide, Adelaide, SA, Australia; CSIRO, Health and Biosecurity, Adelaide, SA, Australia*

Philip Newsholme • *School of Pharmacy and Biomedical Sciences, Curtin Health Innovation Research Institute, Perth, WA, Australia*

Lisa M. Nicholas • *University of Cambridge Metabolic Research Laboratories and MRC Metabolic Diseases Unit, Institute of Metabolic Science, Addenbrooke's Hospital, Cambridge, UK*

Jacqueline F. O'Dowd • *Medical School, University of Buckingham, Buckingham, Buckinghamshire, UK*

Laura P. O'Neill • *Institute of Biomedical Research, College of Medical and Dental Sciences, University of Birmingham, Birmingham, UK*

Chloe L. Rackham • *Diabetes Research Group, School of Life Course Sciences, King's College London, London, UK*
Ionel Sandovici • *Metabolic Research Laboratories, Medical Research Council Metabolic Diseases Unit, Department of Obstetrics and Gynaecology, University of Cambridge, Cambridge, UK; Centre for Trophoblast Research, Department of Physiology, Development and Neuroscience, University of Cambridge, Cambridge, UK*
Joanne L. Selway • *Medical School, University of Buckingham, Buckingham, UK*
Claire J. Stocker • *Medical School, University of Buckingham, Buckingham, Buckinghamshire, UK*
Carla Toop • *Sansom Institute for Health Research, School of Pharmacy and Medical Sciences, University of South Australia, Adelaide, SA, Australia*
Michelle B. Trevino • *Department of Internal Medicine, Strelitz Diabetes Center, Eastern Virginia Medical School, Norfolk, VA, USA*
Edward T. Wargent • *Buckingham Institute of Translational Medicine, University of Buckingham, Buckingham, UK*
Mohamed S. Zaibi • *Buckingham Institute of Translational Medicine, University of Buckingham, Buckingham, UK*

# Chapter 1

# Sixty Years of Drug Discovery for Type 2 Diabetes: Where Are We Now?

John C. Clapham

## Abstract

Today, excluding insulin, there are eight classes of anti-diabetic medicines that have been added to the pharmacy since the introduction of metformin in the mid-1950s; the sulfonylureas, biguanides, thiazolidinediones, α-glucosidase inhibitors, meglitinides, incretins, and sodium glucose transport 2 inhibitors. Does the fact that metformin is still first-line treatment suggest that our drug discovery efforts over the past 60 years have not been good enough? Or does it suggest that diabetes is such a complex disorder that no single treatment, other than gastric bypass surgery, can affect true normalization of not only blood sugar but also the underlying pathologies? Our understanding of the disease has most definitely improved which may bring hope for the future in terms of science, but for it to be beneficial, this science has to be translated into better drug treatments for the disease. In this review, I have examined the eight classes of anti-diabetes drugs from a drug discovery perspective.

**Key words** Type-2-diabetes, Drug discovery, Metformin, Sulfonylureas, Biguanides, Thiazolidinediones, α-Glucosidase inhibitors, DPPIV inhibitors, GLP-1, SGLT2 inhibitors, Pharmaceutical industry

## 1 Introduction

Modern drug discovery programs often start with a hypothesis, based on some prior knowledge, that modulation of target X in pathway Y will result in a positive therapeutic effect in a particular disease area. The key to this approach is discovering the right target in the right pathway in the right tissue which is amenable to specific interaction with a ligand, a target characteristic that has been referred to as "druggability" [1]. This is "target-based" drug discovery and validates drug targets using molecular genetics techniques [2], though this approach does have its critics [3]. Judging by the huge failure rate, on top of patent expiration [4], this is challenging in practice, more so in complex diseases where the risks are much higher. Normal glucose homeostasis and the etiology of type 2 diabetes are highly complex processes, so, predictably, drug

Claire J. Stocker (ed.), *Type 2 Diabetes: Methods and Protocols*, Methods in Molecular Biology, vol. 2076,
https://doi.org/10.1007/978-1-4939-9882-1_1, 

discovery in this area has been slow with relatively few new entrants to the market in the 60 years since the introduction of today's first-line drug treatment, metformin.

Maintenance of a normal blood glucose level involves a dynamic interplay between glucose absorption, glucose production, and glucose utilization. These in turn are controlled by interactions between circulating hormones (primarily insulin, though there are many others) and the cellular processes involved in insulin (and other hormone) signaling, glucose uptake, and glucose disposal. The principal tissues involved in this interplay are the liver, brain, skeletal muscle, and adipose tissue which in turn differ in their patterns of substrate utilization, production, and recycling which are critical to maintaining normal blood glucose levels in the range of 3.8–6.1 mmol/L (68.4–109.8 mg/dL). Following a meal, the degree to which blood glucose increases is a function of the amount of glucose absorbed, the pancreatic insulin secretory response, suppression of hepatic glucose output and increased glucose uptake by insulin-sensitive (skeletal muscle, liver, adipose tissue—65–70%) and insulin-insensitive organs (brain, kidney—30%) [5–7].

Type 2 diabetes is the pathologic consequence of two concurrent and interacting conditions of insulin resistance and *relative* insulin deficiency. On the one hand, insulin's ability to suppress hepatic glucose output and stimulate glucose uptake and utilization is impaired (resulting in chronically raised insulin levels), and on the other hand, the capacity of the pancreatic β-cell to maintain this hyperinsulinemic state also begins to fail [8, 9]. Type 2 diabetic patients are rarely hypoinsulinemic when compared to nondiabetic individuals [8]. Another twist in the natural history of type 2 diabetes story is that there is also a degenerative process that affects the normal healthy existence of the pancreatic β-cell. In a landmark study, it has been shown that after a point, a relatively small decrease in β-cell mass is all that is required to have profound effects on fasting blood glucose levels [10].

The Diabetes Control and Complications Trial (DCCT) and the UK Prospective Diabetes Study (UKPDS) have shown us that maintaining blood glucose levels to near-normal levels significantly improves type 2 diabetes and its ensuing complications [11–13]. The American Diabetes Association has recommended that treatment should reduce HbA1c levels to less than 7% [14, 15]. This is a relaxation of earlier guidelines which recommended reducing HbA1c to 6.5% or below [16] as such aggressive treatment was found to be associated at best with no additional cardiovascular benefit but at worst with increased mortality [17, 18]. However, in practice, HbA1c of 7% or above should initiate treatment regimens. Regulatory guidelines for new drug treatments usually stipulate an endpoint for a clinically meaningful and statistically significant reduction in HbA1c, usually at least 1%

over placebo with noninferiority against standard therapy, usually metformin.

There is a challenge that any anti-diabetic drug will face. The natural history of type 2 diabetes occurs as a continuum of the interplay described above and that occurs over many years. By the time of diagnosis, the disease is already in its mid stages before any drug treatment can be initiated. The costs of treating diabetes are huge and the drugs bill is a favorite political punch bag. It is of course true; in the UK, the diabetes drugs bill is expensive; in 2010, it was around £2 billion. However, the cost of hospitalization as a consequence of diabetes was £8 billion (Diabetes UK). It is worth noting that drug treatment with oral anti-diabetic agents may actually reduce the hospitalization costs [19].

"Type 2 diabetes therapies" is a topic that is extensively and regularly reviewed. The aim of this chapter, therefore, is to provide an overview of current drug therapy of type 2 diabetes resulting from research dating back many decades but with a flavor of the type of things that might influence drug discovery efforts in this area. It will be confined to small molecule drug inventions (though peptide drugs of the exenatide type are included). "Industrial" drug discovery for type 2 diabetes appears to have started around the mid-twentieth century and since then eight broad classes, excluding insulin, of agents are on the market today. These are presented below in the order of their introduction.

## 2 Sulfonylureas (First Generation)

Insulin secretion from the pancreatic β-cell occurs in response to an increase in blood glucose levels after a meal. Briefly, intracellular ATP levels in the pancreatic β-cell increase in response to a rise in blood glucose levels and this causes closure of an inward-rectifying ion channel, the ATP-sensitive potassium channel ($K_{ATP}$). This depolarizes the β-cell plasma membrane, via calcium entry through L-type (verapamil sensitive) calcium channels, and stimulates insulin exocytosis [20].

Our understanding of the electrophysiology of the $K_{ATP}$ channel, now combined with molecular and genomic insights, allows a comprehensive description of how sulfonylureas work. The $K_{ATP}$ channel is actually a multi-subunit protein complex consisting of four inward rectifying potassium channels (Kir6.2) that form a pore and four regulatory subunits [21, 22]. There are two subtypes of regulatory subunits, SUR1 and SUR2, which differ in their binding affinities for sulfonylureas [23, 24]. The SUR1 regulatory subunit is found in the pancreatic β-cell, while SUR2 is found in cardiac and smooth muscle cells [25].

The anti-diabetic sulfonylureas stimulate insulin secretion from the pancreatic β-cells by mimicking the effect of ATP in the β-cell to

block opening of $K_{ATP}$ channels [26, 27]. They are termed insulin secretagogues.

A first-generation sulfonylurea is tolbutamide. Tolbutamide originated from a war-effort search for antibiotics and the unpleasant side effect of blackouts resulting from hypoglycemia; while unacceptable for an antibiotic, it turned out to be a new therapeutic approach for the treatment of diabetes. Tolbutamide, and an analog, carbutamide, were launched in the mid-1950s [28]. Some studies have suggested that tolbutamide, because of a short duration of action, could have a place today in the treatment of elderly type 2 diabetics [29]. The elderly type 2 diabetic patient is particularly vulnerable to the consequences of hypoglycemic episodes that can make them prone to falls [30] and cardiovascular issues [29]. In practice, however, tolbutamide is rarely prescribed today and it carries an FDA warning regarding cardiovascular mortality.

## 3 Biguanides

The only representative of this class of anti-diabetic drug remaining in use is metformin. Although chemically synthesized, metformin is derived from biguanide compounds obtained from the medicinal plant *Galega officinalis* [31]. It was launched in 1957 as an oral hypoglycemic agent. Other examples in this class were phenformin and buformin.

Metformin is poorly absorbed from the gut [32, 33], a process dependent on the plasma membrane monoamine transporter [34], and large doses (500–2500 mg per day) are required for efficacy. The metformin molecule is not metabolized into any other product by the body and is excreted in the urine as the parent drug with the half-life of elimination of around 5 h [35]. The liver appears to be the main site of action for metformin and uptake into the liver is also facilitated by transporters, primarily OCT1 [36] but its pharmacodynamic mechanism of action in the liver has not been fully elucidated. One wonders how far metformin would have advanced through a modern drug discovery process based on current experience, yet metformin is probably the most widely prescribed anti-diabetic agent in the world. The UKPDS showed that metformin outperformed standard therapies, including sulfonylurea and insulin, on all diabetic endpoints [12]. It is now a first-line therapy in almost all markets and can be used as monotherapy or in combination [37, 38]. Indeed, as we shall see later, it has been used in combination with all of the other classes of anti-diabetic drugs because of its front-line role. Since its use is so widespread in a patient population that may already suffer from other problems requiring medication, attention needs to be paid to the potential risk for drug–drug interactions. Its reliance on the action of transporters for absorption and delivery to target organ means that

other agents using these transporters will influence metformin's activity.

Unlike sulfonylureas, metformin reduces raised blood glucose levels only in the presence of hyperglycemia and without stimulating insulin levels [39–41]. Metformin exerts its anti-diabetic effect primarily by enhancing the effect of insulin in suppressing gluconeogenesis and thereby reducing hepatic glucose output [42]. Secondarily, metformin increases muscle tissue insulin sensitivity [43]. Information is being gleaned on the pathways involved in the mechanism of action of metformin but its precise molecular target is still unknown; we do not yet know what it binds to. One of the first breakthroughs was reported in 2002 [44] which showed that metformin, along with thiazolidinedione and rosiglitazone, activated AMP-activated protein kinase (AMPK) by two different mechanisms.

AMPK is a multi-subunit enzyme playing a central role in cellular stress responses through marked pleiotropic effects on metabolism [45]. It initiates cellular cascades to increase fat oxidation, decrease anabolic pathways in fat metabolism, and enhance glucose uptake in order to preserve cellular energy stores [46]. Thus, AMPK orchestrates the flux of fatty acids away from triglyceride synthesis and into β-oxidation via modulation of many downstream proteins. However, metformin does not bind to the AMPK complex directly in order to activate it; AMPK is sensitive to the cellular milieu, in this case the AMP:ATP intracellular ratio. It is suggested that metformin induces changes in the AMP:ATP ratio by disrupting normal mitochondrial function by interfering with complex 1 of the respiratory transport chain [47]. This alteration of the energetic state of the cell elicits an effect on AMPK but independently of a direct interaction with the AMPK molecule. Furthermore, AMPK is itself upregulated by other kinases lying upstream, including the LKB1 tumor suppressor protein kinase [48], which, incidentally, may also be a pathway affected by metformin. A later study, however, has shown that metformin could still inhibit gluconeogenesis in hepatocytes lacking either AMPK or LKB1, perhaps via a reduction in glucose-6-phosphatase expression. Thus, the precise molecular target(s) of metformin have yet to be elucidated—somewhat anachronistic in todays "Big Data" world with emphasis on identifying precise molecular targets even before a drug discovery project starts.

Another advantage of metformin is that it is associated with weight loss in obese subjects with or without type 2 diabetes [49]. This could be via activation of the oxidative pathways outlined above which can be thermogenic and increase energy expenditure [50] with an additional effect to reduce food intake [51] or a combination of both.

A rare side effect of metformin is lactic acidosis. Lactic acidosis has been reported to occur in patients with or without renal

insufficiency [52]. Metformin is extensively cleared via the kidneys [33] so care must be exercised in the elderly or people with a history of kidney disease. The effect of inhibiting complex 1 of the mitochondrial respiratory chain, while possibly explaining inhibition of gluconeogenesis from lactate, may also contribute to the rare cases of lactic acidosis [47]. Early competitors to metformin, phenformin and buformin, were more potent and more efficacious but were eventually withdrawn in the 1970s because of higher incidence of lactic acidosis [31]. Metformin can also cause severe gastrointestinal problems in some patients, possibly via an effect on bile salt absorption [53], though this can be mitigated to a large extent using a prolonged release formulation [54]. There have been occasional reports of metformin-induced pancreatitis in both with [55] or without [56] pre-existing renal disease.

An aspect of drug discovery that has been gaining prominence over the last decade or so is the search for new indications for old (in this case very old) drugs in a drug discovery paradigm called "repurposing" [57]. The potentially positive effects of metformin in cancer, polycystic ovary syndrome, and nonalcohol fatty liver disease are in themselves well-reviewed areas [58–60].

## 4 Sulfonylureas (Second Generation)

This group is represented by the drugs glibenclamide (glyburide), gliclizide, and glimepiride. Glibenclamide was approved by the FDA in 1984. These agents are still used but predominantly as second-line add-on after metformin. As a drug class, they have been extensively reviewed and meta-analysis of clinical trial data reveals that they lower HbA1c by around 1.5% [61]. Hypoglycemia is a common issue with these agents but that is hardly surprising since their mechanism of action is independent of any glucose-sensing remaining in the β-cell or the prevailing blood glucose levels. The liability for hypoglycemia seems to be greater for glyburide than the others. Weight gain is another common unwanted effect of this class of oral anti-diabetic agent.

The second-generation sulfonylureas are metabolized in the liver via the cytochrome P450 system and eliminated via the kidneys. The biotransformation of glyburide in the liver results in the production of active metabolites [62] which will be particularly troublesome in patents with renal insufficiency. No active metabolites of gliclizide and glimeripiride have been identified to date.

When drugs have been in clinical use for so long and in so many patients, any *lurking skeletons* in the cupboard usually make themselves known. Drug discovery efforts are inconveniently, and frequently, hampered by two major causes of attrition: failure in efficacy, failure in safety or both [63].

### 4.1 Failure in Efficacy

Although the meta-analysis reassures us that they are effective in lowering HbA1c, both as monotherapy or on top of other agents, the issue with sulfonylureas with regard to efficacy is durability. In other words, while reasonable efficacy is seen at the start of treatment, it declines with continued use [64, 65] in a phenomenon called "secondary failure." Secondary failure in response to sulfonylurea appears to be specific as long-term treatment with sulfonylureas can selectively reduce the insulin secretory response to an acute dose of another sulfonylurea but not to glucagon [66]. The exact mechanism is not known though sulfonylureas appear to induce β-cell apoptosis in cultured human islets [67].

### 4.2 Failure in Safety

The other issue for the sulfonylureas is the increased risk of cardiovascular side effects, an issue that has been debated since the 1970s. The Sulfonylurea glyburide was shown to have a greater risk of cardiovascular mortality than metformin [68] in a study that raised the question about the manner in which blood glucose can be safely reduced. Since then, several studies, using metformin as a comparator, have reported that a number second-generation sulfonylureas share this cardiovascular risk [64, 65]. There also appears to be differences between different sulfonylureas on the degree of risk [67]. Increased cardiovascular risk with these agents is probably beyond doubt now and has serious implications for developing economies that rely on cheap drugs [69] as preferred treatments.

The increased cardiovascular risk is probably due to the interaction with cardiac $K_{ATP}$ channels [70]. In patients with already increased risk of cardiovascular disease, sulfonylureas acting on cardiac $K_{ATP}$ could mask ST-segment elevation causing opportunities for life-saving interventions to be missed [71].

## 5 Thiazolidinediones

The thiazolidinediones, troglitazone, rosiglitazone, and pioglitazone, were launched in the late 1990s. They exert their antidiabetic effects principally by alleviating insulin resistance. Unlike metformin, whose main site of action is the liver and secondarily skeletal muscle, the thiazolidinediones act primarily on adipose tissue and secondarily skeletal muscle. The molecular mechanism of the thiazolidinediones is activation of the nuclear hormone receptor, Peroxisome Proliferator Activated Receptor-γ (PPAR-γ). There are a number of classes of PPAR [72] and all appear to be involved in the regulation of metabolism; for example, PPAR-α activates pathways for fatty acid oxidation [73]. The thiazolidinediones mentioned above were not a result of rational drug design based on knowledge of their molecular target but rather through the observation that certain drugs, fibrates, originally developed for dyslipidemia and acting via PPAR-α, lowered blood glucose levels

but through a different, then unknown, mechanism. They were well into their clinical development when PPAR-γ was identified as their primary molecular target; the thiazolidinediones were identified by what we now call phenotypic screening, the precursor methodology to target-based approaches. However, almost from the start, they were beset with problems.

Troglitazone, which was approved in 1997, was shown to be efficacious as monotherapy or in combination with sulfonylureas or metformin [74]. But there were early signs of trouble; even in clinical trials, there were indications of the hepatotoxicity [75] that eventually led to its withdrawal from the UK market in 1997 and the US market in 2000. The background to this story and the reasons for the almost immediate withdrawal by GlaxoSmithKline in the UK and its persistence on the US and Japanese markets are sobering reading, and underlies how different companies have very different attitudes to patient safety risk [76]. The other thiazolidinediones, rosiglitazone and pioglitazone, did not share this particular liability.

Rosiglitazone and pioglitazone are efficacious; they lower HbA1c by between 1.0% and 1.5% over placebo control in monotherapy trials [65]. They did however cause fluid retention and an increase in body weight [77]. The thiazolidinediones also lower elevated free fatty acids, particularly in combination with metformin [78, 79]. This is good and has the potential to reduce lipotoxicity which is thought to be a mechanism contributing to β-cell dysfunction in type 2 diabetes [80, 81]. Long-term treatment of *fa/fa* rats with rosiglitazone, using either prevention or intervention protocols, has hugely beneficial effects on islet morphology [82]. Together these sets of results suggest that the thiazolidinediones could have had the potential for improving β-cell health. Sadly, we will never know for sure, as further calamity overtook this class of agent.

Two very controversial meta-analyses suggested that rosiglitazone increased risk of myocardial infarction [83, 84]. The resulting public outcry and media storm [85] condemned the drug and led to its withdrawal by the company in 2007 even though an FDA advisory committee did not think that there was sufficient evidence to actually call for its withdrawal [86]. The methodologies in the meta-analyses have been subsequently questioned and other studies did not find the increased risk of myocardial infarction, and perhaps even a positive finding for rosiglitazone [87, 88]. This controversy seriously knocked the confidence of patients and physicians but it is sad to note that the manufacturer no longer invests in in-house diabetes drug discovery research. In late 2013, after reviewing the data of Rosiglitazone Evaluated for Cardiovascular Outcomes and Regulation of Glycemia in Diabetes (RECORD) trial [89], the FDA removed marketing restrictions on rosiglitazone but the patent on rosiglitazone had expired in 2012.

But the pain did not end there. Pioglitazone sparked some further concern surrounding increased risk of bladder cancer [90]. Thiazolidinediones are also associated with fractures, particularly in postmenopausal women [91] and macular oedema [92], which appears to be reversible on discontinuation of therapy [93]. Thiazolidinediones are available in their generic form but really only as third-line therapies.

## 6 α-Glucosidase Inhibitors

Carbohydrates constitute a large proportion of our energy intake, especially for those of us living in the Western world. Worryingly, over the last 50 years or so, the proportion of refined sugars entering our diet has also increased dramatically [94, 95] as we consume more and more processed foods. The majority of the carbohydrate consumed in food is polysaccharide in the form of starch or oligosaccharides such as sucrose.

Monosaccharides, such as glucose, are readily absorbed through the intestinal epithelium via the sodium-dependent glucose co-transporter-1 (SGLT1) [96]. Oligosaccharides and polysaccharides are not readily absorbed and have to be broken down to monosaccharides first. Starch is broken down into smaller oligosaccharides by α-amylase in the small intestine. The resulting oligomers (or dietary oligomers) are further broken down by a membrane-bound enzyme family into (primarily) glucose, galactose, and fructose [97] which can then be transported through the gut epithelia and on into the blood stream. These latter enzymes reside in the brush border of the small intestine and are the α-glucosidases (formally known as the maltases) and they hydrolyze O-linked glycosidic bonds [98].

As mentioned in the introduction with regard to a potential drug discovery program, a clear hypothesis presents itself here; sugar consumption is increasing and so is type 2 diabetes. In the absence of restraint from ourselves or moderation of added sugars to processed foods by manufacturers, inhibition of α-glucosidases by drugs will reduce absorption of dietary sugar and the hypothesis assumes that this will improve glycemic control, and this is essentially what has happened. The α-glucosidase inhibitors, acarbose, voglibose, and miglitol, are pseudo-carbohydrates and were launched between 1994 and 1996. Acarbose and voglibose are poorly absorbed and are consequently excreted in the feces [99] while miglitol is fully absorbed and excreted as parent compound by the kidneys [100].

Acarbose has been shown to be an effective monotherapy where diet modification is insufficient to control fasting plasma glucose. A marked reduction in postprandial hyperglycemia was reported in one study where a 0.65% reduction in HbA1c after

24 weeks treatment was observed [101]. The efficacy of acarbose is reasonable compared to other oral anti-diabetic agents such as metformin and gliclizide [102, 103]. α-Glucosidase inhibitors may also be useful in reducing insulin requirement of type 1 diabetic patients [104]. Side effects of the α-glucosidase inhibitors are, unsurprisingly, mainly gastrointestinal: diarrhea, flatulence, and abdominal distension (meteorism).

The α-glucosidase inhibitors also appear to have a positive effect on disease markers of cardiovascular dysfunction [105], an effect that may be related to the suppression of postprandial hyperglycemia seen with these agents. Postprandial hyperglycemia is associated with oxidative stress [106] and oxidative stress is linked to vascular endothelial dysfunction [107, 108]. Thus, the α-glucosidase inhibitors have the potential of being a useful add-on treatment to existing anti-diabetic agents to improve postprandial hyperglycemia and perhaps could confer benefits with regard to cardiovascular function.

## 7 Meglitinides

The insulin response to glucose occurs in two phases: an immediate early phase increase within minutes and, a later, more prolonged increase over 2–3 h. The biphasic nature of the insulin response is more discernible in response to intravenous administration of glucose but the episodic nature of the insulin response to prandial glucose is less clearly defined [109]. The liver is an important target organ for the early-phase insulin response, where insulin acts to suppress hepatic glucose output [110, 111].

In type 2 diabetes, there is a loss of the early insulin response to a meal and this may be a marker for impairment at the level of the β-cell [112, 113]. Thus, restoring the first-phase insulin response is an important therapeutic goal [114]. An early proof of concept to this idea was shown in newly diagnosed type 2 diabetics; insulin was infused to mimic the first-phase insulin response and resulted in a marked reduction in elevated postprandial glucose excursions [115]. Thus, the hypothesis that drugs that restore first-phase insulin response will produce an important beneficial therapeutic effect was a clear "go" signal for project work.

The meglitinides are short-acting insulin secretagogues that are readily absorbed from the gastrointestinal tract [116]. This makes them a much more suitable option than infusing insulin. Examples of these agents are repaglinide and nateglinide launched in 1997 and 2000, respectively. Like the sulfonylureas, the meglitinides reduce the probability of $K_{ATP}$ channel opening in β-cells to depolarize the cell by allowing calcium influx through L-type calcium channels [117]. Repaglinide and nateglinide also bind competitively to the SUR1 sulfonylurea receptor with $K_i$ of 100 nM and

240 nM, respectively, compared to 2.3 nM for glibenclamide [118]. Furthermore, nateglinide differs from repaglinide in that it dissociates from the SUR1 receptor very rapidly [118].

Clinical experience, either as monotherapy or in combination, show that this class of anti-diabetic agent is effective, particularly with respect to mealtime glucose excursions. For example, in a double-blind, placebo-controlled study, repaglinide (0.5–1.0 mg) taken at meal times improved glycemic control and reduced HbA1c by 1.14% after 4 weeks of dosing without a significant effect on body weight [119]. This study also highlighted the flexibility of these agents; repaglinide has a rapid onset of action and short duration and has utility where meal patterns may change from day to day. In a 16-week head-to-head trial, repaglinide and nateglinide were compared as monotherapies in type 2 diabetic patients [120]. While both agents have similar effects on postprandial glucose excursions, repaglinide was more effective at reducing HbA1c and fasting plasma glucose though it did induce more weight gain than nateglinide. While repaglinide and nateglinide both block the $K_{ATP}$ channel, their mode of interaction with the regulatory subunit, SUR1, differs [121] which may partly explain their therapeutic differences. Similarly, repaglinide was shown to be slightly more effective that the sulfonylurea, glipizide [122].

The meglitinides are unlikely to be a first-line drug therapy; as the majority of patients will be on metformin, however, where metformin is contraindicated, these agents may be used [123] but there are questions with regard to durability of effect and long-term usefulness as monotherapy [124]. Meglitinides may still be a useful add-on therapy in subjects where their diabetes is hard to control despite diet, exercise, and metformin treatment. In such a case, addition of repaglinide resulted in better control compared to metformin (or repaglinide) monotherapy [125]. Weight gain was reported as well as a greater incidence of mild-to-moderate hypoglycemic incidents.

The rapid onset and short duration of action of the meglitinides seems to confer advantages over the second-generation sulfonylureas with respect to postprandial glucose control, and their pharmacokinetic properties allow flexibility with respect to meal patterns. As we saw with the α-glucosidase inhibitors, this property will have other beneficial effects, particularly on cardiovascular risk, and this does seem to be the case for repaglinide compared to the sulfonylureas [126].

## 8 Incretins

### *8.1 GLP-1 Mimetics*

The discovery of the polypeptide hormones, glucose-dependent insulinotropic polypeptide (GIP), and glucagon-like peptide-1 (GLP-1), followed from the well-known observation that oral,

but not intravenous, administration of glucose enhanced insulin secretion from pancreatic β-cells [127]. These are the incretin hormones and both GIP and GLP-1 are major contributors to meal-induced insulin secretion [128]. GIP is secreted from duodenal K-cells while GLP-1 is secreted from L-cells located further down the gastrointestinal tract at the distal ileum and colon [129]. Glucose sensing by SGLT1 plays a crucial role in the stimulus–secretion coupling in L-cells [130]. GLP-1 reduces the secretion of glucagon from pancreatic β-cells to reduce glycogenolysis while GIP increases glucagon secretion. In the blood stream, both GIP and GLP-1 are rapidly inactivated by N-terminal cleavage of two amino acids by dipeptidyl peptidase IV (DPPIV). Within the 2–4 min that the incretins are active, they interact with GIP receptors and GLP-1 G-protein-coupled receptors on the pancreatic β-cell to effect an increase in cAMP and ultimately insulin secretion [131–133].

The biology of GIP and GLP-1 has been well documented and the reader is referred to a comprehensive review where their biology has been compared and contrasted [134]. The first objective for a therapeutic agent activating the incretin pathway will be to have an active half-life for considerably longer than the 2 min enjoyed by GLP-1. This goal spurned a great deal of industrial activity to screen and identify a small molecular agent to activate the GLP-1 receptor. Agonists are harder than antagonists to identify and Class-B GPCRs are notoriously resistant to drug discovery efforts. This is because of a large and complex N-terminal domain that appears to shield the extracellular binding face of the receptor; to activate the receptor, peptide ligands have to bind to both the N-terminal domain and to the active site [135]. Since the GLP-1 receptor is a Class-B GPCR and an agonist is the therapeutic modality, the odds were stacked against small molecule discovery efforts from the start. Small molecule approaches have been traditionally preferred because they, in the main, are oral therapies. There have been many attempts to identify small molecule activators of the GLP-1 receptor using the shotgun approach of high throughput screening. It is likely that millions of compounds from a variety of libraries from several companies were screened to largely no avail. However, there are some examples of small molecule agonists of the GLP-1 receptor [136]. Molecules of interest, arising from research in China, are substituted cyclobutane compounds which appear to avoid the barriers to small molecule activation of the GLP-1 receptor. The lead compound, designated Boc5, appears to exert GLP-1 agonistic effects in animal models of diabetes [137, 138]. Sadly, these are non-druggable molecules [136], meaning that there is little or no scope for optimization, but they at least encourage us that a small molecule approach is not as improbable as we originally believed.

However, in the present world, the main therapeutic GLP-1 agonists are all peptidic, and therefore require injection. Analogs of GLP-1, such as exenatide which was approved in 2005 and liraglutide which was approved in 2010, were the results of the effort to find longer acting GLP-1s. Unlike the very short half-life of native GLP-1, exenatide has a half-life of around 2.5 h [139] which still necessitates multiple daily doses. Liraglutide, a fatty acid derivative of GLP-1, was approved in 2010 and displays a much longer half-life as a result of this modification [140]. The HbA1c lowering of GLP-1 mimetics is related to half-life, and a longer acting version of exenatide was introduced which allowed for once weekly dosing [141].

The anti-diabetic effects of exenatide and liraglutide have been extensively reviewed [142] and have been shown to be effective treatments in trials either as monotherapy or in combination; in real-world medicine, they are more likely to be given in combination. It is possible that liraglutide outperforms exenatide with respect to HbA1c [143] but that the effect is marginal and the longer acting version of exenatide may mitigate this difference. These agents have some interesting side properties that are beneficial—in the future, these additional properties (over and above HbA1c lowering) will determine the commercial success of any agent for the treatment for type 2 diabetes. Exenatide has been shown to lower body weight, most likely mediated by a central effect on appetite [144, 145]. This may be very useful in the treatment of hyperphagic obesity of hypothalamic origin [146, 147]. Given the experience with the thiazolidinediones and sulfonylureas, this is a desirable add-on effect in drug discovery programs.

β-Cell decompensation [148] and declining β-cell mass [10] are key morbidities in the type 2 diabetes continuum. Therapeutic agents that could reverse this decline in β-cell mass would be game changers as this would result in the in vivo generation of new β-cells. As we have seen, the thiazolidinedione drug class may have had this ability via an attenuation of lipotoxicity, but the world will never really know. However, the general idea of reversing the decline in β-cell mass is generating plenty of interest as a biological effect area in its own right with the realization that the pancreas is actually flexible enough to generate new β-cells either by replication or by neogenesis [149].

It seems that drugs acting via the incretin system appear to have very interesting effects on β-cell biology with the finding that GLP-1 mimetics appear to improve measures of β-cell function [150] or responsiveness [151] in diabetic patients. However, this sort of finding does not imply the effects are due to neogenesis which is currently impossible to measure in living patients. Experimental data from animals [152] and from isolated human islets [153] suggest that this is an area indeed worthy of continued

study especially in the clinical setting. In another twist to the biology of GLP-1 mimetics, exenatide has been shown to reduce β-cell apoptosis in neonatal rat or human isolated islet preparations [154, 155], one of the destructive influences on β-cells in type 2 diabetes [156]. Sadly, since β-cell depletion by apoptosis is a process that occurs over many years, it is hard to envisage a viable clinical study protocol designed to confirm that an anti-apoptotic effect contributes to improvements in β-cell function or mass. As we have seen before [10], after a certain point, only a small reduction in β-cell mass results in overt hyperglycemia. Conversely, perhaps only a small increase in β-cell mass could delay the switch-over to overt, insulin requiring diabetes. However, expansion of β-cell mass in mice may be different and perhaps more amenable than in human islets as the difference in islet structure, and perhaps behavior, between the two species is marked [157–159].

Despite the promise of some very interesting pharmacology with regard to glycemic control, weight loss, and perhaps β-cell mass, a potentially very serious safety concern has been flagged and this has been hotly debated; acute pancreatitis and pancreatic cancer. If probable expansion of β-cell number is due to a proliferative effect, could this occur in other cell types?

Pancreatitis was reported as a potential risk by the FDA in late 2006 and has been subsequently confirmed in many studies [160]. This article summarizes these reports and offers a plausible mechanism for this side effect. Briefly, GLP-1 receptors are present in pancreatic duct cells [161] and following chronic stimulation of these receptors during treatment with GLP-1 mimetics, the duct cells may proliferate and block pancreatic ducts leading to pancreatitis and ultimately pancreatic cancer [160]. The degree of risk posed by these agents has been challenged on the basis that the data neither prove nor disprove the hypothesis that the acute pancreatitis progresses to malignant disease [162]. Nevertheless, diabetes is itself a risk factor for pancreatitis [163] and extreme care must therefore be taken if agents have the potential to superimpose risk where there is already vulnerability.

### 8.2 DPPIV Inhibitors

An alternative strategy to the very challenging approach of producing Class-B GPCR agonists is to extend the half-life of the endogenous hormones; this has been achieved by inhibiting the DPPIV enzyme. This is generally an easier option for the drug hunter and pharmaceutical industry.

DPPIV is a 766-amino acid glycoprotein and is well conserved across species, which is very useful from a drug discovery perspective to reduce the number of screens required. It is a serine protease, so called due to the presence of a serine residue in a catalytic triad comprising serine-624, aspartic acid-702, and histidine-734. As a serine protease, DPPIV removes a dipeptide from the N-terminus of peptide hormones of around 30 amino acids in

length and recognizes its substrates via amino acid motifs. For DPPIV, peptides which have proline or alanine as the penultimate amino acid are favored substrates (i.e., $N_2$H-x-Pro-). Although well conserved across species, DPPIV lacks similarity to the classical serine proteases such as chymotrypsin [164]. However, there are other peptidases that favor the $N_2$H-x-Pro- motif, DPPVIII, and DPPIX, where inhibition of these enzymes, as an off-target effect, could result in severe adverse effects [165].

DPPIV is a type 2 cell surface protein in terms of its spatial arrangement; most of the heavily glycosylated molecule is exposed to the extracellular space and is anchored to the cell membrane by virtue of a transmembrane helix anchor [166]. A soluble form of DPPIV, which lacks the anchor, was discovered in human plasma [167]. In the context of its therapeutic role, its most important substrates are GIP and GLP-1. However, neuropeptide Y (NPY), peptide YY, Substance P, and chemokines such as RANTES are also substrates; indeed, we have found that DPPIV inhibition enhances the antilipolytic activity of NPY in human adipose tissue [168]. The crystal structure of DPPIV was solved in 2003 [169] and subsequently many structures have been published co-crystallizing DPPIV with small molecule ligands and peptides [170]. This is a hugely valuable resource in drug discovery as it increases confidence and facilitates rational drug design.

Therapeutic inhibitors of DPPIV fall broadly into three types: reversible substrate analogs (no example on market), covalently bound substrate analogs such as vildagliptin and saxagliptin and reversible nonpeptidic heterocycles such as sitagliptin [171]. The development path for launch of sitagliptin is worthy of mention. Sitaglitptin (MK-0431) was nominated as the lead candidate for development in January 2002 and by only 2006 was approved by the FDA and by the EMEA the following year; this was a spectacular achievement for Merck and was an example to the industry of what clear planning and crisp decision-making looks like. Sitagliptin was the first DPPIV inhibitor to market.

This drug class has been extensively reviewed (for example, *see* [165, 172–175]). All marketed DPP-IV inhibitors show augmentation of GIP and GLP-1 levels and produce broadly similar reductions in HbA1c of around 1–1.5%, close to that produced by metformin. However, metformin is superior with respect to fasting plasma glucose levels. DPP-IV inhibitors have a low risk for hypoglycemia in monotherapy and are weight-neutral. All DPPIV inhibitors can be given with other oral hypoglycemic agents, and as the diabetes advances, they can be given with insulin in the late stages of the disease where perhaps combination with metformin fails to produce the desired level of glucose control [176].

As expected for agents working in a common pathway, similar effects of DPP-IV inhibitors to GLP-1 mimetics on β-cell biology have been reported. Clinical studies in type 2 diabetics also show an

apparently beneficial effect on the β-cell when using insulin: proinsulin ratio as a surrogate of β-cell function [177–179]. Animal studies, where β-cell mass can be measured directly, show that DPP-IV inhibition preserves (perhaps increases) β-cell mass [180]. Also not surprising is that acute pancreatitis, and the same associated issues, has also been reported with the DPP-IV inhibitors in some [181, 182] but not all [183] studies. While there are no reports of improved cardiovascular outcomes, DPP-IV inhibitors as a class, with perhaps the exception of sitagliptin, appear to be relatively free from major adverse cardiovascular events [184].

Where there are agents with different modalities acting in the same pathway, comparison is inevitable. In one study comparing outcomes of GLP-1 receptor agonists and DPP-IV outcomes, the conclusion was that the GLP-1 receptor agonists were superior in terms of HBA1c and body weight reduction [185]. They also conclude, quite diplomatically, that since DPP-IV inhibitors can be taken orally rather than by injection and where overweight is not a medical issue, DPP-IV inhibitors may be preferred. Nevertheless, it does indicate that there is useful flexibility in treatment options.

## 9 SGLT2 Inhibitors

The SGLT2 inhibitors are the latest oral anti-hyperglycemic agents to be approved and launched. Their rationale is based on the hypothesis that increasing glucosuria will facilitate glycemic control by removing glucose from the blood. In healthy individuals, plasma glucose levels are maintained between 3.8 and 6.1 mmol/L (68.4–109.8 mg/dL). All plasma glucose is filtered freely through the glomerulus and into the proximal convoluted tubule, yet less than 1% of this glucose enters the loop of Henle, glucose is virtually all reabsorbed into the circulation. Glucose is a highly polar molecule; it will not diffuse across biological membranes on its own and a sodium–potassium ATPase is required to power a sodium concentration gradient that provides the drive to transport glucose across the membrane via a sodium–glucose co-transporter. There is a family of renal sodium–glucose transporters and their molecular biology and biochemistry are very well reviewed [186, 187].

The highly industrialized process of glucose reabsorption from the tubular lumen occurs in the earlier part of the proximal convoluted tubule where over 80% of all the glucose is reabsorbed [186]. It is mediated by a high-capacity, low-affinity sodium–glucose co-transporter (SGLT2) present in the luminal brush border membrane. Further along the proximal tubule, there is a low-capacity, high-affinity sodium–glucose co-transporter (SGLT1) which accounts for the remaining glucose removal. Although SGLT2 and SGLT1 differ in their capacities and affinities, they both operate via a common mechanism [188]. SGLT2

was cloned in 1992 [189] and is expressed at very high levels in the early proximal tubule [190], very suggestive of a bulk transport role.

Over the course of 24 h, the kidneys of a normal individual will have reabsorbed over 160 g of glucose [191] which equates to "energy conservation" of the order of 2560 kJ (600 kcal) per day. This degree of reabsorption is well within the maximum renal absorptive capacity for a normal individual and gives the system resilience. However, when plasma glucose levels exceed 10.0 mmol/L (180.0 mg/dL), as seen in diabetes, glucose starts appearing in the urine, a condition known as glucosuria.

Before significant investment is committed to initiating and progressing drug discovery programs, various levels of comfort are required. The highest level is of course when a first-in-class drug is successfully launched; but then it really should be too late for anyone else to follow because of the decade-long lead-time. Commonly, in drug discovery projects, some form of human target validation is sought early in the projects lifetime, perhaps even before a formal investment decision. For SGLT2, there was luck in two respects. First, a form of human target validation presented itself in the form of loss of function mutations (human gene knockouts if you will) that exist and result in glucosuria [192, 193]. Second, there was a competitive inhibitor that has been known to science since the mid-1880s: phlorizin, a naturally occurring dihydrochalcone glucoside found in the bark of pear, apple, and cherry trees. In a study conducted in the 1930s, phlorizin was reported to promote glucosuria and reduce plasma glucose levels in humans [194]. In a reversal of the normal linear process, 50 years elapsed in order to find a study in animals where phlorizin was shown to ameliorate hyperglycemia and, interestingly, improve insulin sensitivity in partially pancreatectomized diabetic rats [195]. Phlorizin was subsequently found to be a competitive inhibitor of SGLT2 with a $K_i$ of around 220 nM [187]. For a project start-up, this is "*gold dust*"!

However, phlorizin has a number of issues: [1] it is poorly absorbed, [2] it is nonselective with regard to other SGLTs, [3] it is poorly bioavailable, and it needs to get to its target, and [4] has unpleasant gastric side effects probably due to point 2. These are all features that can be fixed by a decent medicinal chemistry approach and indeed the currently approved SGLT2 inhibitors used phlorizin as a molecular starting point. Early attempts were not so successful since they, like phlorizin itself, were O-linked glycosides and very prone to rapid metabolism [196]. This was solved by changing the O-linked bond to a C-glucosidic bond to yield canagliflozin [197], dapagliflozin [198], and empagliflozin [199] which gained FDA approval in the order cited here between late 2013 and autumn of 2014. The structural parameters in order to mass-produce SGLT2 inhibitors are well defined [200] as evidenced by

these approvals occurring in rapid succession with yet others waiting in the wings [201, 202]. This may well be a drug class where the "me-too" criticism may well resurface. Differentiation will then be a challenge to get a decent return on investment and additional benefit to the patient.

However, depite being on the market for a relatively short time, there have been several reviews of the SGLT2 inhibitors in diabetes [199, 201–204]. As a class, they appear to have good pharmacokinetic properties [205, 206] and access their molecular target from the luminal side of the proximal tubule [207]. They are well tolerated [205, 208] and reduce HbA1c by the usual 1% or so over placebo [197, 199, 203]. They also appear to be good, perhaps excellent, add-on therapy to metformin, glimeperide, sitagliptin, and insulin [203, 204].

Given that all of the energy contained in glucose is not recycled following SGLT2 inhibition, weight loss is perhaps not surprising [209, 210] and could even be a useful add-on to problematic agents like sulfonylureas where weight gain is a concern [211].

One potentially serious issue that needs careful monitoring is the increased risk of urinary tract infections and an increase incidence has been reported for all members of this class [205, 208]. In an analysis of the literature sponsored by one of the manufacturers, they could not find a definitive dose relationship between SGLT2 inhibitors and urinary tract infection [212]. Of course, the infection risk may well be real, just not related to the dose of drug; it boils down to a question of the integrity of protocol design. Despite this, there has not yet been sufficient time to lapse given the years that diabetic patients will be on their treatments, and given the track record of other classes of drugs when they get into clinical practice, careful monitoring of safety and durability is essential.

There are early signs of additional cardiovascular benefit in this class—a major boon for an oral anti-diabetes therapy—the use of these agents as add-on therapy to metformin and the results of large cardiovascular outcomes trials, DECLARE TIMI-58 for dapagliflozon [213] and EMPA-REG for empagliflozin [214], are eagerly awaited.

An increasingly important challenge for pharmaceutical companies is to demonstrate that their new drug is cost-effective, especially where taxpayers money is involved. Although not mentioned for the previous drug classes, these agents were launched at a time where costs of medicines have never been higher on the agenda of the funders and are worth commenting on. Despite a very optimistic cost–benefit analysis performed by the manufacturer, it does seem that these agents do have some modest cost benefits when modeled using more stringent methods, particularly when compared to sulfonylureas, pioglitazone, and DPP-IV inhibitors [215]. In subjects with uncontrolled diabetes, cost savings

may be indirect. A retrospective study in such patients from India showed that in "real-world clinical practice," there was a compensatory reduction in the amount of insulin required by these patients [216].

## 10 Where Are We Now?

In this chapter, I have outlined the eight classes of anti-diabetic drugs in the chronological order of their appearance as medicines since the 1950s from a drug discovery perspective; so quite a narrow perspective. What is evident is that these agents are the result of research and development activities performed in pharmaceutical companies using knowledge originating from academic research. In future, this paradigm will have to remain the norm. However, pipeline attrition in this disease area is high; numerous publications have appeared on new drug targets optimistically predicting a novel approach only to ultimately end in failure, with stearoyl-CoA desaturase-1 (SCD-1) [217], 11β-hydroxysteroid dehydrogenase-1 (11β-HSD-1) [218], and diacylglycerol acyl transferase-1 (DGAT-1) [219] being relatively recent examples. Nevertheless, potential future targets for type 2 diabetes are reviewed frequently [220–223] showing that science can deliver new ideas. In particular, a class of GPCRs, the fatty acid receptors, seem to be very interesting in this therapeutic area [221].

However, for there to be a real future for anti-diabetes drug development, there needs to be a vibrant pharmaceutical industry with the ability to invest in, or facilitate, the whole journey. Today the costs involved in bringing a drug to market are enormous and appear to have risen hugely over the past decade or so. A report published in 2011 suggests that the cost is between 0.3 and 0.9 billion dollars per drug [224]. However, this analysis does not seem to account for the global costs involved which includes the potentially debilitating costs of failure which have caused serious productivity issues in the industry [225]. An article in Forbes [226] used a rather simplistic but useful calculation where total research and development expenditure over a 10-year period was divided by the number of product launches over the same period. This revealed a truly shocking reality—drug discovery in the pharmaceutical industry, as we know it today, is unsustainable. The numbers suggest that the giants with greatest loss of productivity are spending in excess of $10 billion per drug launch. The industry has been forced to undergo change, often traumatic, as many ex-employees will testify, and there is also the risk of retrenching effort away from the high-risk, high-cost endeavors such as chronic diseases to areas where risk can more comfortably be predicted and managed.

Apart from cost, the next challenge is return on investment: what can new drugs be reasonably sold for? New modalities such as

antibody therapeutics seem to hold many possibilities not dreamed of by the small molecule mindset that I was involved in when I started my career in the 1970s, but they are very expensive which could render them unaffordable no matter how good they are, particularly in the developing economies where future need will be greatest. Then there is the developing sophistication of users and prescribers who will demand more than just HbA1c lowering; weight loss and improved cardiovascular outcomes have been seen with agents; though this was probably a result of serendipity, this is much harder to design in from the beginning. Disease reversal may also be a demand if β-cell biology delivers. Also, new drugs should have to be very safe, probably the hardest thing of all, as nasty surprises are often revealed post-launch when drugs are prescribed to much larger numbers of patients, and the thiazolidinedione story and the more recent potential pancreatitis issue with the incretin agents and urinary tract infection risk with the SGLT2 inhibitors are heightening awareness. Highly effective, safe, and affordable drugs are still urgently needed and type 2 diabetes is, I believe, still an unmet medical need despite six decades of drug discovery research. The prospects are not impossible but the probability is hard to predict.

## References


1. Sugiyama Y (2005) Druggability: selecting optimized drug candidates. Drug Discov Today 10:1577–1579
2. Allen MJ, Carey AH (2004) Target identification and validation through genetics. Drug Discov Today TARGETS 3:183–190
3. Sams-Dodd F (2005) Target-based drug discovery: is something wrong? Drug Discov Today 10:139–147
4. Paul SM, Mytelka DS, Dunwiddie CT, Persinger CC, Munos BH, Lindborg SR, Schact AL (2010) How to improve R&D productivity: the pharmaceutical industry's grand challenge. Nat Rev Drug Discov 9:203–214
5. Bouzakri K, Koistinen HA, Zierath JR (2005) Molecular mechanisms of skeletal muscle insulin resistance in type 2 diabetes. Curr Diabetes Rev 1:167–174
6. Gerich JE, Mitrakou A, Kelley D, Mandarino L, Nurjhan N, Reilly J, Jenssen T, Veneman T, Consoli A (1990) Contribution of impaired muscle glucose clearance to reduced postabsorptive systemic glucose clearance in NIDDM. Diabetes 39:211–216
7. Consoli A (1992) Role of liver in pathophysiology of NIDDM. Diabetes Care 15:430–441
8. Reaven GM (2014) Pathophysiology of insulin resistance in human disease. Physiol Rev 75:473–486
9. Reaven GM (1988) Role of insulin resistance in human disease. Diabetes 37:1595–1607
10. Ritzel RA, Butler AE, Rizza RA, Veldhuis JD, Butler PC (2006) Relationship between b-cell mass and fasting blood glucose concentration in humans. Diabetes Care 29:717–718
11. The Diabetes Control and Complications Trial Research Group (1993) The effect of intensive treatment of diabetes on the development and progression of long-term complications in insulin-dependent diabetes mellitus. N Engl J Med 329:977–986
12. UK Prospective Diabetes Study (UKPDS) Group (1998) Effect of intensive blood-glucose control with metformin on complications in overweight patients with type 2 diabetes (UKPDS 34). Lancet 352:854–865
13. UK Prospective Diabetes Study (UKPDS) Group (1998) Intensive blood-glucose control with sulphonylureas or insulin compared with conventional treatment and risk of complications in patients with type 2 diabetes (UKPDS 33). Lancet 352:837–853

14. American Diabetes Association (2011) Executive summary: standards of medical care in diabetes - 2011. Diabetes Care 34:S4–S10
15. Nathan DM, Buse JB, Davidson MB, Ferrannini E, Holman RR, Sherwin R, Zinman B (2009) Medical management of hyperglycemia in type 2 diabetes: a consensus algorithm for the initiation and adjustment of therapy: a consensus statement of the American Diabetes Association and the European Association for the Study of Diabetes. Diabetes Care 32:193–203
16. Nathan DM, Buse JB, Davidson MB, Heine RJ, Holman RR, Sherwin R, Zinman B (2006) Management of hyperglycemia in type 2 diabetes: a consensus algorithm for the initiation and adjustment of therapy: a consensus statement from the American Diabetes Association and the European Association for the study of diabetes. Diabetes Care 29:1963–1972
17. The ADVANCE Collaborative Group (2008) Intensive blood glucose control and vascular outcomes in patients with type 2 diabetes. N Engl J Med 358:2560–2572
18. The Action to Control Cardiovascular Risk in Diabetes Study Group (2008) Effects of intensive glucose lowering in type 2 diabetes. N Engl J Med 358:2545–2559
19. Herman WH, Dirani RG, O'Neill MC, Kravitz B, Heise A, Bakst A, Freed.M.I. (2005) Reduction in use of healthcare services with combination sulfonylurea and rosiglitazone: findings from the Rosiglitazone Early vs SULfonylurea Titration (RESULT) study. Am J Manag Care 11:273–278
20. Proks P, Reimann F, Green N, Gribble F, Ashcroft F (2002) Sulfonylurea stimulation of insulin secretion. Diabetes 51:S368–S376
21. Nichols CG (2006) KATP channels as molecular sensors of cellular metabolism. Nature 440:470–476
22. Ashcroft FM (2007) ATP-sensitive K channels and disease: from molecule to malady. Am J Physiol Endocrinol Metab 293:E880–E889
23. Inagaki N, Gonoi T, Clement JP, Wang CZ, Aguilar-Bryan L, Bryan J, Seino S (1996) A family of sulfonylurea receptors determines the pharmacological properties of ATP-sensitive $K^+$ channels. Neuron 16:1011–1017
24. Aittoniemi J, Fotinou C, Craig TJ, de Wet H, Proks P, Ashcroft FM (2009) SUR1: a unique ATP-binding cassette protein that functions as an ion channel regulator. Philos Trans R Soc B 364:257–267
25. Gribble FM, Tucker SJ, Seino S, Ashcroft FM (1998) Tissue specificity of sulfonylureas: studies on cloned cardiac and beta-cell K (ATP) channels. Diabetes 47:1412–1418
26. Zünkler BJ, Lenzen S, Männer K, Panten U, Trube G (2014) Concentration-dependent effects of tolbutamide, meglitinide, glipizide, glibenclamide and diazoxide on ATP-regulated $K^+$ currents in pancreatic b-cells. Naunyn Schmiedebergs Arch Pharmacol 337:225–230
27. Sturgess NC, Kozlowski RZ, Carrington CA, Hales CN, Ashford ML (1988) Effects of sulphonylureas and diazoxide on insulin secretion and nucleotide-sensitive channels in an insulin-secreting cell line. Br J Pharmacol 95:83–94
28. Splitter S, Brown FR, Friskey RW, Grindell L, Kinsell LW (1956) Treatment of diabetic patients-observations on the use of carbutamide and tolbutamide. Calif Med 85:285–288
29. Graal MB, Wolffenbuttel BHR (1999) The use of sulphonylureas in the elderly. Drugs Aging 15:471–481
30. Malabu UH, Vangaveti VN, Kennedy LR (2014) Disease burden evaluation of fall-related events in the elderly due to hypoglycemia and other diabetic complications: a clinical review. Clin Epidemiol 6:287–294
31. Bailey CJ, Day C (2004) Metformin: its botanical background. Pract Diabetes Int 21:115–117
32. Bailey CJ (1992) Biguanides and NIDDM. Diabetes Care 15:755–772
33. Tucker GT, Casey C, Phillips PJ, Connor H, Ward JD, Woods HF (1981) Metformin kinetics in healthy subjects and in patients with diabetes mellitus. Br J Clin Pharmacol 12:235–246
34. Zhou M, Xia L, Wang J (2007) Metformin transport by a newly cloned proton-stimulated organic cation transporter (Plasma Membrane Monoamine Transporter) expressed in human intestine. Drug Metab Dispos 35:1956–1962
35. Gong L, Goswami S, Giacomini KM, Altman RB, Klein TE (2012) Metformin pathways: pharmacokinetics and pharmacodynamics. Pharmacogenet Genomics 22:820–827
36. Graham GG, Punt J, Arora M, Day RO, Doogue MP, Duong J, Furlong TJ, Greenfield JR, Greenup LC, Kirkpatrick CM, Ray JE, Timmins P, Williams KM (2011) Clinical pharmacokinetics of metformin. Clin Pharmacokinet 50:81–98

37. Strack T (2008) Metformin: a review. Drugs Today 44:303–314
38. Campbell RK, White JR, Saulie BA (1996) Metformin: a new oral biguanide. Clin Ther 18:360–371
39. DeFronzo RA, Goodman AM (1995) Efficacy of metformin in patients with non-insulin-dependent diabetes mellitus. N Engl J Med 333:541–549
40. Bailey CJ, Turner RC (1996) Metformin. N Engl J Med 334:574–579
41. Stumvoll M, Nurjhan N, Perriello G, Dailey G, Gerich JE (1995) Metabolic effects of metformin in non-insulin-dependent diabetes mellitus. N Engl J Med 333:550–554
42. Hundal RS, Krssak M, Dufour S, Laurent D, Lebon V, Chandramouli V, Inzucchi SE, Schumann WC, Petersen KF, Landau BR, Shulman GI (2000) Mechanism by which metformin reduces glucose production in type 2 diabetes. Diabetes 49:2063–2069
43. Klip A, Leiter LA (1990) Cellular mechanism of action of metformin. Diabetes Care 13:696–704
44. Fryer LGD, Parbu-Patel A, Carling D (2002) The anti-diabetic drugs rosiglitazone and metformin stimulate AMP-activated protein kinase through distinct signaling pathways. J Biol Chem 277:25226–25232
45. Hardie DG (2008) AMPK: a key regulator of energy balance in the single cell and the whole organism. Int J Obes Relat Metab Disord 32: S7–S12
46. Ruderman N, Prentki M (2004) AMP-kinase and malonyl-CoA: targets for therapy of the metabolic syndrome. Nat Rev Drug Discov 3:340–351
47. Owen MR, Doran E, Halestrap AP (2000) Evidence that metformin exerts its anti-diabetic effects through inhibition of complex 1 of the mitochondrial respiratory chain. Biochem J 348:607–614
48. Sakamoto K, Göransson O, Hardie DG, Alessi DR (2004) Activity of LKB1 and AMPK-related kinases in skeletal muscle: effects of contraction, phenformin, and AICAR. Am J Physiol Endocrinol Metab 287:E310–E317
49. Golay A (2007) Metformin and body weight. Int J Obes Relat Metab Disord 32:61–72
50. Clapham JC, Arch JR (2008) Influencing energy expenditure and substrate utilisation. In: Pharmacotherapy of obesity, Milestones in drug therapy. Birkhäuser, Basel, pp 101–115
51. Paolisso G, Amato L, Eccellente R, Gambardella A, Tagliamonte MR, Varricchio G, Carella C, Giugliano D, D'onofrio F (1998) Effect of metformin on food intake in obese subjects. Eur J Clin Invest 28:441–446
52. Bruijstens LA, van Luin M, Buscher-Jungerhans PM, Bosch FH (2008) Reality of severe metformin-induced lactic acidosis in the absence of chronic renal impairment. Neth J Med 66:185–190
53. Carter D, Howlett HCS, Wiernsperger NF, Bailey CJ (2003) Differential effects of metformin on bile salt absorption from the jejunum and ileum. Diabetes Obes Metab 5:120–125
54. Davidson J, Howlett H (2004) New prolonged-release metformin improves gastrointestinal tolerability. Br J Diabetes Vasc Dis 4:273–277
55. Mallick S (2004) Metformin induced acute pancreatitis precipitated by renal failure. Postgrad Med J 80:239–240
56. Alsubaie S, Almalki MH (2013) Metformin induced acute pancreatitis. Derm Endocrinol 5:317–318
57. Oprea TI, Bauman JE, Bologa CG, Buranda T, Chigaev A, Edwards BS, Jarvik JW, Gresham HD, Haynes MK, Hjelle B, Hromas R, Hudson L, Mackenzie DA, Muller CY, Reed JC, Simons PC, Smagley Y, Strouse J, Surviladze Z, Thompson T, Ursu O, Waller A, Wandinger-Ness A, Winter SS, Wu Y, Young SM, Larson RS, Willman C, Sklar LA (2011) Drug repurposing from an academic perspective. Drug Discov Today Ther Strat 8:61
58. Kasznicki J, Sliwinska A, Drzewoski J (2014) Metformin in cancer prevention and therapy. Ann Transl Med 2:57
59. Diamanti-Kandarakis E, Christakou CD, Kandaraki E, Economou FN (2010) Metformin: an old medication of new fashion: evolving new molecular mechanisms and clinical implications in polycystic ovary syndrome. Eur J Endocrinol 162:193–212
60. Scarpello JHB, Howlett HCS (2008) Metformin therapy and clinical uses. Diabetes Vasc Dis Res 5:157–167
61. Hirst JA, Farmer AJ, Dyar A, Lung TWC, Stevens RJ (2013) Estimating the effect of sulfonylurea on HbA1c in diabetes: a systematic review and meta-analysis. Diabetologia 56:973–984
62. Rydberg T, Jönsson A, Karlsson MO, Melander A (1997) Concentration-effect relations of glibenclamide and its active metabolites in man: modelling of Pharmacokinetics and Pharmacodynamics. Br J Clin Pharmacol 43:373–381

63. Kola I, Landis J (2004) Can the pharmaceutical industry reduce attrition rates? Nat Rev Drug Discov 3:711–716
64. Rosengren A, Jing X, Eliasson L, Renstrøm E (2008) Why treatment fails in type 2 diabetes. PLoS Med 5:e215
65. Kahn SE, Haffner SM, Heise MA, Herman WH, Holman RR, Jones NP, Kravitz BG, Lachin JM, O'Neill MC, Zinman B, Viberti G (2006) Glycemic durability of rosiglitazone, metformin, or glyburide monotherapy. N Engl J Med 355:2427–2443
66. Karam JH, Sanz N, Salamon E, Nolte MS (1986) Selective unresponsiveness of pancreatic b-cells to acute sulfonylurea stimulation during sulfonylurea therapy in NIDDM. Diabetes 35:1314–1320
67. Pantalone KM, Kattan MW, Yu C, Wells BJ, Arrigain S, Jain A, Atreja A, Zimmerman RS (2012) Increase in overall mortality risk in patients with type 2 diabetes receiving glipizide, glyburide or glimepiride monotherapy versus metformin: a retrospective analysis. Diabetes Obes Metab 14:803–809
68. Rustenbeck I, Wienbergen A, Bleck C, Jörns A (2004) Desensitization of insulin secretion by depolarizing insulin secretagogues. Diabetes 53:S140–S150
69. Sadikot SM, Mogensen CE (2008) Risk of coronary artery disease associated with initial sulphonylurea treatment of patients with type 2 diabetes: a matched case-control study. Diabetes Res Clin Pract 82:391–395
70. Lefer DJ, Nichols CG, Coetzee WA (2009) Sulfonylurea receptor 1 subunits of ATP-sensitive potassium channels and myocardial Ischemia/reperfusion Injury. Trends Cardiovasc Med 19:61–67
71. Bell DSH (2006) Do sulfonylurea drugs increase the risk of cardiac events? Can Med Assoc J 174:185–186
72. Grygiel-Górniak B (2014) Peroxisome proliferator-activated receptors and their ligands: nutritional and clinical implications - a review. Nutr J 13:17
73. Glosli H, Gudbrandsen OA, Mullen AJ, Halvorsen B, Røst TH, Wergedahl H, Prydz H, Aukrust P, Berge RK (2005) Down-regulated expression of PPARa target genes, reduced fatty acid oxidation and altered fatty acid composition in the liver of mice transgenic for hTNFa. Biochim Biophys Acta 1734:235–246
74. Turner NC, Clapham JC (1998) Insulin resistance, impaired glucose tolerance and non-insulin-dependent diabetes, pathologic mechanisms and treatment: current status and therapeutic possibilities. Prog Drug Res 51:33–94
75. Henry RR (1997) Thiazolidinediones. Endocrinol Metab Clin 26:553–573
76. Gale EAM (2006) Troglitazone: the lesson that nobody learned? Diabetologia 49:1–6
77. Barnett AH (2009) Redefining the role of thiazolidinediones in the management of type 2 diabetes. Vasc Health Risk Manag 5:141–151
78. Phillips LS, Grunberger G, Miller E, Patwardhan R, Rappaport EB, Salzman A (2001) Once- and twice-daily dosing with rosiglitazone improves glycemic control in patients with type 2 diabetes. Diabetes Care 24:308–315
79. Fonseca V, Rosenstock J, Patwardhan R, Salzman A (2000) Effect of metformin and rosiglitazone combination therapy in patients with type 2 diabetes mellitus: a randomized controlled trial. JAMA 283:1695–1702
80. Poitout V (2004) b-cell lipotoxicity: burning fat into heat? Endocrinology 145:3563–3565
81. Nolan CJ, Prentki M (2008) The islet b-cell: fuel responsive and vulnerable. Trends Endocrinol Metab 19:285–291
82. Buckingham RE, Al-Barazanji KA, Toseland CDN, Slaughter M, Connor SC, West A, Bond B, Turner NC, Clapham JC (1998) Peroxisome proliferator-activated receptor-g agonist, rosiglitazone, protects against nephropathy and pancreatic islet abnormalities in Zucker fatty rats. Diabetes 47:1326–1334
83. Nissen SE, Wolski K (2007) Effect of rosiglitazone on the risk of myocardial infarction and death from cardiovascular causes. N Engl J Med 356:2457–2471
84. Singh S, Loke YK, Furberg CD (2007) Thiazolidinediones and heart failure: a teleoanalysis. Diabetes Care 30:2148–2153
85. Bloomgarden ZT (2007) The avandia debate. Diabetes Care 30:2401–2408
86. Misbin RI (2007) Lessons from the avandia controversy: a new paradigm for the development of drugs to treat type 2 diabetes. Diabetes Care 30:3141–3144
87. Bhatt DL, Chew DP, Grines C, Mukherjee D, Leesar M, Gilchrist IC, Corbelli JC, Blankenship JC, Eres A, Steinhubl S, Tan WA, Resar JR, Al Mahameed A, Abdel-Latif A, Tang HW, Brennan D, McErlean E, Hazen SL, Topol EJ (2007) Peroxisome proliferator-activated receptor g agonists for the prevention of adverse events following percutaneous coronary revascularizationG-results of the PPAR study. Am Heart J 154:137–143

88. McAfee AT, Koro C, Landon J, Ziyadeh N, Walker AM (2007) Coronary heart disease outcomes in patients receiving antidiabetic agents. Pharmacoepidem Drug Safe 16:711–725
89. Home PD, Pocock SJ, Beck-Nielsen H, Gomis R, Hanefeld M, Dargie H, Komajda M, Gubb J, Biswas N, Jones NP (2005) Rosiglitazone evaluated for cardiac outcomes and regulation of glycaemia in diabetes (RECORD): study design and protocol. Diabetologia 48:1726–1735
90. Hillaire-Buys D, Faillie JL, Montastruc JL (2011) Pioglitazone and bladder cancer. Lancet 378:1543–1544
91. Grey A (2009) Thiazolidinedione-induced skeletal fragility - mechanisms and implications. Diabetes Obes Metab 11:275–284
92. Oshitari T, Asaumi N, Watanabe M, Kumagai K, Mitamura Y (2008) Severe macular edema induced by pioglitazone in a patient with diabetic retinopathy: a case study. Vasc Health Risk Manag 4:1137–1140
93. Liazos E, Broadbent DM, Beare N, Kumar N (2008) Spontaneous resolution of diabetic macular oedema after discontinuation of thiazolidenediones. Diabet Med 25:860–862
94. Cordain L, Eaton SB, Sebastian A, Mann N, Lindeberg S, Watkins BA, O'Keefe JH, Brand-Miller J (2005) Origins and evolution of the Western diet: health implications for the 21st century. Am J Clin Nutr 81:341–354
95. Prentice AM, Jebb SA (1995) Obesity in Britain: gluttony or sloth? Br Med J 311:437–439
96. Röder PV, Geillinger KE, Zietek TS, Thorens B, Koepsell H, Hannelore D (2014) The role of SGLT1 and GLUT2 in intestinal glucose transport and sensing. PLoS One 9: e89977
97. Caspary WF (1992) Physiology and pathophysiology of intestinal absorption. Am J Clin Nutr 55:299S–308S
98. Chiba S (1997) Molecular mechanism in alpha-glucosidase and glucoamylase. Biosci Biotechnol Biochem 61:1233–1239
99. Göke B, Fuder H, Wieckhorst G, Theiss U, Stridde E, Littke T, Kleist P, Arnold R, Lücker PW (1995) Voglibose (AO-128) is an efficient a-glucosidase inhibitor and mobilizes the endogenous GLP-1 reserve. Digestion 56:493–501
100. Standl E, Schernthaner G, Rybka J, Hanefeld M, Raptis SA, Naditch L (2001) Improved glycaemic control with miglitol in inadequately-controlled type 2 diabetics. Diabetes Res Clin Pract 51:205–213
101. Hanefeld M, Fischer S, Schulze J, Spengler M, Wargenau M, Schollberg K, Fücker K (1991) Therapeutic potentials of acarbose as first-line drug in NIDDM insufficiently treated with diet alone. Diabetes Care 14:732–737
102. Salman S, Salman F, Satman I, Yilmaz Y, Özer E, Sengül A, Özer H, Demirel HO, Karsidag K, Dinççag N, Yilmaz MT (2001) Comparison of acarbose and gliclazide as first-line agents in patients with type 2 diabetes. Curr Med Res Opin 16:296–306
103. Wang G, Liu J, Yang N, Gao X, Fan H, Xu Y, Yang W (2014) MARCH2:comparative assessment of therapeutic effects of acarbose and metformin in newly diagnosed type 2 diabetes patients. PLoS One 9:e105698
104. Dabhi AS, Bhatt NR, Shah MJ (2013) Voglibose: an alpha glucosidase inhibitor. J Clin Diagn Res 7:3023–3027
105. Standl E, Theodorakis MJ, Erbach M, Schnell O, Tuomilehto J (2014) On the potential of acarbose to reduce cardiovascular disease. Cardiovasc Diabetol 13:81
106. Ceriello A, Taboga C, Giacomello R, Stel L, Motz E, Pirisi M (1996) Post-meal coagulation activation in diabetes mellitus: the effect of acarbose. Diabetologia 39:469–473
107. Kawano H, Motoyama T, Hirashima O, Hirai N, Miyao Y, Sakamoto T, Kugiyama K, Ogawa H, Yasue H (1999) Hyperglycemia rapidly suppresses flow-mediated endothelium-dependent vasodilation of brachial artery. J Am Coll Cardiol 34:146–154
108. Heitzer T, Schlinzig T, Krohn K, Meinertz T, Münzel T (2001) Endothelial dysfunction, oxidative stress, and risk of cardiovascular events in patients with coronary artery disease. Circulation 104:2673–2678
109. Caumo A, Luzi L (2004) First-phase insulin secretion: does it exist in real life? Considerations on shape and function. Am J Physiol Endocrinol Metab 287:E371–E385
110. Lewis GF, Zinman B, Groenewoud Y, Vranic M, Giacca A (1996) Hepatic glucose production is regulated both by direct hepatic and extrahepatic effects of insulin in Humans. Diabetes 45:454–462
111. Calles-Escandon J, Robbins DC (1987) Loss of early phase of insulin release in humans impairs glucose tolerance and blunts thermic effect of glucose. Diabetes 36:1167–1172
112. Del Prato S, Miccoli R, Penno G (2005) The importance of effective early phase insulin secretion. Br J Diabetes Vasc Dis 5:198–202
113. Gerich JE (2002) Is reduced first-phase insulin release the earliest detectable abnormality

in individuals destined to develop type 2 diabetes? Diabetes 51:S117–S121

114. Bruce DG, Chisholm DJ, Storlien LH, Kraegen EW (1988) Physiological importance of deficiency in early prandial insulin secretion in non-insulin-dependent diabetes. Diabetes 37:736–744
115. Luzio SD, Owens DR, Vora J, Dolben J, Smith H (1991) Intravenous insulin simulates early insulin peak and reduces post-prandial hyperglycaemia/hyperinsulinaemia in type 2 (non-insulin-dependent) diabetes mellitus. Diabetes Res 16:63–67
116. Owens DR, Luzio SD, Ismail I, Bayer T (2000) Increased prandial insulin secretion after administration of a single preprandial oral dose of repaglinide in patients with type 2 diabetes. Diabetes Care 23:518–523
117. Gromada J, Dissing S, Kofod H, Frøkjær-Jensen J (1995) Effects of the hypoglycaemic drugs repaglinide and glibenclamide on ATP-sensitive potassium-channels and cytosolic calcium levels in TC3 cells and rat pancreatic beta cells. Diabetologia 38:1025–1032
118. Hu S, Wang S, Fanelli B, Bell PA, Dunning BE, Geisse S, Schmitz R, Boettcher BR (2000) Pancreatic b-cell K ATP channel activity and membrane-binding studies with nateglinide: a comparison with sulfonylureas and repaglinide. J Pharmacol Exp Ther 293:444–452
119. Moses RG, Gomis R, Frandsen KB, Schlienger JL, Dedov I (2001) Flexible meal-related dosing with repaglinide facilitates glycemic control in therapy-naive Type 2 diabetes. Diabetes Care 24:11–15
120. Rosenstock J, Hassman DR, Madder RD, Brazinsky SA, Farrell J, Khutoryansky N, Hale PM (2004) Repaglinide versus nateglinide monotherapy: a randomized, multicenter study. Diabetes Care 27:1265–1270
121. Hansen AM, Christensen IT, Hansen JB, Carr RD, Ashcroft FM, Wahl P (2002) Differential interactions of nateglinide and repaglinide on the human b-cell sulphonylurea receptor 1. Diabetes 51:2789–2795
122. Madsbad S, Kilhovd B, Lager I, Mustajoki P, Dejgaard A, for the Scandinavian Repaglinide Group (2001) Comparison between repaglinide and glipizide in type 2 diabetes mellitus: a 1-year multicentre study. Diabet Med 18:395–401
123. Inzucchi SE, Bergenstal RM, Buse JB, Diamant M, Ferrannini E, Nauck M, Peters AL, Tsapas A, Wender R, Matthews DR (2012) Management of hyperglycemia in type 2 diabetes: a patient-centered approach. Diabetes Care 35:1364
124. Ekström N, Svensson AM, Miftaraj M, Andersson SK, Cederholm J, Zethelius B, Eliasson B, Gudbjörnsdottir S (2015) Durability of oral hypoglycemic agents in drug naïve patients with type 2 diabetes: report from the Swedish National Diabetes Register (NDR). BMJ Open Diabetes Res Care 3: e000059
125. Moses R, Slobodniuk R, Boyages S, Colagiuri S, Kidson W, Carter J, Donnelly T, Moffitt P, Hopkins H (1999) Effect of repaglinide addition to metformin monotherapy on glycemic control in patients with type 2 diabetes. Diabetes Care 22:119–124
126. Schramm TK, Gislason GH, Vaag A, Rasmussen JN, Folke F, Hansen ML, Fosbøl EL, Køber L, Norgaard ML, Madsen M, Hansen PR, Torp-Pedersen C (2011) Mortality and cardiovascular risk associated with different insulin secretagogues compared with metformin in type 2 diabetes, with or without a previous myocardial infarction: a nationwide study. Eur Heart J 32:1900–1908
127. Creutzfeldt W (2005) The [pre-] history of the incretin concept. Regul Pept 128:87–91
128. Vilsbøll T, Krarup T, Madsbad S, Holst JJ (2003) Both GLP-1 and GIP are insulinotropic at basal and postprandial glucose levels and contribute nearly equally to the incretin effect of a meal in healthy subjects. Regul Pept 114:115–121
129. Eissele R, Göke R, Willemer S, Harthus HP, Vermeer H, Arnold R, Göke B (1992) Glucagon-like peptide-1 cells in the gastrointestinal tract and pancreas of rat, pig and man. Eur J Clin Invest 22:283–291
130. Gorboulev V, Schürmann A, Vallon V, Kipp H, Jaschke A, Klessen D, Friedrich A, Scherneck S, Rieg T, Cunard R, Veyhl-Wichmann M, Srinivasan A, Balen D, Breljak D, Rexhepaj R, Parker HE, Gribble FM, Reimann F, Lang F, Wiese S, Sabolic I, Sendtner M, Koepsell H (2012) $Na^+$-d-glucose cotransporter SGLT1 is pivotal for intestinal glucose absorption and glucose-dependent incretin secretion. Diabetes 61:187–196
131. Thorens B (1992) Expression cloning of the pancreatic beta cell receptor for the glucoincretin hormone glucagon-like peptide 1. Proc Natl Acad Sci U S A 89:8641–8645
132. Dillon JS, Tanizawa Y, Wheeler MB, Leng XH, Ligon BB, Rabin DU, Yoo-Warren H, Permutt MA, Boyd AE (1993) Cloning and functional expression of the human glucagon-

like peptide-1 (GLP-1) receptor. Endocrinology 133:1907–1910

133. Gremlich S, Porret A, Hani EH, Cherif D, Vionnet N, Froguel P, Thorens B (1995) Cloning, functional expression, and chromosomal localization of the human pancreatic islet glucose-dependent insulinotropic polypeptide receptor. Diabetes 44:1202–1208
134. Seino Y, Fukushima M, Yabe D (2010) GIP and GLP-1, the two incretin hormones: similarities and differences. J Diabetes Invest 1:8–23
135. Salon JA, Lodowski DT, Palczewski K (2011) The significance of G protein-coupled receptor crystallography for drug discovery. Pharmacol Rev 63:901–937
136. Wang MW, Liu Q, Zhou C (2010) Non-peptidic glucose-like peptide-1 receptor agonists: aftermath of a serendipitous discovery. Acta Pharmacol Sin 31:1026–1030
137. Su H, He M, Li H, Liu Q, Wang J, Wang Y, Gao W, Zhou L, Liao J, Young AA, Wang MW (2008) Boc5, a non-peptidic glucagon-like peptide-1 receptor agonist, invokes sustained glycemic control and weight loss in diabetic mice. PLoS One 3:e2892
138. Chen D, Liao J, Li N, Zhou C, Liu Q, Wang G, Zhang R, Zhang S, Lin L, Chen K, Nan F, Young AA, Wang MW (2007) A non-peptidic agonist of glucagon-like peptide 1 receptors with efficacy in diabetic db/db mice. Proc Natl Acad Sci U S A 104:943–948
139. Kolterman OG, Kim DD, Shen L, Ruggles JA, Nielsen LL, Fineman MS, Baron AD (2005) Pharmacokinetics, pharmacodynamics, and safety of exenatide in patients with type 2 diabetes mellitus. Am J Health Syst Pharm 62:173–181
140. Agersø H, Jensen LB, Elbrønd B, Rolan P, Zdravkovic M (2002) The pharmacokinetics, pharmacodynamics, safety and tolerability of NN2211, a new long-acting GLP-1 derivative, in healthy men. Diabetologia 45:195–202
141. Cai Y, Wei L, Ma L, Huang X, Tao A, Liu Z, Yuan W (2013) Long-acting preparations of exenatide. Drug Des Devel Ther 7:963–970
142. Hansen KB, Vilsbøll T, Knop FK (2010) Incretin mimetics: a novel therapeutic option for patients with type 2 diabetes - a review. Diabetes Metab Syndr Obes 17:155–163
143. Pinkney J, Fox T, Ranganath L (2010) Selecting GLP-1 agonists in the management of type 2 diabetes: differential pharmacology and therapeutic benefits of liraglutide and exenatide. Ther Clin Risk Manag 6:401–411
144. Schlögl H, Kabisch S, Horstmann A, Lohmann G, Müller K, Lepsien J, Busse-Voigt F, Kratzsch J, Pleger B, Villringer A, Stumvoll M (2013) Exenatide-induced reduction in energy intake is associated with increase in hypothalamic connectivity. Diabetes Care 36:1933–1940
145. Edwards CM, Stanley SA, Davis R, Brynes AE, Frost GS, Seal LJ, Ghatei MA, Bloom SR (2001) Exendin-4 reduces fasting and postprandial glucose and decreases energy intake in healthy volunteers. Am J Physiol Endocrinol Metab 281:E155–E161
146. Ando T, Haraguchi A, Matsunaga T, Natsuda S, Yamasaki H, Usa T, Kawakami A (2014) Liraglutide as a potentially useful agent for regulating appetite in diabetic patients with hypothalamic hyperphagia and obesity. Intern Med 53:1791–1795
147. Zoicas F, Droste M, Mayr B, Buchfelder M, Schöfl C (2013) GLP-1 analogues as a new treatment option for hypothalamic obesity in adults: report of nine cases. Eur J Endocrinol 168:699–706
148. Matveyenko AV, Butler PC (2008) Relationship between b-cell mass and diabetes onset. Diabetes Obes Metab 10:23–31
149. Demeterco C, Hao E, Lee SH, Itkin-Ansari P, Levine F (2009) Adult human b-cell neogenesis? Diabetes Obes Metab 11:46–53
150. Bunck MC, Cornér A, Eliasson B, Heine RJ, Shaginian RM, Taskinen MR, Smith U, Yki-Järvinen H, Diamant M (2011) Effects of exenatide on measures of b-cell function after 3 years in metformin-treated patients with type 2 diabetes. Diabetes Care 34:2041–2047
151. Kjems LL, Holst JJ, Vølund A, Madsbad S (2003) The influence of GLP-1 on glucose-stimulated insulin secretion: effects on β-cell sensitivity in type 2 and nondiabetic subjects. Diabetes 52:380–386
152. Mondragon A, Davidsson D, Kyriakoudi S, Bertling A, Gomes-Faria R, Cohen P, Rothery S, Chabosseau P, Rutter GA, da Silva Xavier G (2014) Divergent effects of liraglutide, exendin-4, and sitagliptin on beta-cell mass and indicators of pancreatitis in a mouse model of hyperglycaemia. PLoS One 9:e104873
153. Rutti S, Sauter NS, Bouzakri K, Prazak R, Halban PA, Donath MY (2012) In vitro proliferation of adult human beta-cells. PLoS One 7:e35801
154. Toso C, McCall M, Emamaullee J, Merani S, Davis J, Edgar R, Pawlick R, Kin T, Knudsen LB, Shapiro AMJ (2010) Liraglutide, a long-

acting human glucagon-like peptide 1 analogue, improves human islet survival in culture. Transpl Int 23:259–265

155. Bregenholt S, Møldrup A, Blume N, Karlsen AE, Friedrichsen BN, Tornhave D, Knudsen LB, Petersen JS (2005) The long-acting glucagon-like peptide-1 analogue, liraglutide, inhibits b-cell apoptosis *in vitro*. Biochem Biophys Res Commun 330:577–584
156. Butler AE, Janson J, Bonner-Weir S, Ritzel R, Rizza RA, Butler PC (2003) b-Cell deficit and Increased β-cell apoptosis in humans with type 2 diabetes. Diabetes 52:102–110
157. Bosco D, Armanet M, Morel P, Niclauss N, Sgroi A, Muller YD, Giovannoni L, Parnaud G, Berney T (2010) Unique arrangement of α- and β-cells in human Islets of Langerhans. Diabetes 59:1202–1210
158. Cabrera O, Berman DM, Kenyon NS, Ricordi C, Berggren PO, Caicedo A (2006) The unique cytoarchitecture of human pancreatic islets has implications for islet cell function. Proc Natl Acad Sci U S A 103:2334–2339
159. Steiner DJ, Kim A, Miller K, Hara M (2010) Pancreatic islet plasticity: interspecies comparison of islet architecture and composition. Islets 2:135–145
160. Butler PC, Elashoff M, Elashoff R, Gale EAM (2013) A critical analysis of the clinical use of incretin-based therapies: are the GLP-1 therapies safe? Diabetes Care 36:2118–2125
161. Perfetti R, Zhou J, Doyle ME, Egan JM (2000) Glucagon-like peptide-1 induces cell proliferation and pancreatic-duodenum homeobox-1 expression and increases endocrine cell mass in the pancreas of old, glucose intolerant rats. Endocrinology 141:4600–4605
162. Nauck MA, Friedrich N (2013) Do GLP-1-based therapies increase cancer risk? Diabetes Care 36:S245–S252
163. Noel RA, Braun DK, Patterson RE, Bloomgren GL (2009) Increased risk of acute pancreatitis and biliary disease observed in patients with type 2 diabetes: a retrospective cohort study. Diabetes Care 32:834–838
164. David F, Bernard AM, Pierres M, Marguet D (1993) Identification of serine 624, aspartic acid 702, and histidine 734 as the catalytic triad residues of mouse dipeptidyl-peptidase IV (CD26). A member of a novel family of nonclassical serine hydrolases. J Biol Chem 268:17247–17252
165. Lankas GR, Leiting B, Roy RS, Eiermann GJ, Beconi MG, Biftu T, Chan CC, Edmondson S, Feeney WP, Huaibing H, Ippolito DE, Kim D, Lyons KA, Ok HO, Patel RA, Petrov AN, Pryor KA, Qian X, Reigle L, Woods A, Wu JK, Zaller D, Zhang X, Zhu L, Weber AE, Thornberry NA (2005) Dipeptidyl peptidase IV inhibition for the treatment of type 2 diabetes: potential importance of selectivity over dipeptidyl peptidases 8 and 9. Diabetes 54:2988–2994
166. Lambeir A-M, Durinx C, Scharpé S, De Meester I (2013) Dipeptidyl-peptidase IV from bench to bedside: an update on structural properties, functions, and clinical aspects of the enzyme DPPIV. Crit Rev Clin Lab Sci 40:209–294
167. Durinx C, Lambeir AM, Bosmans E, Falmagne JB, Berghmans R, Haemers A, Scharpé S, De Meester I (2000) Molecular characterization of dipeptidyl peptidase activity in serum. Eur J Biochem 267:5608–5613
168. Kos K, Baker AR, Jernas M, Harte AL, Clapham JC, O'Hare JP, Carlsson L, Kumar S, McTernan PG (2009) DPP-IV inhibition enhances the antilipolytic action of NPY in human adipose tissue. Diabetes Obes Metab 11:285–292
169. Engel M, Hoffmann T, Wagner L, Wermann M, Heiser U, Kiefersauer R, Huber R, Bode W, Demuth HU, Brandstetter H (2003) The crystal structure of dipeptidyl peptidase IV (CD26) reveals its functional regulation and enzymatic mechanism. Proc Natl Acad Sci U S A 100:5063–5068
170. Aertgeerts K, Ye S, Tennant MG, Kraus ML, Rogers J, Sang BC, Skene RJ, Webb DR, Prasad GS (2004) Crystal structure of human dipeptidyl peptidase IV in complex with a decapeptide reveals details on substrate specificity and tetrahedral intermediate formation. Protein Sci 13:412–421
171. Sebokova E, Christ AD, Boehringer M, Mizrahi J (2015) Dipeptidyl peptidase IV inhibitors: the next generation of new promising therapies for the management of type 2 diabetes. Curr Top Med Chem 7:547–555
172. Shubrook J, Colucci R, Guo A, Schwartz F (2011) Saxagliptin: a selective DPP-4 inhibitor for the treatment of type 2 diabetes mellitus. Clin Med Insights Endocrinol Diab 4:1–12
173. Toth PP (2015) Overview of saxagliptin efficacy and safety in patients with type 2 diabetes and cardiovascular disease or risk factors for cardiovascular disease. Vasc Health Risk Manag 11:9–23
174. Banerjee M, Younis N, Soran H (2009) Vildagliptin in clinical practice: a review of

literature. Expert Opin Pharmacother 10:2745–2757

175. Dhillon S (2010) Sitagliptin: a review of its use in the management of type 2 diabetes mellitus. Drugs 70:489–512
176. Ahrén B (2014) Insulin plus incretin: a glucose-lowering strategy for type 2-diabetes. World J Diabetes 5:40–51
177. Pratley RE, Schweizer A, Rosenstock J, Foley JE, Banerji MA, Pi-Sunyer FX, Mills D, Dejager S (2008) Robust improvements in fasting and prandial measures of b-cell function with vildagliptin in drug-naïve patients: analysis of pooled vildagliptin monotherapy database. Diabetes Obes Metab 10:931–938
178. Del Prato S, Barnett AH, Huisman H, Neubacher D, Woerle HJ, Dugi KA (2011) Effect of linagliptin monotherapy on glycaemic control and markers of b-cell function in patients with inadequately controlled type 2 diabetes: a randomized controlled trial. Diabetes Obes Metab 13:258–267
179. Ahrén B, Pacini G, Tura A, Foley JE, Schweizer A (2007) Improved meal-related insulin processing contributes to the enhancement of b-cell function by the DPP-4 inhibitor vldagliptin in patients with type 2 diabetes. Horm Metab Res 39:826–829
180. Yeom JA, Kim ES, Park HS, Ham DS, Sun K, Kim JW, Cho JH, Yoon KH (2011) Both sitagliptin analogue & pioglitazone preserve the beta-cell proportion in the islets with different mechanism in non-obese and obese diabetic mice. BMB Rep 44:713–718
181. Girgis CM, Champion BL (2011) Vildagliptin-induced acute pancreatitis. Endocr Pract 17:e48–e50
182. Lee CF, Sun MS, Tai YK (2014) Saxagliptin-induced recurrent acute pancreatitis. Intern Med 53:1351–1354
183. Chang CH, Lin JW, Chen ST, Lai MS, Cuang LM, Chang YC (2016) Dipeptidyl peptidase-4 inhibitor use is not associated with acute pancreatitis in high-risk type 2 diabetic patients: a nationwide cohort study. Medicine 95:e2603–e2609
184. Karagiannis T, Bekiari E, Boura P, Tsapas A (2015) Cardiovascular risk with DPP-4 inhibitors: latest evidence and clinical implications. Ther Adv Drug Saf 7:36–38
185. Brunton S (2014) GLP-1 receptor agonists vs. DPP-4 inhibitors for type 2 diabetes: is one approach more successful or preferable than the other? Int J Clin Pract 68:557–567
186. Wright EM, Loo DDF, Hirayama BA (2011) Biology of human sodium glucose transporters. Physiol Rev 91:733–794
187. Wright EM (2001) Renal $Na^+$-glucose cotransporters. Am J Physiol Renal Physiol 280:F10–F18
188. Mackenzie B, Loo DDF, Panayotova-Heiermann M, Wright EM (1996) Biophysical characteristics of the pig kidney Na+/Glucose cotransporter SGLT2 reveal a common mechanism for SGLT1 and SGLT2. J Biol Chem 271:32678–32683
189. Wells RG, Pajor AM, Kanai Y, Turk E, Wright EM, Hediger MA (1992) Cloning of a human kidney cDNA with similarity to the sodium-glucose cotransporter. Am J Physiol Renal Physiol 263:F459–F465
190. Kanai Y, Lee WS, You G, Brown D, Hediger MA (1994) The human kidney low affinity Na +/glucose cotransporter SGLT2. Delineation of the major renal reabsorptive mechanism for D-glucose. J Clin Invest 93:397–404
191. DeFronzo RA, Hompesch M, Kasichayanula S, Liu X, Hong Y, Pfister M, Morrow LA, Leslie BR, Boulton DW, Ching A, LaCreta FP, Griffen SC (2013) Characterization of renal glucose reabsorption in response to dapagliflozin in healthy subjects and subjects with type 2 diabetes. Diabetes Care 36:3169–3176
192. Calado J, Soto K, Clemente C, Correia P, Rueff J (2004) Novel compound heterozygous mutations in SLC5A2 are responsible for autosomal recessive renal glucosuria. Hum Genet 114:314–316
193. van den Heuvel L, Assink K, Willemsen M, Monnens L (2002) Autosomal recessive renal glucosuria attributable to a mutation in the sodium glucose cotransporter (SGLT2). Hum Genet 111:544–547
194. Gallo LA, Wright EM, Vallon V (2015) Probing SGLT2 as a therapeutic target for diabetes: basic physiology and consequences. Diabetes Vasc Dis Res 12:78–89
195. Rossetti L, Smith D, Shulman GI, Papachristou D, DeFronzo RA (1987) Correction of hyperglycemia with phlorizin normalizes tissue sensitivity to insulin in diabetic rats. J Clin Invest 79:1510–1515
196. Isaji M (2011) SGLT2 inhibitors: molecular design and potential differences in effect. Kidney Int 79:S14–S19
197. Nomura S, Sakamaki S, Hongu M, Kawanishi E, Koga Y, Sakamoto T, Yamamoto Y, Ueta K, Kimata H, Nakayama K, Tsuda-Tsukimoto M (2010) Discovery of canagliflozin, a novel

C-glucoside with thiophene ring, as sodium-dependent glucose cotransporter 2 inhibitor for the treatment of type 2 diabetes Mellitus. J Med Chem 53:6355–6360

198. Meng W, Ellsworth BA, Nirschl AA, McCann PJ, Patel M, Girotra RN, Wu G, Sher PM, Morrison EP, Biller SA, Zahler R, Deshpande PP, Pullockaran A, Hagan DL, Morgan N, Taylor JR, Obermeier MT, Humphreys WG, Khanna A, Discenza L, Robertson JG, Wang A, Han S, Wetterau JR, Janovitz EB, Flint OP, Whaley JM, Washburn WN (2008) Discovery of dapagliflozin: a potent, selective renal sodium-dependent glucose cotransporter 2 (SGLT2) inhibitor for the treatment of type 2 diabetes. J Med Chem 51:1145–1149
199. Neumiller JJ (2014) Empagliflozin: a new sodium-glucose co-transporter 2 (SGLT2) inhibitor for the treatment of type 2 diabetes. Drugs Context 3:212262
200. Hummel CS, Lu C, Liu J, Ghezzi C, Hirayama BA, Loo DDF, Kepe V, Barrio JR, Wright EM (2011) Structural selectivity of human SGLT inhibitors. Am J Physiol Cell Physiol 302:C373–C382
201. Valentine V (2015) The role of the kidney and sodium-glucose cotransporter-2 inhibition in diabetes management. Clin Diab 30:151–155
202. Kalra S (2014) Sodium glucose co-transporter-2 (SGLT2) inhibitors: a review of their basic and clinical pharmacology. Diabetes Ther 5:355–366
203. Dietrich E, Powell J, Taylor JR (2013) Canagliflozin: a novel treatment option for type 2 diabetes. Drug Des Devel Ther 7:1399–1408
204. Aylsworth A, Dean Z, VanNorman C, Okere AN (2014) Dapagliflozin for the treatment of type 2 diabetes mellitus. Ann Pharmacother 48:1202–1208
205. Heise T, Seman L, Macha S, Jones P, Marquart A, Pinnetti S, Woerle HJ, Dugi K (2013) Safety, tolerability, pharmacokinetics, and pharmacodynamics of multiple rising doses of empagliflozin in patients with type 2 diabetes mellitus. Diabetes Ther 4:331–345
206. Kasichayanula S, Liu X, LaCreta F, Griffen SC, Boulton DW (2014) Clinical pharmacokinetics and pharmacodynamics of dapagliflozin, a selective inhibitor of sodium-glucose co-transporter type 2. Clin Pharmacokinet 53:17–27
207. Ghezzi C, Hirayama BA, Gorraitz E, Loo DDF, Liang Y, Wright EM (2014) SGLT2 inhibitors act from the extracellular surface of the cell membrane. Physiol Rep 2:e12058
208. Anderson SL (2014) Dapagliflozin efficacy and safety: a perspective review. Ther Adv Drug Saf 5:242–254
209. Bolinder J, Ljunggren Ö, Kullberg J, Johansson L, Wilding J, Langkilde AM, Sugg J, Parikh S (2011) Effects of dapagliflozin on body weight, total fat mass, and regional adipose tissue distribution in patients with type 2 diabetes mellitus with inadequate glycemic control on metformin. J Clin Endocrinol Metabol 97:1020–1031
210. Nauck MA, Del Prato S, Meier JJ, Durán-García S, Rohwedder K, Elze M, Parikh SJ (2011) Dapagliflozin versus glipizide as add-on therapy in patients with type 2 diabetes who have inadequate glycemic control with metformin: a randomized, 52-week, double-blind, active-controlled noninferiority trial. Diabetes Care 34:2015–2022
211. Strojek K, Yoon KH, Hruba V, Sugg J, Langkilde A, Parikh S (2014) Dapagliflozin added to glimepiride in patients with type 2 diabetes mellitus sustains glycemic control and weight loss Over 48-weeks: a randomized, double-blind, parallel-group, placebo-controlled trial. Diabetes Ther 5:267–283
212. Geerlings S, Fonseca V, Castro-Diaz D, List J, Parikh S (2014) Genital and urinary tract infections in diabetes: impact of pharmacologically-induced glucosuria. Diabetes Res Clin Pract 103:373–381
213. Sonesson C, Johansson PA, Johnsson E, Gause-Nilsson I (2016) Cardiovascular effects of dapagliflozin in patients with type 2 diabetes and different risk categories: a meta-analysis. Cardiovasc Diabetol 15:37
214. MacIsaac RJ, Jerums G, Ekinci EI (2016) Cardio-renal protection with empagliflozin. Ann Transl Med 4:409–412
215. Liakos A, Karagiannis T, Bekiari E, Boura P, Tsapas A (2014) Update on long-term efficacy and safety of dapagliflozin in patients with type 2 diabetes mellitus. Ther Adv Endocrinol Metab 6:61–67
216. Sosale B, Sosale A, Bhattacharyya A (2016) Clinical effectiveness and impact on insulin therapy cost after addition of dapagliflozin to patients with uncontrolled type 2 diabetes. Diabetes Ther 7:765–776
217. Issandou M, Bouillot A, Brusq J, Forest M, Grillot D, Guillard R, Martin S, Michiels C, Sulpice T, Daugan A (2009) Pharmacological inhibition of Stearoyl-CoA Desaturase 1 improves insulin sensitivity in insulin-resistant rat models. Eur J Pharmacol 618:28–36

218. Lepifre F, Christmann-Franck S, Roche D, Leriche C, Carniato D, Charon C, Bozec S, Doare L, Schmidlin F, Lecomte M, Valeur E (2009) Discovery and structure-guided drug design of inhibitors of 11b-hydroxysteroid-dehydrogenase type I based on a spiro-carboxamide scaffold. Bioorg Med Chem Lett 19:3682
219. Birch AM, Buckett LK, Turnbull AV (2010) DGAT1 inhibitors as anti-obesity and anti-diabetic agents. Curr Opin Drug Discov Devel 13:489–496
220. Kaiser D, Oetjen E (2014) Something old, something new and something very old: drugs for treating type 2 diabetes. Br J Pharmacol 171:2940–2950
221. Ichimura A, Hasegawa S, Kasubuchi M, Kimura I (2014) Free fatty acid receptors as therapeutic targets for the treatment of diabetes. Front Pharmacol 5:236
222. Miller BR, Nguyen H, Hu CJH, Lin C, Nguyen QT (2014) New and emerging drugs and targets for type 2 diabetes: reviewing the evidence. Am Health Drug Benefits 7:452–463
223. Cornell S (2015) Continual evolution of type 2 diabetes: an update on pathophysiology and emerging treatment options. Ther Clin Risk Manag 11:621–632
224. Morgan S, Grootendorst P, Lexchin J, Cunningham C, Greyson D (2011) The cost of drug development: a systematic review. Health Policy 100:4–17
225. Paul SM, Mytelka DS, Dunwiddie CT, Persinger CC, Munos BH, Lindborg SR, Schacht AL (2010) How to improve R&D productivity: the pharmaceutical industry's grand challenge. Nat Rev Drug Discov 9:203–214
226. Herper M (2012) The truly staggering cost of inventing new drugs. Forbes. https://www.forbes.com/sites/matthewherper/2012/02/10/the-truly-staggering-cost-of-inventing-new-drugs/

# Chapter 2

# Practical Considerations for In Vivo Mouse Studies

Edward T. Wargent

## Abstract

Obesity and type 2 diabetes are serious conditions that have reached pandemic proportions. The underlying physiology is complex with multiorgan interactions involved and, consequently, multiorgan approaches are necessary for researchers to elucidate and find treatments. As such, in vivo models are an invaluable resource for these studies and mice are, for many reasons, by far the most common species used. The use of animals comes with responsibilities to ensure their welfare and well-being: primarily for the sake of the mice themselves, but also to ensure quality of data. Physiological stress responses, such as adrenalin (epinephrine) and corticosterone release among others, have major consequences on metabolism. Additionally, behavioral stress responses are also a source of data variance. This chapter looks at the main in vivo procedures incorporated in mouse obesity/diabetes protocols and considers the practical factors involved that can be considered to minimize animal stress and improve study data quality.

**Key words** Mouse, In vivo, Stress, Data quality, 3Rs

## 1 Introduction

Type 2 diabetes and obesity are worldwide major public health problems. As well as its adverse psychosocial impact, obesity increases susceptibility to type 2 diabetes (markedly), cardiovascular disease (both dependent and independent of diabetes), and certain cancers. By some estimates, it is close to becoming the biggest killer in our society. Diabetes increases myocardial infarction, stroke, kidney failure, blindness, and peripheral vascular disease and is a major cause of male impotence.

The onus of obesity treatment traditionally lies with the patients themselves expected to take responsibility for management of their own condition [1]. This approach persists despite the increasing prevalence of both diseases. Patients are rightly advised to eat less and exercise more, but this simplistic therapy is evidently insufficient. Currently, there are several anti-obesity medications available, but orlistat is the only worldwide-approved drug

Claire J. Stocker (ed.), *Type 2 Diabetes: Methods and Protocols*, Methods in Molecular Biology, vol. 2076,
https://doi.org/10.1007/978-1-4939-9882-1_2, 

remaining for the treatment of obesity (the only one licensed in the UK, for example). However, the effectiveness of orlistat is slim with an average weight loss of only 2.9 kg (or about 2.3 kg for the over-the-counter dose). There are more therapeutic options for type 2 diabetes, but the older drugs merely slow the advance of the disease by a few years (at most), and the newer ones are either suspected of having a poor benefit-to-risk ratio, or their ability to halt the advance of the disease has yet to be demonstrated. There is a need for better treatments for diabetes and obesity in the form of drugs, nutraceuticals (since much of the diabetes epidemic is occurring in countries and populations that cannot afford Western drugs), diets or lifestyle modifications. To achieve this, we need to understand better the causes of the diseases, identify potential therapeutic targets, and investigate whether and how potential interventions work. Control of metabolism, growth, and body composition involve the interaction of many body organs including brain, liver, adipose tissue, muscle, and endocrine organs. Neither cell or tissue cultures nor nonvertebrate organisms can replicate such mammalian whole body systems. Computational methods are still in a developmental stage, requiring further experimental data before they can reliably replace whole animals.

The use of animals in scientific research comes with responsibilities to ensure the welfare and ethical treatment of those animals. It is every in vivo researcher's duty to explore ways to replace animals with other means to answer the questions postulated; to reduce the numbers of animals used; and the refine the procedures employed to reduce harm and distress experienced by experimental animals. When studying conditions such as obesity and diabetes, the reduction of stress is also necessary as it impacts greatly upon metabolism [2]. Consequently, reducing stress is the single most important factor to be considered when designing reliable and reproducible experiments and reducing the variation of the data generated.

For manifold reasons, including finance, ethics, genetics, time scales, etc., rodents and mice are by far the most widely employed species in obesity and diabetes studies and this chapter describes the typical in vivo procedures used in a manner intended to minimize stress by exposing the rodents to no more than transient pain, distress or harm. When carried out in the ways described, each procedure can be classified as mild. However, animals should be monitored before and after each procedure to ensure no compound suffering from consecutive procedures. The recovery times detailed below are minimal and the health of each animal should be monitored carefully during and after each procedure.

## 2 General Output Measures

Relevant output measures fall into three groups: obesity, insulin sensitivity/glucose tolerance, and energy balance. Specific details are stated where animal quality of life and experimental variance will be improved. Further details can be obtained from the National Centre for the Replacement, Refinement and Reduction of Animals in Research (https://www.nc3rs.org.uk).

### 2.1 Obesity

Body weight and composition may be determined in vivo by quantitative magnetic resonance (QMR) or dual-energy X-ray absorptiometry (DEXA) scanning. QMR measurements can be made without the need for anesthesia. In this procedure, mice are unrestrained in a plastic cylinder with freedom to turn about but limited vertical movement and placed in the scanner. Measurement is completed within 1–2 min. DEXA scanning requires animals to be under light general anesthesia to prevent movement.

### 2.2 Insulin Resistance and Glucose Tolerance

#### 2.2.1 Blood Levels of Markers of Insulin Resistance

Blood levels of markers of insulin resistance and type 2 diabetes in either the fed state or fasted state include glucose, insulin, lipids, incretins, and pro- and anti-inflammatory molecules such as cytokines and chemokines. Blood samples will typically be taken from a superficial blood vessel or by removing the tip of the tail (~1 mm). Repeat samples can then be collected by removing the scab and gently massaging the tail. Not more than 10% blood volume should be taken in a single day and not more than 15% in a 28-day period. On average, mice have around 58.5 mL of blood per kg of bodyweight and this approximation should be used for the above calculation, e.g., a 20.0 g mouse will be estimated to have 1.17 mL blood and therefore blood sampling should be no more than 117 μL in a day or 175 μL in any 28-day period.

#### 2.2.2 Glucose Tolerance Test (GTT)

GTTs assess the disposal of a glucose load administered via oral gavage or intraperitoneal/intravenous injection. The response to a GTT is determined by insulin secretion and insulin resistance and is impaired in obesity-related diabetes. Mice are fasted for 5–6 h to ensure steady-state blood glucose levels. An aqueous glucose load is administered in a volume of 10 mL/kg and blood glucose is measured over a span of 2–3 h. The glucose load is typically 2–3 g/kg and may be adjusted based on lean body mass body composition data if available due to muscle being the main tissue responsible for glucose clearance in a GTT (the liver second). A glucose load of 3 g/kg is sufficient to cause a doubling of blood glucose concentration after 30 min in normal mice. Insulin-resistant mice require less glucose to effectuate a doubling in blood glucose concentration: 2.5 g/kg is recommended in diet-induced obese mice and 2 g/kg in more extreme models of insulin resistance such as *ob/ob* or *db/db* mice. A doubling in blood

glucose concentration is desirable as it produces a statistically significant effect without overloading the system, thus providing a window to show treatments that either increase or decrease insulin sensitivity. The GTT duration varies for the same reason, with blood glucose concentration taking 2 h to return to pre-dose levels in normal mice. GTTs in insulin-resistant mice may not have returned to pre-dose levels even after 3 h, but the purpose of the GTT will have been fulfilled after this time and so the GTT should be no longer than this. Typically, a blood sample (10 μL or less) is taken prior to the glucose load (for baseline measurements) and then at 30-min intervals for the duration of the experiment (for 3-h GTTs, a 150 min time point does not improve the quality of the data and should be omitted for refinement purposes). Thirty-minute intervals are recommended, as the stress-induced increase in blood glucose following handling/bleeding will usually be insignificant by then. An additional blood 30 min before glucose load can be performed to demonstrate this (and this may be a convenient time for a treatment dose, should the GTT incorporate one in addition to the glucose load). Oral GTTs represent the most physiological route of entry of glucose. Mice like the taste of glucose water and it is sometimes possible to train unstressed mice to drink a small volume from the tip of a syringe. Experimenters should conduct preliminary tests to see if their mice will voluntarily drink the glucose load. Alternatively, it may be administered by gavage or administered with a feeding needle. The appearance and clearance of blood glucose during an oral GTT is affected by the rate of gastric emptying and the incretin effect and if it is necessary to circumvent these processes, the glucose may be given by the intraperitoneal or intravenous routes. Blood samples for the measurement of plasma insulin are taken 30 min before and 30 min after the administration of glucose. These are much larger sample sizes, taking longer to collect and increasing the stress the mouse experiences, and should be limited to these time points only for the sake of the animal and the quality of the GTT.

### *2.2.3 Sensitivity to Insulin, by Euglycemic/Hyperinsulinemic Clamp*

This is the gold standard technique for measuring insulin sensitivity. Mice are fasted for 4–6 h to prevent the appearance of meal-derived glucose, but not deplete liver glycogen stores. Mice then receive a constant infusion of insulin to achieve a steady-state hyperinsulinemia above fasting insulin level. A variable glucose infusion is administered to maintain euglycemia. Infusions are administered via a previously implanted indwelling catheter. The glucose infusion rate is determined by measuring blood glucose at regular intervals, typically every 10 min, and adjusting the glucose infusion accordingly. This variable rate of glucose infusion indicates whole-body insulin action, as mice with enhanced insulin action require a greater infusion of glucose. Isotopic tracer infusions can be applied to assess sites where insulin action is affected.

### 2.2.4 Sensitivity to Insulin, by Insulin Tolerance Test (ITT)

Following a short (4 h) fast, glucose concentration is monitored every 15–30 min for 60–90 min following a bolus of insulin administered via intraperitoneal or intravenous injection. A bolus insulin dose to fasting mice comes with a risk of hypoglycemia and death, and the shorter fasting period in ITTs compared to GTTs, albeit only an hour, provides a significantly safer procedure in terms of mouse mortality. The safety factor far outweighs the risk of having a small amount of glucose still entering the blood from the gut. The degree to which glucose falls following the insulin bolus is indicative of whole-body insulin action. The insulin dose will be determined according to lean body mass where appropriate and may be higher if there is insulin resistance. A dose is chosen which is not expected to produce hypoglycemia: typically, 0.5 mU/kg in normal mice and 0.75 mU/kg in insulin-resistant mice (severely insulin-resistant phenotypes may require an even higher insulin dose, e.g., *ob/ob* and *db/db* mice may require up to 1.5 mU/kg, but alternatives to such studies should be carefully considered due to the variability and uncertain success rate). A lower dose can be used in phenotyping studies as it gives a good response in wild-type animals without reducing blood glucose to dangerous levels. If the genotype causes insulin resistance, then no reduction is seen in this group. In mice with diet-induced insulin resistance, the insulin dose used needs to be higher to elicit a borderline nonsignificant reduction in glucose. Drugs that improve insulin sensitivity therefore have the best chance to have their effect detected at this insulin dose. For the same reason, the insulin dose will alter in genetically insulin-resistant mice, though the exact dose will vary for each transgenic/mutant. Any animal that shows signs of torpor after insulin administration should immediately be given glucose and glucagon (amount of glucagon equal to counteract the insulin dose) by the intraperitoneal route, monitored continuously, and culled if it fails to respond to stimulation or does not recover within 20 min (treatment with both glucose and glucagon should recover 95% of mice experiencing torpor). If it is suspected that a strain of mouse may be overly sensitive to insulin, then small pilot studies should be performed.

### 2.2.5 Real-Time Minute-by-Minute Changes in Insulin Secretion

Under in vivo conditions, the study of physiological and pharmacological functions of an organ is difficult due to whole-body interactions with the organ. In vitro perfusion of isolated pancreas is required for physiologic and response studies, including the investigation of endocrine function and secretory responsiveness under a variety of diabetes-associated conditions and treatments. Animals are terminally anesthetized, and the pancreas isolated from the connecting spleen, stomach, and duodenum and transferred to a pre-warmed chamber, where it is perfused in isolation from all other organs and the perfusate collected for analysis of insulin secretion.

#### 2.2.6 Blood Pressure

Hypertension is associated with hyperinsulinemia, and the same programming conditions that cause increased risk of obesity and diabetes also increase the susceptibility to hypertension. Therefore, blood pressure is an important measure and can be done satisfactorily by the noninvasive tail cuff method. Systolic blood pressure equal to or greater to 140 mmHg is considered to be hypertensive. A positive outcome of treatment would be to reduce systolic blood pressure below 130 mmHg.

### 2.3 Energy Balance

(a) Measurement of food intake and measurement of overall daily energy expenditure using indirect calorimetry measuring the amount of oxygen consumed and carbon dioxide produced in expired air.

(b) Measurement of basal metabolic rate by measuring the utilization of glucose and release of carbon dioxide in animals in a thermoneutral environment over 8 h. The only difference from normal measurements of energy expenditure is that the ambient temperature raised to 28–30 °C and measurements are limited to 8 h during the light period.

(c) Measurement of brown adipose tissue activity after administration of a thermogenic agent (such as a beta 3-adrenoceptor agonist) by measuring oxygen consumption and carbon dioxide output and blood pressure indirectly by the tail cuff method. Brown adipose tissue thermogenic capacity will also be assessed ex vivo by determining the expression of uncoupling protein-1.

## 3 Considerations for In Vivo Procedures in Obesity and Diabetes Protocols

### 3.1 Strain

Many strains of mice are available for the study of obesity and type 2 diabetes and the question of a "right model" per se a complex, and possibly unanswerable, one [3]. Genetically modified mice will usually be generated on a 129 background and thereafter transferred to the strain of choice, usually C57Bl/6 mice because of their susceptibility to environmentally induced obesity and insulin resistance. However, the strain employed will depend on the question being posed by the study. For example, studies into browning of adipose tissue may well be suited to being on the 129 strain because they exhibit a propensity for browning of white adipose tissue and so have a window to both upregulate and downregulate this physiological effect. Experimental consequences will occur with all strain, e.g., in the case of 129 mice, the propensity for browning might make them suitable to study promoters of browning, but will make them resistant to the effects of a high-fat diet and so require a longer period before they develop insulin resistance and require a 60% fat diet rather than a 40% fat diet. The complex

physiology of obesity and diabetes makes a study of strain suitability within the confines of a single book chapter impossible. Fortunately, there are mouse strain resources that researchers can consult in addition to literature tapping, e.g., International Mouse Strain Resource (https://www.jax.org/research-and-faculty/resources/international-mouse-strain-resource).

### 3.2 Single Housing

Animals should be group housed wherever possible. For some studies, it may be necessary to house animals singly so that individual food intake can be measured, or to remove any effect of hierarchy or aggression on feeding behavior.

### 3.3 Food and Feeding

#### 3.3.1 Feeding a Modified Diet

Modified diets should be adequate with respect to all known nutrients including vitamins and minerals. As such, commercial rodent feeds are preferable to handcrafted feeds, and these are also consistent in constitution. Diets should be stored under appropriate conditions to prevent deterioration and be given a defined shelf-life. Feeding high-fat diets may reduce wear of the teeth. Overgrowth of teeth will reduce the animal's ability to feed and drink resulting in loss of weight. All experimental animals should have their teeth checked for malocclusion, with the weighing times a good time to do this. Where possible, animals should be provided with environmental enrichment, such as wooden sticks, to help increase teeth wear. Advice on treatment or culling should be sought from a veterinary surgeon if teeth become overgrown. Likewise, diets with a high sugar intake may increase the risk of dental caries, which may cause pain and a reduction in food intake. Mice on these diets should have their teeth inspected weekly (when weighed would be ideal). If evidence of dental caries is observed, the advice on tooth management should be sought from a veterinary surgeon.

#### 3.3.2 Pair-Feeding

In the event of an experimental group having reduced food intake, it may be necessary to pair-feed a group of control animals so that they receive the same amount of food. A reduction in food intake results in an improvement in insulin sensitivity and pair-feeding allows differentiation between the insulin sensitizing effects of reduced food intake and the primary mechanistic actions being investigated in the study. This reduction in food intake should be no less than 40% of normal on any one occasion (up to a maximum of 72 h) and no more than 25% over the period of an experiment to minimize the stress imposed on an animal. Body weight must be measured to assess the impact of pair-feeding on the control animals and should not drop below 80% of the weight of normal mice on standard diet.

### 3.3.3 Fasting

The withholding of food from rodents is stressful but some studies require deprivation of food for a defined period. The minimal period of food withdrawal commensurate with the objectives of the experiment should therefore always be used and should never be greater than 18 h, which may be required if it is necessary to deplete the primary nutrient stores of glycogen and mobilize lipid stores from adipose tissue. Measurements of lipid dysregulation are more likely to be seen if the animal is fasted for 18 h in mice weighing 20 g or more and 5 h in mice less than 20 g. Animals should have a minimum of 3 days with continuous availability of food between any periods of fasting. There is no evidence that mice that are hyperphagic show an enhanced level of fasting stress.

For some studies, animals may need to be deprived of food for a defined period. Glucose tolerance and insulin sensitivity tests require there to be no uncontrolled glucose appearance into the blood and require a fasting period (typically 5 h) that is long enough to ensure that the gut is empty, but short enough not to stimulate hepatic gluconeogenesis. This is typically 5 h in mice.

## 3.4 Temperature

The topic of appropriate housing temperature for mice is currently under debate. With appropriate nesting material, mouse housing temperatures are generally maintained 1–2 °C above the room temperature. Thermoneutrality (the temperature with the minimum of physiological thermoregulation) is achieved with a room temperature of 28–30 °C. Below this zone, mice start to generate their own heat by increased skeletal muscle and brown adipose tissue activity, resulting in increased fat catabolism. Therefore, studies designed to study the adverse effects of fat accumulation (particularly those investigating chemical or genetic resistance to these effects) would benefit from higher temperatures, e.g., high-fat diet-induced obesity and insulin resistance is promoted at temperatures close to thermoneutrality (with a tendency toward reduced variation in data generated). However, mouse aggression also increases with temperature and mice housed at thermoneutrality tend to fight more and for this reason, mice should only be housed at thermoneutrality when necessary. C57Bl/6 mice, a strain commonly employed in metabolic studies because of its physiological suitability, are naturally aggressive and an alternative strain should be considered if housing at thermoneutrality for extended periods be intended. Behavioral studies have shown that mice prefer temperatures higher than the usual housing conditions of around 20–24 °C; however, temperatures in the thermoneutral range are only preferred during periods of rest. Taking the metabolic and behavioral aspects into consideration, the ethically recommended temperature range for in vivo mice protocols is 24–26 °C. Procedures investigating energy expenditure at thermoneutrality should be performed during the light phase for a maximum period of 8 h.

### 3.5 Blood Sampling

Blood sampling would preferably be taken either from a superficial blood vessel or from the tip of the tail after removal of no more than 0.5 mm of the tip of the tail on the first occasion and on subsequent occasions after removal of the scab. Blood sampling from a superficial vessel will be as noninvasive as possible. Pain from tail tipping for blood samples can be controlled by local anesthetic. The volume of blood taken should not exceed 10% of total blood volume on a single occasion or 15% in a 28-day period.

Blood sampling may be facilitated by placing the animals in a warm environment for the period of the sampling, but this will not have any adverse effects on the animal. Animals should be checked for bleeding at 1 and 12 h after the procedure and more frequently if required. Any other than minor bleeding after blood sampling should be controlled by the temporary application of pressure and a clotting agent. A veterinary surgeon should be consulted for advice on wound healing if any animal showing signs of bleeding more than 24 h after the last sampling. Any animal showing signs of excessive blood loss such as torpor lethargy or anemia should be culled.

Repeat sampling from the tip of the tail may result in bruising if too much pressure is applied when massaging. If hematomas and localized inflammation are noted at the tip of the tail, then animals should be carefully monitored. Localized inflammation and redness should recede within 24 h. If prolonged redness is observed or is accompanied by swelling or darkening of the tail, the animal should be removed from any further procedures. Any animal showing signs of necrosis, infection or delayed healing more than 24 h after the last sampling should be culled.

Long-term studies should have a maximum of five tolerance tests each requiring repeat blood sampling during the procedure. Animals should be assessed prior to each test to ensure the animal has healed fully from the previous procedure, and if there is any sign of hyperalgesia or abnormal healing, the animal should not be used.

### 3.6 Administration of Test Compounds

#### *3.6.1 Implantation of an Osmotic Mini-pump for Delivery of Compound by Constant Infusion*

The mini-pump could be either intraperitoneal or subcutaneous and should not be removed or re-used. Animals are expected to recover quickly and to show no adverse effects from the surgery other than a small and transient reduction in food intake. It is expected that the mini-pump will initiate the formation of a fibrous coat around itself, but this will cause minimum pain, distress, or lasting harm. Pumps should be neither replaced nor removed. Following surgery, body weight should be measured daily to assess for any post-operative loss in bodyweight. A loss of 20% body weight should be the humane end-point at which an animal will be culled. The skin of obese and diabetic animals does not have the same elasticity as that of normal animals and wound healing can be impaired. A special watch should be kept on such animals and the animals culled by an appropriate method if tears appear. Animals

with implanted pumps should not be kept more than 7 days after the expected exhaustion of the pump, nor should they undergo measurement of body composition by QMR.

### 3.6.2 Administration of Test Agents in the Food or Water

This is the first choice of route for chronic dosing as no discomfort or distress is expected from feeding compounds in the diet and should be employed if compounds can be homogenously distributed with no degradation. If this is not possible, or if taste aversion occurs, another method will need to be considered. Waste measurement for accurate assessment of dosage is also a consideration. Leaky water bottles, "shredding" of solid diets and dispersal of powdered diets out of the food tray are complications that may arise. There are no fool proof methods for overcoming these issues, e.g., trays with a wire top tend to accumulate urinary and fecal waste and wire-bottomed cages with a waste tray underneath can cause weight loss in the mice. Another disadvantage to this route is that this is not a method that would be used in humans, and so some studies, by necessity, require a bolus dosing route.

### 3.6.3 Oral Gavage

Dosing by oral gavage in mice should be at a maximum of 20 mL/kg, and preferably 10 mL/kg. Some minor discomfort and transient distress is expected on each occasion, and on rare occasions, the esophagus becomes damaged or a small volume may inadvertently enter the lungs. Animals should be observed immediately after dosing. Any animal showing signs of mis-dosing or damage such as by coughing/choking or collapsing after administration of substances should be culled. A mis-dose directly into the lungs is extremely unlikely and results in immediate collapse shortly followed by death. Should collapse occur, the mouse should be immediately culled. More likely than a direct dose into the lungs is the event of a small amount of fluid ending up in the lungs. This happens when the dosing tube is inserted into the esophagus rather than the stomach, combined with too rapid a dosing. Detection is by careful listening immediately after dosing—a rasping sound will indicate this has happened. If this happens, the animal should be immediately culled, as death will occur slowly within 2 days and cause pain and distress.

### 3.6.4 Subcutaneous Injection

Substances should be administered by the subcutaneous route at a maximum volume of 20 mL/kg, and preferably 10 mL/kg. Some minor discomfort and transient distress is expected on each occasion. On repeat dosing, the injection site should be alternated over five subcutaneous areas in the flank and scapula (except for when direct exposure of brown adipose tissue is undesired, which case the scapula will not be used). Animals should be observed immediately after dosing and monitored throughout the treatment period for signs of discomfort, pain, or distress. Signs to look for are lumps/bumps or skin ulcerations and localized inflammation/redness: should this exceed a diameter of 5 mm, these mice should receive no further doses.

#### 3.6.5 Intraperitoneal Injection

Substances should be administered by the intravenous route at a maximum volume of 20 mL/kg, and preferably 10 mL/kg. Some minor discomfort and transient distress is expected on each occasion. Occasionally, a superficial blood vessel may be punctured. On repeat dosing, the injection site should be alternated over four areas in the peritoneum. Animals should be observed immediately after dosing and if treatment is for a prolonged period of time, the mice should be monitored for signs of pain and distress that may indicate peritonitis (hunching, subdued behavior, hind limb extension). Any animal showing signs of peritonitis should be culled. In obese mice, intraperitoneal dosing should be performed only when no other route is suitable as a proportion of animals will receive the dose in the fat pads instead. Data from tolerance tests can be analyzed for lack of appearance of glucose (although exclusion of data solely on this basis is not good practice).

#### 3.6.6 Intravenous Injection

Substances may be administered by the intravenous route at a maximum volume of 10 mL/kg, but preferably at 5 mL/kg. Some minor discomfort and transient distress is expected on each occasion. The main adverse effects of intravenous administration are needle stick injuries, bruising (which may be a result of the animal aggravating the site by licking and rubbing particularly when placed back in the cage), and loss of visibility of the vein. These adverse effects can be minimized using a suitable restraint, and good dosing technique (by administering slowly), including use of appropriately sized needles and warming the procedure room to ~25 °C to facilitate vasodilatation. Any bleeding after dosing should be controlled by the application of local pressure. On repeat dosing, the site of injection should be altered.

### 3.7 Energy Expenditure

Energy expenditure may be measured by whole body calorimetry at room temperature or at thermoneutrality (28–30 °C). The equipment draws air out of the enclosed animal cage which has a small air inlet hole to allow replacement and an alarm should be incorporated to detect if air ceases to be drawn from the cage. This can be linked to a mobile phone device.

#### 3.7.1 Measurement of Energy Expenditure at Room Temperature

Energy expenditure should be measured in the normal housing cages so as not to change behavior. No stress is expected from measuring energy expenditure at room temperature.

#### 3.7.2 Measurement of Energy Expenditure at Thermoneutrality

Energy expenditure measured at thermoneutrality (28–30 °C) should be done for no more than 8 h during the light period and the temperature of the room should be regularly monitored. Animals kept at thermoneutrality are expected to show a relaxed postural extension.

They should be observed at least every hour to ensure that this behavior is not altered to one of heat stress. This can be recognized by locomotor activity (to escape to a cooler environment) and excessive grooming (to spread saliva). Animals showing signs of heat stress should be moved to a normal environment, and if these signs do not begin to decrease within 20 min, they should be culled by an approved method. When animals have been treated in a way that might increase their energy expenditure or interfere with heat loss mechanisms, they must be checked every 30 min for the first 2 h.

## References

1. Bessesen DH, Van Gaal LF (2018) Progress and challenges in anti-obesity pharmacotherapy. Lancet Diabetes Endocrinol 6:237–248
2. Rabassa C, Dickson SL (2016) Impact of stress on metabolism and energy balance. Curr Opin Behav Sci 9:71–77
3. Leiter EH (2009) Selecting the "right" mouse model for metabolic syndrome and type 2 diabetes research. Methods Mol Biol 560:1–17

# Chapter 3

# Nutritional Models of Type 2 Diabetes Mellitus

**Beverly Sara Mühlhäusler, Carla Toop, and Sheridan Gentili**

## Abstract

In order to better understand the events that precede and precipitate the onset of type 2 diabetes (T2DM), several nutritional animal models have been developed. These models are generated by manipulating the diet of either the animal itself, or its mother during her pregnancy, and in comparison to traditional genetic and knock out models, have the advantage that they more accurately reflect the etiology of human T2DM. This chapter will discuss some of the most widely used nutritional models of T2DM: Diet-induced obesity (DIO) in adult rodents, and studies of offspring of mothers fed a low-protein, high-fat and/or high-sugar diet during pregnancy and/or lactation. Several common mechanisms have been identified through which these nutritional manipulations can lead to metabolic disease, including pancreatic beta-cell dysfunction, impaired insulin signaling in skeletal muscle, and the excess accumulation of visceral adipose tissue and consequent deposition of nonesterified fatty acids in peripheral tissues. In addition, there is an emerging concept that obesity/poor quality diets result in increased production and release of pro-inflammatory cytokines from adipose tissue leading to a state of chronic low-grade inflammation, and that this is likely to represent an important link between obesity/diet and metabolic dysfunction. The following chapter will discuss the most common nutritional models of T2DM in experimental animals, their application, and relationship to human etiology, and will highlight the important insights these models have provided into the pathogenesis of T2DM.

**Key words** Type 2 diabetes, Obesity, Insulin resistance, Animal models, Nutrition, High-fat diet, Programming

## 1 Introduction

While the human is undoubtedly the model of choice when studying the pathophysiology of human disease, the study of the underlying mechanisms of disease in living humans has a number of logistical and ethical limitations. Therefore, to better understand the events which precede and precipitate the onset of type 2 diabetes (T2DM), there is a need to develop in vivo animal models of this disease. Commonly used genetic models of T2DM, including *ob/ob* and *db/db* mice and Zucker *fa/fa* rats, have been useful in understanding some of the mechanisms which may contribute to altered glucose and insulin metabolism; however, none of these are

Claire J. Stocker (ed.), *Type 2 Diabetes: Methods and Protocols*, Methods in Molecular Biology, vol. 2076,
https://doi.org/10.1007/978-1-4939-9882-1_3, 

an ideal disease model, since these gene mutations are extremely rare in human populations [1]. Similarly, experimental animal models of T2DM induced by chemical destruction or removal of a portion of the pancreas [2] are not representative of the etiology of T2DM in humans, which is typically preceded by obesity [3, 4].

This has led to the development of a number of nutritional animal models of T2DM, which more closely mimic the etiology of the disease in human populations. These nutritional models involve the manipulation of the diet of either the animal itself, or its mother during pregnancy and/or lactation. A number of dietary approaches have been utilized in an attempt to best mimic the features of insulin resistance and T2DM in humans; however, the majority involve increases in dietary fat, in particular saturated fat, and/or increases in sugar (sucrose/fructose). This chapter will present an overview of these nutritional models of T2DM, with a particular focus on different dietary approaches used in these studies. It will discuss the application and relationship of these models to human T2DM etiology and the mechanisms contributing to the development of insulin resistance/T2DM that these nutritional models have provided.

## 2 Diet-Induced Obesity

A significant proportion of T2DM in human populations is linked to an excessive accumulation of body fat, particularly in the abdominal region [4–6]. This fact makes the diet-induced obesity model (DIO) particularly relevant for studying the underlying mechanisms through which an excessive accumulation of body fat and/or an excessive dietary fat and/or sugar intake can lead to the development of insulin resistance and T2DM. The two most widely used models for the study of obesity-induced T2DM are high-fat/high-sugar feeding in rodents and the sand rat (*Psammomys obesus*), which develops obesity spontaneously when fed on a standard rodent laboratory diet.

### 2.1 Diet-Induced Obesity: Rats and Mice

The DIO rodent model involves a regimen in which healthy, non-obese mice or rats are provided with *ad libitum* access to a highly palatable high-fat, high-energy diet. C57BL/6J mice were originally selected for this model because in early studies, these mice developed clear-cut diabetes more rapidly than other strains fed the same high-fat diet, suggesting a genetic predisposition to T2DM in this strain [7]. In this model, male C57BL/6J (B6) mice are maintained on these diets for 8–12 weeks, and as a result, become obese, mildly to moderately hyperglycemic, and develop impaired glucose tolerance [7]. Studies where the animals are maintained on the diets for longer periods have also demonstrated that after 16 weeks on a high-fat diet, C57BL/6 mice exhibit adipocyte hyperplasia and hypertrophy, and are insulin resistant [8]. For similar reasons, that

is, due to their propensity toward diet-induced insulin resistance in comparison to other common breeds, Wistar and Sprague-Dawley rats have been the rat strains of choice for studying the metabolic effects of diet-induced obesity [1].

The use of high-energy diets to induce obesity in laboratory animals for the purpose of studying obesity-related disorders has been widely adopted, and the scope of these diets is now quite extensive, ranging from an oil-based diet to free access to a variety of human junk foods, including pies, cakes and chocolate, termed a "cafeteria diet" [9–13]. The composition of these diets varies considerably between studies. However, the most common nutritional models involve increasing the dietary content of fat and/or sugar in combination with an increase in energy density. The response of the animals to these diets depends both on the specific dietary composition and the breed/strain of the animal, and both must therefore be considered when selecting an appropriate nutritional approach for a given study. We will briefly consider the different dietary approaches below.

### 2.1.1 High-Fat Diets

The majority of high-fat diets used in rodents provide between 40% and 60% energy as fat, as compared to ~10% energy from fat in standard laboratory diets [14]. Historically, the major source of fat in these diets has been lard, and therefore, most studies to date have predominately increased the dietary saturated fat content. Feeding rodents diets containing high levels of saturated fat has consistently been shown to promote fat deposition, increase the production of pro-inflammatory cytokines, and result in the development of insulin resistance, hypertriglyceridemia, hyperphagia, hypertension, and nonalcoholic fatty liver disease [14–16].

Over recent years, it has also become increasingly clear, however, that different types of dietary fats can have profoundly different physiological effects. Consequently, not all high-fat diets provide a suitable nutritional approach for inducing insulin resistance/T2DM. This is particularly true of diets which contain high levels of the omega-3 long-chain polyunsaturated fatty acids ($n-3$ LCPUFA), eicosapentaenoic acid (EPA) and docosahexaenoic acid (DHA), since these $n-3$ LCPUFA, unlike saturated and omega-6 polyunsaturated fats, have been reported to have both antilipogenic/adipogenic and insulin-sensitizing effects in vitro and in vivo [17, 18].

The insulin sensitizing and anti-obesity actions of $n-3$ LCPUFA have been attributed to both direct effects on insulin-sensitive tissues, and the effects of the bioactive derivatives of this class of fatty acids. Studies in vitro and in adult rodents have shown that both EPA and DHA act to suppress expression of genes involved in preadipocyte proliferation/differentiation, thereby inhibiting the expansion of adipose depots by hyperplasia [17]. In addition, these fatty acids also suppress expression/activity of the

lipogenic transcription factor, SREBP-1c in mature adipocytes, and thus inhibit the accumulation of triglycerides in mature adipose depots [18, 19]. This suppression of both hyperplastic and hypertrophic expansion of fat depots is thought to underlie the beneficial effect of $n-3$ LCPUFA on fat deposition. However, despite the strong biochemical data, and the encouraging results of rodent studies, results from human trials investigating the potential of $n-3$ LCPUFA in assisting weight loss have been disappointing. One possible explanation for this is the high level of omega-6 PUFA which are present in most typical human diets in Western countries, since this class of fat has been shown to have proadipogenic and prolipogenic actions in vitro and in vivo [20, 21].

The insulin-sensitizing effects of the $n-3$ LCPUFA are again driven both by direct and indirect effects. Both EPA and DHA activate the transcription factor PPARγ in adipose tissue, which increases the synthesis and secretion of the insulin-sensitizing adipokine, adiponectin [22]. Adiponectin then acts via its receptors on peripheral insulin-sensitive tissues, in particular, the skeletal muscle and liver, to improve peripheral insulin sensitivity [22]. The $n-3$ LCPUFA also give rise to bioactive derivatives which either oppose/dampen the pro-inflammatory effects of the $n-6$ PUFA derivatives or have inherent anti-inflammatory properties [23]. These therefore act to suppress inflammatory processes and production of pro-inflammatory cytokines in adipose and other tissues which is thought to be a major contributor to the development of insulin resistance and T2DM in humans [24].

These data are important to consider when designing nutritional models of insulin resistance/T2DM, since they imply that the balance of $n-6$ and $n-3$ PUFA in the diet are likely to be important determinants of the effects of the diet on fat deposition and insulin action. Therefore, the content of both these fatty acid classes needs to be taken into account in the design of nutritional approaches for inducing insulin resistance/T2DM in experimental animal models.

### 2.1.2 High-Sucrose and High-Fructose Diets

In recent years, there has been an increasing focus on the contribution of added sugars in foods/beverages to the current epidemic of obesity and T2DM in human populations worldwide. This interest has been heightened by data from epidemiological studies, which have demonstrated that consumption of one or more sugar-sweetened beverage per day is associated with an elevated risk of developing high blood pressure, metabolic syndrome [25], and a 22% increase in the risk of developing T2DM [26]. These data have resulted in the American Heart Association advising that daily added sugar intake be limited to 100 cal and 150 cal for women and men respectively [27], which is equivalent to approximately 5–10% of daily energy intake. More recently, the World Health

Organization recommended that guidelines for added sugar intake be reduced to 25 g per day, less than a single can of sugar-sweetened beverage [28]. Depsite these recommendations, however, the average daily consumption of added sugars in Western countries remains high, with average daily intakes of ≥15% total energy intake in the United States, United Kingdom, and Australia [27, 29, 30].

Sucrose (cane/table sugar) is the most commonly used sweetener worldwide; however, the use of high-fructose corn syrup-55 (HFCS-55), is becoming more widespread, particulary in the United States. Following ingestion, sucrose (a disaccharide of glucose and fructose) is hydrolyzed into its monosaccharides prior to absorption, whereas the free glucose and fructose in HFCS-55 (55% fructose, 42% glucose) can be absorbed directly into the circulation [31]. The absorption of free fructose is limited by the physiological capacity of the glucose transporters (GLUTs), and this can result in malabsorption if consumed in large amounts [32]. The metabolic effects of sucrose and HFCS-55 are thought to more closely mimic those of fructose consumption alone; hence, the adverse metabolic outcomes, including dyslipidemia, ectopic fat deposition, impaired glucose tolerance and insulin resistance, associated with excess sugar consumption have been attributed to the fructose component [33].

A number of rodent studies have begun to utilize high-sucrose and high-fructose diets as a nutritional strategy for inducing obesity and insulin resistance. However, the results of these studies have not been consistent, apparently because of variation in the metabolic response to the diets both between species/strains, concentration and the way in which the sucrose/fructose are administered. Studies looking at fructose and sucrose range from a 10% w/v beverage to 60–70% fructose or sucrose content of chow, and many use a supra-physiological dose of sucrose or fructose, commonly 60% content of chow [33, 34]. In Wistar rats, providing sucrose either in solid form (e.g., as a component added to the feed) or in the drinking water (as a 10–30% w/v sucrose solution) has been associated with both increased visceral fat accumulation and insulin resistance in both liver and skeletal muscle in male animals [35–37]. In mice, however, adding sucrose to drinking water has had more varied effects. Providing additional sucrose to C57BL/6 mice fails to induce obesity; however, recent data suggests that this does induce more subtle changes in the metabolic phenotype of the animals, including adipocyte hypertrophy, glucose intolerance, hyperinsulinemia, hyperlipidemia, fatty liver, and increased levels of inflammatory cytokines [38]. Further studies in the area of high-sucrose feeding are required in order to establish whether this is an appropriate model of T2DM in humans and to fully elucidate the effects of sucrose/fructose consumption on male and female animals.

While fructose does not acutely increase insulin levels, chronic exposure to high-fructose diets in both rats and mice has been associated with the development of obesity, insulin resistance, impaired glucose tolerance, hyperinsulinemia, and hypertriglyceridemia [34]. In one study, feeding rats a 66% fructose diet for only 2 weeks was associated with a reduced abundance of the insulin receptor in both skeletal muscle and liver, and these changes preceded any changes in insulin sensitivity, plasma glucose or insulin concentrations in these animals [39]. High-fructose diets in rodents have also been associated with increased accumulation of nonesterified free fatty acids in tissues, resulting in lipotoxicity and ultimately leading to the development of insulin resistance [33]. Fructose feeding also stimulates expression of pro-lipogenic genes, SREBP-1 mRNA and FAS mRNA, in liver, and these molecular changes are implicated in the development of fatty liver and hepatic insulin resistance [39, 40]. While there are still relatively few studies which have utilized high-fructose feeding as a model of T2DM, the data to date are encouraging and support the utility of this nutritional strategy as an appropriate model of T2DM in humans [34].

#### *2.1.3 Studies of Obesity-Prone and Obesity-Resistant Animals*

It is now widely accepted that the susceptibility to developing obesity and T2DM varies between individuals, and there is considerable interest in understanding the genetic and physiological basis of this difference. This question has been addressed using an adaptation of the DIO model in which adult Sprague-Dawley rats are fed a purified diet with a moderately high fat content. The rats are subsequently selected as either obesity-prone or obesity-resistant according to their response (i.e., degree of weight gain and increase in percentage body fat) on the high-energy diet [41]. The obesity-prone rats typically eat approximately 16% more calories over the first 30 days compared to the obesity-resistant strain and exhibit a phenotype comparable to human metabolic syndrome, including glucose intolerance, hyperinsulinemia, and T2DM [41, 42]. Selective breeding has enabled these researchers to generate obesity-resistant and obesity-prone strains, and to study these two populations in order to determine factors which may underlie an increased propensity to obesity [43, 44]. This is a useful model, in that it provides a means of distinguishing between the effects due to high dietary fat content as distinct from those related to the effects of excess body fat.

#### *2.1.4 Summary: Diet-Induced Obesity as a Model of Human T2DM*

Irrespective of the precise nature of the diet, diet-induced obesity results in many of the same changes as seen in human obesity, including the development of central and peripheral insulin and leptin resistance [9], increased lipid accumulation in peripheral tissues, a pro-inflammatory state and in the altered expression of

adipokines which are known to contribute to the regulation of peripheral insulin sensitivity, in particular adiponectin and resistin [45].

DIO rodent models have been widely utilized in order to investigate the defects within specific tissues that may contribute to the development of insulin resistance in obese individuals. By comparing the profile of gene expression and protein content in specific tissues of DIO mice with those from lean controls using micro-array or 2D gel electrophoresis, it is possible to quickly identify genes which may be involved in the development of T2DM. Using this approach, DIO was shown to be associated with a reduced pancreatic abundance of enzymes involved in the clearance of reactive oxygen species, providing a potential mechanism for the deterioration of pancreatic function seen in the later stages of T2DM [46]. In addition, DIO is associated with adipocyte hypertrophy [47] and the induction of hepatic steatosis and hepatic insulin resistance [48], which again resembles the human obese state. More recently, high-fat diets, high-sugar diets, and excess fat accumulation have been linked to increased production of pro-inflammatory cytokines by adipose tissue and infiltration of these into peripheral tissues, resulting in a state of chronic low-grade inflammation [49]. This heightened inflammatory state is now considered to be a key factor which links excess adipose tissue deposition with the development of insulin resistance (Fig. 1).

Overall, the major advantage of the DIO model lies in the fact that these rats share many of the same characteristics as humans with obesity-related diabetes ("diabesity"). These therefore provide a model for measuring the cellular events through which excess accumulation of body fat and/or excessive dietary fat and/or sugar intake result in the degradation of insulin action in key insulin-sensitive tissues. Another advantage of this model is that DIO mice and rats can now be ordered directly from commercial suppliers. While this is obviously more expensive than an in-house option, it does have the potential to save the researcher the 8–12 weeks that it would normally take to generate the DIO rodents. In addition, a variety of high-fat diets are now available from commercial animal feed manufacturers. Most of these suppliers are able to adapt these diets according to the particular requirements of the study, which provides researchers with added flexibility and the potential to focus studies on one or more specific dietary component.

While the DIO model has many positive attributes, it also has some potential limitations. Perhaps, the major limitation is the lack of standardization of the feeding regimen of different studies, which has meant that the phenotype of the animals varies between experiments. The high-fat diets which have been used consist of anywhere from 20% to 60% energy content from fat, and the fat

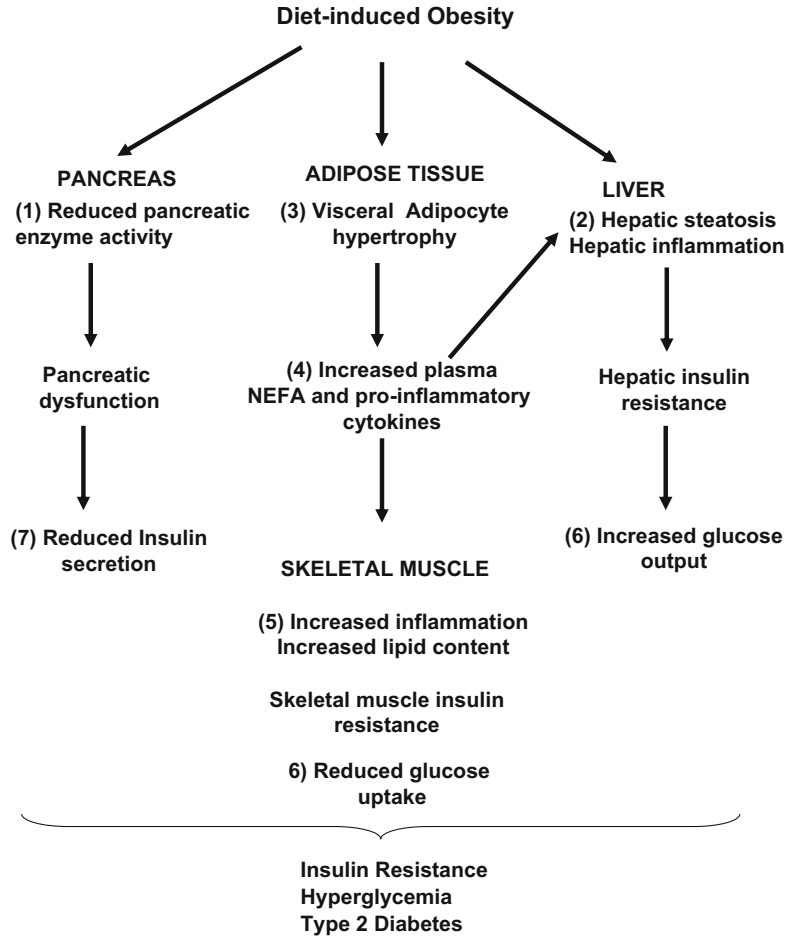


**Fig. 1** Summary of proposed mechanisms involved in the development of type 2 diabetes in models of diet-induced obesity in adult rodents. Increased dietary fat intake is associated with (1) reduced activity of pancreatic enzymes, leading to impaired pancreatic function and reduced insulin secretion, and (2) increased accumulation of lipids in the liver (hepatic steatosis) which results in hepatic insulin resistance and increased hepatic glucose output. In addition, increased accumulation of adipose tissue in the visceral compartment results in (3) increased production and secretion of pro-inflammatory cytokines resulting in chronic low-grade inflammation and (4) increased plasma concentrations of nonesterified free fatty acids (NEFAs) (4) which are deposited in liver and skeletal muscle. Both the chronic low-grade inflammation and ectopic fat deposition further contribute to insulin resistance in peripheral tissues. Together, this results in an impaired glucose uptake by skeletal muscle (5), increased hepatic glucose output (6) and impaired insulin secretion (7) and precipitates the development of whole-body insulin resistance and type 2 diabetes

source (i.e., animal vs. plant), fatty acid composition (i.e., the content of saturated, monounsaturated, and polyunsaturated fats), the balance of $n-6$ and $n-3$ PUFA and the level of trans fats also varies between studies [1, 14]. Similarly, high-sucrose

and/or high-fructose diets vary in their sugar content and the form in which the sugar is delivered, as well as the background fat and protein content of the diet. While there is no clear indication of which type of nutritional treatment represents the best model of the metabolic disturbances seen in human obesity, two publications focused on various types of diets employed in these experiments concluded that a "cafeteria diet" approach, in which rats/mice were provided with a selection of high-fat/high-sugar "junk foods," produced the metabolic phenotype that was most similar to that seen in human diet-induced obesity [1, 50]. However, it is also important to note that the composition of "cafeteria diets" is highly variable between laboratories and their effects variable between breeds. Therefore, it is important to critically evaluate the extent to which the diet used in nutritional models of human T2DM reflects the typical "poor quality western style diet," including the proportion of energy derived from fat/sugar and fat composition, and the precise phenotype of the strain under investigation when interpreting results and extrapolating these to humans.

### 2.2 *Diet-Induced Obesity:* Psammomys Obesus

The sand rat (*Psammomys obesus*) has been another popular model for studying the degradation of metabolic function associated with obesity. This is an attractive model because the sand rat rapidly develops obesity when fed a standard laboratory chow in standard animal housing conditions, which is considerably less expensive than custom-made high-fat diets. Many of the pathophysiological changes found in the obese sand rat are similar to those seen in human type 2 diabetic patients [51], and this model therefore appears to provide an appropriate nutritional model of human T2DM. When provided with *ad libitum* access to laboratory chow, the adult sand rat progress through from normoglycemia and normoinsulinemia, to hyperinsulinemia with marked insulin resistance, followed by pronounced hyperinsulinemia with hyperglycemia, and after a further 6–10 weeks of chow feeding, gradual beta-cell degradation and disappearance of beta-cell insulin which eventually results in severe insulin deficiency and overt diabetes [52]. The obese sand rat exhibits profound insulin resistance in both skeletal muscle and liver, and provides an attractive model for studying the mechanisms which underlie the development of diabetes in human obesity [53]. Studies utilizing this model have reported that GLUT4 protein content is reduced in skeletal muscle, resulting in a reduced peripheral glucose uptake and hyperglycemia [52]. In addition, hepatic PEPCK activity is increased, suggesting that the ability of insulin to inhibit hepatic glucose production is impaired [54]. Extensive use has been made of the obese sand rats for the purpose of testing potential T2DM drugs, including tyrosine phosphatase inhibitors and glucagon like peptide-1 (GLP-1) analogues [52].

The major limitations of this model are that the sand rat exhibits insulin resistance even when fed on a low energy diet, suggesting that the physiology of this desert-adapted animal may not be entirely comparable with humans. The link between weight gain and the development of insulin resistance in this model has yet to be clearly defined; however, the phenotype is normalized by dietary restriction. Nevertheless, this model has been utilized extensively for the study of obesity-induced diabetes, and continues to provide important insights into the cellular defects, which contribute to the development of central and peripheral insulin resistance.

## 3 Prenatal Nutritional Models of T2DM

The fetal or developmental origins of adult disease hypothesis states that insults during critical windows of development result in adaptive changes within fetal tissues and organ systems, which have lifetime consequences for the health of an individual. The hypothesis was first derived from studies of the Hertfordshire birth cohort by Professor David Barker in the early 1990s which showed that there was an inverse relationship between birth weight and the incidence of cardiovascular disease in adult life [55]. This was followed by a series of studies in human populations which all demonstrated that being of low birth weight was associated with an increased incidence of adult metabolic and cardiovascular disease [56, 57].

The Dutch Winter Hunger Famine was a 5-month period in World War II during which the food supply to Amsterdam, Holland was severely restricted, resulting in a substantial decrease in the daily energy intake of the population [58]. Subsequent studies of the children of women who were pregnant during the famine showed that those exposed to famine in the last 5 months of gestation had a significantly greater incidence of glucose intolerance, obesity and T2DM in adult life compared to those children whose mothers were not exposed to the famine [58, 59]. Similarly, early studies in infants of diabetic mothers clearly showed that exposure to high glucose levels in the pre- and perinatal period was associated with an increased incidence of hyperglycemia and T2DM in the offspring in postnatal life [60]. These studies provided the first evidence that exposure to an inappropriately low, or inappropriately high nutrient supply during early development was associated with a permanent alteration of metabolic function in the offspring. An increasing number of epidemiological and experimental animal studies have since continued to highlight the importance of both the prenatal and early postnatal nutritional environment for the determination of later metabolic health [57, 61, 62].

Together, these studies have clearly demonstrated that a low birth weight followed by a period of accelerated postnatal growth, or a high birth weight as a consequence of prenatal overnutrition, are each associated with an increased propensity toward the development of insulin resistance, glucose intolerance, and T2DM in adult life [63–65]. As a result, both spontaneous and experimentally induced fetal growth restriction (in utero growth restriction (IUGR)) and prenatal overnutrition in animal models have been widely employed in order to understand the physiological basis of reduced insulin sensitivity. It has also been demonstrated that global undernutrition in the pregnant rodent is associated with later onset of T2DM in the offspring [66]. This is, however, considered to be largely a consequence of impaired insulin secretion rather than defects in insulin signaling [67], and is therefore not regarded as an appropriate model for the pathophysiological process which contributes to T2DM in the majority of human patients.

### 3.1 The Maternal Low-Protein Model

The maternal low-protein model is one of the most extensively studied models of fetal growth restriction. In this model, pregnant dams are fed a diet containing approximately 8% of energy as protein, compared to approximately 20% in controls, and this is associated with low birth weight in the offspring, followed by accelerated postnatal growth [68, 69]. The period of rapid postnatal growth is due to enhanced insulin sensitivity in the period immediately after birth; however, this is not maintained beyond the early postnatal period, and the offspring develop insulin resistance by the age of 15 months, frank T2DM by 17 months [65, 70], and the deterioration of metabolic function is accelerated by a postnatal high-fat diet [71]. The phenotype of the low-protein offspring has many similarities to that of human type 2 diabetics, including insulin resistance, altered regulation of hepatic glucose output and pancreatic dysfunction [68]. As a result, this model has been used extensively to explore and characterize the cellular defects within the insulin signaling pathway which may contribute to reduced insulin sensitivity. These studies have demonstrated that prenatal exposure to a low-protein diet results in defects in several peripheral insulin-sensitive tissues, which are central to the maintenance of glucose homeostasis. In the pancreas, the islets of Langerhans are smaller and exhibit a reduced insulin secretion in response to amino acid stimulation [72]. While there is no obvious defect in glucose-stimulated insulin release in offspring fed a control chow diet postweaning, a reduction in the capacity of glucose to stimulate insulin release emerges if these offspring are fed on a high-fat diet postweaning. The liver of the low-protein offspring is unresponsive to the action of glucagon, and insulin stimulates, rather than suppresses, hepatic glucose output [73]. Furthermore, adipose cells exhibit increased basal and insulin-stimulated glucose uptake, leading to an increased accumulation of fat in the visceral compartment

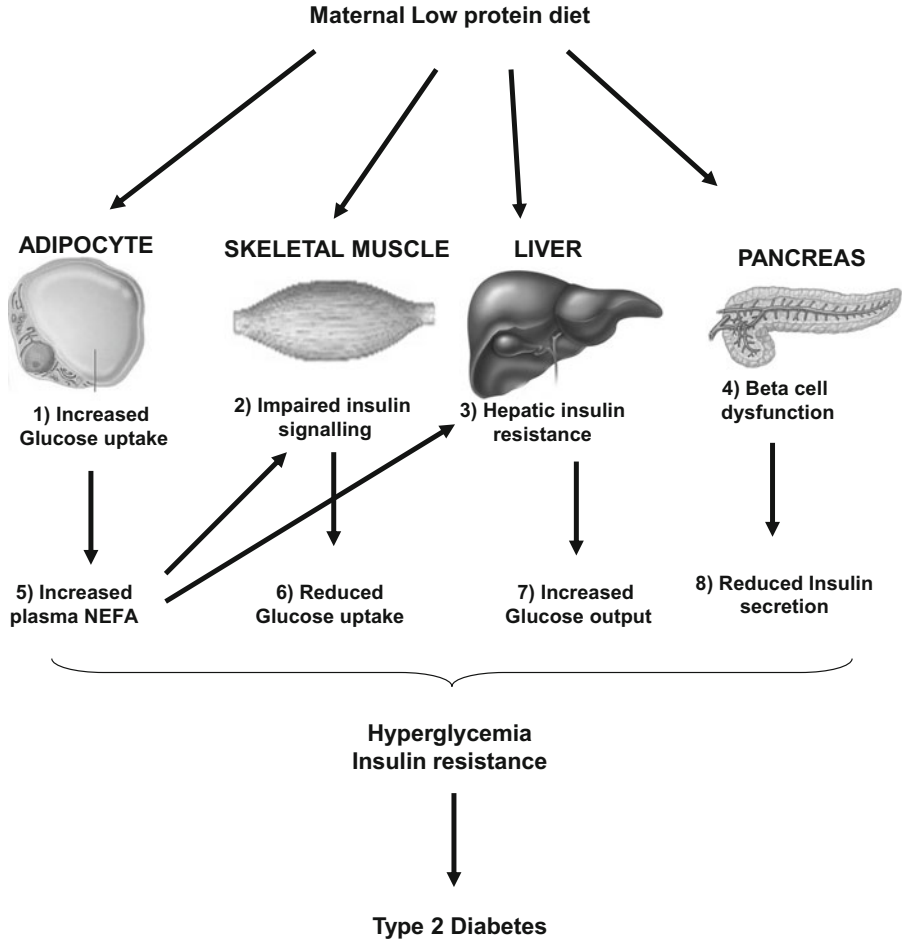


**Fig. 2** Summary of mechanisms proposed to contribute to the programming of type 2 diabetes of offspring in the maternal low-protein model. Prenatal exposure to a low-protein diet results in (1) an increased capacity for glucose uptake by visceral adipocytes (2) impaired insulin signaling in skeletal muscle, (3) hepatic insulin resistance and (4) impaired pancreatic function. The increased glucose uptake by visceral adipocytes results in an increased accumulation of visceral adipose tissue, resulting in elevated plasma concentrations of nonesterified free fatty acids (NEFAs) (5) which are deposited in peripheral tissues (liver and skeletal muscle), further reducing insulin sensitivity. This reduced insulin sensitivity is associated with impaired glucose uptake by skeletal muscle (6), increased glucose output by the liver (7) and reduced insulin secretion by the pancreas (8), resulting in peripheral hyperglycemia, insulin resistance and type 2 diabetes

and ectopic fat storage in liver and skeletal muscle, which further contributes to the peripheral insulin resistance [74] (Fig. 2).

Given that muscle represents the major site of postprandial glucose disposal, it is not surprising that changes in the functional characteristics of muscle fibers during the perinatal period are important in the programming of insulin resistance and diabetes (Fig. 2). Isolated muscle strips from these low-protein animals exhibit enhanced basal and insulin-stimulated glucose uptake, and this increase in insulin sensitivity is associated with a twofold

increase in the abundance of insulin receptors in muscle membranes [75]. By 15 months of age, however, there is a decrease in the insulin sensitivity of glucose uptake in skeletal muscle from the group exposed to the low-protein diet in utero [76]. This impaired insulin action is not associated with changes in the expression of either the insulin receptor or GLUT4, but is associated with a decrease in the abundance of signaling molecules downstream of the insulin receptor, including the zeta-isoform of protein kinase C, an isoform that is positively involved in GLUT4-mediated glucose transport [76] and p85 PI3K [69] (Fig. 2). In addition to defects in insulin signaling, it has also been reported that prenatal undernutrition is associated with impaired mitochondrial biogenesis and impaired mitochondrial oxidative capacity in skeletal muscle, which has previously been associated with reductions in insulin sensitivity in this tissue [77, 78].

While these studies have provided important insights into the cellular defects which contribute to deteriorations in insulin sensitivity in peripheral tissues, it is still unclear whether these defects are the same as those seen in human T2DM, which typically develops secondary to increased body fat accumulation. There is recent evidence that the mechanisms involved in the prenatal programming of insulin resistance may be quite distinct from those in insulin resistance which develops in response to diet-induced obesity [67]. Nevertheless, the obvious importance of the early environment in determining metabolic health in later life may well explain why it is that some individuals are more susceptible to insulin resistance than others at the same degree of body fatness and same nutritional/environmental conditions.

### 3.2 Prenatal Overnutrition, Postnatal Obesity, and T2DM

There is increasing evidence that prenatal exposure to a high plane of nutrition is also associated with an increased risk of obesity and T2DM in postnatal life [61]. The rat and sheep represent the two main animal models that have been utilized thus far for investigating the effects of prenatal overnutrition on the offspring, and there is increasing evidence pointing to the negative impact of intrauterine exposure to maternal obesity and/or high-fat/high-sugar diets on insulin signaling in the offspring [61, 79]. Studies to date have suggested that the deterioration of metabolic function in these individuals is associated with altered development of pancreatic beta cells, mitochondrial dysfunction and programming of the central appetite-regulating network [11, 80–82]. Several studies have also suggested that the deterioration of metabolic function may be secondary to the increased accumulation of adipose tissue in these offspring (Fig. 3) [82, 83]; however, it is not clear whether this is the case in all models of prenatal overnutrition.

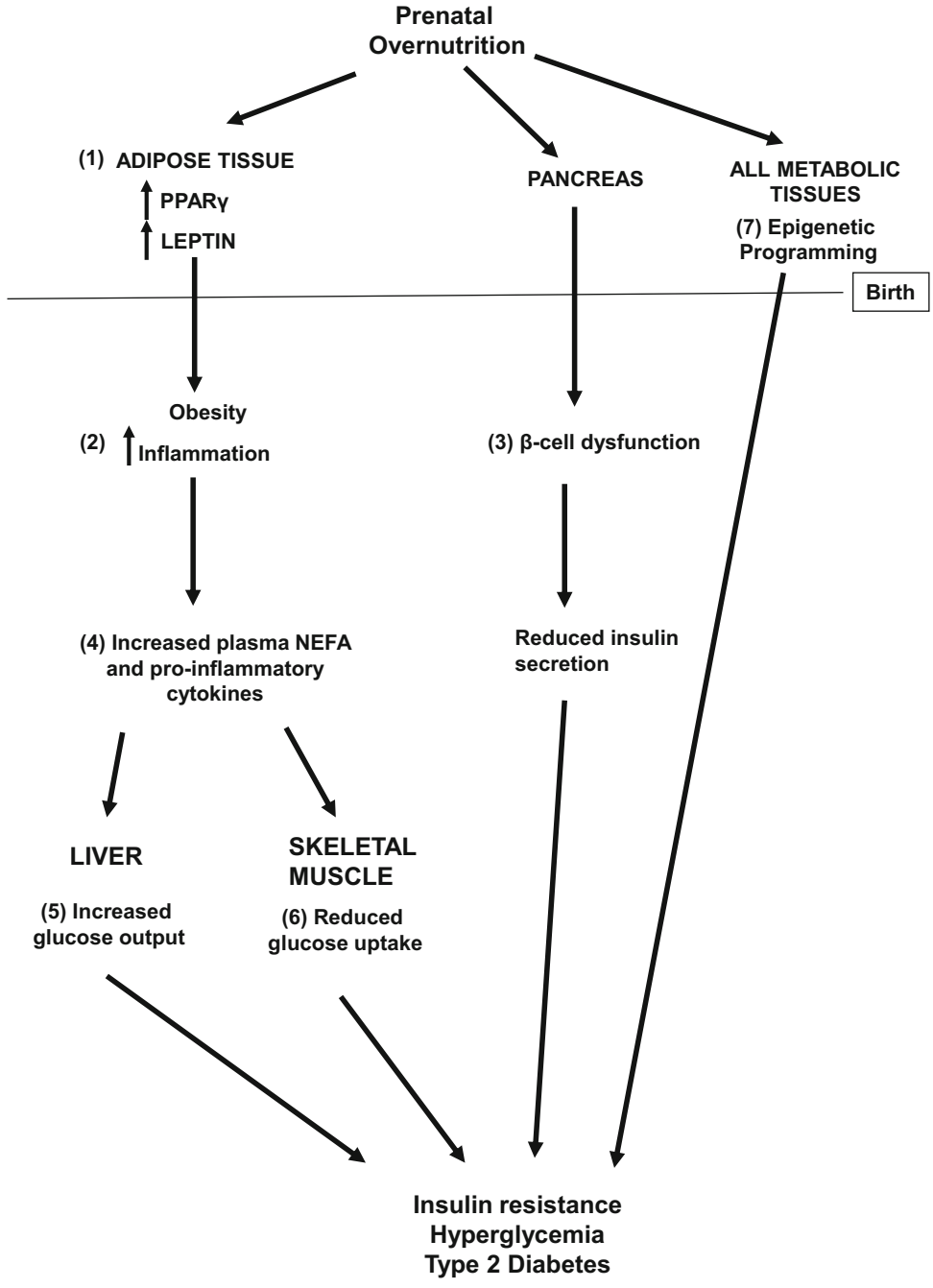


**Fig. 3** Potential mechanisms contributing to the programming of type 2 diabetes following prenatal overnutrition. It has been demonstrated that prenatal overnutrition is associated with an increased lipogenic capacity of adipose cells (1), which results in increased fat accumulation after birth (2) and predisposes these offspring to obesity in later life. In addition, prenatal high-fat diets result in impaired pancreatic development, and beta-cell dysfunction in postnatal life (3) and increased inflammation in key metabolic tissues, both of which contribute to increased insulin resistance. The increased accumulation of body fat further contributes to metabolic dysfunction by elevating plasma nonesterified free fatty acid (NEFA) concentrations (4) which are

In the sheep, feeding ewes approximately 55% above their maintenance energy requirements in later pregnancy results in an increase in fetal glucose and insulin concentrations in the last third of gestation [84], and is associated with an increased accumulation of subcutaneous adipose tissue at the end of the first month of postnatal life [82]. The offspring of overfed ewes exhibit elevated glucose concentrations during the first month after birth [82], although whether this is associated with reduced insulin sensitivity during this period has yet to be determined.

In the rat, maternal high-fat feeding results in disturbed glucose homeostasis in the offspring at weaning and in adult life, including an impaired glucose tolerance and reduced whole-body insulin sensitivity [81, 85]. As with adult rodents, however, the type of fat in the maternal diet also appears to be an important determinant of the effects of offspring physiology/metabolism. Patel and colleagues found that feeding rats on a chow containing high levels of saturated fat during pregnancy and lactation resulted in offspring that were significantly heavier than controls, and had elevated plasma concentrations of insulin, glucose, free fatty acids and triglycerides and exhibited glucose intolerance [80]. When they investigated the pancreatic islets in these animals, they found that those from male offspring exhibited an increased insulin secretory response at low glucose concentrations compared to controls, suggesting that high-fat feeding resulted in altered pancreatic development [86]. This was also the case in a separate study, in which feeding pregnant rats a high-saturated fat diet during pregnancy and lactation was associated with hyperglycemia and evidence of compromised beta-cell function in the weanling offspring [87]. Similarly, the offspring of Sprague-Dawley rats fed a lard-rich diet during pregnancy and lactation exhibited whole-body insulin resistance and a reduced glucose-stimulated insulin secretion in isolated islets at 9 months [11], again supporting the thesis that maternal high-fat feeding is associated with impaired pancreatic function in the offspring. Maternal consumption of diets high in saturated fat has also been linked to increased hepatic triglyceride accumulation in the offspring both in nonhuman primates and rodents, with a consequent reduction in hepatic insulin sensitivity [88].

### *3.3 Omega-6 and Omega-3 PUFA and Metabolic Programming*

The pro-adipogenic and pro-lipogenic actions of omega-6 PUFA, as discussed above, coupled with the substantial increase in the level of these fatty acids in the typical diets of many Western countries over the past 3–4 decades, have led to the suggestion that these

**Fig. 3** (continued) deposited in skeletal muscle and liver, resulting in insulin resistance in these tissues (5) and (6). Epigenetic changes which occur before birth (7) may also play a role in metabolic programming after prenatal overnutrition. Together, these changes result in peripheral insulin resistance and, ultimately, type 2 diabetes

fatty acids in the maternal diet could program an increased propensity to obesity and T2DM in the offspring [89, 90]. In support of this, a recent study by Massiera and colleagues demonstrated that intakes of omega-6 PUFA at levels comparable to those in modern western diets, in the absence of an increase in saturated fat intake, was sufficient to program a transgenerational increase in adipose tissue deposition in C57BL6/J mice [91]. Further studies are required, however, to establish whether maternal diets high in omega-6 fats could represent a suitable model to study the intergenerational programming of insulin resistance/T2DM in humans.

Despite the established role of $n-3$ LCPUFA in suppressing fat storage and promoting insulin resistance in vitro and in adults, the data from studies in which maternal $n-3$ LCPUFA intake is increased have failed to provide robust evidence that this is associated with an improved metabolic phenotype in the offspring [92, 93]. Indeed, in one study, offspring of dams who were provided with a DHA-supplemented diet during pregnancy and lactation actually had a higher relative fat mass in adolescence [94]. The potential for maternal $n-3$ LCPUFA supplementation to produce improvements in insulin sensitivity of the offspring has yet to be studied directly in either humans or animal models, and this remains an important area for future research.

### 3.4 Maternal High-Sucrose/High-Fructose Diets and Metabolic Programming

The adverse metabolic effects associated with excess consumption of additional sweeteners in adults have led to a growing interest in the potential role of these substances in the maternal diet in the programming of insulin resistance and T2DM. In epidemiological studies, excess consumption of sugar-sweetened beverages prior to pregnancy has been associated with an increased risk of developing gestational diabetes [95], which is known to be a risk factor for obesity and T2DM in the offspring [79]. The consumption of these sugar-sweetened beverage has also been linked to an increased birth weight [96]. Thus far, however, there have been relatively few experimental studies which have attempted to address the effects of sucrose/fructose in the maternal diet at levels typically encountered in Western diets on the long-term metabolic health of the offspring.

There is evidence from rodent studies, however, that maternal consumption of high levels of fructose or fructose containing sugars during pregnancy is associated with metabolic dysfunction in the mother, including increased adiposity, weight gain and hepatic insulin resistance, and adverse effects on placental and fetal development [97–103]. As discussed above, the metabolic effects of fructose in combination with glucose are different from fructose alone; however, few studies have investigated the separate effects of sucrose or fructose during pregnancy on maternal and

offspring outcomes [104]. Further studies in this area are clearly warranted, given that the evidence from the studies to date suggests that elevated intakes of both sucrose and fructose are associated with negative metabolic outcomes in the offspring. Therefore, maternal high-sucrose and/or high-fructose diets may offer an alternative experimental animal model of T2DM to maternal high-fat diets.

## 4 Possible Mechanisms for Metabolic Programming

### 4.1 The Adipocyte

In large animal models, there is evidence that exposure to prenatal overnutrition or undernutrition can act to permanently alter the function of adipocytes, and result in an increased lipogenic capacity in adipose depots in postnatal life. In sheep, which have a similar profile of adipose cell development to humans, exposure to increased glucose concentrations in late fetal life increases the expression of genes within adipose cells that are responsible for promoting lipid storage and forming new adipocytes [105]. This is associated with increased adipose tissue mass by the end of the first month of life, due primarily to an increase in adipocyte cell size [82]. In pigs, adipocytes exposed to high glucose levels before birth also exhibit a dramatic increase in their capacity for lipogenesis [106] and this precedes the development of obesity in the piglets [107]. These findings have since been supported by work in rodents, in which maternal junk food feeding during pregnancy and lactation in rats and an obesogenic diet during this same period in mice were each associated with increased adiposity and increased expression of lipogenic genes and insulin-independent glucose transporters in the perirenal adipose depot [83, 108]. It would therefore appear that fat cells exposed to an excess substrate supply during critical windows in their development have an increased capacity for storing lipid in postnatal life. This enhanced lipogenic capacity would render these individuals more likely to store excess energy in the form of fat, and increase their susceptibility to weight gain, obesity and, consequently, to the excess deposition of fatty acids in liver and skeletal muscle, resulting in peripheral insulin resistance, hyperglycemia, and ultimately, T2DM [109] (Fig. 3).

In individuals exposed to low nutrition levels before birth, adipocyte development is initially sacrificed in favor of "essential" organs [57, 110]. If an in utero "restricted" individual is born into a postnatal environment where nutrient supply is no longer constrained, a period of "catch-up" fat deposition ensues, mainly in the visceral adipose depot [111]. These individuals are thus at increased risk of visceral obesity [112], and consequently, to the development of insulin resistance and T2DM [113–115]. It is the increased

accumulation of visceral adipose tissue that has also been demonstrated in animal models of IUGR, including the sheep, guinea pig, and rodent [115–117]. Therefore, exposure of the developing adipocyte to suboptimal nutrition, particularly of the visceral adipose tissue which is the first adipose depot to develop in sheep and humans [118, 119], also appears to play a critical role in defining an individual's propensity for accumulating visceral body fat later in life, that is, a central pattern of fat accumulation, which is the fat pattern linked to increased risk of metabolic dysfunction and T2DM [6].

### 4.2 Mitochondrial Biogenesis

Mitochondria play a central role in the regulation of cellular energy metabolism, and impaired mitochondrial function and reduction in mitochondrial oxidative capacity in skeletal muscle have been associated with the onset of insulin resistance and T2DM both in experimental animal models and in human subjects [120]. In experimental animal studies, both diet-induced obesity and prenatal undernutrition have been associated with impaired mitochondrial biogenesis and reduced abundance of oxidative enzymes in skeletal muscle. Importantly, there is evidence that the reduction of mitochondrial biogenesis in adult rats exposed to prenatal undernutrition precedes the development of insulin resistance and glucose intolerance in this model [77, 78], therefore, implicating impaired mitochondrial function in the causal pathway linking prenatal undernutrition to later metabolic disease. The role of mitochondrial dysfunction in metabolic programming has yet to be explored in large animal models, and the potential role of mitochondrial dysfunction in the development of T2DM remains an important area for future investigation.

### 4.3 Increased Inflammation

The established role of chronic low-grade inflammation in the etiology of metabolic disease and T2DM in adults [49] has led to the suggestion that the impact of nutritional exposures experienced during the perinatal period on insulin sensitivity in the offspring could be mediated via altered inflammatory status in the offspring [121]. This premise has been supported by a number of experimental animal studies. These studies have demonstrated that both maternal undernutrition and maternal high-fat feeding results in a state of chronic low-grade inflammation in the mother, and that this is transferred both to the placenta and to a number of organs of the offspring, including the liver, adipose tissue, cardiovascular system and brain [122–124]. In one study in mice, offspring of high-fat fed dams exhibited increased expression of a number of key inflammatory factors, including TNFα, CD68, and MCP-1, in their subcutaneous adipose tissue, in conjunction with decreased GLUT4 mRNA expression, which supports the suggestion that maternal obesity can affect fetal insulin sensitivity via the alteration of inflammatory pathways [124]. Similarly, in a sheep model of maternal obesity, suppression of insulin receptor expression and

insulin signaling occurred in conjunction with an upregulation of inflammation in skeletal muscle in the offspring [123]. While fewer studies have focused on the potential role of chronic inflammation in the programming of T2DM by maternal nutritional deficits, there is recent evidence implicating exposure to maternal undernutrition in altered immune development in the offspring [122].

### 4.4 Epigenetics

The concept that changes in phenotype could be elicited by modification of the DNA in the absence of changes in DNA sequence, that is, epigenetic changes, provides a new basis for understanding of phenotypic programming. The two most well-characterized epigenetic modifications include DNA methylation and histone acetylation, which both act to suppress gene expression [125, 126]. Recent evidence has demonstrated that exposure to an inappropriate nutrient supply during early development may result in epigenetic modifications in the fetus which have the potential to permanently alter the function of important metabolic systems. Waterland and colleagues demonstrated that when mice with a genetic tendency toward obesity were fed a standard diet during pregnancy, the degree of obesity in the offspring increased progressively with each generation. This effect was, however, completely abolished if mice were fed a diet high in methyl groups (which increases DNA methylation) during pregnancy, and the offspring remained lean. These findings suggested that reduced DNA methylation in genes which play a role in the regulation of energy balance and fat storage, as a result of early nutritional programming, may contribute to the later development of obesity and metabolic disease [127]. The early work of Waterland has since been supported by a large number of subsequent experimental animal studies, and the importance of epigenetics in mediating metabolic programming is now well established. There is also increasing evidence that exposure to a suboptimal nutrient supply before birth can also alter methylation of a series of genes involved in growth and energy homeostasis, and that this may explain the link between both fetal growth restriction and maternal nutritional imbalance and later metabolic dysfunction. In rodent studies, Burdge and Lilycrop have reported altered methylation of a number of key hepatic genes, including those involved in carbohydrate metabolism, in offspring exposed to maternal undernutrition in utero [128]. Importantly, these studies have provided the evidence of transgenerational programming effects, such that epigenetic alterations persist into the F2 generation [129]. There is also emerging evidence of epigenetic programming in human studies, including a study reporting altered Igf2 methylation in adults whose mothers were exposed to the Dutch Winter Hunger Famine during pregnancy [130]. Overall, the role of epigenetics in the developmental origins of metabolic disease is certainly an exciting area of research, and has been the subject of a number of excellent reviews [131–134].

## 5 Summary

The dramatic increase in the incidence of T2DM over the past decade has highlighted the need to better understand the pathophysiology of this disease. The use of nutritional animal models which mimic the disease progression in humans is essential in order to investigate the cellular mechanisms which contribute to the deterioration of insulin metabolism in key insulin-sensitive tissues. This criterion is not fulfilled by genetic models, or models in which the pancreas is surgically ablated, since these causes account for only a relatively minor proportion of the humans who will develop T2DM. A number of nutritional models of T2DM have now been developed, and have made a significant contribution to our current understanding of the cellular defects which emerge in insulin-sensitive tissues in response to an excess accumulation of body fat or excessive intake of dietary fat, and which result in the development of peripheral insulin resistance. It has also become clear that exposure to an inappropriate nutritional environment in utero is associated with an increased susceptibility to T2DM in adult life, and that the detailed study of the cellular and molecular defects in these offspring has the potential to provide novel insights into why some individuals are more prone to the development of insulin resistance and T2DM than others.

The study of diet-induced obesity and models of prenatal undernutrition and overnutrition has revealed several common mechanisms which contribute to the onset of insulin resistance and T2DM in these different models (Fig. 4). This has provided important insights into the etiology of T2DM in humans, and identified possible targets for intervention. As with all animal models, it is important to recognize that animal data may not always be directly extrapolated to the human situation, where other factors, in particular, socioeconomic status and demographic variations, also contribute to the risk of metabolic disease [135]. It is therefore important to exercise caution when extrapolating results to human clinical practice. Nevertheless, it is clear that nutritional studies in the animal models discussed in this chapter have been critical in shaping our current understanding of the pathophysiology of T2DM and offer significant opportunities for identifying and testing potential clinical interventions.

## Acknowledgments

BSM is supported by a Career Development Fellowship from the National Health and Medical Research Council of Australia (NHMRC).

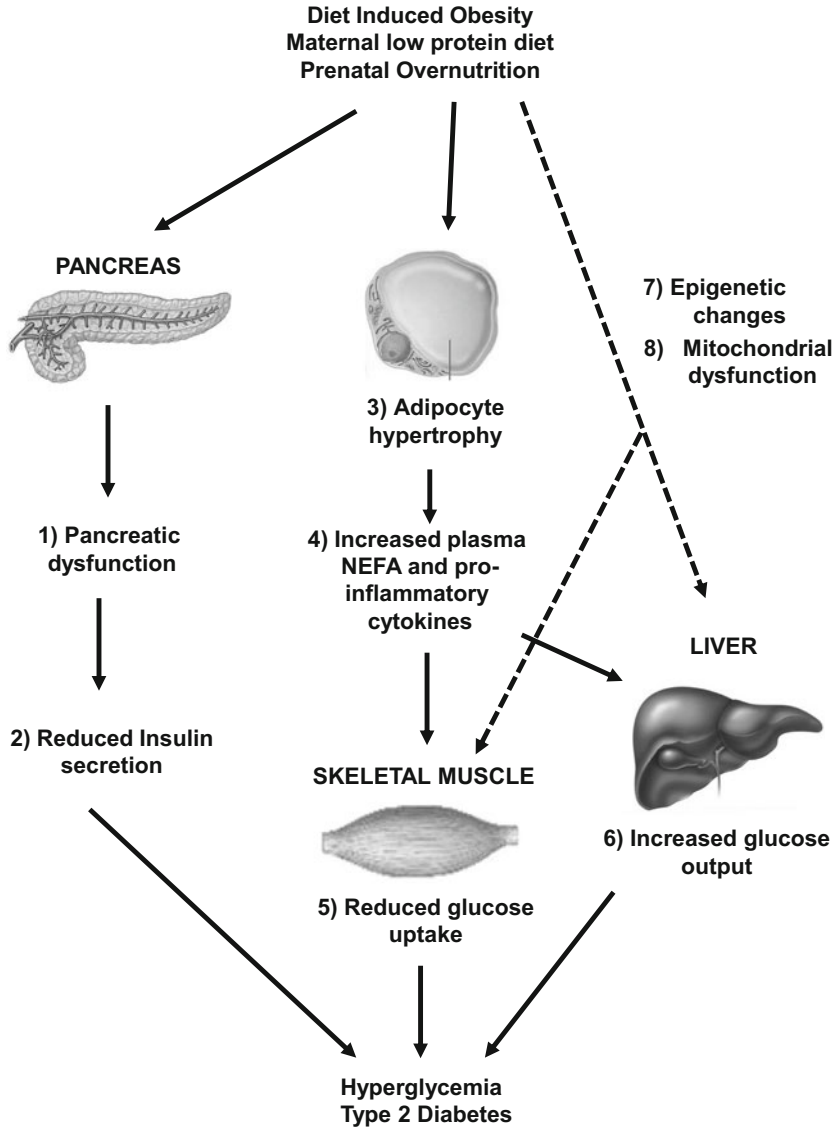


**Fig. 4** Summary of common mechanisms identified in all nutritional models of type 2 diabetes. Both diet-induced obesity and prenatal nutritional interventions are associated with pancreatic dysfunction (1) and impaired insulin secretion (2), which contributes to peripheral hyperglycemia. In addition, adipocyte hypertrophy, in particular within the visceral compartment (3), is associated with increased circulating concentrations of nonesterified free fatty acids (NEFA) (4) and increased production and release of pro-inflammatory cytokines (5). The infiltration of NEFA and pro-inflammatory cytokines liver and skeletal muscle results in development of insulin resistance in these tissues, and consequently, reduced glucose uptake by skeletal muscle (5) and increased hepatic glucose output (6). In addition, epigenetic changes and mitochondrial dysfunction in liver and skeletal muscle may also contribute to development of metabolic disorders

## References


1. Buettner R, Scholmerich J, Bollheimer LC (2007) High-fat diets: modeling the metabolic disorders of human obesity in rodents. Obesity 15:798–808
2. Portha B, Blondel O, Serradas P, McEvoy R, Giroix MH, Kergoat M, Bailbe D (1989) The rat models of non-insulin dependent diabetes induced by neonatal streptozotocin. Diabete Metab 15:61–75
3. Bray GA (2004) Medical consequences of obesity. J Clin Endocrinol Metab 89:2583–2589
4. Goralski KB, Sinal CJ (2007) Type 2 diabetes and cardiovascular disease: getting to the fat of the matter. Can J Physiol Pharmacol 85:113–132
5. Smith SR, Lovejoy JC, Greenway F, Ryan D, deJonge L, de la Bretonne J, Volafova J, Bray GA (2001) Contributions of total body fat, abdominal subcutaneous adipose tissue compartments, and visceral adipose tissue to the metabolic complications of obesity. Metabolism 50:425–435
6. Ravussin E, Smith SR (2002) Increased fat uptake, impaired fat oxidation, and failure of fat cell proliferation result in ectopic fat storage, insulin resistance, and type 2 diabetes. Ann N Y Acad Sci 967:363–378
7. Surwit R, Kuhn C, Cochrane C, McCubbin J, Feinglos M (1988) Diet-induced type II diabetes in C57BL/6J mice. Diabetes 37:1163–1167
8. Black BL, Croom J, Eisen EJ, Petro AE, Edwards CL, Surwit RS (1998) Differential effects of fat and sucrose on body composition in A/J and C57BL/6 mice. Metabolism 47:1354–1359
9. Roberts CK, Berger JJ, Barnard RJ (2002) Long-term effects of diet on leptin, energy intake, and activity in a model of diet-induced obesity. J Appl Physiol 93:887–893
10. Bayol SA, Farrington SJ, Stickland NC (2007) A maternal 'junk food' diet in pregnancy and lactation promotes an exacerbated taste for 'junk food' and a greater propensity for obesity in rat offspring. Br J Nutr 98:843–851
11. Taylor PD, McConnell J, Khan IY, Holemans K, Lawrence KM, Asare-Anane H, Persaud SJ, Jones PM, Petrie L, Hanson MA, Poston L (2005) Impaired glucose homeostasis and mitochondrial abnormalities in offspring of rats fed a fat-rich diet in pregnancy. Am J Physiol Regul Integr Comp Physiol 288: R134–R139
12. Ong ZY, Wanasuria AF, Lin MZP, Hiscock J, Muhlhausler BS (2013) Chronic intake of a cafeteria diet and subsequent abstinence. Sex-specific effects on gene expression in the mesolimbic reward system. Appetite 65:189–199
13. Reichelt AC, Morris MJ, Westbrook RF (2014) Cafeteria diet impairs expression of sensory-specific satiety and stimulus-outcome learning. Front Psychol 5:852
14. Hariri N, Thibault L (2010) High-fat diet-induced obesity in animal models. Nutr Res Rev 23:270–299
15. Flanagan AM, Brown JL, Santiago CA, Aad PY, Spicer LJ, Spicer MT (2008) High-fat diets promote insulin resistance through cytokine gene expression in growing female rats. J Nutr Biochem 19:505–513
16. Barbosa-da-Silva S, da Silva NC, Aguila MB, Mandarim-de-Lacerda CA (2013) Liver damage is not reversed during the lean period in diet-induced weight cycling in mice. Hepatol Res 18:12138
17. Flachs P, Rossmeisl M, Bryhn M, Kopecky J (2009) Cellular and molecular effects of n-3 polyunsaturated fatty acids on adipose tissue biology and metabolism. Clin Sci (Lond) 116:1–16
18. Muhlhausler BS, Cook-Johnson R, James M, Miljkovic D, Duthoit E, Gibson R (2010) Opposing effects of omega-3 and omega-6 long chain polyunsaturated fatty acids on the expression of lipogenic genes in omental and retroperitoneal adipose depots in the rat. J Nutr Metab
19. Ruzickova J, Rossmeisl M, Prazak T, Flachs P, Sponarova J, Veck M, Tvrzicka E, Bryhn M, Kopecky J (2004) Omega-3 PUFA of marine origin limit diet-induced obesity in mice by reducing cellularity of adipose tissue. Lipids 39:1177–1185
20. Massiera F, Guesnet P, Ailhaud G (2006) The crucial role of dietary n-6 polyunsaturated fatty acids in excessive adipose tissue development: relationship to childhood obesity. Nestle Nutr Workshop Ser Pediatr Program 57:235–242
21. Massiera F, Saint-Marc P, Seydoux J, Murata T, Kobayashi T, Narumiya S, Guesnet P, Amri E-Z, Negrel R, Ailhaud G (2003) Arachidonic acid and prostacyclin signaling promote adipose tissue development: a human health concern? J Lipid Res 44:271–279

22. Semple RK, Chatterjee VK, O'Rahilly S (2006) PPAR gamma and human metabolic disease. J Clin Invest 116:581–589
23. De Caterina R, Basta G (2001) n-3 Fatty acids and the inflammatory response — biological background. Eur Heart J Suppl 3:D42–D49
24. Chandalia M, Abate N (2007) Metabolic complications of obesity: inflated or inflamed? J Diabetes Complications 21:128–136
25. Malik VS, Popkin BM, Bray GA, Despres JP, Hu FB (2010) Sugar-sweetened beverages, obesity, type 2 diabetes mellitus, and cardiovascular disease risk. Circulation 121:1356–1364
26. Romaguera D, Norat T, Wark PA, Vergnaud AC, Schulze MB, van Woudenbergh GJ, Drogan D, Amiano P, Molina-Montes E, Sanchez MJ, Balkau B, Barricarte A, Beulens JW, Clavel-Chapelon F, Crispim SP, Fagherazzi G, Franks PW, Grote VA, Huybrechts I, Key TJ, Khaw KT, Nilsson P, Overvad K, Palli D, Panico S, Quiros JR, Rolandsson O, Sacerdote C, Sieri S, Slimani N, Spijkerman AM, Tjonneland A, Tormo MJ, Tumino R, van den Berg SW, Wermeling PR, Zamara-Ros R, Feskens EJ, Langenberg C, Sharp SJ, Foroughi NG, Riboli E, Wareham NJ (2013) Consumption of sweet beverages and type 2 diabetes incidence in European adults: results from EPIC-InterAct. Diabetologia 56:1520–1530
27. Johnson RK, Appel LJ, Brands M, Howard BV, Lefevre M, Lustig RH, Sacks F, Steffen LM, Wylie-Rosett J (2009) Dietary sugars intake and cardiovascular health: a scientific statement from the American Heart Association. Circulation 120:1011–1020
28. Te Morenga L, Mallard S, Mann J (2012) Dietary sugars and body weight: systematic review and meta-analyses of randomised controlled trials and cohort studies. BMJ 346: e7492
29. Willett WC, Ludwig DS (2013) Science souring on sugar. BMJ 346:e8077
30. McLennan W, Podger A (1998) National nutrition survey nutrient intakes and physical measurements 1995. Canberra, ACT, Australian Bureau of Statistics
31. Tappy L, Le KA (2010) Metabolic effects of fructose and the worldwide increase in obesity. Physiol Rev 90:23–46
32. Douard V, Ferraris RP (2013) The role of fructose transporters in diseases linked to excessive fructose intake. J Physiol 591:401–414
33. Lustig RH (2013) Fructose: it's "alcohol without the buzz". Adv Nutr 4:226–235
34. Tran LT, Yuen VG, McNeill JH (2009) The fructose-fed rat: a review on the mechanisms of fructose-induced insulin resistance and hypertension. Mol Cell Biochem 332:145–159
35. Pagliassotti MJ, Prach PA, Koppenhafer TA, Pan DA (1996) Changes in insulin action, triglycerides, and lipid composition during sucrose feeding in rats. Am J Physiol 271: R1319–R1326
36. Sheludiakova A, Rooney K, Boakes RA (2012) Metabolic and behavioural effects of sucrose and fructose/glucose drinks in the rat. Eur J Nutr 51:445–454
37. Chicco A, D'Alessandro ME, Karabatas L, Pastorale C, Basabe JC, Lombardo YB (2003) Muscle lipid metabolism and insulin secretion are altered in insulin-resistant rats fed a high sucrose diet. J Nutr 133:127–133
38. Oliveira LS, Santos DA, Barbosa-da-Silva S, Mandarim-de-Lacerda CA, Aguila MB (2014) The inflammatory profile and liver damage of a sucrose-rich diet in mice. J Nutr Biochem 25:193–200
39. Catena C, Giacchetti G, Novello M, Colussi G, Cavarape A, Sechi L (2003) Cellular mechanisms of insulin resistance in rats with fructose-induced hypertension. Am J Hypertens 16:973–978
40. Kazumi T, Odaka H, Hozumi T, Ishida Y, Amano N, Yoshino G (1997) Effects of dietary fructose or glucose on triglyceride production and lipogenic enzyme activities in the liver of Wistar fatty rats, an animal model of NIDDM. Endocr J 44:239–245
41. Levin BE, Hogan S, Sullivan AC (1989) Initiation and perpetuation of obesity and obesity resistance in rats. Am J Physiol Regul Integr Comp Physiol 256:R766–R771
42. Clegg DJ, Benoit SC, Reed JA, Woods SC, Dunn-Meynell A, Levin BE (2005) Reduced anorexic effects of insulin in obesity-prone rats fed a moderate-fat diet. Am J Physiol Regul Integr Comp Physiol 288:R981–R986
43. Levin BE, Dunn-Meynell AA, Balkan B, Keesey RE (1997) Selective breeding for diet-induced obesity and resistance in Sprague-Dawley rats. Am J Physiol Regul Integr Comp Physiol 273:R725–R730
44. Tkacs NC, Levin BE (2004) Obesity-prone rats have preexisting defects in their counter regulatory response to insulin-induced hypoglycemia. Am J Physiol Regul Integr Comp Physiol 287:R1110–R1115
45. Woods SC, Seeley RJ, Rushing PA, D'Alessio D, Tso P (2003) A controlled high-fat diet induces an obese syndrome in rats. J Nutr 133:1081–1087

46. Qiu L, List EO, Kopchick JJ (2005) Differentially expressed proteins in the pancreas of diet-induced diabetic mice. Mol Cell Proteomics 4:1311–1318
47. Corbett SW, Stern JS, Keesey RE (1986) Energy expenditure in rats with diet-induced obesity. Am J Clin Nutr 44:173–180
48. Yaqoob P, Sherrington EJ, Jeffery NM, Sanderson P, Harvey DJ, Newsholme EA, Calder PC (1995) Comparison of the effects of a range of dietary lipids upon serum and tissue lipid composition in the rat. Int J Biochem Cell Biol 27:297–310
49. Dandona P, Aljada A, Bandyopadhyay A (2004) Inflammation: the link between insulin resistance, obesity and diabetes. Trends Immunol 25:4–7
50. Higa TS, Spinola AV, Fonseca-Alaniz MH, Evangelista FSA (2014) Comparison between cafeteria and high-fat diets in the induction of metabolic dysfunction in mice. Int J Physiol Pathophysiol Pharmacol 6:47–54
51. Wassink AM, Olijhoek JK, Visseren FL (2007) The metabolic syndrome: metabolic changes with vascular consequences. Eur J Clin Invest 37:8–17
52. Shafrir E, Ziv E, Kalman R (2006) Nutritionally induced diabetes in desert rodents as models of type 2 diabetes: acomys cahirinus (spiny mice) and Psammomys obesus (desert gerbil). ILAR J 47:212–224
53. Kaiser N, Nesher R, Donath MY, Fraenkel M, Behar V, Magnan C, Ktorza A, Cerasi E, Leibowitz G (2005) Psammomys obesus, a model for environment-gene interactions in type 2 diabetes. Diabetes 54:S137–S144
54. Maislos M, Medvedovskv V, Sztarkier I, Yaari A, Sikuler E (2006) Psammomys obesus (sand rat), a new animal model of non-alcoholic fatty liver disease. Diabetes Res Clin Pract 72:1–5
55. Barker DJP, Bull AR, Osmond C, Simmonds SJ (1990) Fetal and placental size and risk of hypertension in adult life. Br Med J 301:259–262
56. Hales CN, Barker DJP (2001) The thrifty phenotype hypothesis. Br Med Bull 60:5–20
57. McMillen IC, Robinson JS (2005) Developmental origins of the metabolic syndrome: prediction, plasticity, and programming. Physiol Rev 85:571–633
58. Ravelli AC, van der Meulen JH, Osmond C, Barker DJ, Bleker OP (1999) Obesity at the age of 50 y in men and women exposed to famine prenatally. Am J Clin Nutr 70:811–816
59. Ravelli ACJ, van der Meulen JHP, Michels RPJ, Osmond C, Barker DJP, Hales CN, Bleker OP (1998) Glucose tolerance in adults after prenatal exposure to famine. Lancet 351:173–177
60. Pettit DJ, Knowler WC (1998) Long-term effects of the intrauterine environment, birth weight, and breast-feeding in Pima Indians. Diabetes Care 21:B138–B141
61. Rkhzay-Jaf J, O'Dowd JF, Stocker CJ (2012) Maternal obesity and the fetal origins of the metabolic syndrome. Curr Cardiovasc Risk Rep 6:487–495
62. Muhlhausler BS, Ong ZY (2011) The fetal origins of obesity: early origins of altered food intake. Endocr Metab Immune Disord Drug Targets 11:189–197
63. Bavdekar A, Yajnik C, Fall C, Bapat S, Pandit A, Deshpande V, Bhave S, Kellingray S, Joglekar C (1999) Insulin resistance syndrome in 8-year-old Indian children: small at birth, big at 8 years, or both? Diabetes 48:2422–2429
64. McMillen IC, Adam CL, Muhlhausler BS (2005) Early origins of obesity: programming the appetite regulatory system. J Physiol 565:9–17
65. Hales CN, Barker DJP (2001) The thrifty phenotype hypothesis: type 2 diabetes. Br Med Bull 60:5–20
66. Holemans K, Verhaeghe J, Dequeker J, Van Assche FA (1996) Insulin sensitivity in adult female rats subjected to malnutrition during the perinatal period. J Soc Gynecol Investig 3:71–77
67. Thompson NM, Norman AM, Donkin SS, Shankar RR, Vickers MH, Miles JL, Breier BH (2007) Prenatal and postnatal pathways to obesity: different underlying mechanisms, different metabolic outcomes. Endocrinol Metab Clin North Am 148:2345–2354
68. Ozanne SE (2001) Metabolic programming in animals: type 2 diabetes. Br Med Bull 60:143–152
69. Ozanne SE, Jensen CB, Tingey KJ, Storgaard H, Madsbad S, Vaag AA (2005) Low birthweight is associated with specific changes in muscle insulin-signalling protein expression. Diabetologia 48:547–552
70. Hales CN, Desai M, Ozanne SE, Crowther NJ (1996) Fishing in the stream of diabetes: from measuring insulin to the control of fetal organogenesis. Biochem Soc Trans 24:341–350
71. Petry CJ, Ozanne SE, Wang CL, Hales CN (1997) Early protein restriction and obesity independently induce hypertension in 1-year-old rats. Clin Sci (Lond) 93:147–152
72. Snoeck A, Remacle C, Reusens B, Hoet JJ (1990) Effect of a low protein diet during

pregnancy on the fetal rat endocrine pancreas. Biol Neonate 57:107–118

73. Ozanne SE, Smith GD, Tikerpae J, Hales CN (1996) Altered regulation of hepatic glucose output in the male offspring of protein-malnourished rat dams. Am J Physiol Endocrinol Metab 270:E559–E564
74. Ozanne SE, Nave BT, Wang CL, Shepherd PR, Prins J, Smith GD (1997) Poor fetal nutrition causes long-term changes in expression of insulin signaling components in adipocytes. Am J Physiol Endocrinol Metab 273: E46–E51
75. Ozanne SE, Wang CL, Coleman N, Smith GD (1996) Altered muscle insulin sensitivity in the male offspring of protein-malnourished rats. Am J Physiol Endocrinol Metab 271: E1128–E1134
76. Ozanne SE, Olsen GS, Hansen LL, Tingey KJ, Nave BT, Wang CL, Hartil K, Petry CJ, Buckley AJ, Mosthaf-Seedorf L (2003) Early growth restriction leads to down regulation of protein kinase C zeta and insulin resistance in skeletal muscle. J Endocrinol 177:235–241
77. Wadley GD, Siebel AL, Cooney GJ, McConell GK, Wlodek ME, Owens JA (2008) Uteroplacental insufficiency and reducing litter size alters skeletal muscle mitochondrial biogenesis in a sex-specific manner in the adult rat. Am J Physiol Endocrinol Metab 294:E861–E869
78. Siebel AL, Mibus A, De Blasio MJ, Westcott KT, Morris MJ, Prior L, Owens JA, Wlodek ME (2008) Improved lactational nutrition and postnatal growth ameliorates impairment of glucose tolerance by uteroplacental insufficiency in male rat offspring. Endocrinology 149:3067–3076
79. Poston L (2011) Intergenerational transmission of insulin resistance and type 2 diabetes. Prog Biophys Mol Biol 106:315–322
80. Srinivasan M, Katewa SD, Palaniyappan A, Pandya JD, Patel MS (2006) Maternal high-fat diet consumption results in fetal malprogramming predisposing to the onset of metabolic syndrome-like phenotype in adulthood. Am J Physiol Endocrinol Metab 291: E792–E799
81. Cerf ME, Muller CJ, Du Toit DF, Louw J, Wolfe-Coote SA (2006) Hyperglycaemia and reduced glucokinase expression in weanling offspring from dams maintained on a high-fat diet. Br J Nutr 95:391–396
82. Muhlhausler BS, Adam CL, Findlay PA, Duffield JA, McMillen IC (2006) Increased maternal nutrition alters development of the appetite-regulating network in the brain. FASEB J 20:1257–1259
83. Samuelsson A-M, Matthews PA, Argenton M, Christie MR, McConnell JM, Jansen EHJM, Piersma AH, Ozanne SE, Twinn DF, Remacle C, Rowlerson A, Poston L, Taylor PD (2008) Diet-induced obesity in female mice leads to offspring hyperphagia, adiposity, hypertension, and insulin resistance: a novel murine model of developmental programming. Hypertension 51:383–392
84. Muhlhausler BS, Roberts CT, McFarlane JR, Kauter KG, McMillen IC (2002) Fetal leptin is a signal of fat mass independent of maternal nutrition in ewes fed at or above maintenance energy requirements. Biol Reprod 67:493–499
85. Bruce KD, Cagampang FR, Argenton M, Zhang J, Ethirajan PL, Burdge GC, Bateman AC, Clough GF, Poston L, Hanson MA, McConnell JM, Byrne CD (2009) Maternal high-fat feeding primes steatohepatitis in adult mice offspring, involving mitochondrial dysfunction and altered lipogenesis gene expression. Hepatology 50:1796–1808
86. Srinivasan M, Aalinkeel R, Song F, Mitrani P, Pandya JD, Strutt B, Hill DJ, Patel MS (2006) Maternal hyperinsulinemia predisposes rat fetuses for hyperinsulinemia, and adult-onset obesity and maternal mild food restriction reverses this phenotype. Am J Physiol Endocrinol Metab 290:E129–E134
87. Cerf ME, Williams K, Chapman CS, Louw J (2007) Compromised beta-cell development and beta-cell dysfunction in weanling offspring from dams maintained on a high-fat diet during gestation. Pancreas 34:347–353
88. McCurdy CE, Bishop JM, Williams SM, Grayson BE, Smith MS, Friedman JE, Grove KL (2009) Maternal high-fat diet triggers lipotoxicity in the fetal livers of nonhuman primates. J Clin Invest 119:323–335
89. Ailhaud G, Massiera F, Weill P, Legrand P, Alessandri JM, Guesnet P (2006) Temporal changes in dietary fats: role of n-6 polyunsaturated fatty acids in excessive adipose tissue development and relationship to obesity. Prog Lipid Res 45:203–236
90. Muhlhausler BS, Ailhaud GP (2013) Omega-6 polyunsaturated fatty acids and the early origins of obesity. Curr Opin Endocrinol Diabetes Obes 20:56–61
91. Massiera F, Barbry P, Guesnet P, Joly A, Luquet S, Moreilhon-Brest C, Mohsen-Kanson T, Amri E-Z, Ailhaud G (2010) A Western-like fat diet is sufficient to induce a gradual enhancement in fat mass over generations. J Lipid Res 51:2352–2361
92. Muhlhausler BS, Gibson RA, Makrides M (2011) The effect of maternal omega-3

long-chain polyunsaturated fatty acid (n-3 LCPUFA) supplementation during pregnancy and/or lactation on body fat mass in the offspring: a systematic review of animal studies. Prostaglandins Leukot Essent Fatty Acids 85:83–88

93. Muhlhausler BS, Gibson RA, Makrides M (2010) Effect of long-chain polyunsaturated fatty acid supplementation during pregnancy or lactation on infant and child body composition: a systematic review. Am J Clin Nutr 92:857–863
94. Muhlhausler BS, Miljkovic D, Fong L, Xian CJ, Duthoit E, Gibson RA (2011) Maternal omega-3 supplementation increases fat mass in male and female rat offspring. Front Genet 2:48
95. Chen L, Hu FB, Yeung E, Willett W, Zhang C (2009) Prospective study of pre-gravid sugar-sweetened beverage consumption and the risk of gestational diabetes mellitus. Diabetes Care 32:2236–2241
96. Phelan S, Hart C, Phipps M, Abrams B, Schaffner A, Adams A, Wing R (2011) Maternal behaviors during pregnancy impact offspring obesity risk. Exp Diabetes Res 985139:26
97. Toop CR, Muhlhausler BS, O'Dea K, Gentili S (2014) Consumption of sucrose, but not high fructose corn syrup, leads to increased adiposity and dyslipidaemia in the pregnant and lactating rat. J Dev Orig Health Dis 19:1–9
98. Goran MI, Dumke K, Bouret SG, Kayser B, Walker RW, Blumberg B (2013) The obesogenic effect of high fructose exposure during early development. Nat Rev Endocrinol 9:494–500
99. Sloboda DM, Li M, Patel R, Clayton ZE, Yap C, Vickers MH (2014) Early life exposure to fructose and offspring phenotype: implications for long term metabolic homeostasis. J Obesity 203474:23
100. Vickers MH, Clayton ZE, Yap C, Sloboda DM (2011) Maternal fructose intake during pregnancy and lactation alters placental growth and leads to sex-specific changes in fetal and neonatal endocrine function. Endocrinology 152:1378–1387
101. Mukai Y, Kumazawa M, Sato S (2013) Fructose intake during pregnancy up-regulates the expression of maternal and fetal hepatic sterol regulatory element-binding protein-1c in rats. Endocrine 44:79–86
102. Rodriguez L, Panadero MI, Roglans N, Otero P, Alvarez-Millan JJ, Laguna JC, Bocos C (2013) Fructose during pregnancy affects maternal and fetal leptin signaling. J Nutr Biochem 24:1709–1716
103. Samuelsson AM, Matthews PA, Jansen E, Taylor PD, Poston L (2013) Sucrose feeding in mouse pregnancy leads to hypertension, and sex-linked obesity and insulin resistance in female offspring. Front Physiol 4:14
104. Regnault TR, Gentili S, Sarr O, Toop CR, Sloboda DM (2013) Fructose, pregnancy and later life impacts. Clin Exp Pharmacol Physiol 40:824–837
105. Muhlhausler BS, Duffield JA, McMillen IC (2007) Increased maternal nutrition stimulates peroxisome proliferator activated receptor-{gamma} (PPAR{gamma}), adiponectin and leptin mRNA expression in adipose tissue before birth. Endocrinology 148:878–885
106. Kasser TR, Martin RJ, Allen CE (1981) Effect of gestational alloxan diabetes and fasting on fetal lipogenesis and lipid deposition in pigs. Biol Neonate 40:105–112
107. Ezekwe MO, Martin RJ (1980) The effects of maternal alloxan diabetes on body composition, liver enzymes and metabolism and serum metabolites and hormones of fetal pigs. Horm Metab Res 12:136–139
108. Bayol SA, Simbi BH, Bertrand JA, Stickland NC (2008) Offspring from mothers fed a 'junk food' diet in pregnancy and lactation exhibit exacerbated adiposity that is more pronounced in females. J Physiol 586:3219–3230
109. Muhlhausler B, Smith SR (2009) Early-life origins of metabolic dysfunction: role of the adipocyte. Trends Endocrinol Metab 20:51–57
110. Padoan A, Rigano S, Ferrazzi E, Beaty BL, Battaglia FC, Galan HL (2004) Differences in fat and lean mass proportions in normal and growth-restricted fetuses. Am J Obstet Gynecol 191:1459–1464
111. Crescenzo R, Samec S, Antic V, Rohner-Jeanrenaud F, Seydoux J, Montani J-P, Dulloo AG (2003) A role for suppressed thermogenesis favoring catch-up fat in the pathophysiology of catch-up growth. Acta Paediatr 52:1090–1097
112. Ibanez L, Ong K, Dunger DB, de Zegher F (2006) Early development of aiposity and insulin resistance after catch-up weight gain in small-for-gestational-age children. J Clin Endocrinol Metab 91:2153–2158
113. Jaquet D, Gaboriau A, Czernichow P, Levy-Marchal C (2000) Insulin resistance early in adulthood in subjects born with intrauterine growth retardation. J Clin Endocrinol Metab 85:1401–1406

114. De Blasio MJ, Gatford KL, McMillen IC, Robinson JS, Owens JA (2006) Placental restriction of fetal growth increases insulin action, growth and adiposity in the young lamb. Endocrinology 148:1350–1358
115. De Blasio MJ, Gatford KL, Robinson JS, Owens JA (2007) Placental restriction of fetal growth reduces size at birth and alters postnatal growth, feeding activity, and adiposity in the young lamb. Am J Physiol Regul Integr Comp Physiol 292:R875–R886
116. Ozanne SE (2001) Metabolic programming in animals. Br Med Bull 60:143–152
117. Kind KL, Clifton PM, Grant PA, Owens PC, Sohlstrom A, Roberts CT, Robinson JS, Owens JA (2003) Effect of maternal feed restriction during pregnancy on glucose tolerance in the adult guinea pig. Am J Physiol Regul Integr Comp Physiol 284:R140–R152
118. Alexander G (1978) Quantitative development of adipose tissue in foetal sheep. Aust J Biol Sci 31:489–503
119. Merklin RJ (1973) Growth and distribution of human fetal brown fat. Anat Res 178:637–646
120. Højlund K, Mogensen M, Sahlin K, Beck-Nielsen H (2008) Mitochondrial dysfunction in type 2 diabetes and obesity. Endocrinol Metab Clin North Am 37:713–731
121. Howie GJ, Sloboda DM, Reynolds CM, Vickers MH (2013) Timing of maternal exposure to a high fat diet and development of obesity and hyperinsulinemia in male rat offspring: same metabolic phenotype, different developmental pathways? J Nutr Metab 517384:13
122. Palmer AC (2011) Nutritionally mediated programming of the developing immune system. Adv Nutr 2:377–395
123. Zhu MJ, Du M, Nathanielsz PW, Ford SP (2010) Maternal obesity up-regulates inflammatory signaling pathways and enhances cytokine expression in the mid-gestation sheep placenta. Placenta 31:387–391
124. Murabayashi N, Sugiyama T, Zhang L, Kamimoto Y, Umekawa T, Ma N, Sagawa N (2013) Maternal high-fat diets cause insulin resistance through inflammatory changes in fetal adipose tissue. Eur J Obstet Gynecol Reprod Biol 169:39–44
125. Junien C, Gallou-Kabani C, Vigé A, Gross MS (2005) Nutritional epigenomics: consequences of unbalanced diets on epigenetics processes of programming during lifespan and between generations. Ann Endocrinol (Paris) 66:S19–S28
126. Gallou-Kabani C, Junien C (2005) Nutritional epigenomics of metabolic syndrome: new perspective against the epidemic. Diabetes 54:1899–1906
127. Waterland RA, Travisano M, Tahiliani KG, Rached MT, Mirza S (2008) Methyl donor supplementation prevents transgenerational amplification of obesity. Int J Obes (Lond) 32:1373–1379
128. Burdge GC, Hanson MA, Slater-Jefferies JL, Lillycrop KA (2007) Epigenetic regulation of transcription: a mechanism for inducing variations in phenotype (fetal programming) by differences in nutrition during early life? Br J Nutr 97:1036–1046
129. Burdge GC, Slater-Jefferies J, Torrens C, Phillips ES, Hanson MA, Lillycrop KA (2007) Dietary protein restriction of pregnant rats in the F0 generation induces altered methylation of hepatic gene promoters in the adult male offspring in the F1 and F2 generations. Br J Nutr 97:435–439
130. Tobi EW, Slagboom PE, van Dongen J, Kremer D, Stein AD, Putter H, Heijmans BT, Lumey LH (2012) Prenatal famine and genetic variation are independently and additively associated with DNA methylation at regulatory loci within IGF2/H19. PLoS One 7:30
131. Hanley B, Dijane J, Fewtrell M, Grynberg A, Hummel S, Junien C, Koletzko B, Lewis S, Renz H, Symonds M, Gros M, Harthoorn L, Mace K, Samuels F, van Der Beek EM (2010) Metabolic imprinting, programming and epigenetics – a review of present priorities and future opportunities. Br J Nutr 104:S1–S25
132. Heerwagen MJR, Miller MR, Barbour LA, Friedman JE (2010) Maternal obesity and fetal metabolic programming: a fertile epigenetic soil. Am J Physiol 299:R711–R722
133. Li CC, Maloney CA, Cropley JE, Suter CM (2010) Epigenetic programming by maternal nutrition: shaping future generations. Epigenomics 2:539–549
134. Li CC, Young PE, Maloney CA, Eaton SA, Cowley MJ, Buckland ME, Preiss T, Henstridge DC, Cooney GJ, Febbraio MA, Martin DI, Cropley JE, Suter CM (2013) Maternal obesity and diabetes induces latent metabolic defects and widespread epigenetic changes in isogenic mice. Epigenetics 8:602
135. Haslam DW, James WP (2005) Obesity. Lancet 366:1197–1209

# Chapter 4

# Cheminformatics in the Identification of Drug Classes for the Treatment of Type 2 Diabetes

**Paul W. Finn**

## Abstract

Computer-Aided Drug Design has developed into a powerful suite of methods that complement experimental approaches to the identification of new pharmacologically active compounds. In particular, virtual screening has become a standard tool for lead identification. Diverse examples of the application of virtual screening applied to T2DM target proteins have been reported. While several of these indicate successful identification of new lead compounds from synthetic chemical and natural product databases, many of them have been performed on a small scale and with limited validation. Careful study design and collaboration with cheminformaticians and computational chemists will enable these approaches to fulfil their potential for T2DM.

**Key words** Cheminformatics, Virtual screening, Molecular modeling, Chemical database

## 1 Introduction

The goal of Computer-Aided Drug Design (CADD) is to use computational approaches to understand the relationship between the chemical structures of drug molecules and their biological activities, and to use this understanding to assist in identifying new and improved compounds. CADD began in the 1960s with simple statistical regression models. As our theoretical understanding of molecular interactions and the processing power of computers has increased, CADD has grown in scope and sophistication to now encompass a large toolbox of machine learning and simulation methods.

One of the most widely used CADD methods is "virtual screening." Virtual screening simulates experimental testing; in particular, the High-Throughput Screening performed in Pharma and Biotech companies. To perform a virtual screen, two components are required. The first is a cheminformatics database, which stores the compounds' chemical structures, names (identifiers), and typically a range of computed and/or experimentally determined

Claire J. Stocker (ed.), *Type 2 Diabetes: Methods and Protocols*, Methods in Molecular Biology, vol. 2076,
https://doi.org/10.1007/978-1-4939-9882-1_4, 

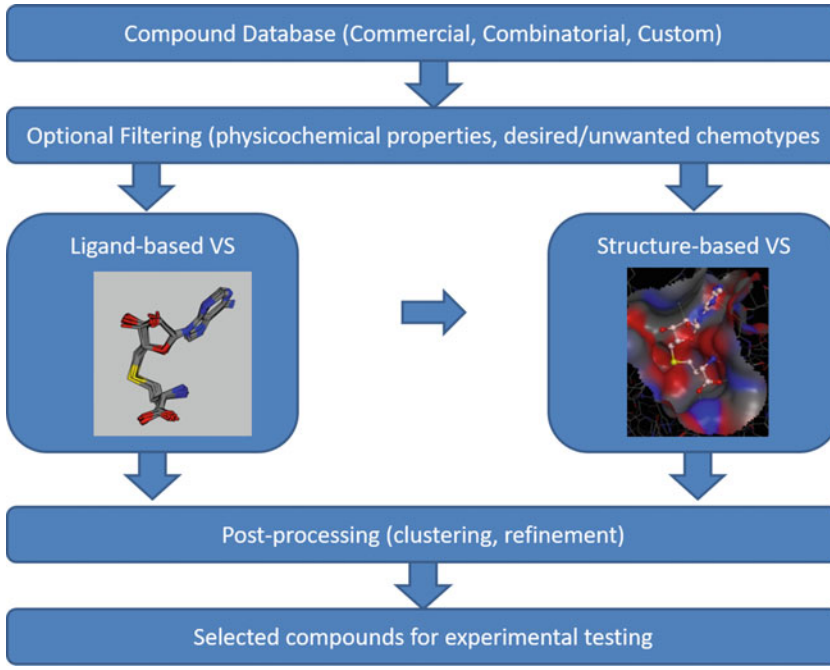


**Fig. 1** A typical virtual screening pipeline. An input database, which may contain tens of millions of unique chemical structures, is searched against either a ligand or structure-based model of activity. Typically, the initial rank-ordered list of "hits" is further processed by additional cheminformatic criteria and by manual selection to identify the compounds to be tested experimentally. The final numbers chosen range from a handful to several hundreds or thousands

chemical properties. The second is a computer model of the requirements for a particular biological activity. A diverse range of models have been used, but they can be categorized at a high level into two main classes. *Ligand-based virtual screening* compares the database compounds to a query compound of known activity through a quantitative measure of molecular similarity. The similarity metric could, for example, be overall molecular shape or a geometric pattern of interaction features (known as a pharmacophore) the presence of which in a compound confers the desired biological activity. *Structure-based virtual screening* assesses the shape and property complementarity of each database compound to a binding site (usually the active site, but possibly an allosteric site) of a target protein (Fig. 1).

One of the main driving forces behind the development of virtual screening methods has been the exponential growth in the availability of experimental data on which these methods can be applied. Protein X-ray crystallography methodology and investment in structural genomics initiatives are delivering the atomic resolution three-dimensional structures of the protein targets of drugs at an ever-increasing rate (Fig. 2), such that in 2016, over 10,000 new protein X-ray structures were deposited in the Protein Data Bank.

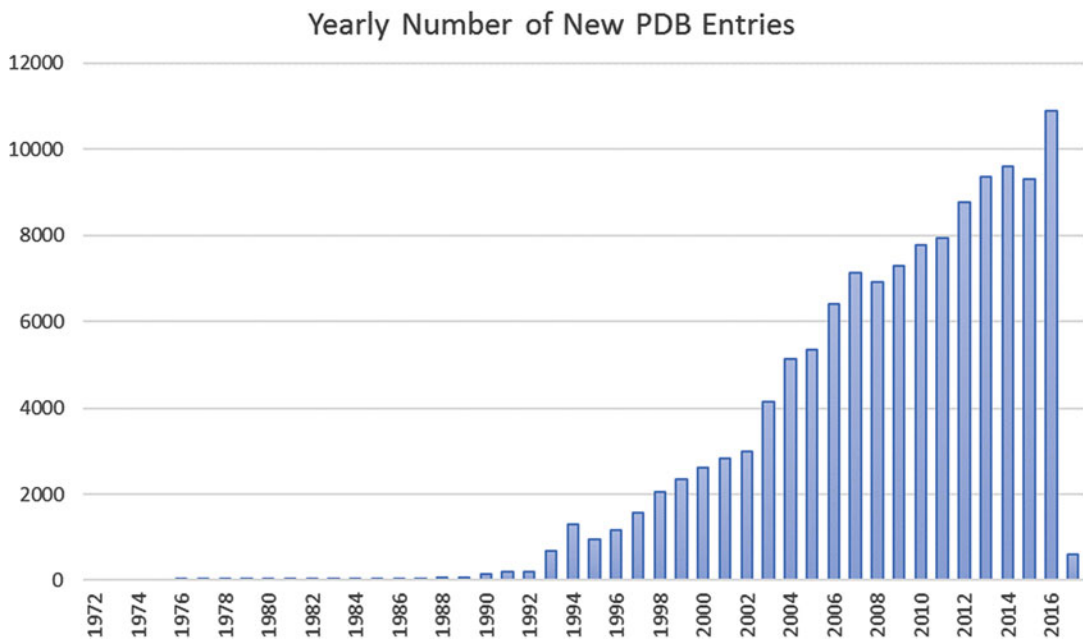


**Fig. 2** Since the mid-1990s there has been continual growth in the number of new protein structures that can be used as input to computational methods

Equally important has been the growth in public domain sources of chemical structure databases of commercially available and literature compounds. The popular ZINC database [1] is in the public domain and contains approximately 4.5 million chemical structures appropriate for virtual screening experiments and available for commercial suppliers. Other examples of useful cheminformatics databases include ChemSpider [2], maintained by the UK Royal Society of Chemistry, which includes information on over 30 million structures collated from over 450 data sources, including analytical data and literature and patent references and ChEMBL [3], a database of over 1.5 million compounds combining chemical structure and biological activity data mostly extracted from the open scientific literature. A non-exhaustive summary of software tools and databases for virtual screening is provided in Table 1.

Type 2 diabetes (T2DM) is a complex disease presenting a great variety of potential drug targets. Many of these can be investigated by CADD methodologies. The remaining sections of this review chapter summarize some of the recent T2DM CADD literature to provide an overview of the scope of these methods to uncover new chemotypes (drug classes) as lead compounds for drug discovery and development. While there are a number of success stories in the drug discovery literature, CADD methods, and their application are far from mature technologies and there are many pitfalls to their successful application. Some of these

**Table 1**
**Tools and databases for virtual screening**

| | |
|---|---|
| *Structure-based virtual screening* | |
| AutoDock/autodock vina | Autdock.scripps.edu |
| Dock | Dock.compbio.ucsf.edu/Overview_of_DOCK/index.htm |
| GOLD | www.ccdc.cam.ac.uk/solutions/csd-discovery/components/gold/ |
| Glide | www.schrodinger.com/Glide |
| FlexX | www.biosolveit.de/flexx/index.htm |
| Blaster | Blaster.docking.org |
| *Ligand-based virtual screening* | |
| Pharmer | smoothdock.ccbb.pitt.edu/pharmer/ |
| LiSiCa | insilab.org/lisica/ |
| LigandScout | www.inteligand.com/ligandscout/ |
| *Compound databases* | |
| Zinc | zinc15.docking.org/ |
| ChEMBL | www.ebi.ac.uk/chembl/ |
| ChemSpider | www.chemspider.com |
| DrugBank | www.drugbank.ca |

limitations are highlighted in the context of T2DM studies in the hope that this will be helpful to diabetes researchers stimulated to apply CADD in their own research.

## 2 Virtual Screening

There are many examples in the literature of the use of virtual screening and related approaches to identify novel compounds with the potential to treat type 2 diabetes. It is not possible to provide a detailed review of this extensive literature, but the following recent examples provide an impression of the current state-of-the-art.

Virtual screening and "core-hopping" studies have been reported to find dual agonists of PPAR-α and PPAR-γ. One study was based on GW409554 [4] and the other employed the ZINC screening database [5]. The protocol combines multiple computational approaches and included prediction of ADME properties, resulting in the design of ten putative dual agonists in each case. Using similar methods, the same group has recently reported the design of a multitargeted PPARα/γ/δ pan agonist [6]. However, no experimental confirmation of the design ideas is reported in any

of these publications, and thus, the hypotheses must currently be regarded as speculative given the current limited performance of computational design approaches.

In another application of the ZINC database, a combination of QSAR and docking methods was used to perform virtual screening of more than 25 million compounds in the ZINC library. The QSAR model was developed using 1,517 compounds, identifying 42,378 potential PPARγ agonists. Of these, 10,000 were selected for docking with PPARγ based on their diversity. Several steps were used to refine the docking results, and finally 30 potentially highly active ligands were identified. Four compounds were subsequently tested for their in vitro activity, with one compound found to have a $K_i$ value of $<5$ μM [7].

Tanwar et al. [8] performed structure-based virtual screening against dipeptidyl peptidase IV using the Molecular Diversity Preservation International (MDPI) database and the docking programs Glide and GOLD. Six hits were tested for DPP-IV inhibition, of which the most potent had an $IC_{50}$ of 0.73 μM and glucose lowering effects in fed hyperglycemic female Wistar rats. For the same target, pharmacophore-based virtual screening against the NCI database identified a small number of hits, although activity was very weak with the most potent compound, paroxetine, showing only 20% inhibition at 10 μM.

Another widely studied diabetes target is aldose reductase (AR). AR is an aldo–keto reductase that has been widely investigated as an enzyme crucially involved in the pathogenesis of chronic complications associated with diabetes mellitus as well as acting as a key mediator of oxidative and inflammatory signaling pathways involved in the development of other human pathologies, such as cardiovascular disorders, sepsis, and cancer [9]. Wang et al. [10] have described the identification of novel aldose reductase inhibitors through virtual screening. Notable aspects of this study are the use of multiple binding site conformations and the extensive use of molecular dynamics, a computationally expensive process which require the use of Graphics-Processor-Unit (GPU) hardware to make the computation tractable. The library screened was very small for a virtual screening experiment, at only 7,249 compounds, but a respectable 14% hit rate was obtained.

The farnesoid X receptor (FXR), a ligand-dependent transcription factor of the nuclear hormone receptor superfamily, is involved in the regulation of glucose and lipid metabolism and is thus a potential target for T2DM and other metabolic diseases. Workers at the University of Innsbruck and their collaborators have undertaken a thorough pharmacophore-based approach to discover FXR agonists. Pharmacophore models were developed based on multiple structures available in the PDB. Known FXR agonists were obtained from ChEMBL-DB (FXR-Actives, 221 compounds) as were a property-matched set of inactive compounds (FXR-Decoys,

5,598 compounds). Property matching involves ensuring that the inactive compounds display a similar distribution of physicochemical and pharmacophoric feature ranges (logP, molecular weight, hydrogen bonds, etc.). If this is not done, then it is easy to develop computer models that distinguish actives from inactives on the basis of these simple properties, but such models have no predictive value. Three other databases were also used in this study, DrugBank [11] and an in-house "Virtual DB" were used for validation and the NCI Developmental Therapeutics Program database for prediction. Validation studies on these datasets enabled the selection of the best-performing pharmacophore models and the selection of virtual screening hits from the NCI database for biological testing. Only eight compounds were tested; two showed dose-dependent FXR agonism, with the remaining six being inactive [12]. The same approach was also applied to the identification of novel FXR agonists from natural sources (see below).

## 3 Natural Products

A significant percentage of small molecule drugs are either natural products or natural product derivatives. Plants and plant extracts have been used since ancient times for the treatment of T2DM, with a great number of species being used [13].

Historically, many of the sources of natural product used for experimental screening consisted of uncharacterized or only partly characterized samples. This limited the potential for computational virtual screening approaches, which typically require a well-defined chemical structure to associate with the screening sample. However, a number of natural product computer databases have now been developed, for example, the Analyticon database of over 5,000 natural products is available for download (www.ac-discovery.com) and several other companies maintain natural product databases. The website Super Natural II (bioinf-applied.charite.de/supernatural_new/index.php) allows access to a database of 325,508 natural compounds through collecting offerings from a number of commercial suppliers and academic collections.

There are a number of literature reports of efforts to explore the PPAR-γ-activating potential of a wide range of natural products originating from traditionally used medicinal plants or dietary sources. Cheminformatics approaches have been applied to natural product databases and again PPAR-γ has been a frequently used target structure.

Fakhrudin et al. [14] used a structure-based pharmacophore model to screen natural compound databases. The model was based on the PDB entry identifier 2G0G and consists of three hydrophobic features, one aromatic ring, one hydrogen bond acceptor, and exclusion volume spheres lining the ligand-binding domain of

PPAR-γ. Sixty-one hits were identified, including several neolignans, including magnolol, as partial PPAR-γ agonists with $EC_{50}$ values in the low micromolar or submicromolar range and the ability to induce adipocyte differentiation in 3T3-L1 adipocytes. The prediction that magnolol binds to PPAR-γ was subsequently confirmed by X-ray crystallography, although the binding mode was different from that predicted by modeling [15]. Magnolol was also demonstrated to bind to the RXRα receptor, indicating potential polypharmacology (see below). Subsequently [16], further computational modeling experiments identified another natural product neolignan, honokiol, a major constituent of the traditional Chinese herbal drug Magnolia bark. Honokiol was reported to directly bind to the purified human PPARγ ligand-binding domain in vitro with a $K_i$ of 22.86 μM, but unlike previously identified neolignans, it did not induce PPAR-γ-dependent lipid accumulation in 3T3-L1 adipocytes. However, other reports question the ability of honokiol to interact directly with PPAR receptors [17]. Also, using a structure-based pharmacophore model, in this case based on the common interactions of four different agonists with the PPARγ structure, Tanrikulu et al. [18] screened the Analyticon database, leading to the discovery of two α-santonin derivatives as PPARγ activators.

In another example [19], a ligand-derived PPARγ pharmacophore was created, starting from an analysis of 13 selective partial agonists. The derived pharmacophore, simpler than the structure-based one as it consists only of a hydrogen bond acceptor and three hydrophobic features, was used to search the Chinese Natural Product Database, comprising over 57,000 constituents of Traditional Chinese Medicine. One compound selected from the hitlist, methyl oleanonate, is found in Chios mastic gum. The acid of methyl oleanonate, oleanonic acid, was identified as a modestly active PPARγ agonist through bioassay-guided chromatographic fractionation of Chios mastic gum fractions.

Rupp et al. [20] used a machine learning method, descriptor-based Gaussian process regression, to search for PPARγ agonists based on a data set of 144 published PPAR-γ ligands. Fifteen compounds were selected for experimental testing in PPAR-α and PPAR-γ agonist assays, based on a combination of their performance in the prediction models and manual selection. Eight of these exhibited agonist activity toward at least one of the receptors. The most active compound, a truxillic acid derivative, was a selective PPAR-γ agonist with an $EC_{50}$ of 10 μM.

Lewis et al. [21] used docking to evaluate various natural products as putative PPARγ agonists. They were able to demonstrate a docking pose for α-eleostearic acid, a conjugated triene, and a compound already known as an activator of PPARγ [22].

A further structure-based virtual screening study [23] of the PPARγ- ligand-binding domain against a natural product library

identified 29 potential agonists. Of these, six flavonoids stimulated PPARγ transcriptional activity in a transcriptional factor assay with the most potent, psi-baptigenin-possessing an $EC_{50}$ of 2.9 μM. Evidence that the compound was working through the intended mechanism of action was provided by the finding that psi-baptigenin's-induced PPARγ activity was abolished in the presence of a selective PPARγ antagonist, GW9662.

Much of the computational analysis of natural product libraries has focused on PPAR-γ as the molecular target, but other proteins have also been investigated. Building on their previously developed FXR pharmacophore work (see above) Grienke et al. have explored an in-house Chinese Herbal Medicine database. This identified mainly lanostane-type triterpenes of the fungus *Ganoderma lucidum* Karst as putative FXR ligands. Extracts of *Ganoderma* fruit bodies and isolated compounds exhibited FXR inducing effects at 100 μg/mL.

DPP-IV inhibitors from natural sources have also been studied [24]. Starting with a database of 89,000 natural compounds taken from ZINC, a structure-derived pharmacophore and docking study identified 446 potential hit compounds. To focus on those compounds that contained novel elements, the hitlist was merged with 2,342 known DPP-IV inhibitors taken from the BindingDB database [25] and clustered based on 2D structural fingerprints. Of the resulting 50 clusters, 12 exclusively contained natural products. A total of nine compounds were selected from seven of these 12 clusters and tested in an in vitro assay. The compounds showed activity, but were tested at very high concentrations (between 100 μM and 1 mM). A computational analysis suggested analogues with predicted higher binding affinity, but no compounds were synthesized or tested. The weak affinity of the identified compounds and the lack of any experimental confirmation of the proposed binding mode make the conclusions drawn highly speculative at this time. A follow-up study suggested further compounds from natural extracts as DPP-IV inhibitors, but without any supporting evidence [26].

An alternative strategy to the search for natural product antidiabetic compounds has been described by Pathania et al. [27]. Here, the search was focused on compounds contained in a specific plant *Rauvolfia serpentina*, a medicinal plant endemic to the Himalayas known to be effective in relieving diabetes and its complications. This focus naturally led to a rather small dataset of compounds, only 142 unique chemical structures. The search specifically focused on the identification of putative inhibitors of aldose reductase. Docking studies against a high-resolution aldose reductase crystal structure were followed by molecular dynamics refinement, leading to two indole alkaloids, indobine and indobinine being suggested as novel aldose reductase inhibitors. The computational characterization of the compounds is relatively thorough,

but the conclusions are again unsupported by experimental validation. It can be difficult, of course, to obtain sufficient sample of well-characterized natural products. The authors, however, suggest structurally related compounds from the ZINC database that they also predict to be active through the same screening workflow. Such compounds are often available commercially at modest cost for a screening sample. Testing these commercial compounds could have been an effective way to add support to their conclusions.

## 4 Polypharmacology

The vast majority of drug discovery activities undertaken over the last 50 years have conformed to the classical one-compound–one-target paradigm derived from the "magic bullet" hypothesis of Ehrlich [28]. Nonetheless, modulation of unintended targets that can play a fundamental role in explaining pharmacological profiles, for example, of drugs acting on the central nervous system, which can bind to many different receptors [29] and for some multi-kinase inhibitors in oncology [30]. In many cases, such "polypharmacology" arose serendipitously, but it suggests that there is potential in purposely designing compounds with multiple targets, and researchers have begun to explicitly consider systems pharmacology and the functioning of drug targets as part of a network, rather than individually [31–33].

In this context, Gu et al. have created a natural product database and have explored its network properties as a source of compounds with polypharmacology [34, 35]. The analysis was limited by a lack of experimental activity data on the compounds, so this was supplemented with computational virtual screening data against 332 protein targets. The structure of the derived network indicated that the database should be rich in compounds with polypharmacological properties. Related work has investigated the mechanism of action of components of a Traditional Chinese Medicine (TCM) used for the treatment of T2DM. It was found that multiple compounds in the preparation were predicted to target proteins implicated in T2DM, and that this would have an effect at the network level. Several additional compounds with no reported pharmacological activity in T2DM were also highlighted. More recently, Tian et al. [36], combined docking, pharmacophore mapping and machine learning methods to establish a compound–-target interaction network for TCMs. Approximately, 20% of the predicted inhibitors could interact with multiple targets and some of these predictions were experimentally validated. The authors speculate that the antidiabetic efficacy of TCMs derives from a combination of substituents that are active against T2DM-related targets supplemented by bioactivities that are more indirectly related, in particular compounds with free radical scavenging and antioxidant activities.

## 5 Conclusions

Computational methods continue to develop in speed and sophistication and have great potential to identify novel synthetic and natural product compounds as leads for the development of new T2DM therapies. However, the computational methods present many technical difficulties at every stage of their application and there are many pitfalls which can trap nonexperts and lead to false conclusions.

Most molecular modeling protocols involve the sequential application of a number of steps, many of these requiring choices to be made by the scientists involved. In many studies, it is difficult to determine the degree to which the various modeling steps involved contributed to the identification of the active compound, and more importantly, the lack of any control experiments makes judging the effectiveness of the method overall problematic. For example, could a simpler method have performed as well, or is the success largely determined by the manual selection of compounds for testing, which is typically the final step in many protocols?

Several 2D and 3D virtual screening approaches summarized above have reported structurally diverse natural products modulators of T2DM targets, which at face value indicates that natural products could be a rich source for novel compounds for the treatment of T2DM. However, in many of these reports, the number of compounds subjected to experimental testing is very small, often barely into double figures. If, say, two of these compounds are active in the assay, it is very hard to judge the significance of the finding. This is particularly the case if the compounds have been tested at high concentrations. It is not rare to see concentrations as high as 100 μM, or even higher, being used. The pharmacological relevance of effects at these concentrations must be doubtful.

Of the compounds reported as, for example, PPARγ modulators, certain chemical families (chemotypes) occur quite frequently. Of course, at one level, this is expected, as from the similarity principle that guides medicinal chemistry, similar compounds will tend to share similar biological effects. However, often the binding modes of these compounds are different to the thiazolidinedione agonists and their effects in animal models are different (sometimes beneficially so, through reduction in side effects). Example compounds include genistein, biochanin A, sargaquinoic acid, resveratrol, amorphastilbol, magnolol, honokiol, and amorfrutin 1 (Fig. 3). In most cases, predicted binding modes were not followed up with experimental verification through X-ray crystallography.

There is also growing awareness that many compounds have the potential to interact nonspecifically with many biological systems and are thus frequently identified in high-throughput and

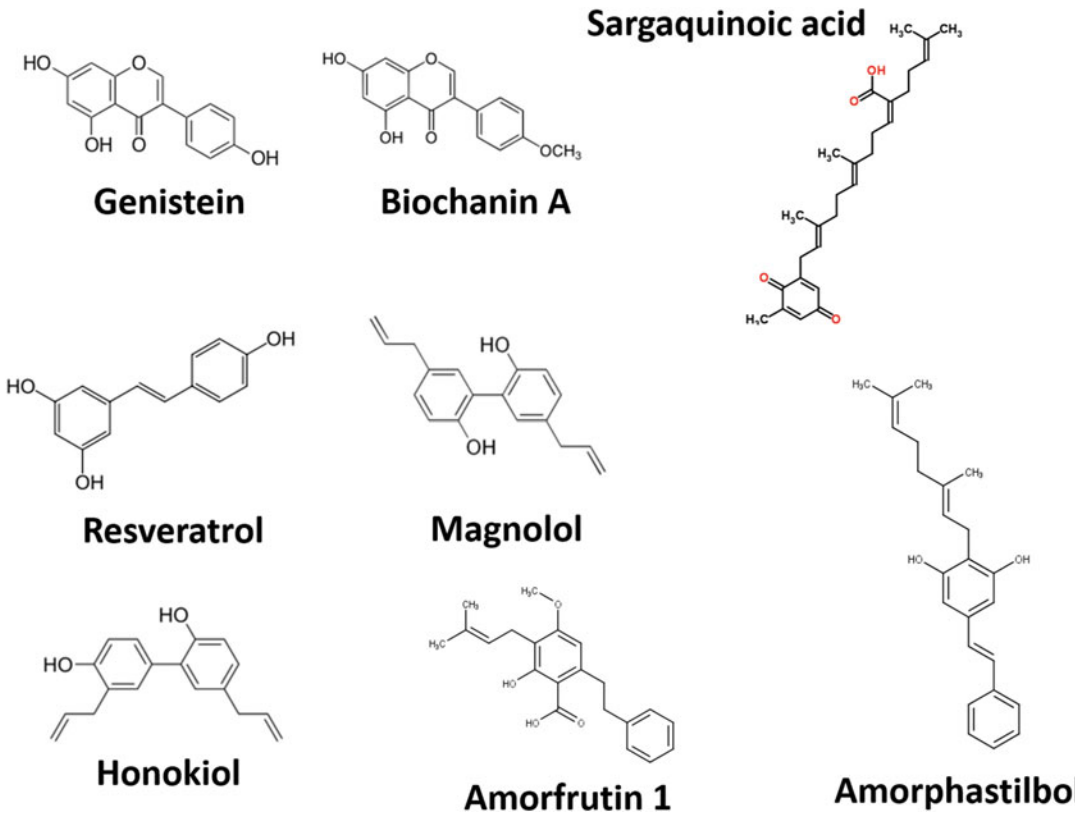


**Fig. 3** Chemical structures of selected natural product PPAR modulators reported in the literature

computational screening exercises. Such compounds have been dubbed PAINS, pan-assay interference compounds [37] and it has been estimated that 5–12% of a typical academic screening library consists of PAINS. Well-known examples include polyhydroxylated natural compounds such as resveratrol, curcumin, and genistein. Compounds of this type require careful characterization if they are to be suggested as interesting drug leads, as their potential to interact nonspecifically with multiple biological systems is well documented [38, 39]. This may be particularly the case with receptors such as PPARγ, which appears to be rather promiscuous in its ability to bind a wide variety of structurally diverse compounds. A good example of the characterization that can be performed can be seen in the identification of the amorfrutins (through experimental screening) as partial agonists of PPARγ and as potent antidiabetic natural products [40].

Among the important points for someone wishing to apply virtual screening to carefully consider are the following:

1. Choice of software tool. Comparative studies of the methodologies listed in Table 1, and others, shows that they tend to have

similar levels of performance overall. However, there is much variability from target to target and it can be difficult to know in advance which method will work best for any particular target. Ideally, one may wish to choose a method that has been shown to perform well against similar targets or binding sites.

2. Beware of artifacts that could arise from the choice of compound database or methodology. Compare performance with a simpler method and evaluate the performance statistically [41]. Guidelines are available to help avoid the most serious pitfalls [42].
3. The "hit rates" for virtual screening reported in the literature of often derived from retrospective studies. The performance in prospective studies is usually much lower. It is unlikely that active compounds will be found unless a large number (probably hundreds) of compounds are tested experimentally. Also, test at a reasonable concentration (at most low micromolar). Beware PAINS and potential nonspecific activities—demonstrate a dose–response.

There has never been a greater need for the development of new treatments for T2DM, and there would be great benefit globally from identification of compounds of natural origin as aspects of therapeutic regimens. Our improving knowledge of the pathophysiology of the disease and the development of ever-expanding databases and screening methods offers much promise. To deliver on this promise, closer collaboration between experimentalists with T2DM domain expertise and expert cheminformaticians is needed if we are to identify compounds with genuine potential to address the unmet medical need.

## References

1. Sterling T, Irwin JJ (2015) ZINC 15 – ligand discovery for everyone. J Chem Inf Model 55:2324–2337
2. Pence HE, Williams A (2010) ChemSpider: an online chemical information resource. J Chem Educ 87:1123–1124
3. Gaulton A, Bellis LJ, Bento AP et al (2011) ChEMBL: a large-scale bioactivity database for drug discovery. Nucleic Acids Res 40: D1100–D1107
4. Ma Y, Wang S-Q, Xu W-R et al (2012) Design novel dual agonists for treating type-2 diabetes by targeting peroxisome proliferator-activated receptors with core hopping approach. PLoS One 7:e38546. https://doi.org/10.1371/journal.pone.0038546
5. Liu L, Ma Y, Wang R-L et al (2013) Find novel dual-agonist drugs for treating type 2 diabetes by means of cheminformatics. Drug Des Devel Ther 7:279–288
6. Wang X-J, Zhang J, Wang S-Q et al (2014) Identification of novel multitargeted PPARα/γ/δ pan agonists by core hopping of rosiglitazone. Drug Des Devel Ther 8:2255–2262
7. Gee VM, Wong FS, Ramachandran L et al (2014) Identification of novel peroxisome proliferator-activated receptor-gamma (PPARγ) agonists using molecular modeling method. J Comput Aided Mol Des 28:1143–1151
8. Tanwar O, Tanwar L, Shaquiquzzaman M et al (2014) Structure based virtual screening of MDPI database: discovery of structurally diverse and novel DPP-IV inhibitors. Bioorg Med Chem Lett 24:3447–3451

9. Maccari R, Ottanà R (2015) Targeting aldose reductase for the treatment of diabetes complications and inflammatory diseases: new insights and future directions. J Med Chem 58:2047–2067
10. Wang L, Gu Q, Zheng X et al (2013) Discovery of new selective human aldose reductase inhibitors through virtual screening multiple binding pocket conformations. J Chem Inf Model 53:2409–2422
11. Wishart DS, Knox C, Guo AC et al (2006) DrugBank: a comprehensive resource for in silico drug discovery and exploration. Nucleic Acids Res 34:D668–D672
12. Schuster D, Markt P, Grienke U et al (2011) Pharmacophore-based discovery of FXR agonists. Part 1. Model development and experimental validation. Bioorg Med Chem 19:7168–7180
13. Bnouham N, Ziyyat A, Mekhfi H et al (2006) Medicinal plants with potential antidiabetic activity – a review of ten years of herbal medicine research (1990-2000). Int J Diabetes & Metab 14:1–25
14. Fakhrudin N, Ladurner A, Atanasov AG et al (2010) Computer-aided discovery, validation, and mechanistic characterization of novel neolignan activators of peroxisome proliferator-activated receptor gamma. Mol Pharmacol 77:559–566
15. Zhang H, Xu X et al (2011) Molecular determinants of magnolol targeting both RXRα and PPARγ. PLoS One 6(11):e28253
16. Atanasov AG, Wang JN, Gu SP et al (2013) Honokiol: a non-adipogenic PPARγ agonist from nature. Biochim Biophys Acta 1830:4813–4819
17. Choi SS, Cha BY, Iida K et al (2011) Honokiol enhances adipocyte differentiation by potentiating insulin signaling in 3T3-L1 preadipocytes. J Nat Med 65:424–430
18. Tanrikulu Y, Rau O, Schwarz O et al (2009) Structure-based pharmacophore screening for natural-product-derived PPARgamma agonists. Chembiochem 10:75–78
19. Petersen RK, Christensen KB, Assimopoulou AN et al (2011) Pharmacophore-driven identification of PPARgamma agonists from natural sources. J Comput Aided Mol Des 25:107–116
20. Rupp M, Schroeter T, Steri R et al (2010) From machine learning to natural product derivatives that selectively activate transcription factor PPARgamma. ChemMedChem 5:191–194
21. Lewis SN, Brannan L, Guri AJ et al (2011) Dietary alpha-eleostearic acid ameliorates experimental inflammatory bowel disease in mice by activating peroxisome proliferator-activated receptor-gamma. PLoS One 6: e24031
22. Moon H-S, Guo D-D, Lee H-G et al (2009) Alpha-eleostearic acid suppresses proliferation of MCF-7 breast cancer cells via activation of PPARγ and inhibition of ERK1/2. Cancer Sci 101:396–402
23. Salam NK, Huang TH, Kota BP et al (2008) Novel PPAR-gamma agonists identified from a natural product library: a virtual screening, induced-fit docking and biological assay study. Chem Biol Drug Des 71:57–70
24. Guash L, Ojeda MJ, Gonzalez-Abuin N et al (2012) Identification of novel human dipeptidyl peptidase-IV inhibitors of natural origin (Part I): virtual screening and activity assays. PLoS One 7:e44791
25. Chen X, Liu M, Gilson MK (2001) BindingDB: a web-accessible molecular recognition database. Comb Chem High Throughput Screen 4:719–725
26. Guasch L, Sala E, Ojeda MJ et al (2012) Identification of novel human dipeptidyl-IV inhibitors of natural origin (Part II): in silico prediction in antidiabetic extracts. PLoS One 7:e44792
27. Pathania S, Randhawa V, Bagler G (2013) Prospecting for novel plant-derived molecules of *Rauvolfia serpentina* as inhibitors of aldose reductase, a potent drug target for diabetes and its complications. PLoS One 8:e61327
28. Ehrlich P (1907) On immunity with special reference to the relationship between distribution and action of antigens. J R Inst Pub Health 15:321–340
29. Roth BL, Sheffler DJ, Kroeze WK (2004) Magic shotguns versus magic bullets: selectively non-selective drugs for mood disorders and schizophrenia. Nat Rev Drug Discov 3:353–359
30. Knight ZA, Lin H, Shokat KM (2010) Targeting the cancer kinome through polypharmacology. Nat Rev Cancer 10:130–137
31. Hopkins AL (2008) Network pharmacology: the next paradigm in drug discovery. Nat Chem Biol 4:682–690
32. Berger SI, Iyengar R (2009) Network analyses in systems pharmacology. Bioinformatics 25:2466–2472
33. Vogt I, Mestres J (2010) Drug-target networks. Mol Informatics 29:10–14
34. Gu J, Gui Y, Chen L et al (2013) Use of natural products as chemical library for drug discovery and network pharmacology. PLoS One 8: e62839

35. Gu J, Chen L, Yuan G et al (2013) A drug-target network-based approach to evaluate the efficacy of medicinal plants for type II diabetes mellitus. Evid Based Complement Alternat Med 2013:203614
36. Tian S, Li Y, Li D et al (2013) Modelling compound-target interaction network of traditional Chinese medicines for type II diabetes mellitus: insight for polypharmacology and drug design. J Chem Inf Model 53:1787–1803
37. Baell JB, Holloway GA (2010) New substructure filters for removal of pan assay interference compounds (PAINS) from screening libraries and for their exclusion in bioassays. J Med Chem 53:2719–2740
38. Priyadarsini KI (2013) Chemical and structural features influencing the biological activity of curcumin. Curr Pharm Des 19:2093–2100
39. Ingólfsson HI et al (2014) Phytochemicals perturb membranes and promiscuously alter protein function. ACS Chem Biol 9:1788–1798
40. Weidner C et al (2012) Amorfrutins are potent antidiabetic dietary natural products. Proc Natl Acad Sci U S A 109:7257–7262
41. Zhou W, Hevener KE et al (2009) A statistical framework to evaluate virtual screening. BMC Bioinformatics 10:225
42. Scior T, Bender A et al (2012) Recognizing pitfalls in virtual screening: a critical review. J Chem Inf Model 52:867–881

# Chapter 5

# Whole-Exome Sequencing (WES) for Illumina Short Read Sequencers Using Solution-Based Capture

**Milind C. Mahajan and Andrew S. McLellan**

## Abstract

Next-generation sequencing (NGS) is transforming clinical research and diagnostics, vastly enhancing our ability to identify novel disease-causing genetic mutations and perform comprehensive diagnostic testing in the clinic. Whole-exome sequencing (WES) is a commonly used method which captures the majority of coding regions of the genome for sequencing, as these regions contain the majority of disease-causing mutations. The clinical applications of WES are not limited to diagnosis; the technique can be employed to help determine an optimal therapeutic strategy for a patient considering their mutation profile. WES may also be used to predict a patient's risk of developing a disease, e.g., type 2 diabetes (T2D), and can therefore be used to tailor advice for the patient about lifestyle choices that could mitigate those risks. Thus, genome sequencing strategies, such as WES, underpin the emerging field of personalized medicine. Initiatives also exist for sharing WES data in public repositories, e.g., the Exome Aggregation Consortium (ExAC) database. In time, by mining these valuable data resources, we will acquire a better understanding of the roles of both single rare mutations and specific combinations of common mutations (mutation signatures) in the pathology of complex diseases such as diabetes.

Herein, we describe a protocol for performing WES on genomic DNA extracted from blood or saliva. Starting with gDNA extraction, we document preparation of a library for sequencing on Illumina instruments and the enrichment of the protein-coding regions from the library using the Roche NimbleGen SeqCap EZ Exome v3 kit; a solution-based capture method. We include details of how to efficiently purify the products of each step using the AMPure XP System and describe how to use qPCR to test the efficiency of capture, and thus determine finished library quality.

**Key words** NGS, WES, Exome-seq, Sequencing, AMPure XP, NEBNext, Illumina, qPCR

## 1 Introduction

Next-generation sequencing (NGS) technology emerged only a decade and a half ago, but is fast becoming an essential tool in research and the clinic. It aids in the discovery of genetic variation that causes disease and can assist with diagnosis and disease prevention. For type 2 diabetes (T2D) is a complex disease, which arises out of the interaction of many genes and the environment [1, 2]. Deep sequencing of exonic regions of the genome

Claire J. Stocker (ed.), *Type 2 Diabetes: Methods and Protocols*, Methods in Molecular Biology, vol. 2076,
https://doi.org/10.1007/978-1-4939-9882-1_5, 

employing NGS serves as a high precision tool for the identification of new disease-causing variants, being capable of efficiently detecting complex and rare variants that have not been previously uncovered by non-NGS methods [1].

Since the publication of the human genome sequence in 2001 [3], the technology used to sequence DNA has evolved at an incredible pace exceeding Moore's law (an observation originally used to define the exponential rate of increase in the number of transistors on integrated circuits which double approximately every 2 years) [4, 5]. The first-generation (Sanger) sequencing-based techniques used to sequence the human genome were slow, laborious, and expensive to complete. The desire for cost-effective cheaper and faster sequencing has brought us into the era of next-generation sequencing (NGS) which has progressed to the point that a human genome can be sequenced for as low as $1000 in less than a week, compared to the estimated $3 billion accomplished in about 13 years for the first human genome sequenced in 2003 [5]. Over the past decade, the enhancements and reduced cost of sequencing technology and host of methods being developed around it have unleashed significant potential for understanding mechanisms of complex diseases, e.g., type 2 diabetes. While genome-wide association studies (GWAS) have helped identify over 153 variants from 120 loci which reliably associate with T2D [1, 6], most of the heritable basis for T2D still remains undiscovered and it was thought to be explained by rare variants with minor allele frequencies (MAFs) <5% (omitted from GWAS studies) [7]. NGS facilitates the contribution of rare variants to be assessed, and a recent NGS-based study of more than 120,000 Europeans, with and without T2D, has revealed that rare variants do not provide a significant contribution to T2D development [8]. It was concluded that most variation associated with the disease was still mostly linked to common variants observed in the same regions of the genome implicated by GWAS.

NGS technologies for assessment of genome variation, e.g., custom targeted sequencing, whole-exome sequencing (WES), and whole genome sequencing (WGS), are becoming cheaper and more commonly utilized in both research and clinical settings as the cost per base decreases and the utility in discovering pathogenic (disease-causing) variants and using them for genetic testing gains traction [9]. NGS techniques are capable of uncovering any type of genomic variation, all of which have the potential to cause disease by altering the structure and function of a protein product, or by modifying the regulation of expression of a protein, which can lead to loss or gain of function. The variant types include single nucleotide variants (SNVs), e.g., an A → T mutation, small insertions and deletions (indels), e.g., an AGT → TAAA change, copy number variants (CNVs), e.g., deletion or duplication of a genomic region or even whole chromosomes, and other structural variants (SVs)

including genomic rearrangements. Custom targeted NGS is commonly used clinically for diagnostic sequencing, where a set of known high impact pathogenic variants (typically rare with a population frequency of <1%) can be screened in a patient at low cost. For example, a targeted NGS-based diagnostic test has been developed to detect mutations in all genes known to cause monogenic and neonatal diabetes [10]. This technology typically uses hybridization capture or amplicon-based methods to enrich only the regions of the genome of interest. Hybridization capture-based methods use libraries of synthesized DNA or RNA oligonucleotide sequences, called "probes" or "baits," that span the genomic regions to be sequenced [11]. They can be either attached to magnetic beads (solution-based hybridization) or a solid surface (array-based hybridization) to capture complementary DNA from ultrasonically or enzymatically fragmented genomic DNA [11, 12]. "Solution"-based hybridization capture is a more recent development, requiring less input DNA, being more efficient and enabling capture of smaller genomic fragments [11, 12]. Newer "amplicon"-based methods simplify preparation and require even less starting material, but a recent study showed that they can miss variants detected by traditional hybridization capture methods [12]. Costs are reduced by combining many samples within a single sequencing reaction (multiplexing). Of course, use of targeted sequencing comes with the caveat of potentially missing causative mutations, because only a limited portion of the genome is sequenced, although, in a clinical setting, restricting the genomic regions being analyzed leads to less risk of incidental findings (observing potentially disease-causing mutations that were not part of the contracted test) which may have ethical implications.

WES is a specific implementation of targeted sequencing, targeting 95% of the protein-encoding parts of the genome [13]. This helps with the discovery of causative mutations, but is more expensive and involves a greater burden of analysis, increased computation, and greater storage needs. In a clinical setting, WES comes with challenges with respect to filtering the variants so that all the potentially pathogenic and uncertain variants are retained while the majority of benign variants are discarded; a signal to noise ratio problem. An example of WES being used in the clinic is documented by Bonneford et al. [14] who describe its application in the discovery of a novel non-synonymous mutation in the ABCC8 gene using DNA from a patient presenting with non-autoimmune neonatal diabetes mellitus (NDM). This finding indicated that oral sulfonylurea may be effective as a treatment instead of insulin therapy. In a recent clinical case, a family study, WES was used to study the heritability of T2D in a family from which three brothers and their mother were affected, implicating four genes in their disease pathology [15].

To maximize the chances of discovering disease-causing genetic aberrations, WGS is the technique of choice [9, 13, 16]. Targeted sequencing and WES may indicate the existence of SVs and large genomic rearrangements, e.g., CNV detection is possible; however, WGS is also capable of accurately describing the precise nature of the variation. Moreover, capture methods require greater coverage (the number of uniquely captured DNA fragments that overlap a genomic region) in the order of two- to threefold at each locus to achieve a sensitivity comparable to WGS [11, 13]. This results from capture bias, as baits have different target binding affinities and coverage loss may occur due to off-target binding [13]. In a recent comparison using a cohort of more than 500 patients, WGS was pitted against a commonly used targeted NGS test for the diagnosis of inherited retinal disease (IRD) [16]. WGS increased diagnostic yield by 29% by detecting disease-causing variants that were missed by targeted NGSs. An obvious limitation of WGS, given the enormous amount of sequencing required, is that the cost of both sequencing and analysis is significantly higher for WGS. Costs of data storage also increase as more raw data is collected, and depending on local regulations, in clinical settings, all raw data may need to be archived for in excess of a decade. Over time, however, decreasing sequencing costs, improved analytical algorithms, faster computation, and cheaper storage will lead to the increasing use of WGS. At this juncture, as the exome represents approximately 1–2% of the genome but contains an estimated 85% of pathogenic variants [17, 18], WES is, therefore, a good compromise for most purposes.

The NGS techniques described are currently employed in clinical use for diagnosing simple (Mendelian) diseases, e.g., monogenic diabetes [14, 19]. For complex diseases, such as T2D, the complex interplay of myriad genetic and environmental factors means that NGS is not yet readily amenable to diagnostic use [20]; nevertheless, employment of NGS is already advancing our ability to understand the genetic basis of the disease [1, 8, 15]. With continually increasing amounts of NGS data becoming available for bioinformatic interrogation, improved classification of disease subtypes and development of better artificial intelligence (AI) approaches to elucidate predictive signals from the data, it may one day be possible to use a patient's WES or WGS data routinely in the clinic to help target lifestyle advice to genetically at risk but asymptomatic individuals and prescribe the most appropriate treatments for patients as part of a personalized medicine strategy [1, 17, 18]. Two such data repositories are maintained by The Exome Aggregation Consortium (ExAC) [21] and the T2D-GENES (Type 2 Diabetes Genetic Exploration by Next-generation sequencing in multi-Ethnic Samples) consortium [8]. The latter aims to identify genetic variants for T2D through multiethnic NGS, and are performing deep WES in 10,000 people from five ethnicities. The more WES

datasets annotated and placed into the public domain, the more accurate predictions of pathogenicity become.

WES is commonly performed using short-read sequencing using Illumina platforms (NextSeq, HiSeq series, and NovaSeq series), which use the sequencing by synthesis (SBS) method [22, 23]. Sequencing may be up to 150 bp, but can be performed "paired-end" meaning that both ends of a DNA fragment are sequenced, aiding alignment. Illumina are the market leader in short read NGS technologies [22, 23], but there are other platforms available which have their strengths and weaknesses. For example, short read sequencing has limited use in de-novo assembly or for resolving large structural variants and complex or repetitive regions. Long-read sequencing platforms, e.g., the Pacific BioSciences RSII and Sequel, excel in this space, being able to sequence regions 8–20 kb in length [22, 23].

We herein provide a working protocol for the preparation of a gDNA library followed by exome enrichment using the Roche NimbleGen SeqCap v3 kit to obtain a final WES library designed for sequencing on the Illumina family of sequencers. A diagram of the entire workflow is shown in Fig. 1. This protocol is by no means a promotion of the reagents and kits used, but is intended as a general practical guide that can be used for any WES library preparation kit of choice. Increasingly, kits for library preparation are becoming available that provide faster turnaround time with reduced amplification cycles and which combine several reactions into one step. We have chosen the NEBNext kit, which yields excellent quality WES libraries compatible with the Illumina HiSeq and NovaSeq sequencers (we currently use the NovaSeq). This protocol is designed to be used for the preparation of WES libraries from 10 to 12 DNA samples simultaneously using Eppendorf tubes. However, the protocol can easily be adapted for high-throughput WES library preparation in a 96-well format, using liquid handlers and automation.

## 2 Materials

### 2.1 Purification and Size Selection of DNA

1. AMPure XP System (SPRI beads) (Beckman Coulter, Brea, CA, USA).
2. SPRI binding buffer (20% PEG, 2.5 M NaCl): Prepare 40% PEG8000 by weighing out 16 g of PEG into a sterile 50 mL conical tube. Bring the volume up to 40 μL with nuclease-free water. Shake on a plate shaker machine for 4 h, or overnight. Mix equal volumes of 5 M NaCl and 40% PEG for 20% PEG, 2.5 M NaCl solution. Vortex well and allow any air bubbles to settle before using. Store at 4 °C and bring to room temperature before use.

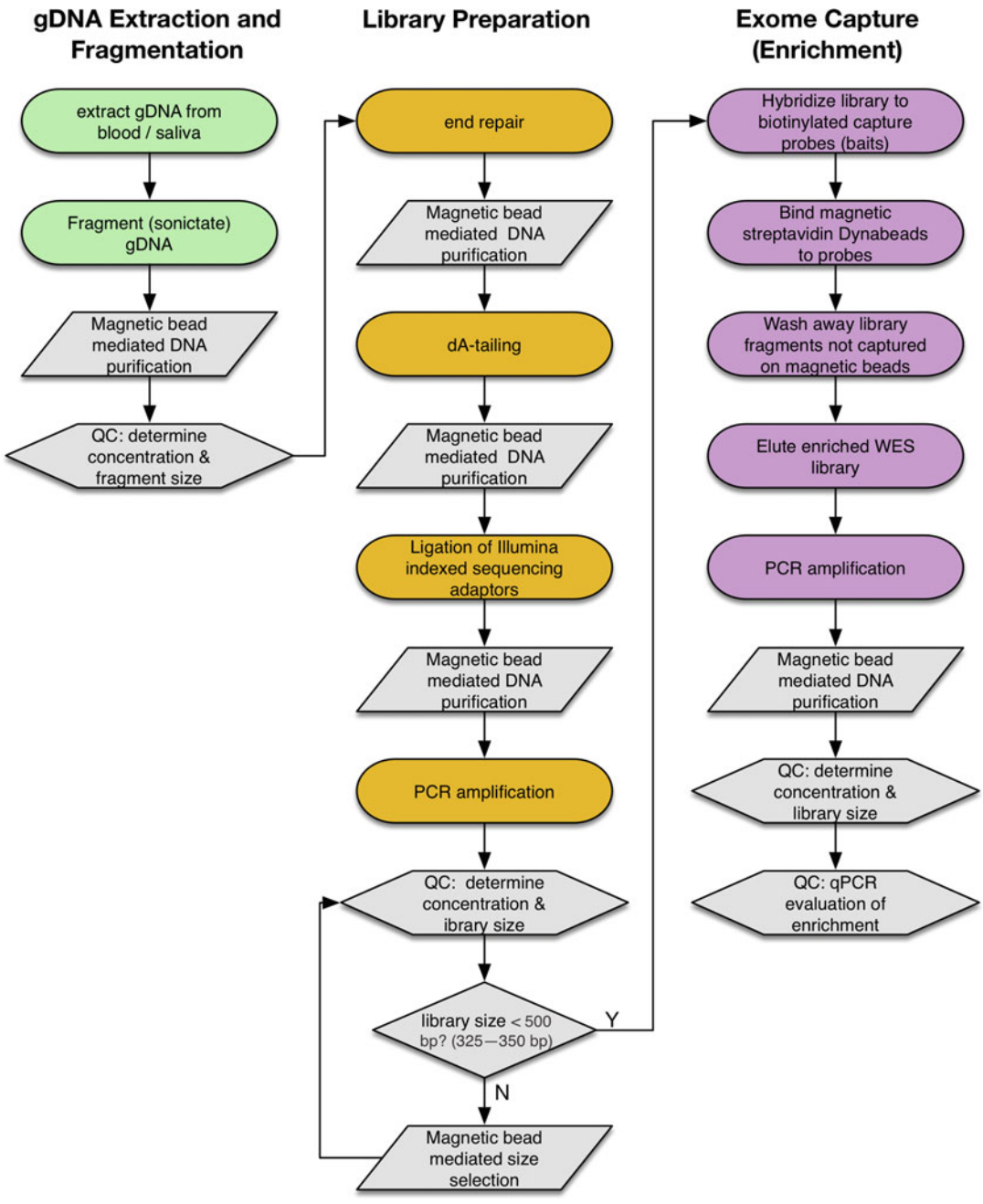


**Fig. 1** A diagram to summarize the workflow of the whole-exome capture procedure

3. SPRI elution buffer: 20 mM Tris-HCl, pH 8 or can use Qiagen Buffer EB (Qiagen, Germantown, MD, USA): 10 mM Tris-HCl, pH 8.5.
4. Magnet stand (Life Technologies Ref # 12027).
5. Covaris sonicator (LE220) (Covaris, Woburn, MA, USA).
6. Bioanalyzer 2100 (Agilent, Santa Clara, CA, USA).

### 2.2 Preparation of the gDNA Sequencing Library

1. NEBNext DNA Library Prep Master Mix Set for Illumina (NEB, Ipswich, MA).
2. KAPA HiFi HotStart ReadyMix (KAPA Biosystems, Wilmington, MA, USA): KAPA HiFi HotStart DNA Polymerase in a proprietary reaction buffer, dNTPs (0.3 mM of each dNTP at 1×), $MgCl_2$ (2.5 mM at 1×) and stabilizers.
3. Qubit dsDNA BR Assay Kit (ThermoFisher Scientific, Waltham, MA, USA).

### 2.3 Exonic Sequence Library Capture and Quality Assessment

1. Roche NimbleGen SeqCap EZ Exome v3 (Roche, Indianapolis, IN, USA).
2. COT Human DNA, Fluorometric Grade 1 mg/mL, 1 mL (Roche, Indianapolis, IN, USA).
3. Dynabeads M-270 Streptavidin (ThermoFisher Scientific, Waltham, MA, USA).
4. NanoDrop ND-1000 (ThermoFisher Scientific, Waltham, MA, USA).
5. Qubit Fluorometer (Thermofisher Scientific, Waltham, MA, USA).
6. SYBR Green PCR Master Mix (Roche Molecular Systems, Ct # 04707516001).
7. ABI 7900HT Real-Time PCR System (Applied Biosystems, Foster City, CA, USA).

## 3 Methods

### 3.1 Purification and Size Selection of DNA During WES Library Preparation Steps

Purification and size selection of DNA can be carried out by conventional agarose gel chromatography. However, it is a low-throughput and time-consuming process that requires a large amount of input DNA and the gel extraction process results in the loss of a large proportion of the gel-isolated fraction. Thus, Solid Phase Reversible Immobilisation (SPRI) beads are used to achieve efficient purification and size selection of nanogram to microgram levels of DNA [24]. SPRI beads are paramagnetic, which prevents them from clumping and falling out of solution. Each bead is made of polystyrene surrounded by a layer of magnetite and is coated with carboxyl molecules that are variably protonated/deprotonated depending on pH. These carboxylic groups reversibly bind DNA in the presence of polyethylene glycol (PEG) and salt (20% PEG, 2.5 M NaCl) binding buffer and can be eluted by 10–20 mM Tris-HCl pH 8–8.5. This system is ideally suited to purifying from low concentrations of DNA, is easy to use, and is amenable to automation, facilitating high-throughput DNA purification and size selection (*see* **Note 1**).

### 3.1.1 Random Fragmentation of Genomic DNA by Sonication

Classically, fragmentation of gDNA has been achieved via physical shearing of the DNA, which yields unbiased random DNA fragments representing the whole genome in the final library. Recently, however, several vendors including Kapa Biosystems and NEB have developed enzymatic shearing protocols, using endonucleases to create double-stranded breaks in the DNA. The advantage of enzymatic fragmentation is that it does not require any specialized equipment; however, efficacy, consistency, and reliability of enzymatic shearing needs to be established. Hence, we describe Covaris-based ultrasonic shearing of DNA for the preparation of WES libraries.

The Covaris sonicator transmits focused acoustic energy waves to randomly fragment DNA (by physical shearing). Prior to use, the sonicator must be set up (*see* **Note 2**).

1. Transfer 0.5–3 μg of gDNA in 120 μL of nuclease-free water into Covaris MicroTubes.
2. Vortex MicroTubes containing DNA samples briefly, then centrifuge to remove air bubbles (*see* **Note 3**). If air bubbles remain, a second centrifugation step may be necessary.
3. Place the MicroTubes in the MicroTube rack (*see* **Note 4**), then place the rack in the sonication chamber. We use the following parameters to obtain a DNA size range of 150–400 base pairs, with mean peak size in the range of 200–250 base pairs: time = 600 s, duty = 5%, intensity = 2, cycle per burst = 50 (*see* **Note 5**).
4. After fragmentation is complete, remove the shearing plate from the sonicator, wipe the water from the outside of the tubes and pulse spin in a centrifuge.
5. For each sample, transfer the sheared DNA to a 1.5 mL Eppendorf tube.
6. Assess the quality of the sheared genomic DNA using an Agilent 2100 Bioanalyzer: Run sheared DNA on the DNA HS chip using the Bioanalyzer to determine the size of sheared DNA (Fig. 2).
7. You may pause the protocol at this point (*see* **Note 6**).

### 3.1.2 Purification of Sheared DNA

1. AMPure XP beads should be removed from storage at 4 °C, at least 30 min prior to use, to allow them to equilibrate to room temperature.
2. Mix the reagents well so that the bead suspension appears homogeneous.
3. Aliquot 216 μL of completely resuspended room temperature AMPure XP beads to an Eppendorf tube (one tube per sample).

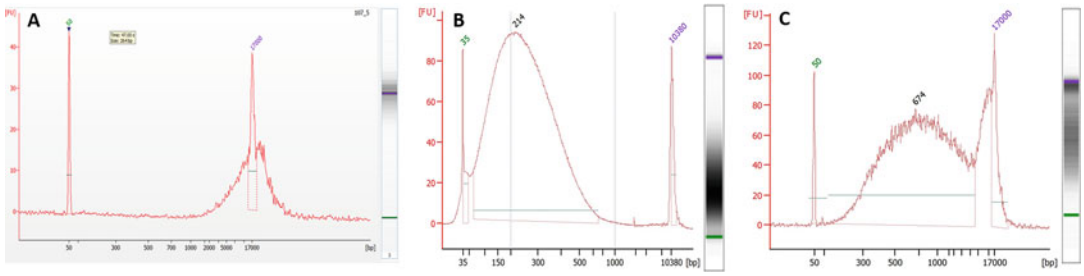


**Fig. 2** Determining optimal shearing of DNA using the Bioanalyzer. (**a**) Bioanalyzer trace of the input DNA, showing size and integrity. (**b**) Optimally sheared gDNA. (**c**) Poorly sheared gDNA

4. For each sample, transfer the total volume of fragmented DNA (0.5–3 μg in ~119 μL) from the Covaris tube into an Eppendorf tube containing AMPure XP beads (the volume of beads added is 1.8× the original DNA volume).
5. Mix well and incubate at room temperature for 5 min with intermittent mixing using a pipette to keep the beads in suspension throughout.
6. Spin the tubes for 1 min at 3000 × *g* in a microcentrifuge, then place them in a magnetic stand for 3 min or until the solution is clear.
7. Without disturbing the beads, remove 330 μL of the supernatant and discard (*see* **Note 7**).
8. Keeping the tubes in the magnetic stand, dispense 400 μL of freshly prepared 70% ethanol into each and incubate for 30 s.
9. Remove and discard the ethanol and any remaining supernatant.
10. Dry the beads at 37 °C for 5 min or until the residual ethanol has completely evaporated.
11. Add 42.5 μL of SPRI elution buffer and resuspend the beads by gently pipetting.
12. You may pause the protocol at this point (*see* **Note 8**).

### *3.2 Preparation of the Whole Genome DNA (gDNA) Sequencing Library*

The NEB Next™ DNA Sample Prep kit is used for constructing the gDNA library from the fragmented DNA. This kit contains master mixes of enzymes and reagents for end repair of fragmented DNA, dA-tailing, ligation of synthetic oligonucleotide adaptors and amplification of the adaptor-ligated DNA, using adaptor-specific barcoded PCR primers, to obtain the final gDNA library. After each of these four steps, DNA is purified using AMPure beads (*see* **Note 9**), selecting a binding buffer with the appropriate concentration of PEG and NaCl (as detailed above).

### 3.2.1 End Repair of Sheared DNA

Bead-bound purified sheared DNA from **step 11** above (Subheading 3.1.2) is used to create blunt-ended DNA by end repair.

1. For each sample, set up the end repair reaction mix as follows: 5 μL of NEB Next End Repair Reaction Buffer (10×), 2.5 μL of NEBNext End Repair Enzyme Mix, 42.5 μL of AMPure bead-bound sheared DNA (50 μL total).
2. Incubate in a thermocycler for 30 min at 20 °C to complete the end repair reaction.

### 3.2.2 Cleaning Up End-Repaired DNA

Prior to using the end-repaired DNA, it must first be purified as follows:

1. Add 90 μL of SPRI binding buffer (20% PEG-2.5 M NaCl) solution to the 50 μL of end repair reaction mix to bind the DNA back to the beads.
2. Pipette up and down 20 times to resuspend the beads and incubate at room temperature for 5 min.
3. Spin the tube for 1 min at 3000 × *g* in a microcentrifuge. Place the tube on the magnetic stand for 3 min or until the solution is clear.
4. Without disturbing the beads, remove 135 μL of supernatant and discard. A small volume of supernatant will be left in each well.
5. Continue to keep the tube on the magnetic stand and add 200 μL of freshly prepared 70% ethanol, incubate for 30 s then discard the ethanol.
6. Repeat **step 5** for a total of two ethanol washes.
7. Dry the samples at room temperature for 10 min or until the residual ethanol completely evaporates.
8. Add 42 μL of SPRI elution buffer and pipette up and down 15 times to resuspend the beads. The bead-bound DNA is now ready for dA-tailing.
9. You may pause the protocol at this point to continue next day or proceed to the dA-tailing step described below in Subheading 3.2.3 (*see* **Note 8**).

### 3.2.3 Addition of Deoxyadenine to the 3′ End of Blunt-Ended DNA (dA-Tailing)

1. Prepare the dA-tailing reaction mix using reagents from the NEBNext DNA Library Prep Master Mix Set for Illumina as follows: 5 μL of NEBNext dA-Tailing Reaction Buffer (10×), 3 μL of Klenow Fragment (3′ → 5′ exo$^-$), 42 μL of DNA-bead mix after end repair step (total of 50 μL).
2. Incubate the reaction mix at 37 °C for 30 min to obtain DNA fragments with dA-overhangs on the 3′ end.

*3.2.4 Cleaning Up the dA-Tailed DNA*

1. Add 90 μL of 20% PEG, 2.5 M NaCl to ~50 μL of dA-tailed DNA reaction mix, then mix the contents thoroughly using a pipette and incubate at room temperature for 5 min.
2. Spin tube at 3000 × *g* in a microcentrifuge. Place the tube on the magnetic stand for 3 min or until the solution is clear.
3. Without disturbing the beads, remove 135 μL of supernatant and discard. A small volume of supernatant will be left in each well.
4. Continue to keep the tube on the magnetic stand and add 200 μL of freshly prepared 70% ethanol, incubate for 30 s then discard the ethanol.
5. Repeat **step 4** for a total of two ethanol washes.
6. Dry the samples at 37 °C for 5 min or until any residual ethanol has completely evaporated.
7. Add 25 μL of Qiagen elution buffer and pipette up and down 15 times to resuspend the beads. You should proceed directly to the next step (*see* **Note 10**).

*3.2.5 Ligation of Illumina Adaptors to dA-Tailed DNA*

1. Prepare the Adaptor Ligation reaction mix as follows: 10 μL of NEBNext Quick Ligation Reaction Buffer (5×), 10 μL of DNA Multiplex Adaptor (10 μM), 5 μL of Quick T4 DNA Ligase, 25 μL of Quick T4 DNA Ligase (total volume of 50 μL). Adaptor sequences are shown in Table 1.
2. Incubate for 60 min at 20 °C to allow ligation to occur.

*3.2.6 Cleaning Up and Size Selection of the Adaptor-Ligated DNA*

1. Add 60 μL of SPRI binding buffer to 50 μL of adaptor ligation reaction mix to get to 1.2× ratio of SPRI binding buffer/beads to ligation mix (*see* **Note 11**).
2. Mix well by briefly vortexing each tube then incubate at room temperature for 5 min. Place the tubes in the magnetic stand for 3 min or until the solution becomes clear.
3. Without disturbing the beads, remove the supernatant and discard. A small volume of supernatant will be left in each well.
4. Continue to keep the tube on the magnetic stand and add 200 μL of freshly prepared 70% ethanol, incubate for 30 s then discard the ethanol.
5. Repeat **step 4** for a total of two ethanol washes.
6. Dry the sample at 37 °C for 5 min or until any residual ethanol has completely evaporated.
7. Add 20 μL of nuclease-free PCR grade water and pipette up and down 15 times to resuspend the beads and incubate for 5 min at room temperature, pipetting intermittently to keep the beads in suspension.

**Table 1**
**Illumina Adaptor sequences ligated to dA-tailed gDNA during library preparation (rows 1 and 2)**

| Primer name | Sequence (5′–3′) | Direction |
|---|---|---|
| Multiplex adap. 1 | P-GATCGGAAGAGCACACGTCT | |
| Multiplex adap. 2 | ACACTCTTTCCCTACACGACGCTCTTCCGATC∗T | |
| PE PCR primer-F | AATGATACGGCGACCACCGAGATCTACACTCTTTCCC TACACGACGCTCTTCCGATCT | F |
| PE PCR primer-R | CAAGCAGAAGACGGCATACGAGAT[CGTGAT] GTGACTGGAGTTCAGACGTGTGCTCTTCCGATCT | R |
| PE PCR primer F-BLOCK | AATGATACGGCGACCACCGAGATCTACACTCTTTCCC TACACGACGCTCTTCCGATCT | F |
| Idx01-Long-BLOCK | CAAGCAGAAGACGGCATACGAGAT[CGTGAT∗] GTGACTGGAGTTCAGACGTGTGCTCTTCCGATCT | R |
| IS 5 | AATGATACGGCGACCACCGA | F |
| IS 6 | CAAGCAGAAGACGGCATACGA | R |

NEBNext Universal PCR Primer (F) and an example NEBNext Index Primer (R) (rows 3 and 4). Blocking oligos used during exome-capture step (rows 5 and 6). PCR primers used for the post-capture amplification of WES library (rows 7 and 8). The index sequence of the blocking oligos is the same as that used for the NEBNext Index Primer in the gDNA library preparation for a given sample. Index sequences are shown within square brackets. ∗indicates a phosphorothioate bond

8. Pulse spin in a microcentrifuge, then place the tube on the magnetic stand for 3 min or until the solution is clear.
9. Transfer the eluate (~20 μL) to a new PCR tube and discard the beads.

*3.2.7 Amplification of the gDNA Library*

The quantity of adaptor-ligated gDNA library is currently too small to proceed with exome capture by solution hybridization. It must first be amplified by a few PCR cycles as necessary to obtain a yield of ≥500 ng.

1. Prepare the PCR mix in a pre-PCR hood (to reduce the risk of contamination with aerosolized PCR products) as follows: 25 μL KAPA HiFi HotStart ReadyMix, 2.5 μL of forward PCR primer (10 μM), 2.5 μL of indexed reverse primer (10 μM), 20 μL of adaptor-ligated DNA (50 μL total volume). PCR primer sequences are shown in Table 1.
2. Set up the PCR reaction on a thermocycler using the following program: 98 °C for 5 min (denaturation), followed by 8 cycles of 98 °C for 1 min, 60 °C for 30 s and 72 °C for 45 s (amplification), then finish with 72 °C for 10 min (extension). Hold at 4 °C until ready for the next stage.
3. Clean up 50 μL of PCR amplified DNA using 60 μL of AMPure XP beads as described in Subheading 3.2.6 (*see* **Note 12**).

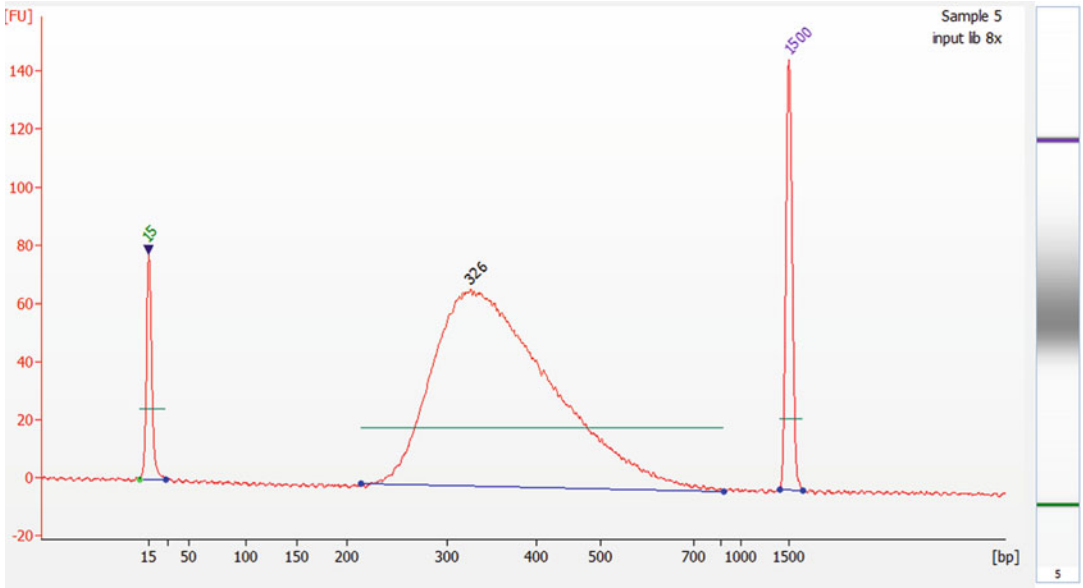


**Fig. 3** A Bioanalyzer trace showing the profile of an optimally prepared genomic DNA library

4. Elute DNA in 30 μL of SPRI elution buffer.

At this point the gDNA library is ready for exome enrichment, but, before proceeding, it is necessary to estimate the quantity and size of the gDNA library on the Bioanalyzer and verify that the PCR primers have been removed. Note the following features on the electropherogram provided by the Bioanalyzer:

- Concentration of each library.
- Average library size.
- Any other peaks besides the library.

For most samples, the majority of the gDNA obtained after initial shearing should have been sized between 200 and 250 base pairs (Fig. 2b). Thus, the mean peak size of the finished library will be around 325–350 base pairs, which is suitable for sequencing (Fig. 3). If, for some reason, the library exhibits a broad molecular weight range or shows a peak greater than 400 base pairs (Fig. 4), then use the following protocol to remove high molecular weight DNA from the gDNA Seq library.

### *3.2.8 Removal of High Molecular Weight DNA from the gDNA Library*

1. Remove a stock tube of AMPure XP beads from storage at 4 °C and allow to equilibrate to room temperature.
2. Centrifuge the sample plate at 300 × *g* for 30 s to ensure all components are collected at the bottom of each well.
3. To 30 μL of PCR amplified WES library, add 19.5 μL of AMPure beads. This is a 0.65× ratio of beads to sample

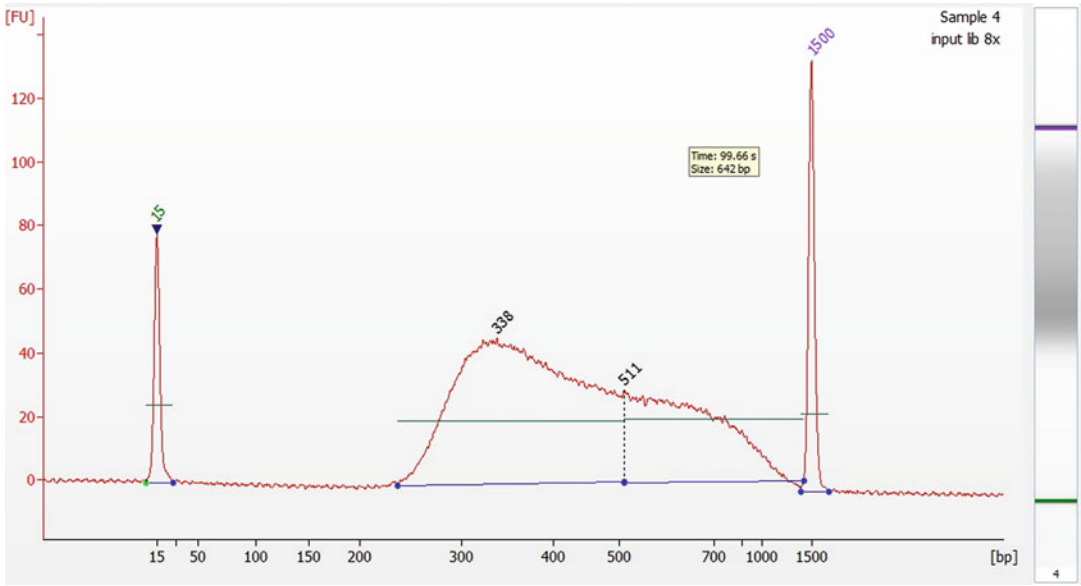


**Fig. 4** A Bioanalyzer trace obtained before removal of high molecular weight DNA from a genomic DNA library

volume, optimal for binding the high molecular weight material in the library.

4. Pipette up and down 20 times to resuspend the beads.
5. Incubate at room temperature for 5 min with intermittent mixing by gentle pipetting.
6. Spin the tube for 1 min at 3000 × *g* in a microcentrifuge then place the tube on the magnetic stand for 3 min or until the solution is clear.
7. Transfer the supernatant containing unbound ~350 base pairs of WES library DNA to a new Eppendorf tube. Add 16.5 μL of AMPure beds to the DNA in the supernatant to obtain a 1.2× ratio of beads to sample volume.
8. Repeat **steps 5** and **6**.
9. Without disturbing the beads, remove 40 μL of supernatant and discard. A small volume of supernatant will be left in the tube.
10. Continue to keep the tube on the magnetic stand and add 200 μL of freshly prepared 70% ethanol, incubate for 30 s then discard the ethanol.
11. Repeat **step 10** for a total of two ethanol washes.
12. Dry the samples in an incubator at 37 °C for 5 min or until the residual ethanol has evaporated.
13. Add 20 μL of nuclease-free PCR grade water and pipette up and down 15 times to resuspend the beads.

14. Repeat **steps 5** and **6**.
15. Transfer the eluate (~20 μL) to a new 1.5 mL Eppendorf tube. Run some of the eluted DNA on a Bioanalyzer for size determination and estimation of concentration. This is the final gDNA library ready for exome enrichment (Fig. 3).
16. Store the gDNA library overnight at −20 °C or until needed for the exome enrichment process described as in Subheading 3.3 below.

### *3.3 Enrichment of Exonic Content of the gDNA Library (Exome Enrichment)*

The gDNA library prepared as described above comprises sequence content from the entire genome out of which only ~2% belongs to the coding portion of the genome. To isolate/enrich this relatively tiny fraction of the total gDNA library, a solution hybridization-based capture method can be employed. There is an assortment of vendors producing kits for generating capture libraries for WES and most use tiled or overlapping biotinylated DNA or RNA capture probes (baits) and streptavidin-coated magnetic beads to isolate the fragments containing exonic sequence. Of these, the most popular kits are produced by Illumina, Roche NimbleGen, Agilent, Integrated DNA Technologies (IDT) and Twist Bioscience. Illumina offers three kits based on the Nextera Rapid Capture enrichment method. The Nextera Rapid Capture Exome kit targets all coding sequence (~37 megabases), the Nextera Rapid Capture Expanded Exome kit also captures non-coding regions, UTRs and miRNAs (~62 megabases) and the TrueSight One kit captures a reduced set of exons (~12 megabases) that have been implicated in at least one disease. Roche NimbleGen provides a similar selection with its SeqCap EZ Exome Library v3.0 (~64 megabases), SeqCap EZ Exome + UTR Library (~96 megabases), and SeqCap EZ HGSC VCRome (~45 megabases) solution-based capture kits. Agilent's SureSelectXT Human All Exon V6 (~58 megabases), SureSelectXT Human All Exon V6 + UTR (size not specified), and SureSelectXT Focused Exon Capture (~12 megabases) are equivalent. IDT offers the xGen Exome Research Panel (~39Mb), and several disease specific and custom targeted panels, boasting a comprehensively high on-target rate and uniform coverage, even across GC-rich regions. Twist Bioscience is the latest entrant in the growing list of vendors offering whole exome and targeted capture solutions. It offers the Human Core Exome Kit (~33 Mb of highly conserved protein-coding regions) and custom panels. The company has developed high-fidelity double stranded oligos which are uniquely designed to capture both DNA strands, providing enhanced specificity and uniformity across targeted regions without unexpected dropouts. Some of these manufacturers also allow for the addition of custom probes to the exome panel. While there are widely reported advantages and disadvantages to specific kits [17, 25] in general they appear to perform similarly and it is

important to realize that no single kit has complete coverage of all exons. It is difficult to use comparisons reported in the literature as the results tend to vary considerably, particularly as kits are modified and improved over time; however, the choice of kit should include consideration of relative coverage of exome databases, target coverage sensitivity, GC bias (which is traditionally more pronounced in Illumina Nextera kits as they exhibit an increase in read depth for sequences with at least 60% GC content [25]), and sensitivity in detecting single nucleotide variants (SNVs) and indels. Other factors to take into account include platform compatibility, cost, fragmentation preference (enzymatic or sonication), required input DNA quantity and amenability toward automation should this feature be desirable.

Here we describe exome enrichment procedure using the Roche SeqCap EZ Exome v3 reagent kit, a solution-based capture method using a 64 megabase sequence capture design based on the human genome build GRCh37/hg19 [26].

### *3.3.1 Hybridization of gDNA Library to the Exome Capture System*

Before commencing the exome capture procedure it is necessary to complete the following steps:

1. Set a heat block to 95 °C and allow to equilibrate.
2. Remove an appropriate number of 4.5 μL SeqCap Exome Oligo pool aliquots (1 per capture) from −65 °C storage and allow them to thaw on ice. Thaw freezer stored COT DNA and Blocking Oligos (Table 1) to room temperature.
3. Set up a pre-hybridization as follows: 1 μL of COT DNA (1 mg/mL), 1 μg forward blocking oligo (1 mM), 1 μL of indexed reverse blocking oligo (1 mM) and 500–750 ng of gDNA library in 10–15 μL (as in Subheading 3.2.7).
4. Lyophilize the amplified sample library/COT DNA/PE-HE Oligos in a DNA vacuum concentrator at 65 °C (*see* **Note 13**).
5. Add 7.5 μL of 2× SC Hybridization Buffer and 3 μL of SC Hybridization Component.
6. Cap and vortex the tube for 10 s then microcentrifuge for 10 s.
7. Place the samples in a 95 °C heat block for 10 min to denature the DNA, then pulse-spin in a microcentrifuge.
8. Transfer the ~10.5 μL of amplified sample library/COT DNA/PE-HE Oligos/Hybridization cocktail to the 4.5 μL aliquot of SeqCap EZ Exome v3 oligonucleotide pool that has been thawing on ice.
9. Vortex the contents of the tube briefly and centrifuge at maximum speed for 10 s.
10. Incubate in a thermocycler (with a heated lid) at 47 °C for 64–72 h (*see* **Note 14**).

**Table 2**
**Preparation of wash buffers for washing and recovery of hybridized samples using Streptavidin Dynabeads**

| Stock concentrated buffer | Volume of concentrated buffer for 1× (μL) | Volume of water for 1× (μL) | Total volume (μL) |
|---|---|---|---|
| 10× Stringent wash buffer (vial 4) | 40 | 360 | 400 |
| 10× Wash buffer I (vial 1) | 30 | 270 | 300 |
| 10× Wash buffer II (vial 2) | 20 | 180 | 200 |
| 10× Wash buffer III (vial 3) | 20 | 180 | 200 |
| 2.5× Bead wash buffer (vial 7) | 200 | 300 | 500 |

### *3.3.2 Wash and Recovery of Hybridized Samples*

Step 1. Prepare Sequence Capture Wash Buffers

1. Dilute stock Stringent Wash Buffer, SC Wash Buffers (I, II, and III), and Bead Wash Buffer to create 1× working solutions as shown in Table 2. The values in the table are for a single exome capture. For more exome captures, simply multiply each volume by the number of samples (*see* **Notes 15**–**17**).
2. Preheat 1× Stringent Wash Buffer and one-third of the volume of 1× SC Wash Buffer I to 47 °C in a water bath.

Step 2. Prepare the Streptavidin Dynabeads

1. Allow the Streptavidin Dynabeads M270 to equilibrate at room temperature for 20 min prior to use.
2. Mix the beads thoroughly by vortexing for 1 min.
3. Aliquot 100 μL of beads per capture into a single 1.5 mL tube (i.e., for one capture use 100 μL of beads and for four captures use 400 μL of beads—*see* **Note 18**).
4. Centrifuge the 1.5 mL tube at maximum speed for 10 s in a microcentrifuge, then place the tube in a magnetic stand. When the beads separate and liquid becomes clear, carefully remove and discard the liquid without disturbing the beads. Any remaining traces of liquid will be removed with subsequent wash steps. Proceed immediately to the next step (*see* **Note 19**).
5. Take the 1.5 mL tube off the magnetic stand and add twice the initial bead volume of 1× Bead Wash Buffer (i.e., for one capture add 200 μL of buffer and for four captures add 800 μL of buffer).
6. Vortex for 10 s, then centrifuge at full speed for 10 s.
7. Return the tube to the magnetic stand to bind the beads. Again, once clear, remove and discard the liquid.
8. Repeat **steps 5**–**7** for a total of two washes.

9. After removing the buffer following the second wash, resuspend the beads by vortexing in 1× the original volume using the Streptavidin Dynabead Binding and Wash Buffer that was prepared in Step 1 (i.e., for one capture use 100 μL of buffer and for four captures use 400 μL of buffer).
10. Aliquot 100 μL of resuspended beads into a new individual PCR tube or strip tube.
11. Use the 96-well magnetic plate to bind the beads by placing the tube on the magnet for 5 min. Remove and discard the liquid when clear.
12. The Streptavidin Dynabeads are now ready to bind the captured DNA. Remove the tubes containing the beads from the magnetic plate.

Step 3. Bind DNA to the Streptavidin Dynabeads

1. Transfer the ~15 μL of amplified sample library/COT DNA/PE-HE Oligos/Hybridization cocktail (which should have been hybridized for 64–72 h) to the Streptavidin Dynabeads prepared in **step 2**.
2. Mix thoroughly by pipetting up and down 10 times.
3. Bind the captured sample to the beads by placing the tubes containing the beads and DNA in a thermocycler at 47 °C for 45 min. Mix the samples by vortexing for 3 s every 15 min to ensure that the beads remain in suspension (*see* **Note 20**).

Step 4. Wash the Streptavidin Dynabeads Plus Bound DNA

1. If more than eight captures are being washed, transfer the entire contents (~115 μL) of each tube to a 96-deep well plate. If less than eight captures are being washed, samples may remain in strip tubes.
2. Place the strip tube or 96-deep well plate on the magnet. Remove the supernatant immediately once clear.
3. Add 100 μL of SC Wash Buffer I preheated to 47 °C (*see* **Note 21**).
4. Cap tubes or seal plate and mix by vortexing for 10 s.
5. Place the tubes or plate on the magnet to bind the beads. Remove and discard the liquid immediately once clear.
6. Remove the tubes or plate from the magnet and add 200 μL of Stringent Wash Buffer preheated to 47 °C. Pipette up and down 5 times to mix (*see* **Note 21**).
7. Incubate at 47 °C for 5 min. If captures are in a 96-deep well plate, use an incubation chamber. If samples are in a strip tube, use a PCR block with heated lid.
8. Repeat **steps 5**–**7** for a total of two washes with Stringent Wash Buffer heated to 47 °C.

9. Place the tubes or plate on the magnet to bind the beads. After 5 min remove and discard the supernatant.
10. Add 200 μL of room temperature SC Wash Buffer I and mix by vortexing for 2 min. If liquid has collected in the tube's cap, pulse-spin in a microcentrifuge to collect the liquid into the tube's bottom before continuing to the next step.
11. Place the tubes or plate on the magnet to bind the beads. Remove and discard the liquid once clear.
12. Add 200 μL of room temperature SC Wash Buffer II and mix by vortexing for 1 min. Pulse-spin in a microcentrifuge if necessary.
13. Place the tubes or plate on the magnet to bind the beads. Remove and discard the liquid once clear.
14. Add 200 μL of room temperature SC Wash Buffer III and mix by vortexing for 30 s. Pulse-spin in a microcentrifuge if necessary.
15. Place the tubes or plate on the magnet to bind the beads. Remove and discard the liquid once clear.
16. Remove the tubes or plate from the magnet and add 20 μL of PCR grade water to each tube of bead-bound exome-captured library (*see* **Note 22**).

### 3.4 Final Amplification of Captured Library

The quantity of exome enriched library is usually less than 1 ng, which is too low to be used for sequencing on the Illumina sequencer directly and must be amplified using a limited number of PCR cycles.

1. Generate a PCR Master Mix by adding the following components: 25 μL of KAPA HiFi HotStart ReadyMix, 2.5 μL of IS 5 Primer (10 μM), 2.5 μL of IS 6 Primer (10 μM), 20 μL of exome captured library with beads (total volume of 50 μL). *See* Table 1 for primer sequences.
2. Run the PCR reaction on a thermocycler using the following program: 98 °C for 10 min (denaturation), followed by 12 cycles of 98 °C for 1 min, 60 °C for 30 s and 72 °C for 45 s, then finish with 72 °C for 10 min. Hold at 4 °C until ready for the next stage.
3. Clean up the post-capture PCR product using AMPure XP beads as shown in Subheading 3.2.6.
4. Elute WES library DNA in a final volume of 30 μL of nuclease-free water.
5. Assess library size on a Bioanalyzer and quantify using the Qubit dsDNA BR Assay Kit. On the Bioanalyzer, the trace should look as shown in Fig. 5.

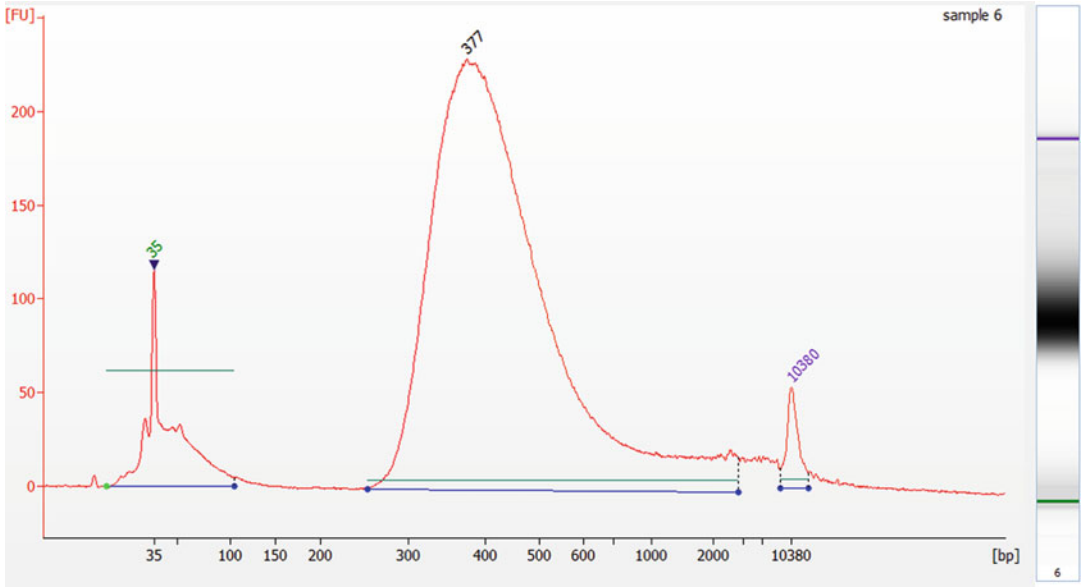


**Fig. 5** A bioanalyzer profile of a successfully captured whole-exome library

### *3.5 Assessing the Quality of Exonic Enrichment in a WES Library by qPCR*

To assess if the exonic regions of the gDNA library were successfully enriched, qPCR can be performed using exon-specific primers for a couple of genes. Significant enrichment of targeted exonic regions in a WES library over the original gDNA library indicates a successful outcome of the exome enrichment process described above. Roche NimbleGen recommends verifying two exonic regions, and also two intronic regions as controls. When running qPCR for verification of exon enrichment, it is necessary to include both the input gDNA Seq library (prepared in Subheading 3.2) and the amplified capture library (prepared in Subheading 3.4). Every qPCR assay must include standard curves for all four amplicons (two exons and two introns) using a dilution series of wild-type human genomic DNA, and a no template control (NTC) must be included. The dissociation curves for all four amplicons must be reviewed to ensure that no unexpected PCR products are generated. Compare the ratios of the results (Ct values) from qPCR of all the exonic and intronic regions in the capture libraries vs. the input libraries to determine whether enrichment of exonic regions has been successful.

1. Determine the concentration of each of the samples using either the Qubit or Bioanalyzer. Each 15 μL of qPCR reaction will contain 0.5 ng of library DNA. Make working dilutions of all libraries to a concentration of 0.1 ng/μL.
2. For quantitation of amplicon enrichment for a given qPCR reaction, each qPCR assay must include a standard curve generated using a dilution series of normal human genomic DNA

with a concentration determined by fluorescence-based quantitation using a Qubit Fluorometer. Within each dilution must be included 5 ng/μL of lambda phage DNA (non-human carrier DNA) to ensure efficient PCR across the dilution series. The dilution series should comprise the following gDNA concentrations: 5, 0.5, and 0.05 ng/μL. The negative control will contain only the 5 ng/μL of lambda (carrier) DNA.

3. Prepare the qPCR mix as follows: 7.5 μL of SYBR Green PCR Master Mix, 0.3 μL Forward/Reverse Primer Mix (5 μM), 5 μL of template DNA (0.1 ng/μL) (total volume of 10 μL).
4. Run qPCR using any standard qPCR instrument using following cycle conditions (in our lab we use the ABI 7900HT): 95 °C for 10 min (denaturation step), followed by 40 cycles of 95 °C for 15 s and 60 °C for 1 min (amplification step), then 1 cycle of 95 °C for 15 s, 60 °C for 15 s, and 95 °C for 15 s (final step to generate a dissociation curve).

The qPCR results obtained with two example samples: "WES Seq library-1" and "WES Seq library-2" are summarized in Tables 3

**Table 3**
**qPCR results for quality control analysis of an example WES library "WES-Seq library-1"**

| | NSC-247.a (exon) | PRKG.b (intron) | THAP3.a (exon) | THAP2.a (intron) |
|---|---|---|---|---|
| gDNA input Ct | 29.06 | 28.88 | 29.58 | 30.35 |
| Post-capture WES library Ct | 21.32 | 30.98 | 20.34 | 30.80 |
| delta Ct | 7.74 | −2.10 | 9.23 | −0.45 |
| delta Ct/3.32 | 2.33 | −0.63 | 2.78 | −0.14 |
| Fold increase | 213.88 | 0.23 | 604.41 | 0.73 |

The cycle parameters show the enrichment/depletion profile for the capture library using four different primer pair sets (two exonic and two intronic)

**Table 4**
**qPCR results for quality control analysis of an example WES library "WES-Seq library-2"**

| | NSC-247.a (exon) | PRKG.b (intron) | THAP3.a (exon) | THAP2.a (intron) |
|---|---|---|---|---|
| gDNA input Ct | 28.89 | 29.51 | 29.58 | 30.12 |
| Post-capture WES library Ct | 20.86 | 29.66 | 20.92 | 31.51 |
| delta Ct | 8.03 | −0.15 | 8.65 | −1.39 |
| delta Ct/3.32 | 2.42 | −0.04 | 2.61 | −0.42 |
| Fold increase | 262.59 | 0.90 | 403.59 | 0.38 |

The cycle parameters show the enrichment/depletion profile for the capture library using four different primer pair sets (two exonic and two intronic)

and 4. The tables indicate the cycle enrichment/depletion for the capture library for four different primer pair sets. For the regions to be captured (exons) there is usually a 6–9 cycle difference or ~65 to 500-fold enrichment (a difference of 3.32 cycles is equivalent to a tenfold enrichment). For regions that were not targeted in the capture (introns), one should see either a decrease in representation or little to no enrichment.

The results in Tables 3 and 4 show an increase of 200- to 600-fold in the exonic regions in the captured WES libraries, indicating successful exome enrichment had been achieved. These libraries are ready for sequencing (*see* **Note 23**).

## 4 Notes

1. Charge-dependent binding of DNA to SPRI beads is directly proportional to the concentration of the PEG and NaCl in the binding buffer (as the charge on a DNA molecule is directly proportional to its length). Consequently, by altering the composition of the PEG and NaCl in the binding buffer, DNA fragments within specific size ranges can be isolated using the SPRI beads.
2. The Covaris sonicator must be turned on, chilled to 6–8 °C and degassed for at least 1.5 h before samples are sheared.
3. Centrifugation helps to remove air bubbles, which can lead to uneven sharing of the DNA.
4. Position the MicroTubes in the bottom half of the MicroTube rack and position the top half of the rack so that that the samples are held tightly.
5. The timing and intensity of sonication needs to be standardized to obtain sheared DNA of an appropriate size.
6. If you do not wish to continue to the next step immediately, the samples may be stored at 4 °C for 24 h or at −20 °C for a longer period.
7. A small volume of supernatant should remain to avoid aspiration of the beads.
8. If you do not wish to continue to the next step immediately, the samples may be stored at 4 °C. Do not freeze the sample/bead mixture.
9. To save on the cost of AMPure beads, and avoid loss of DNA during each purification step and the size selection step, we add AMPure-bound DNA to all the biochemical reactions described. At the end of each step, a binding buffer containing an appropriate amount of PEG and NaCl is added to bind the biochemically modified DNA back to the beads, which are then

purified by placing in the magnetic stand and aspirating off the spent reagents and buffer. The bead-bound purified DNA is then used in the subsequent biochemical reaction step. We refer to this modified protocol as the "on-bead" protocol.

10. Do not stop after dA-tailing the DNA. Long-term storage and freeze-thawing causes the dA-tail to degrade. For optimal results, proceed immediately to the adaptor ligation procedure.
11. A 1.2× ratio of SPRI binding buffer/beads to sample mix ensures that only adaptor-ligated DNA will bind to the beads and any non-ligated adaptors will remain in solution.
12. The 1.2× ratio of SPRI binding buffer/beads to sample mix facilitates removal of any residual primer dimers.
13. Before lyophilizing the sample, cover the opening of the tube with a piece of paraffin tape and make an X-shaped slit through the tape using a clean blade/scalpel. This minimizes the risk of contamination during concentration of the sample.
14. When hybridizing the capture probes to the genomic library, it is preferable to set up the incubation on Friday and hybridize over the weekend to maximize productivity.
15. Be sure to generate enough stock of sequence capture wash buffers for 1–2 extra reactions, or 10% extra, to ensure there is enough for all samples.
16. Diluted 1× sequence capture wash buffers may be stored at room temperature for up to 2 weeks.
17. 1× sequence capture wash buffers must always be equilibrated to 47 °C before use.
18. Enough Streptavidin Dynabeads for six captures can be prepared in a single tube.
19. ***Do not*** allow the Streptavidin Dynabeads to dry out. Small amounts of residual Streptavidin Dynabead Binding and Wash Buffer will not interfere with the binding of DNA to the Streptavidin Dynabeads.
20. It is helpful to have a vortex mixer located close to the thermocycler for this step.
21. Work quickly so that the temperature does not drop much below 47 °C.
22. There is no need to elute DNA off the beads. The beads plus captured DNA will be used as the template in the following steps.
23. If the calculated fold enrichment values are less than 50-fold, the exome capture (i.e., enrichment) has probably failed. If this is the case, the whole-exome library preparation must be repeated.

## References


1. Prasad RB, Groop L (2015) Genetics of type 2 diabetes—pitfalls and possibilities. Genes 6 (1):87–123
2. Murea M, Ma L, Freedman BI (2012) Genetic and environmental factors associated with type 2 diabetes and diabetic vascular complications. Rev Diabet Stud 9(1):6–22
3. Lander ES, Linton LM, Birren B et al (2001) Initial sequencing and analysis of the human genome. Nature 409(6822):860–921
4. Muir P, Li S, Lou S et al (2016) The real cost of sequencing: scaling computation to keep pace with data generation. Genome Biol 17:53
5. Wetterstrand KA (2016) DNA sequencing costs: data from the NHGRI genome sequencing program (GSP). www.genome.gov/sequencingcostsdata. Accessed 27 Feb 2017
6. Dorajoo R, Liu J, Boehm BO (2015) Genetics of type 2 diabetes and clinical utility. Genes 6:372–384
7. Dickson SP, Wang K, Krantz I, Hakonarson H et al (2010) Rare variants create synthetic genome-wide associations. PLoS Biol 8: e1000294. https://doi.org/10.1371/journal.pbio.1000294
8. Fuchsberger C, Flannick J, Teslovich TM et al (2016) The genetic architecture of type 2 diabetes. Nature 536(7614):41–47
9. Katsanis SH, Katsanis N (2013) Molecular genetic testing and the future of clinical genomics. Nat Rev Genet 14(6):415–426
10. Ellard S, Lango Allen H, De Franco E et al (2013) Improved genetic testing for monogenic diabetes using targeted next-generation sequencing. Diabetologia 56:1958
11. Warr A, Robert C, Hume D et al (2015) Exome sequencing: current and future perspectives. G3 5(8):1543–1550
12. Samorodnitsky E, Jewell BM, Hagopian R et al (2015) Evaluation of hybridization capture versus amplicon-based methods for whole-exome sequencing. Hum Mutat 36 (9):903–914
13. Lelieveld SH, Spielmann M, Mundlos S et al (2015) Comparison of exome and genome sequencing technologies for the complete capture of protein-coding regions. Hum Mutat 36 (8):815–822
14. Bonnefond A, Durand E, Sand O et al (2010) Molecular diagnosis of neonatal diabetes mellitus using next-generation sequencing of the whole exome. PLoS One 5(10):e13630
15. Shaer N, Khan JJ, Dallol A, Abuzenadah A (2014) Diabetes personalized: the use of whole-exome sequencing in order to identify familial type 2 diabetes mellitus susceptibility factors. BMC Genomics 15(Suppl 2):P51
16. Ellingford JM, Barton S, Bhaskar S et al (2016) Whole genome sequencing increases molecular diagnostic yield compared with current diagnostic testing for inherited retinal disease. Ophthalmology 123(5):1143–1150
17. Meienberg J, Zerjavic K, Keller I et al (2015) New insights into the performance of human whole-exome capture platforms. Nucleic Acids Res 43(11):e76
18. Rabbani B, Tekin M, Mahdieh N (2014) The promise of whole-exome sequencing in medical genetics. J Hum Genet 59(1):5–15
19. Kwak SH, Jung CH, Ahn CH et al (2016) Clinical whole exome sequencing in early onset diabetes patients. Diabetes Res Clin Pract 122:71–77
20. Lyssenko V, Laakso M (2013) Genetic screening for the risk of type 2 diabetes: worthless or valuable? Diabetes Care 36(Suppl 2): S120–S126
21. Exome Aggregation Consortium, Lek M, Karczewski KJ, Minikel EV et al (2016) Analysis of protein-coding genetic variation in 60,706 humans. Nature 536(7616):285–291
22. Goodwin S, McPherson JD, McCombie WR (2016) Coming of age: ten years of next-generation sequencing technologies. Nat Rev Genet 17(6):333–351
23. Levy SE, Myers RM (2016) Advancements in next-generation sequencing. Annu Rev Genomics Hum Genet 17:95–115
24. DeAngelis MM, Wang DG, Hawkins TL (1995) Solid-phase reversible immobilization for the isolation of PCR products. Nucleic Acids Res 23(22):4742–4743
25. Chilamakuri CSR, Lorenz S, Madoui M-A, Vodák D, Sun J, Hovig E, Myklebost O, Meza-Zepeda LA (2014) Performance comparison of four exome capture systems for deep sequencing. BMC Genomics 15(1):449
26. Roche Sequencing (2017) SeqCap EZ System. http://sequencing.roche.com/products/nimblegen-seqcap-target-enrichment/seqcap-ez-system.html. Accessed 27 Feb 2017

# Chapter 6

# Gene Expression Mining in Type 2 Diabetes Research

Donald R. Dunbar

## Abstract

Gene expression analysis by microarray and more recently by next-generation sequencing has become a core part of biomedical research and its value can be seen in thousands of research papers. A successful gene expression experiment needs to be augmented by specialized data mining techniques if the data are to be fully exploited. Here, tools that concentrate on three areas—gene enrichment analysis, literature mining, and transcription factor binding site analysis—are described for the novice user of microarray and next generation sequencing technologies. The focus of this chapter is on free, publicly available, web-based tools.

**Key words** Bioinformatics, Microarray, Next generation sequencing, Gene expression, Data mining, Gene enrichment, Literature mining, Transcription factor binding site

## 1 Introduction

The methods and utility of microarray gene expression studies have been described in the previous chapter by Drs. White and Kaestner in the first edition of this series. In recent years, next generation sequencing methodologies have begun to compete with microarrays. Although the initial analysis methodologies are very different for microarrays and sequencing (often called RNA-seq) once a gene list is generated, similar challenges remain for both. For biologists, the main limiting step in the process from experiment design to publication of results is usually the interpretation of the data. Modern microarrays and next generation sequencing experiments measure gene expression on a genome-wide level, and depending on the experimental system being studied, routinely identify from tens to thousands of genes that are differentially expressed. This creates a problem for the biologist. The biological annotation for a handful of genes is relatively easy to collate and any strong themes within the data will be simple to spot. However, when presented with a list of a hundred or more genes, interpretation of the biological changes underlying the data becomes an enormous

Claire J. Stocker (ed.), *Type 2 Diabetes: Methods and Protocols*, Methods in Molecular Biology, vol. 2076,
https://doi.org/10.1007/978-1-4939-9882-1_6, 

challenge. High-throughput methods that help the biologist make sense of their gene expression data have been developed over the last few years, and the purpose of this chapter is to guide the inexperienced user of microarrays through a selection of them. The selection includes tools to identify overrepresented biological functions and processes associated with the gene list, to mine the biomedical literature for associations between genes and biological terms of interest, and to identify transcription factor binding sites in the gene sequences. The focus of this chapter will be on free, publicly available, web-based tools.

The method section of this chapter is split into five short sections (one method for preparing gene lists and four web-based tools). Each describes one method or tool that helps the biologist to gain some insight into the biology behind their data. The aim is to give enough information to allow the novice user of microarrays and next-generation sequencing, with little or no bioinformatics support, to use each tool. Each of the tools has additional functionality (and usually adequate online help pages), and indeed, there are many other similar tools available in addition to those described here.

### 1.1 Gene Enrichment Analysis

Gene enrichment analysis uses statistical procedures to discover overrepresented features within a dataset. Given a gene list and some biological information, these tools can identify categories (e.g., biological processes and molecular functions from the Gene Ontology consortium or molecular pathways from KEGG) that appear more often in the gene set that they would by chance in a random gene set of the same size. If a category is overrepresented, then this might have biological significance and point to that part of biology being perturbed in the experiment [1]. Gene enrichment analysis with the online tool DAVID (Database for Annotation, Visualization, and Integrated Discovery) will be described [2]. A tool with a broader and complementary scope than DAVID, Enrichr, has similar functionality to look for enriched biological functions [3, 4] and is used in a very similar way to DAVID. Enrichr gives access to libraries of data including transcription, pathways, ontologies, diseases, and drug and is very intuitive to explore.

### 1.2 Literature Mining

Literature Mining probes the huge body of information available to biomedical scientists, for example in the Medline database [5]. If two or more genes or proteins occur in the same paper, it is possible that they have some sort of association. Two main problems face the biologist when mining the literature, however. First, because there are often hundreds of genes of interest, looking for pairwise associations using manual web-based searching (e.g., through the PubMed web interface) is unfeasible. Computationally, however, these searches are trivial. The PubMatrix text mining tool will be described [6]. Second, genes often have multiple synonyms that are used in the literature. For example, the human gene transcription

factor 7-like 2 (T-cell specific, HMG-box) (official gene symbol, TCF7L2) has several synonyms: HMG box transcription factor 4, hTCF-4, T-cell-specific transcription factor 4, TCF4, TCF-4, and transcription factor 7-like 2. Several of these are used in scientific publications and this makes exact text matching difficult unless a complicated query string is built for each gene. The Information Hyperlinked over Proteins (iHOP) tool makes good use of synonym information, and offers several useful features, and its use will be described here [7]. These text-mining tools give the biologist a good entry to mining the literature. Further tools that include more advanced information extraction and retrieval, entity recognition, and natural language processing will become available to the biologist over time.

### 1.3 Transcription Factor Binding Site (TFBS) Analysis

Transcription factor binding site (TFBS) analysis can identify binding sites that are statistically overrepresented in the sequences of a gene list. Finding such enriched sites can give an idea of the factors that are driving gene expression locally at the cellular level in the experimental model. TFBSs often bind to several similar sequences and computational tools that access TFBS databases can use sequence models to predict binding sites in gene sequences [8]. In addition, if a binding site is conserved between species, it is more likely to be functionally important. Whole Genome RVista allows for identification of conserved (between pairs of species) statistically overrepresented TFBSs in specified regions (e.g., 5 kb upstream) of groups of genes [9].

## 2 Materials

This description of protocols for downstream analysis of high-throughput gene expression data is strongly aimed at the inexperienced user of microarray technology with little or no bioinformatics support. As such, the reader only needs access to the processed, statistically analyzed data, and a computer with web access, spreadsheet (e.g., Microsoft Excel or OpenOffice) software, and text file editing software.

## 3 Methods

The following methods require the user to have a list of selected genes. This will be generated by a statistical tool, often used by a microarray or next generation sequencing facility, and genes will be included or excluded based on a threshold score for some statistics of the gene expression (e.g., $p$-value or fold change). These protocols require that the user can copy a list of gene identifiers (e.g., Affymetrix Probeset IDs or Entrez Gene IDs for Subheadings 3.2

and 3.5; gene symbols and names for Subheading 3.3) for further use. Other identifiers are available and documentation in each of the tools will describe the appropriate one. Data should come to the user in the form of a spreadsheet or a tab delimited text file.

### 3.1 Gene List Preparation

1. Open the file containing gene expression data with spreadsheet software.
2. Copy the gene identifiers.
3. Paste into a new spreadsheet.
4. Sort the identifiers.
5. Remove any duplicate entries (*see* **Note 1**).
6. Save as a plain text file with appropriate name, e.g., "exp1_up_2fold_AffyIDs.txt."

### 3.2 Gene Enrichment Analysis with DAVID

1. Open the gene list text file (*see* **Note 2**).
2. Copy the identifiers, noting their type (e.g., Affymetrix ID, Entrez Gene IDs).
3. Go to DAVID website: https://david.ncifcrf.gov/.
4. Click "Start Analysis" in the menu bar.
5. Paste the gene list into "Step 1: Enter Gene List" box.
6. Select the type of identifier (e.g., AFFY_ID) in "Step 2: Select Identifier".
7. Select "Gene List" from "Step 3: List Type."
8. Submit List (this will take you to the analysis wizard).
9. Click "Rename," rename the list in the dialog box, click "OK."
10. The "Current Background" will be automatically selected (*see* **Note 3**).
11. If your data are Affymetrix IDs, click "Background" in the navigation bar.
12. Click the "+" beside "Affymetrix." Choose the appropriate GeneChip.
13. Click "Functional Annotation Tool" in the analysis wizard.
14. Click "Functional Annotation Chart."
15. Click the "+" for "Options." Check "Fold Enrichment" then "Re-run Using Options."
16. Explore the results (*see* **Note 4**).

### 3.3 Literature Mining with PubMatrix

1. Go to the PubMatrix site (http://pubmatrix.grc.nia.nih.gov/) and register for an account, and then log on to the "authenticated site."
2. Prepare a list of gene names and symbols up to a maximum of 100 (*see* **Note 5**).

3. Prepare a list of relevant words to analyze alongside the genes (e.g., diabetes, obesity, insulin, diet, glucose, metformin, regulate, and expression).
4. Give the "Search Terms" and "Modifier Terms" appropriate names (e.g., "upregulated genes experiment 2," "T2D terms 1–10").
5. Copy the gene list into the "Search Terms" list (or upload a file).
6. Copy the word list into the "Modifier Terms" list (or upload a file).
7. Submit to PubMatrix (*see* **Note 6**).
8. The following day, go to the PubMatrix site and click "Your past results." Check the status of your search, and if completed, click the link.
9. Explore your results. In the matrix displayed, each combination of Search Term (gene) and Modifier Term (extra word) has a number indicating how many abstracts were found. Click one.
10. This takes you to a PubMed search for the titles and abstracts that contain both the search and modifier term (*see* **Note 7**).

### 3.4 Literature Mining with iHOP

1. Go to the iHOP website: http://www.ihop-net.org.
2. Enter a gene name, symbol or ID in the first box.
3. Select the appropriate fields to search (leaving "all fields" is usually fine, if it is a gene ID, select "NCBI Gene"). Select a species if required.
4. Click the "SEARCH" link.
5. Explore your results.
6. If successful, the search gives one or more rows. Click any of the links in the row that matches your gene (all the links in a row are to the same page).
7. This page is the current iHOP page for that gene (highlighted red). Sentences from PubMed abstracts are displayed and other genes and other annotation highlighted and hyperlinked (*see* **Note 8**).
8. Click a link for another gene mentioned in the sentence along with your gene of interest and you will be taken to the iHOP page for that gene.
9. Use some of the other functions available in iHOP (*see* **Note 9**).

### 3.5 Transcription Factor Binding Site Analysis with Whole Genome RVista

1. Go to the Whole Genome RVista site: http://genome-test.lbl.gov/cgi-bin/WGRVistaInputCommon.pl.
2. Choose a genome alignment to use (e.g., Human Feb. 2009 (hg19) vs. Mouse Jul. 2007 (mm9)) and "GO."

3. Select the length of upstream sequence you would like to analyze (5 kb default) and a *p*-value threshold (0.005 by default).
4. Open the file with the Entrez Gene IDs. Copy the IDs into the box select "I am submitting locus link ids" (*see* **Note 10**). Submit.
5. Explore your results. The results table shows overrepresented (statistically significant) conserved transcription factor binding sites, ordered by $-\log_{10}$ *p*-value (a *p*-value of 0.005 gives a $-\log_{10}$ *p*-value of 2.3). Click one of the buttons on the right, marked with a TFBS symbol. This then shows the genes in your list that have this sequence at least once in the region searched (*see* **Note 11**).
6. Back on the main results page, scroll down to the second table. Click on one of the "show" links in the "Summary of all conserved TFBS upstream of this gene" column. This will then show a table of conserved TFBSs upstream of the gene with those overrepresented in the input gene list marked in green.

## 4 Notes

1. Often, lists of genes that are differentially expressed will have two or more entries for the same gene. This is the case for some outputs of microarray analyses where probes/probe sets have been kept separate. This can cause problems in further analysis, especially where statistics require no redundancy. If a gene (e.g., its Entrez Gene ID) is present two or more times in a list, then it will be counted twice in the analyses used, for example, by DAVID (Subheading 3.2) and rVISTA (Subheading 3.5). When working with tools that accept chip identifiers (such as Affymetrix probe set IDs), redundancy is not usually a problem as the chip identifiers will normally be unique. Although many tools deal with this redundancy at the gene level, it is safer to remove it at source. Paste the IDs into a worksheet, sort, and then remove duplicate items, either manually or using a spreadsheet function (Excel has a remove duplicates tool).
2. Many tools allow identifiers or sequences to be input by pasting text or directly form a file. If the file is in the appropriate format, then these methods are equivalent. Choose the method that suits you.
3. Enrichment analysis requires a "benchmark" to test against. A background gene set is used for this and can be the complement of genes on a microarray, or in the whole genome. (The

"Current Background" in DAVID defaults to complete knowledgebase gene set for the input species). If, for example, ten genes in your gene list of 200 (5%) belong to (or map to) one Gene Ontology term (GO term) this might sound exciting. However, if 5% of the genes on the microarray also belong to that GO term, then your finding is no different from chance. But if only 1% of the genes on the microarray map to the GO term, then it is likely that your result is a real enrichment. You can then proceed to investigate the biological significance of the result. Other background gene sets, for example, the lit of genes expressed in a tissue of interest, can be used and may give better enrichment results; however, this may be more advanced than novice users can manage.

4. The DAVID functional annotation chart is a table displaying those terms that are statistically enriched in your gene list. The "term" column gives a hyperlinked name of the enriched term. The hyperlink goes to the database outlined in the "category" column: for example, GOTERM_ goes to QuickGO at EBI, SP_ goes to Uniprot, and KEGG_ and BIOCARTA_ go to those pathway databases stored within DAVID. The links are not all ideal as they can be to text searches rather than direct links to database entries using the ID of the term: these text searches, using the term name can often match more than the term of interest. Further information about the term can be obtained from the "RT" column, which gives a hyperlink to related terms for each term, ranked by relatedness based on overlap of gene lists. This can be useful to get a wider view of the biology around the enriched term. There is usually plenty of redundancy in this list, mainly due to the hierarchical nature of the GO database (e.g., genes in GOTERM_BP_5 are a subset of genes in GOTERM_BP_4). The table is ordered by the p-value for the statistical test (Fisher Exact) used to determine enrichment. In addition, there is a column "Benjamini" that lists the p-value corrected for multiple testing. The "count" indicates the number of genes from our list that is mapped to the term, and "%" is this number as a percentage of the full list of genes mapped to that term. The "fold enrichment" column gives a ratio for the enrichment. Clicking on the blue bar in the "Genes" column will show the genes in the list that map to the term and useful links to the database entry for each gene and a set of related genes.
5. PubMatrix does not map a gene's ID onto its name or symbol, so it is essential to prepare a gene name and symbol list. These of course can be used separately, but they can also be used as a query together separated by "OR." Copy and paste name and symbol for your gene list into a worksheet. Insert a column between them and add the word "OR" to each cell in the

column by filling down, so that we have gene name in column 1, "OR" in column 2, and gene symbol in column 3. Now, in the column 4, add the following function: =CONCATENATE (A1," ",B2," ",C1), and fill or copy it down the column. This will give terms like "aquaporin 4 OR Aqp4." These can then be stored in a text file with an appropriate name and used in a PubMatrix search.

6. Due to restrictions placed on using PubMed servers at NCBI, PubMatrix will only run searches from 5 p.m. to 8 a.m. Eastern Standard Time. Jobs will, however, go into the queue if submitted outside this window and are almost always completed by the next day.
7. PubMatrix searches are fairly crude and as with other text searches of PubMed, and are sensitive to false positives and negatives. False negatives usually happen because none of a gene's synonyms were used in the search. False positives are frequently the fault of gene symbols having an alternative meaning in the literature. Symbols that are also short words or abbreviations are often the culprits. Adding extra synonyms where appropriate and removing problematic symbols can help. Where this occurs, simply resubmit the new list to PubMatrix.
8. The main advantage of using iHOP is its use of synonym data to search the literature and link genes/proteins. This means that searching with one synonym will also find publications that cite other synonyms or symbols for the gene or protein. iHOP makes extensive use of links and markup. Each iHOP page has links to the pages for other genes: this is the essence of iHOP. "Marking up" abstracts means that it is immediately obvious where in the abstract the current and other genes are in addition to informative verbs such as associated, interacts, biding, complexed, affect, inhibits, suppresses, and activates. MESH (Medical Subject Headings) terms and chemical compounds are also marked up and have additional links. Links on the right of the screen will take you to the abstracts within PubMed.
9. An extremely useful feature of iHOP is the "show overview" link. This link takes you to a list of genes that are associated with the gene of interest, ordered by the number of sentences in the literature that co-cite the two genes and whether there is any interaction evidence in several databases including IntAct. This immediately guides you to genes that are highly co-cited with the gene of interest. Click a gene link to see that both the original and linked genes are marked up in the sentences. Enhanced PubMed and Google searches (using all synonyms, symbols, and additional terms) are useful for further searching,

and genes can be added to a useful "Gene Model" that shows interactions visually.

10. Locus link was the predecessor of the Entrez Gene database. Locus link IDs map exactly to Entrez Gene IDs.
11. In the Whole Genome rVISTA output, the "number of hits in the submitted regions" column tells us the total number of hits rather than the number of genes that contain the conserved TFBS sequence. This is compared with the "total number of hits on genome" to generate the statistics. Clicking the "show genes where…" buttons will then show the genes that have the TFBS.

## References


1. Curtis RK, Oresic M, Vidal-Puig A (2005) Pathways to the analysis of microarray data. Trends Biotechnol 23(8):429–435
2. Huang DW, Sherman BT, Lempicki RA (2009) Systematic and integrative analysis of large gene lists using DAVID bioinformatics resources. Nat Protoc 4(1):44–57
3. Chen EY, Tan CM, Kou Y, Duan Q, Wang Z, Meirelles GV et al (2013) Enrichr: interactive and collaborative HTML5 gene list enrichment analysis tool. BMC Bioinformatics 14:128
4. Kuleshov MV, Jones MR, Rouillard AD, Fernandez NF, Duan Q, Wang Z et al (2016) Enrichr: a comprehensive gene set enrichment analysis web server 2016 update. Nucleic Acids Res 44(W1): W90–W97
5. Jensen LJ, Saric J, Bork P (2006) Literature mining for the biologist: from information retrieval to biological discovery. Nat Rev Genet 7(2):119–129
6. Becker KG, Hosack DA, Dennis G, Lempicki RA, Bright TJ, Cheadle C et al (2003) PubMatrix: a tool for multiplex literature mining. BMC Bioinformatics 4:61
7. Hoffmann R, Valencia A (2004) A gene network for navigating the literature. Nat Genet 36 (7):664
8. Elnitski L, Jin VX, Farnham PJ, Jones SJM (2006) Locating mammalian transcription factor binding sites: a survey of computational and experimental techniques. Genome Res 16 (12):1455–1464
9. Zambon AC, Zhang L, Minovitsky S, Kanter JR, Prabhakar S, Salomonis N et al (2005) Gene expression patterns define key transcriptional events in cell-cycle regulation by cAMP and protein kinase A. Proc Natl Acad Sci U S A 102 (24):8561–8566

# Chapter 7

# Pathways Enrichment Analysis of Gene Expression Data in Type 2 Diabetes

**Maysson Ibrahim**

## Abstract

Profiling genome-wide transcriptional changes with advanced high-throughput transcriptional profiling techniques has led to a revolution in biomedical science. It has been challenging to handle the massive data generated by these techniques and draw meaningful conclusions from it. Therefore, computational biologists have developed a number of innovative methods of varying complexity and effectiveness to analyze such complex data. Over the past decade, rich information in pathway repositories has attracted and motivated researchers to incorporate such existing biological knowledge into computational analysis tools to develop what is known as pathway enrichment analysis tools. This chapter describes a new sophisticated pathway enrichment tool that exploits topology of pathway as well as expression of significantly changed genes to identify biologically significant pathways for high-dimensional gene expression datasets. Also, we demonstrate the use of this tool to analyze gene expression data from a type 2 diabetes dataset to identify a list of significantly enriched metabolic pathways.

**Key words** Pathway analysis, Metabolic pathway, Gene expression, Type 2 diabetes, Microarray

## 1 Introduction

Genome-wide transcriptional profiling techniques provide researchers with tools to explore life at the molecular level by quantifying temporal and spatial changes in gene activity. However, meaningful analysis of complex data generated by these techniques remains a challenge despite recent substantial efforts to develop sophisticated analysis methods. Pathway enrichment is one of these analysis methods that have facilitated our understanding of big genetic data by reducing the dimensionality of analyzed data from tens of thousands of individual genes into hundreds of predefined biological pathways curated and stored in public databases [1]. Based on differences in structure and mechanism, biological pathways are grouped and stored in different categories such as biochemical enzyme–substrate pathways, linear or branching signaling cascades pathways or protein–DNA binding. Therefore,

Claire J. Stocker (ed.), *Type 2 Diabetes: Methods and Protocols*, Methods in Molecular Biology, vol. 2076,
https://doi.org/10.1007/978-1-4939-9882-1_7, 

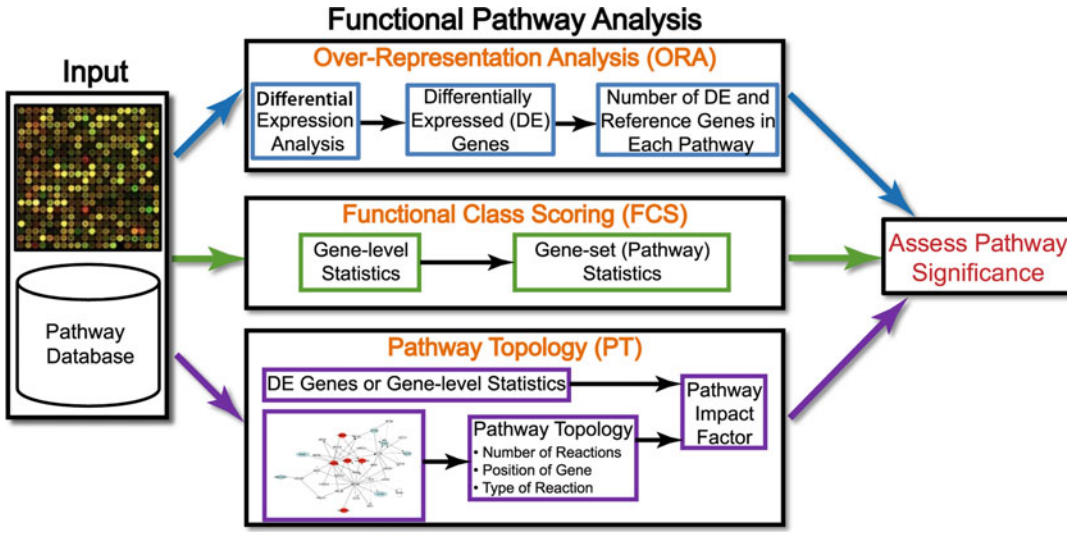


**Fig. 1** Pathway enrichment analysis approaches (Adapted from [2])

defining a one-size-fits-all set of mathematical principles to analyze different groups of pathways is a very challenging task. Pathway enrichment approaches can be generally divided into three generations [2]: Over-Representation Analysis (ORA), Functional Class Scoring (FCS) approaches, and Pathway Topology (PT)-based approaches (Fig. 1). Arguably, the third-generation approaches outperform both ORA and FCS approaches in the rational exploitation of rich biological information such as topology of pathway represented by genes location and interaction (e.g., activation, inhibition, etc.). Several topology-based pathway enrichment tools have been proposed in the literature over the past few years [2]. Some tools rely on topology only in scoring pathways [3, 4], whereas others use topology in addition to other gene expression measurements [5].

This chapter presents a new topology-based pathway enrichment tool for analyzing gene expression data [6]. The underpinning approach utilizes both pathway topology (i.e., the relationships between genes of the network) and magnitude of gene expression changes in formulating a new score for impacted pathways called Pathway Regulation Score (PRS) [7]. The PRS approach was developed to analyze signaling as well as metabolic pathways taking into consideration differences in structural complexity between the two groups. The list of pathways used by this tool was imported from KEGG database (http://www.kegg.jp/kegg/rest/) [8] and then maps were redrawn in MATLAB for two reasons. Firstly, removing any redundancy of genes in pathways map (i.e., some genes are represented multiple times in one pathway map) to mitigate any bias can affect the reliability of the final pathway score, and secondly to facilitate the use of graph theory for

solving the loops problem in pathways in addition to other problems that emerged from working on annotations and topology information. The PRS tool gives users the option of running a statistical test to evaluate the significance of their results. For comparison purposes with traditional pathway enrichment scoring approaches, the tool uses the known *z*-score approach [9] to run overrepresentation analysis in parallel with the PRS approach.

## 2 Materials

1. Microarray gene expression data. There are a number of public gene expression dataset repositories such as Gene Expression Omnibus (GEO) database (http://www.ncbi.nlm.nih.gov/geo/), or ArrayExpress (http://www.ebi.ac.uk/arrayexpress/).
2. Access to PRS software, which is a standalone tool that needs to be downloaded on your PC (*see* Subheading 3.1 for details).
3. Microsoft Excel spreadsheet to create an input file for the tool.
4. Internet access to browse enriched pathways map.

## 3 Methods

### *3.1 Software Installation*

1. If you do not have MATLAB on your PC, you should initially install the MCR (MATLAB Compiler Runtime) as explained in the tool webpage (http://www.buckingham.ac.uk/research/clore-laboratory-diabetes-obesity-and-metabolic-research/staff/maysson-al-haj-ibrahim/prs-tool/).
2. Click on the "Topology-based Pathway Analysis Tool" hyperlink in the tool webpage to download the .zip file.
3. Right-click on the .zip format file to extract all relevant files, and then run the PRS_interface file.

### *3.2 Data Preprocessing*

1. Prior to the analysis of gene expression data, some information should be checked such as the array platform, number of samples per group, species, and whether data is raw or normalized.
2. The tool does not provide a filter to normalize data. Therefore, users should normalize the data before using the tool for analysis (*see* **Note 1**).
3. Data must be saved in a form of simple Excel spreadsheet, in which the first column should be a probe ID, and the following columns are normalized gene expression values from control and test groups (*see* **Note 2**).

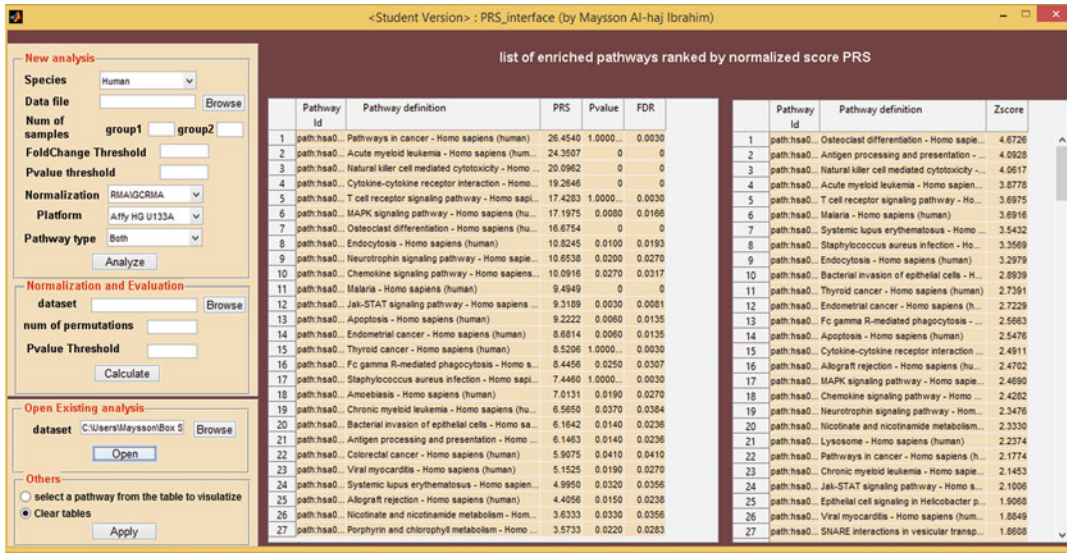


**Fig. 2** PRS tool interface

### *3.3 Pathways Enrichment with PRS*

1. Right-click on the main file to open the GUI (*see* Fig. 2).
2. Select the type of species (e.g., Human, Mouse, Rat) from the drop-down menu.
3. Click the "browse" button to select the input data file (.xls format) pre-prepared in **step 3** of Subheading 3.2.
4. Enter the number of samples in group 1 and 2 (i.e., group1 might refer to control or test group based on which one comes first in the input file).
5. Enter the fold-change threshold for selecting highly changed genes (*see* **Note 3**).
6. Enter the *p*-value threshold for selecting significantly changed genes (*see* **Note 4**).
7. Select the normalization method (e.g., RMA/GCRMA, MAS) used for normalizing your data.
8. Select the platform (e.g., Affy HG U133A, Affy HG U133B, Affy HG U133 Plus 2.0, Affy HG U95A, Agilent) that is compatible with your data.
9. Finally, select which group of pathways (signaling or metabolic pathways, or both) you would like to map your data onto to run the analysis.
10. Press the "Analyze" button to start the analysis and see the results in the main interface (*see* **Note 5**).

### *3.4 Statistical Evaluation*

1. Click the "browse" button to select a results' file (.mat format) that was generated from a previous analysis (*see* **Note 6**).

2. Input the number of permutations for the statistical test (*see* **Note 7**).
3. Input the *p*-value threshold for selecting significant pathways (*see* **Note 8**).
4. Click the "calculate" button to run the evaluation.

### 3.5 Visualizing Enriched Pathway Map

1. In the main interface, activate the "Select a pathway to visualize" checkbox option.
2. From the results' table in the main interface, click on the pathway that you want to visualize.
3. Click the "Apply" button and wait for the pathway map webpage to open (*see* **Note 9**).

## 4 Notes

1. It is important to mention that effective normalization techniques are usually platform-dependent. For example, RMA [10], dChip [11], and MAS5 [12] are between-arrays normalization techniques used with one-channel arrays such as Affymetrix [13]. Whereas Lowess is within-array normalization method and commonly used with Agilent platforms [10]. These methods are implemented in a number of existing software such as Affymetrix Expression Console Software, which can be downloaded from (http://www.affymetrix.com/estore) or other software development platforms such as MATLAB (www.mathworks.com) or Bioconductor (http://www.bioconductor.org/).
2. To format the input file, make sure that your data start from the first row with no headings. Also remember that the order and size of the groups stored in the file should match those you will input in the main interface (**step 4** in Subheading 3.3).
3. Fold-change is a known method for identifying genes that change significantly between two groups. In this method, gene expression medians are calculated for each gene in both control and test groups. The fold-change will be estimated by the ratio of the medians of the two groups. All genes that have fold-change greater than a user-defined threshold are defined as Differentially Expressed Genes (DEGs). Although the threshold is traditionally set to be 1.5 or more, this is relatively arbitrary and may be adapted depending on the number of replicates. Indeed, the selected value should yield a sufficient number of impacted genes to allow pathway mapping.
4. *p*-Value threshold is the other criterion used in combination with fold-change to identify significantly changed genes between groups. Only DEGs that have *p*-values less than a

threshold (user-defined) are considered as significant DEGs. Although the *p*-value threshold is an arbitrary value, 0.01 and 0.05 are most commonly used in this area.

5. By clicking the "Analyze" button, the PRS tool will:
   (a) Read data (probe IDs, groups' samples) from the input file.
   (b) Convert probe IDs to KEGG IDs. It is not always easy to convert from any platform to KEGG ID. For that reason, Entrez ID is used as an intermediate step in the conversion. Firstly, probe IDs are converted into Entrez IDs based on existing mapping tables for different platforms. Secondly, Entrez IDs can be easily converted into KEGG IDs by adding a known prefix to Entrez IDs (e.g., "has": for human, "mmu": for mouse, "rno": for rat).
   (c) Identify a list of significant DEGs based on fold-change and *p*-value criteria. Unlike significant DEGs, nonsignificant genes are assigned a value 1 instead of their fold-change value to mitigate their contribution in the final pathways score.
   (d) Map genes and their values onto the list of curated pathways.
   (e) Build a graph for each pathway. Then, a Depth-First Search (DFS) algorithm is used to solve the loops problem and facilitate traversing the nodes (genes) of each graph (pathway). It also assigns a weight to each node based on its location and the number of significant downstream nodes.
   (f) Calculate a pathway regulation score (PRS) for each weighted graph (pathway) using the weights of significant nodes in that graph in addition to other parameters.
   (g) Calculate the *z*-score for each weighted graph (pathway) for comparison purposes with the PRS approach.
   (h) Rank the pathways in descending order based on their PRS values then export the ranked list to the table in the main interface.
   (i) Repeat the latter step for *z*-score and export the ranked list to a different table for comparison purposes.
   (j) Save the results in two different format files (.mat and . xls).
6. After the analysis and generating a list of scored pathways, statistical significance of the results can be evaluated to test if any of these scores (particularly high scoring pathways) were likely to occur by chance. The null hypothesis assumes that there is no difference between an observed score (PRS) and any random score for the same pathway.

7. A nonparametric permutation approach is used to generate random PRS scores for each pathway. It starts by permuting all genes' values, mapping them back onto pathways, and then recalculating the PRS score for each pathway. This process is repeated n times to generate the null distribution, where n is the number of permutations provided by the user through the interface. This number should be high enough (e.g., $n = 500$, $n = 1000$) to get a reliable test.
8. To decide if a pathway score is statistically significant, all random scores created in **step 7** for a pathway are compared to its observed score. Only the ones that match or exceed the observed score are counted, then the resultant number is divided by the total number of random scores (number of permutations) to give us what is known as the *p*-value. Next, the *p*-values of all pathways are adjusted by the false discovery rate (FDR) to assign a refined *p*-value to each pathway. Finally, all pathways that have a *p*-value smaller than the user-defined threshold are considered statistically significant.
9. The PRS software calls a pathway mapping web service (REST-based API service) hosted on the KEGG website and passes a number of parameters including a list of all expressed genes with their fold-change values, as well as setting colors to differentiate significant genes from nonsignificant genes (*see* Fig. 3).

Herein, we used the PRS tool to run pathways enrichment analysis on type 2 diabetes and pancreatic islets dataset downloaded from the Gene Expression Omnibus database (https://www.ncbi.nlm.nih.gov/geo/; accession #GDS4337). The

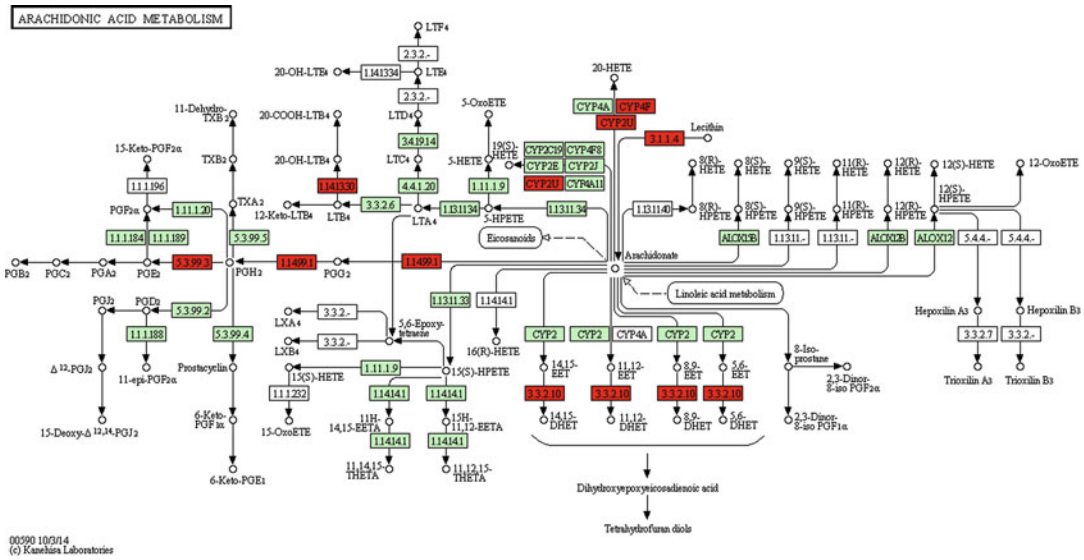


**Fig. 3** "Arachidonic acid metabolism pathway" enriched in T2D dataset (significant genes are colored in red)

**Table 1**
**Input data information for pathways analysis and significance evaluation in T2D and pancreatic islets dataset**

| | |
|---|---|
| **PRS analysis** | |
| Species | Human |
| # of samples in group1 | 9 |
| # of samples in group2 | 54 |
| Fold-change threshold | 1.3 |
| *p*-Value threshold | 0.05 |
| Normalization method | RMA |
| Platform | Affymetrix human gene 1.0 ST |
| Pathway type | Both (metabolic and signaling) |
| **Statistical significance evaluation** | |
| Number of permutations | 1000 |
| *p*-Value threshold | 0.05 |

experiment was designed to compare the gene expression levels in RNA isolated from human pancreatic islets taken from 9 type 2 diabetes (T2D) cadaver donors with RNA samples of pancreatic islets derived from 54 nondiabetic cadaver donors. Affymetrix Human Gene 1.0 ST Array was used for measuring gene expression levels and the resulting values were normalized by Robust Multi-array Analysis (RMA) before being uploaded to the GEO database. To use the PRS tool, we created an input file containing Affymetrix probe IDs and the samples from the two groups. Also, we input in the GUI other parameters (*see* Table 1 for more details about the parameters used in this example) such as number of samples in each group taking into account the groups order in the input file, (group 1 is diabetic and group 2 is nondiabetic in this case), fold-change (FC) and *p*-value thresholds (FC $\geq$1.3 and *p*-value $<$0.05 in this case, as FC $\geq$1.5 yields small number of significant genes which is not sufficient number to allow pathways mapping). Also, we chose to enrich for both signaling and metabolic pathways. Accordingly, the tool found the significant genes, mapped them onto the pathways, and created two scores (PRS and *z*-score) for each pathway. Then, pathways were ranked according to PRS and *z*-score and shown on the GUI in two separate tables (Fig. 2). Table 2 shows the top ten significant pathways ranked by PRS score where only statistically significant pathways (FDR $<$ 0.05) were selected, and Table 3 shows the top ten significant pathways ranked by *z*-score.

**Table 2**
**Top ten pathways ranked by PRS score (T2D and pancreatic islets dataset)**

| Rank | Pathway name | PRS | *p*-Value | FDR |
|---|---|---|---|---|
| 1 | Arachidonic acid metabolism | 3.450412 | 0 | 0 |
| 2 | Cytokine–cytokine receptor interaction | 1.443531 | 0 | 0 |
| 3 | TGF-beta signaling pathway | 1.345376 | 0 | 0 |
| 4 | Complement and coagulation cascades | 1.180362 | 0 | 0 |
| 5 | PPAR signaling pathway | 1.030316 | 0.002 | 0.0065 |
| 6 | Pathways in cancer | 0.910555 | 0.004 | 0.0104 |
| 7 | Type II diabetes mellitus | 0.793327 | 0.002 | 0.0065 |
| 8 | Tryptophan metabolism | 0.754089 | 0.001 | 0.004875 |
| 9 | MAPK signaling pathway | 0.736616 | 0.001 | 0.004875 |
| 10 | Fatty acid metabolism | 0.701842 | 0.004 | 0.0104 |

**Table 3**
**Top ten pathways ranked by z-score (T2D and pancreatic islets dataset)**

| Rank | Pathway name | *z*-Score |
|---|---|---|
| 1 | Arachidonic acid metabolism | 6.103672 |
| 2 | TGF-beta signaling pathway | 5.571651 |
| 3 | Complement and coagulation cascades | 5.468563 |
| 4 | PPAR signaling pathway | 5.302763 |
| 5 | Cytokine–cytokine receptor interaction | 5.102405 |
| 6 | Fatty acid metabolism | 5.050608 |
| 7 | Intestinal immune network for IgA production | 4.748036 |
| 8 | Cell adhesion molecules (CAMs) | 4.601507 |
| 9 | Allograft rejection | 4.480696 |
| 10 | *Staphylococcus aureus* infection | 4.416682 |

Interestingly, some relevant pathways come in the top of the list such as "Arachidonic acid metabolism" [14], "TGF-beta signaling pathway" [15]," Fatty acid metabolism" [16, 17], "PPAR signaling pathway" [18, 19]. In comparison with *z*-score, only PRS picked up "MAPK signaling" and "Type II diabetes mellitus" pathways which are highly related to T2DM.

## References


1. Bauer-Mehren A, Furlong LI, Sanz F (2009) Pathway databases and tools for their exploitation: benefits, current limitations and challenges. Mol Syst Biol 5:290
2. Khatri P, Sirota M, Butte AJ (2012) Ten years of pathway analysis: current approaches and outstanding challenges. PLoS Comput Biol 8 (2):e1002375
3. Gao S, Wang X (2007) TAPPA: topological analysis of pathway phenotype association. Bioinformatics 23(22):3100–3102
4. Vert JP, Kanehisa M (2003) Extracting active pathways from gene expression data. Bioinformatics 19(Suppl 2):ii238–ii244
5. Tarca AL, Draghici S, Khatri P, Hassan SS, Mittal P, Kim J et al (2009) A novel signaling pathway impact analysis. Bioinformatics 25 (1):75–82
6. Ibrahim MA, Jassim S, Cawthorne MA, Langlands K (2014) A MATLAB tool for pathway enrichment using a topology-based pathway regulation score. BMC Bioinformatics 15(1):358
7. Ibrahim MA, Jassim S, Cawthorne MA, Langlands K (2012) A topology-based score for pathway enrichment. J Comput Biol 19 (5):563–573
8. Kanehisa M, Goto S, Kawashima S, Nakaya A (2001) The KEGG databases at GenomeNet. Nucleic Acids Res 2(1):42–46
9. Cheadle C, Vawter MP, Freed WJ, Becker KG (2003) Analysis of microarray data using Z score transformation. J Mol Diagn 5(2):73–81
10. Järvinen A-K, Hautaniemi S, Edgren H, Auvinen P, Saarela J, Kallioniemi O-P et al (2004) Are data from different gene expression microarray platforms comparable? Genomics 83(6):1164–1168
11. Li C, Wong W (2003) DNA-chip analyzer (dChip). http://www.springerlink.com/index/G5V0232463245R24.pdf
12. Pepper SD, Saunders EK, Edwards LE, Wilson CL, Miller CJ (2007) The utility of MAS5 expression summary and detection call algorithms. BMC Bioinformatics 8(1):273
13. Do JH, Choi D (2006) Normalization of microarray data: single-labeled and dual-labeled arrays. Mol Cells 22(3):254
14. Persaud SJ, Muller D, Belin VD, Kitsou-Mylona I, Asare-Anane H, Papadimitriou A et al (2007) The role of Arachidonic acid and its metabolites in insulin secretion from human islets of Langerhans. Diabetes 56(1):197–203
15. Prentki M, Nolan CJ (2006) Islet cell failure in type 2 diabetes. J Clin Invest 116 (7):1802–1812
16. Yaney GC, Corkey BE (2003) Fatty acid metabolism and insulin secretion in pancreatic beta cells. Diabetologia 46(10):1297–1312
17. McGarry JD (2002) Banting lecture 2001 Dysregulation of fatty acid metabolism in the etiology of type 2 diabetes. Diabetes 51(1):7–18
18. Kim H-S, Hwang Y-C, Koo S-H, Park KS, Lee M-S, Kim K-W et al (2013) PPAR-γ activation increases insulin secretion through the up-regulation of the free fatty acid receptor GPR40 in pancreatic β-cells. PLoS One 8(1): e50128
19. Sugden MC, Holness MJ (2004) Potential role of peroxisome proliferator-activated receptor-α in the modulation of glucose-stimulated insulin secretion. Diabetes 53(1):S71–S81

# Chapter 8

# Diagnostic Genetic Testing for Monogenic Diabetes and Congenital Hyperinsulinemia

**Jayne A. L. Houghton**

## Abstract

Monogenic diabetes and hyperinsulinism are genetically heterogeneous disorders. The determination of the genetic etiology defines the diagnostic subtype, predicts prognosis, and importantly can guide clinical management. This chapter focuses on the processes and methodologies utilized in the diagnostic testing for monogenic diabetes and congenital hyperinsulinism (i.e., Sanger sequencing and targeted next-generation sequencing).

**Key words** Sanger sequencing, Targeted next-generation sequencing, Neonatal diabetes, MODY, Hyperinsulinism, *KCNJ11* and *ABCC8*

## 1 Introduction

Monogenic diabetes and hyperinsulinemic hypoglycemia result from a mutation or mutations in a single gene and can be dominantly inherited, recessively inherited, or can arise de novo. Monogenic diabetes is rare and accounts for ~3% of all cases of diabetes in young people. Neonatal diabetes affects ~1:100,000 live births and can be transient, permanent, or part of a syndrome. A genetic diagnosis often leads to improved treatment and can predict prognosis. Genetic testing can define the subtype in ~80% patients diagnosed with neonatal diabetes and about 40% of these patients will have an activating mutation in one of the KATP channel genes *KCNJ11* and *ABCC8*. A rapid genetic test is important, as patients with KATP channel mutations are able to transfer from insulin injections to sulfonylurea tablets which results in an improvement in glycemic control [1]. Approximately 52% of patients with a confirmed diagnosis of maturity onset diabetes of the young (MODY) have a mutation in *HNF1A*, 10% have a mutation in *HNF4A*, and 32% have *GCK* mutations [2]. A genetic diagnosis of MODY is essential to ensure that patients are on the most appropriate treatment, reducing the risk of diabetic complications

Claire J. Stocker (ed.), *Type 2 Diabetes: Methods and Protocols*, Methods in Molecular Biology, vol. 2076,
https://doi.org/10.1007/978-1-4939-9882-1_8, 

in later life. MODY subtypes HNF1A and HNF4A can be treated with low-dose sulfonylureas and those with MODY subtype GCK do not require any pharmacological treatment.

Congenital hyperinsulinism affects about 1:50,000 newborns, although the prevalence is more common in certain populations ~1:2500 [3]. It is characterized by the inappropriate secretion of insulin despite low glucose levels which if untreated can lead to seizures, coma, and death. It has two distinct histological forms, diffuse and focal. In patients with diffuse disease, the whole of the pancreas is affected, whereas a patient with focal disease has only a portion of the pancreas affected. Diffuse disease can be recessively or dominantly inherited, but the inheritance of focal congenital hyperinsulinism is more complex. Focal disease results from a paternally inherited recessive inactivating *KCNJ11* or *ABCC8* mutation and loss of the maternal allele within the pancreas due to paternal uniparental isodisomy during embryonic development. Genetic testing can help to distinguish between the diffuse and focal forms in ~40% of patients with congenital hyperinsulinism and plays an important role in helping to guide appropriate clinical management as it can help identify those patients with congenital hyperinsulinism who can be cured by lesionectomy. A genetic diagnosis also informs families of sibling recurrence risk and the risk for future offspring and can enable predictive genetic testing for asymptomatic relatives.

Current comprehensive genetic testing for patients with monogenic diabetes and congenital hyperinsulinism is performed using a combination of Sanger sequencing and targeted next-generation sequencing. Sanger sequencing of the common causes of monogenic diabetes and hyperinsulinism is performed as the first-line test as this can help guide urgent clinical management. For patients in whom a mutation is not identified in one of the common genetic causes, testing of all the known causes of monogenic diabetes and hyperinsulinism is performed using targeted next-generation sequencing. The aim of this chapter is to provide information for users regarding the methods utilized for the detection of mutations in the diagnostic testing for monogenic diabetes and congenital hyperinsulinism.

## 2 Materials

### 2.1 DNA Sample Preparation

DNA is extracted from peripheral blood in EDTA within 5 days of venesection using standard laboratory protocols or commercial DNA extraction and purification kits. High-quality DNA (nondegraded, $A_{260}/A_{280}$ is 1.8–2.0) is essential for reliable PCR amplification and sequencing.

### 2.2 Sanger Sequencing: PCR Reagents

1. MegaMix Royal (Microzone) contain Taq polymerase in 2× enhancing buffer (6 mM $MgCl_2$) with 400 μM dNTPs, blue MiZn loading dye, and stabilizer.
2. Microforce (MF) (Microzone) enhancing buffer for the amplification of GC-rich templates.
3. AmpliTaq Gold Polymerase (Applied Biosystems) with 10× PCR buffer I containing 15 mM $MgCl_2$.
4. 5 M Betaine.
5. 7-Deaza-dGTP (2 mM) (Roche).
6. dNTPS (Mix 1) (Cat no. AB-0196).
7. dNTPs (Mix 2) to make up 100 μl: 5 μl dTTP (100 mM), 5 μl dTTP (100 mM), 5 μl dTTP (100 mM), 5 μl dTTP (100 mM), and 81.5 μl of sterile water.
8. Deaza dGTP (Mix 3) to make up 100 μl: 10 μl Deaza dGTP (2 mM), 90 μl of sterile water.
9. Dimethyl sulfoxide (DMSO).
10. DNA (10 ng/μl).
11. PCR primers (*see* Table 1 for sequences) (*see* **Note 1**).

### 2.3 Sanger Sequencing: PCR Clean-Up Reagents

1. 5 μl PCR product.
2. Ethanol (85% v/v) (Sigma-Aldrich E7023—500 ml).
3. Agencourt AMPure XP-PCR purification system.
4. 384-Well cycling plate (40 μl well capacity).

### 2.4 Sanger Sequencing: Sequencing Reagents

Sequencing reagents will vary because they will be specific to the laboratory's available sequencing equipment. We have found that the following produce high-quality data and fit with our automated laboratory system.

1. 5× BigDye dilution buffer (Life Technologies Cat# 4336697).
2. BigDye terminator v3.1 (Life Technologies Cat# 4337455).
3. $dH_2O$ (Baxter (UKF7114).
4. M13 sequencing primers (Stock 100 pmol/μl).
5. POP7 Polymer (Life Technologies Cat#4342759).
6. 10× 3730 running buffer (Life Technologies Cat# 4335613).
7. EDTA (0.5 mM).

### 2.5 Sanger Sequencing: Sequencing Reaction Clean-Up Reagents

1. Sequencing reaction product.
2. Agencourt CleanSeq Dye terminator removal.
3. Ethanol (85% v/v) (Sigma-Aldrich E7023—500 ml).
4. Elution buffer ($dH_2O$).

**Table 1**
**List of genes, transcripts, primers and PCR conditions**

| *Gene: ABCC8 Accession No.: U63421 and L78208* | | | | | |
|---|---|---|---|---|---|
| **Exon** | **PCR method** | **Primer concentration (pmol/μl)** | **DNA concentration (ng/μl)** | **Forward and reverse primer sequences (M13 tailed) chromosome number** | **Size (bp)** |
| 1 | MMR | 2 (80% MF) | 10 | ABCC8ex1F_and_ABCC8ex1R agctgcaagggacagagg gagtgaagggatgagctgg 11 | 417 |
| 2 | MMR | 2 | 10 | ABCC8ex2F_and_ABCC8ex2R GAGGCAACAGAGCAAGACC ACCCTGGAGCAGATTCACTT 11 | 422 |
| 3 | MMR | 2 | 10 | ABCC8ex3F_and_ABCC8ex3R gccctgcagcctataaagtg ctccatgaaggcagggatt 11 | 390 |
| 4 | MMR | 2 | 10 | ABCC8ex4F_and_ABCC8ex4R AAATGTACACACCCAGGCAC GGGTAAAACAAGCTGATCCC 11 | 411 |
| 5 | MMR | 2 | 10 | ABCC8ex5F_and_ABCC8ex5R gtgttggggaatccttttcc ccctttgaggtccctctctg 11 | 478 |
| 6 | MMR | 2 | 10 | ABCC8ex6F_and_ABCC8ex6R GTTTCCCCAGACAACAGGAG TGGTAGTGACGGTGAGAGGA 11 | 522 |
| 7 | MMR | 2 | 10 | ABCC8ex7F_and_ABCC8ex7R CAGGGTGTAAGCAACCTTCC TGAGGATGAATAACACTCATGGAC 11 | 453 |
| 8 | MMR | 2 | 10 | ABCC8ex8F_and_ABCC8ex8R AAGTTGGAACGGTGATACAG TGTGAAAGGTACAGGCAAGC 11 | 435 |
| 9 | MMR | 2 | 10 | ABCC8ex9F_and_ABCC8ex9R GATAATTTGGAAACCTGGGC TGAAGTGGCCTACTCAAAGTC 11 | 387 |
| 10 | MMR | 2 | 10 | ABCC8ex10F_and_ABCC8ex10R TCTGGGAAATGGAGTCAATG GAGTCGGATAATCTCAAGGC 11 | 432 |
| 11 | MMR | 2 | 10 | ABCC8ex11F_and_ABCC8ex11R TGCCCCTAGCCTACTGGAG CTGGGCAGCCTGTCACTG 11 | 248 |
| 12 | MMR | 2 | 10 | ABCC8ex12F_and_ABCC8ex12R ATGAAGGTGTCTCCAACTAAAAGAT ATCACTCGAGCAAGCCTTG 11 | 362 |

| | | | | | |
|---|---|---|---|---|---|
| 13 | MMR | 2 | 10 | ABCC8ex13F_and_ABCC8ex13R TTCAGTGTGGGCTTTGTGG GGTGGTTTGGAGGTGAGGA 11 | 390 |
| 14 | MMR | 2 | 10 | ABCC8ex14F_and_ABCC8ex14R GCTGTGTCGGACTTCTGCCTTT GCTCCCTCTGGGAGTTGGTG 11 | 266 |
| 15 | MMR | 2 | 10 | ABCC8ex15F_and_ABCC8ex15R TTTTGGCTTTCATGGAGGAG TGCAGCTTTGTCTTTTTATCTCTATG 11 | 251 |
| 16 | MMR | 2 | 10 | ABCC8ex16F_and_ABCC8ex16R GAGGATGTTGATTTCCAGAAGG TGAGGAGGATGGTTAAAAGGAG 11 | 346 |
| 17 | MMR | 2 | 10 | ABCC8ex17F_and_ABCC8ex17R ACAGAGGCCATTTGGAAAC TCTGAAAATATGTAGGCTGCAC 11 | 298 |
| 18 | MMR | 2 | 10 | ABCC8ex18F_and_ABCC8ex18R TCTCTATGCAGCATTTGTGG AATGGATGCACAGAAACAGC 11 | 366 |
| 19 | MMR | 2 | 10 | ABCC8ex19F_and_ABCC8ex19R AGACCCAGACCTCTCAAACC GGTGCACCATATGGAGAGG 11 | 439 |
| 20 | MMR | 2 | 10 | ABCC8ex20F_and_ABCC8ex20R GAGGCCTATTAAAGCCATTGC CATGTTTGACCTTACTGCAGGC 11 | 350 |
| 21 | MMR | 2 | 10 | ABCC8ex21F_and_ABCC8ex21R AGGTGAGAAGCAGGCAAAGA GGTGGAGGTGGGCAGTTAG 11 | 277 |
| 22 | MMR | 2 | 10 | ABCC8ex22F_and_ABCC8ex22R TCCAAAGCCACACAGCTAAC CCAGTGCTGGTCTCTTATGC 11 | 404 |
| 23 | MMR | 2 | 10 | ABCC8ex23F_and_ABCC8ex23R AGGAGTATGTTGGTTGGGGTAG GGGCACTAAGGACAGGAAGA 11 | 399 |
| 24 | MMR | 2 | 10 | ABCC8ex24F_and_ABCC8ex24R TGAATGTGTGTCTGTCTGCC CAGAGGGAAGCCATTTAATC 11 | 370 |
| 25 | MMR | 2 | 10 | ABCC8ex25F_and_ABCC8ex25R CCCGTTGTCCCCTCAGTAAG CTCAGCCCTTCCCCCATC 11 | 393 |
| 26 | MMR | 2 | 10 | ABCC8ex26F_and_ABCC8ex26R CTGCAGCCAGGAACTGCTC CCATTTTATAGATGGGAAGACTAAGG 11 | 375 |

(continued)

**Table 1**
**(continued)**

| *Gene: ABCC8 Accession No.: U63421 and L78208* | | | | | |
|---|---|---|---|---|---|
| **Exon** | **PCR method** | **Primer concentration (pmol/μl)** | **DNA concentration (ng/μl)** | **Forward and reverse primer sequences (M13 tailed) chromosome number** | **Size (bp)** |
| 27 | MMR | 2 | 10 | ABCC8ex27F_and_ABCC8ex27R TGAATGACTCCAGAGACACTTA AGACAGGAGAAGCCCCCAG 11 | 246 |
| 28 | MMR | 2 | 10 | ABCC8ex28F_and_ABCC8ex28R AGTCTGGGCAACAGTGAGAC TAGGGCGGTGGAATAAGATG 11 | 466 |
| 29 | MMR | 2 | 10 | ABCC8ex29F_and_ABCC8ex29R CACGGGGTAAGAAGCTGAG GCTTGAGAGAGAACGTGTCC 11 | 349 |
| 30 | MMR | 2 | 10 | ABCC8ex30F_and_ABCC8ex30R GACATTCCAGAGAGGGATAGC ACACTAGGAGGACCACCAGG 11 | 411 |
| 31 | MMR | 2 | 10 | ABCC8ex31F_and_ABCC8ex31R CCCTTGTGTGTGTCTGGTG AACCTCCACCTGTCTGGG 11 | 454 |
| 32 | MMR | 2 | 10 | ABCC8ex32F_and_ABCC8ex32R GATGGCAGCAAAAGGAATC AGTTCTTTGGGATCAGCG 11 | 411 |
| 33 | MMR | 2 | 10 | ABCC8ex33F_and_ABCC8ex33R AGTCCAAGGAGGAGTGTGTC AGCATTGGGTTGGGCCCG 11 | 274 |
| 34 | MMR | 2 | 10 | ABCC8ex34F_and_ABCC8ex34R GAAACAAGCCCAAACCTGTG GGTGGCTGTGGGTACACG 11 | 286 |
| 35 | MMR | 2 | 10 | ABCC8ex35F_and_ABCC8ex35R GTGTACCCACAGCCACCAG CAACCCCCTCCTCTTTGTG 11 | 300 |
| 36 | MMR | 2 | 10 | ABCC8ex36F_and_ABCC8ex36R ACCACCTCGGTGCTTCTC TAGGACTAAATGGTCCTGCC 11 | 363 |
| 37 | MMR | 2 | 10 | ABCC8ex37F_and_ABCC8ex37R CCATGCACACATTTTCCAAC ATCCCACTAAACCCTTTCCAA 11 | 289 |

| | | | | | |
|---|---|---|---|---|---|
| 38 | MMR | 2 | 10 | ABCC8ex38F_and_ABCC8ex38R GGACTAGGATCGGGGTCAG CTGCTTCAGGGTTCTTTCTTG 11 | 307 |
| 39 | MMR | 2 | 10 | ABCC8ex39F_and_ABCC8ex39R ACCCCAGGAAAGTGCAGTC tttgctcacacagcttctgc 11 | 495 |
| IVS8 | MMR | 2 | 10 | ABCC8_Cryptic_Donor_FandR AGACACCGGCTCACAAGGT TCTTAGAGGCTGGGAAGTGG 11 | 290 |

***Gene: EIF2AK3 Accession No.: AF110146.1***

| Exon | PCR method | Primer concentration (pmol/μl) | DNA concentration (ng/μl) | Forward and reverse primer sequences (M13 tailed) chromosome number | Size (bp) |
|---|---|---|---|---|---|
| 1F | MMR (5% DMSO) | 2 (5% DMSO) | 10 | EIF2AK3ex1F_and_EIF2AK3ex1R CCTAGCACGTCCTTGCCTTC CCCCTACACCGCATCCTC 2 | 509 |
| 1R | MMR | 2 (5% DMSO) | 10 | EIF2AK3ex1F_and_EIF2AK3ex1R CCTAGCACGTCCTTGCCTTC CCCCTACACCGCATCCTC 2 | 509 |
| 2 | MMR | 2 | 10 | EIF2AK3ex2F_and_EIF2AK3ex2R TGAGCATGTGGGATAAGTG TGCCCTAAAGGGACACAAAC 2 | 369 |
| 3 | MMR | 2 | 10 | EIF2AK3ex3F_and_EIF2AK3ex3R TCAGGATCAAGACTCCAGCTC TGACAACCTCAGGGGAAAAT 2 | 484 |
| 4 | MMR | 2 | 10 | EIF2AK3ex4F_and_EIF2AK3ex4R GTTGGTAATCTAACTGATGC CCAACAGCAACATTA 2 | 358 |
| 5 | MMR | 2 | 10 | EIF2AK3ex5F_and_EIF2AK3ex5R GCCCTCTTGTGGCATAAATC GGGAGAGGAAGAACCGTA 2 | 485 |
| 6 | MMR | 2 | 10 | EIF2AK3ex6F_and_EIF2AK3ex6R TACTTGGGGCTCTCAGCTTG CACTCCTGAAGTAGGAAGG 2 | 410 |
| 7 | MMR | 2 | 10 | EIF2AK3ex7F_and_EIF2AK3ex7R CCCTCCCTGTTTTTGTTGAA GGGCAAAGACAGTCAGGATT 2 | 425 |
| 8 | MMR | 2 | 10 | EIF2AK3ex8F_and_EIF2AK3ex8R CTGGGCCATTTGTTTAACTT TGAAATTGTCTCCCAAGATG 2 | 420 |

(continued)

**Table 1**
**(continued)**

| *Gene: EIF2AK3 Accession No.: AF110146.1* | | | | | |
|---|---|---|---|---|---|
| **Exon** | **PCR method** | **Primer concentration (pmol/μl)** | **DNA concentration (ng/μl)** | **Forward and reverse primer sequences (M13 tailed) chromosome number** | **Size (bp)** |
| 9 | MMR | 2 | 10 | EIF2AK3ex9F_and_EIF2AK3ex9R AAGAAGAGAGACAAAACTTAAAAGGAA GGAAGATCACTGAGAACTTTGG 2 | 388 |
| 10 | MMR | 2 | 10 | EIF2AK3ex10F_and_EIF2AK3ex10R AAGACTGGAGGGATAGCAGT AGATCTTAGGTCATTTCTTCTTTG 2 | 407 |
| 11 | MMR | 2 | 10 | EIF2AK3ex11F_and_EIF2AK3ex11R TGAACTGATTTTCACATTACCAC AATTGGCAGCACTTAGAACC 2 | 376 |
| 12 | MMR | 2 | 10 | EIF2AK3ex12F_and_EIF2AK3ex12R GCCTTCAGTGTTGTCTTACT CATTGTAATCACACAAGCAAA 2 | 420 |
| 13A | MMR | 2 | 10 | EIF2AK3ex13AF_and_EIF2AK3ex13AR ACAGAGGGTGCAGTTCAGGT GCTACTGGTGGGCTTGAAAG 2 | 572 |
| 13B | MMR | 2 | 10 | EIF2AK3ex13BF_and_EIF2AK3ex13BR GAGGGGCACTCCTTTGAAC GATGCTTTTACTCTCCCCAACTC 2 | 589 |
| 14 | MMR | 2 | 10 | EIF2AK3ex14F_and_EIF2AK3ex14R TTGTCACTATTTTCCTGTTAGCC TGGGTTTTAGATTACTGGGTATTT 2 | 384 |
| 15 | MMR | 2 | 10 | EIF2AK3ex15F_and_EIF2AK3ex15R CCTGGGCTTTCCTTCTGTAA TGAGCTTTAAATGGAAGCAAA 2 | 500 |
| 16 | MMR | 2 | 10 | EIF2AK3ex16F_and_EIF2AK3ex16R GATGTACAACCTCTTAGTCATTTTGTT GGGAGCAGGTCTCTTTCCTC 2 | 371 |
| 17 | MMR | 2 | 10 | EIF2AK3ex17F_and_EIF2AK3ex17R TTTTGCCAGCACTGATTTTA TTTCAAGTCTGCAATTTTGG 2 | 403 |

| *Gene: FOXP3 Accession No.: NM_014009.2* | | | | | |
|---|---|---|---|---|---|
| **Exon** | **PCR method** | **Primer concentration (pmol/μl)** | **DNA concentration (ng/μl)** | **Forward and reverse primer sequences (M13 tailed) chromosome number** | **Size (bp)** |
| 1 | MMR | 2 | 10 | FOXP3ex1F_and_FOXP3ex1R TCAAGAAAAGGAGAAACACAGAGAG CACGGTAGCTGGGTACATCC X | 359 |
| 2 | MMR | 2 | 10 | FOXP3ex2F_and_FOXP3ex2R TTTGACCAGAGGAGTGTCCA ACAGTAAAGGTCGGCACCTG X | 414 |
| 3 | MMR | 2 | 10 | FOXP3ex3F_and_FOXP3EX3R tgagcctcagtttccatacg GGGCATCCACCGTTGAG X | 395 |
| 4 | MMR | 2 | 10 | FOXP3ex4F_and_FOXP3EX4R GACAGGCCACATTTCATGC CCAAGCCTCTGAGACCTGAC X | 427 |
| 5 and 6 | MMR | 2 | 10 | FOXP3ex5-6F_and_FOXP3ex5-6R CGCTCAAAATGAGAGGCCTTG CACCCTAGACCTCTCCCCAC X | 391 |
| 7 and 8 | MMR | 2 | 10 | FOXP3ex7-8F_and_FOXP3ex7-8R CCATTCAGAGCATTGAGCCAG CACCGTGCAGACCTCCTC X | 439 |
| 9 | MMR | 2 | 10 | FOXP3ex9F_and_FOXP3ex9R CTTGAATCTGGGAGGTGGG CCGAAAGGAAGCTTTTGTGA X | 546 |
| 10 | MMR | 2 | 10 | FOXP3ex10F_and_FOXP3ex10R ACGGGTGTTGACGGTGAG GGAGGAACCCACTCTGAGG X | 297 |
| 11 and 12 | MMR | 2 | 10 | FOXP3ex11-12F_and_FOXP3ex11-12R CCCTGATTACCTGCCCCTAC CTGCCTCCCACCAGTTTG X | 605 |
| *Gene: GATA4 Accession No.: NM_002052.3* | | | | | |
| **Exon** | **PCR method** | **Primer concentration (pmol/μl)** | **DNA concentration (ng/μl)** | **Forward and reverse primer sequences (M13 tailed) chromosome number** | **Size (bp)** |
| 1 | MMR | 2 | 10 | GATA4ex1F_and_GATA4ex1R CGGAGATGTGGAGTGATTGG CGGAAGGGGAAACTGAGG 8 | 394 |
| 2A | AG60 | 5 | 10 | GATA4ex2AF_and_GATA4ex2AR AAATTGGGATTTTCCGGAGT GTGTGGGCACGTAGACTGG 8 | 477 |

(continued)

**Table 1**
**(continued)**

| *Gene: GATA4 Accession No.: NM_002052.3* | | | | | |
|---|---|---|---|---|---|
| **Exon** | **PCR method** | **Primer concentration (pmol/μl)** | **DNA concentration (ng/μl)** | **Forward and reverse primer sequences (M13 tailed) chromosome number** | **Size (bp)** |
| 2B | AG60 | 5 | 10 | GATA4ex2BF_and_GATA4ex2BR CTCAGCTCGACACGGAGG GTATGGAGGGCTGTCGGC 8 | 350 |
| 2C | AG60 | 5 | 10 | GATA4ex2CF_and_GATA4ex2CR CGCAGGGACCATGTATCAG GGTAGGGGCTGGAGTAGGAG 8 | 497 |
| 2D | AG60 | 5 | 10 | GATA4ex2DF_and_GATA4ex2DR CTGCGGCCTACAGCAGTG CCTCGACAGGGCTCAAGAC 8 | 299 |
| 3 | AG60 | 5 | 10 | GATA4ex3F_and_GATA4ex3R AGCCCGAGGTGGTCTTCT TATTATGGGGCTCTCACCCA 8 | 435 |
| 4 | MMR | 2 | 10 | GATA4ex4F_and_GATA4ex4R CGCAGGTGACAGGAGAGTTAG AAGGAAGAAGACAAGGGAGGA 8 | 373 |
| 5 | MMR | 2 | 10 | GATA4ex5F_and_GATA4ex5R TTGCTTAGGTGTTGCCTTCTC TTTTTGCTGGGCTCTTCATC 8 | 353 |
| 6 | MMR | 2 | 10 | GATA4ex6F_and_GATA4ex6R AGCCATCCCTGTGAGAACTG GCTGGCCTCTGGGACTCT 8 | 387 |
| 7 | MMR | 2 | 10 | GATA4ex7F_and_GATA4ex7R AGAAGTGCTCCTTGGTCCCT TTCCCAGTTGTTGTTCTGGA 8 | 449 |
| *Gene: GATA6 Accession No.: NM_005257.3* | | | | | |
| **Exon** | **PCR method** | **Primer concentration (pmol/μl)** | **DNA concentration (ng/μl)** | **Forward and reverse primer sequences (M13 tailed) chromosome number** | **Size (bp)** |
| 2A | AG60 | 5 | 10 | GATA6ex2AF_and_GATA6ex2AR AAGGAGTGGAGGCGAGGTAG GGTCGAGGTCAGTGAACAGC 18 | 482 |
| 2B | AG60 | 5 | 10 | GATA6ex2BF_and_GATA6ex2BR CTCAGCTCGACACGGAGG GTATGGAGGGCTGTCGGC 18 | 518 |

| | | | | | |
|---|---|---|---|---|---|
| 2C | AG60 | 5 | 10 | GATA6ex2CF_and_GATA6ex2CR CTCTCTCCAGCCAGGGTCC GACAGCGAGCTGTACTGGG 18 | 484 |
| 2D | AG60 | 5 | 10 | GATA6ex2DF_and_GATA6ex2DR GCGCTTCCCCTACTCTCC CTGCAAATCCTTCCTGGGAC 18 | 501 |
| 3 | AG60 | 5 | 10 | GATA6ex3F_and_GATA6ex3R AAAAGCTCAGCCGGGAAG CTAGGGTGGGACCGCAG 18 | 435 |
| 4 | MMR | 2 | 10 | GATA6ex4F_and_GATA6ex4R TCTTGGCCCAGAAAAGTCAG AAAAGCACCTTCAATTCAATAA 18 | 491 |
| 5 and 6 | MMR | 2 | 10 | GATA6ex5and6F_and_GATA6ex5and6R CATGCGCCAACAAGTCTG CAAAACTTCTTGCTTTTACTTGG 18 | 801 |
| 7 | MMR | 2 | 10 | GATA6ex7F_and_GATA6ex7R GAGCAGCTCTGGCCCTG CAAAATAAAGGCACGAGAATCAC 18 | 412 |

***Gene: GCK Accession No.: NM_000162.2***

| Exon | PCR method | Primer concentration (pmol/μl) | DNA concentration (ng/μl) | Forward and reverse primer sequences (M13 tailed) chromosome number | Size (bp) |
|---|---|---|---|---|---|
| 1 | MMR | 2 | 10 | GCKex1F_and_GCKex1R TCCACTTCAGAAGCCTACTG TCAGATTCTGAGGCTCAAAC 7 | 195 |
| 2 | MMR | 2 | 10 | GCKex2F_and_GCKex2R GGGGTCAGAAGACAGAAGGA AGAGGAGCCAAGGGTGAGA 7 | 511 |
| 3 | MMR | 2 | 10 | GCKex3F_and_GCKex3R ATATCCGGGCTCAGTCACC CACCTCCCGTCAGGACTAGC 7 | 332 |
| 4 | MMR | 2 | 10 | GCKex4F_and_GCKex4R TAGCTTGGCTTGAGGCCGTG TGAAGGCAGAGTTCCTCTGG 7 | 308 |
| 5 | MMR | 2 | 10 | GCKex5F_and_GCKex5R tcactcacggcagaagca tggaagccaaggagaaagg 7 | 634 |
| 6 | MMR | 2 | 10 | GCKex6F_and_GCKex6R TGCGAGACGCTATCAAACG GGCTCTGCTCTGACATCACC 7 | 358 |
| 7 | MMR | 2 | 10 | GCKex7F_and_GCKex7R ccattgttccagacaaagca caagcccattatctgcaatg 7 | 436 |

(continued)

**Table 1**
**(continued)**

| *Gene: GCK Accession No.: NM_000162.2* | | | | | |
|---|---|---|---|---|---|
| **Exon** | **PCR method** | **Primer concentration (pmol/μl)** | **DNA concentration (ng/μl)** | **Forward and reverse primer sequences (M13 tailed) chromosome number** | **Size (bp)** |
| 8 | MMR | 2 | 10 | GCKex8F_and_GCKex8R CATTTCTAAAGCTCTGGCTCATT GTCCTGTCCCAGCCTCCT 7 | 634 |
| 9 | MMR | 2 | 10 | GCKex9F_and_GCKex9R ctttggctgggtgaggtg agggggacgagaagaggac 7 | 574 |
| 10 | MMR | 2 | 10 | GCKex10F_and_GCKex10R CCTCTTCTCGTCCCCCTTG ATGGAGCCTGGGTGCTGT 7 | 360 |
| PROM | MMR | 2 (80% MF) | 10 | GCKpromF_and_GCKpromR gctcggcatttcctgct agtcaggctgccaagaggt 7 | 512 |
| *Gene: GLIS3 Accession No.: NM_001042413.1* | | | | | |
| **Exon** | **PCR method** | **Primer concentration (pmol/μl)** | **DNA concentration (ng/μl)** | **Forward and reverse primer sequences (M13 tailed) chromosome number** | **Size (bp)** |
| Prom A | MMR | 2 | 10 | GLIS3 5'UTR(A)F_and_GLIS3 5'UTR(A)R aggaagcagctggctacagg GCTCATTCTCCCCTGCTACA 9 | 398 |
| Prom B | MMR | 2 | 10 | GLIS3 5′UTR(B)F_and_GLIS3 5′UTR(B)R ACGAGGATGAACAGGACAGG GCCTCCTTCGGAAATGAAA 9 | 244 |
| Prom C | MMR | 2 | 10 | GLIS3 5′UTR©F_and_GLIS3 5′UTR©R TGTAGCAGGGGAGAATGAGC gcaaagttcctatggcatcc 9 | 333 |
| 2A | MMR | 2 | 10 | GLIS3ex2AF_GLIS3Ex2AR ttgccgagagcactgtattg CTTCCCATTGGTGAGCATTT 9 | 642 |
| 2B | MMR | 2 | 10 | GLIS3ex2BF_and_GLIS3ex2BR ATCTCAAGATGCCCTCAGGA CTGGCAGAAAATGGGATGG 9 | 284 |
| 3 | MMR | 2 | 10 | GLIS3ex3F_and_GLIS3ex3R attggaattggagaaagcc CGAACGGAAAACACTTGTGGG 9 | 437 |
| 4A | MMR | 2 | 10 | GLIS3ex4AF_and_GLIS3ex4AR gggattgtcaatgcagtg aagccctcgacccgttg 9 | 510 |
| 4B | MMR | 2 | 10 | GLIS3ex4BF_and_GLIS3ex4BR gggattgtcaatgcagtg aagccctcgacccgttg 9 | 510 |

| | | | | | |
|---|---|---|---|---|---|
| 4C | MMR | 2 | 10 | GLIS3ex4CF_and_GLIS3ex4CR gggattgtcaatgcagtg aagccctcgacccgttg 9 | 510 |
| 5 | MMR | 2 | 10 | GLIS3ex5F_and_GLIS3ex5R ccaaatctgatacagaaa cttttaccaggctccact 9 | 527 |
| 6 | MMR | 2 | 10 | GLIS3ex6F_and_GLIS3ex6R Caattggtaacagttcat TCTAAAGCAGGTTATACC 9 | 338 |
| 7 | MMR | 2 | 10 | GLIS3ex7F_and_GLIS3ex7R Atagagcatgatgccttc TCACGTGAGCATTCCTTT 9 | 305 |
| 8 | MMR | 2 | 10 | GLIS3ex8F_and_GLIS3ex8R Tatgcttgctgtcaggct TTCAGCAACTGTCAAGGC 9 | 334 |
| 9 | MMR | 2 | 10 | GLIS3ex9F_and_GLIS3ex9R Gaatttggctttggagag GCATCTGAAATCCACGAC 9 | 345 |
| 10 | MMR | 2 | 10 | GLIS3ex10F_and_GLIS3ex10R Agctgggttggaatgatc GTGCTTGGTCACGTCCAG 9 | 351 |
| 11 | MMR | 2 | 10 | GLIS3ex11F_and_GLIS3ex11R tgtagtgcatttccagtg GCTGACATCCTTCCTCAA 9 | 304 |

***Gene: GLUD1 Accession No.: NM_005271.1***

| Exon | PCR method | Primer concentration (pmol/μl) | DNA concentration (ng/μl) | Forward and reverse primer sequences (M13 tailed) chromosome number | Size (bp) |
|---|---|---|---|---|---|
| 6 | MMR | 2 | 10 | GLUD1ex6F_and_GLUD1ex6R TTAAATGAGAATGTGCTTTGACTT TGAATTTGGTGATAGTTTGGTTG 10 | 496 |
| 7 | MMR | 2 | 10 | GLUD1ex7F_and_GLUD1ex7R AACCAGTTAGTACATTGTTTCTTTTGG AGAATGGACCCATGTTGCTG 10 | 393 |
| 10 | MMR | 2 | 10 | GLUD1ex10F_and_GLUD1ex10R gtgggatgggaaggagtgt ttgtgcatttttggtctaagtttc 10 | 455 |
| 11 | MMR | 2 | 10 | GLUD1ex11F_and_GLUD1ex11R GCAGAGTTTGCAGTGAGCTG TGCCGCAGATGAAATCCA 10 | 374 |
| 12 | MMR | 2 | 10 | GLUD1ex12F_and_GLUD1ex12R gttctgtgtggtgtccctgtt ggctgagatagcatggttgag 10 | 546 |

(continued)

**Table 1**
**(continued)**

| *Gene: HADH (SCHAD) Accession No.: NM_005327.2* | | | | | |
|---|---|---|---|---|---|
| **Exon** | **PCR method** | **Primer concentration (pmol/μl)** | **DNA concentration (ng/μl)** | **Forward and reverse primer sequences (M13 tailed) chromosome number** | **Size (bp)** |
| 1 | MMR | 2 | 10 | HADHex1F_and_HADHex1R CGTGTATACCCGCTCAACG GTGAAAACTCCCTGGTGTCG 4 | 502 |
| 2 | MMR | 2 | 10 | HADHex2F_and_HADHex2R TCGGTATTTTGAATGGAATGG AACCTCAAATCCCACCCAAC 4 | 538 |
| 3 | MMR | 2 | 10 | HADHex3F_and_HADHex3R GAACAGATAGGGTAGGCCAAT GCATGGAACAAAACTGCAC 4 | 436 |
| 4 | MMR | 2 | 10 | HADHex4F_and_HADHex4R CCCAATGGGTCAGGACAAC TATGAGGCTCAGGGACAACC 4 | 425 |
| 5 | MMR | 2 | 10 | HADHex5F_and_HADHex5R TTGTTTCTGGCTTGAGATTCC AACTAGAACAGGAGGCACGG 4 | 439 |
| 6 | MMR | 2 | 10 | HADHex6F_and_HADHex6R TGTACAGCTTGATAAATGGGG TCACAAAGCTAGAAAACAGACACTG 4 | 363 |
| 7 | MMR | 2 | 10 | HADHex7F_and_HADHex7R CCAAGCCAGAAAGTCTCAGTC GTGAGGCAGGATTTTGGAAG 4 | 413 |
| 8 | MMR | 2 | 10 | HADHex8F_and_HADHex8R CACCAGCACAGCCTTCCT TGCTGTAACTGGTGTAATAATCACTTC 4 | 490 |
| IVS5 | MMR | 2 | 10 | HADH_Cryptic_Donor_FandR ttttaggtacagcttggtaaacaca tcatttcagcaactgggatt 4 | 297 |
| *Gene: HNF1A Accession No.: NM_000545.3* | | | | | |
| **Exon** | **PCR method** | **Primer concentration (pmol/μl)** | **DNA concentration (ng/μl)** | **Forward and reverse primer sequences (M13 tailed) chromosome number** | **Size (bp)** |
| 1 | MMR | 2 | 10 | HNF1aEx1F_and_HNF1aEx1R gggtgcaaggagtttggttt ggcccctctaggctctcc 12 | 524 |
| 2 | MMR | 2 | 10 | HNF1aEx2F_and_HNF1aEx2R TGGGCTCCATAACTGCTTTC TCCCACTGACTTCCTTTCC 12 | 588 |

| | | | | | |
|---|---|---|---|---|---|
| 3 | MMR | 2 | 10 | HNF1aEx3F_and_HNF1aEx3R GCATGTGTGCTGTGTGTTTG AAGCCAATATCAGGAGTTCTCG 12 | 501 |
| 4 | MMR | 2 | 10 | HNF1aEx4F_and_HNF1aEx4R ACTGTCAATTGCCCAAGGTC GAATGGAATGGAACCAAACTG 12 | 540 |
| 5 | MMR | 2 | 10 | HNF1Aex5F_and_HNF1Aex5R tggagtttgaagtgctgagg gccaaggaaagatgaggttg 12 | 320 |
| 6 | MMR | 2 | 10 | HNF1aEx6F_and_HNF1aEx6R TGTAAGGAAAACCCAACCTCA AGTGGCTCTTCCAGCTCCT 12 | 430 |
| 7 | MMR | 2 | 10 | HNF1aEx7F_and_HNF1aEx7R AAGTCACCGCCTGCCTCT GCCAACCTCTATCATCATCTCC 12 | 516 |
| 8 | MMR | 2 (80% MF) | 10 | HNF1aEx8F_and_HNF1aEx8R ACAAGAGGAGCTGGAGTTGG AGACCTGGGGGAGCAGAG 12 | 513 |
| 9 | MMR | 2 (80% MF) | 10 | HNF1aEx9F_and_HNF1aEx9R ACCAAGCAGGTAAGGTCCAG GTGACGGACAGCAACAGAAG 12 | 331 |
| 10 | MMR | 2 | 10 | HNF1aEx10F_and_HNF1aEx10R GTACCCCTAGGGACAGGCAGG ACCCCCCAAGCAGGCAGTACA 12 | 328 |
| Prom | MMR | 2 | 10 | HNF1aPrmF_and_HNF1aPrmR ACAAGGTTCTTTCGGGGGTG TCTTTGCTCAGCCCTGACTC 12 | 550 |

***Gene: HNF1B Accession No.: NM_000458.1***

| Exon | PCR method | Primer concentration (pmol/μl) | DNA concentration (ng/μl) | Forward and reverse primer sequences (M13 tailed) chromosome number | Size (bp) |
|---|---|---|---|---|---|
| 1 | MMR | 2 | 10 | HNF1bEx1F_and_HNF1bEx1R CTGGATTTGGGGTTTGCTT CGGGGGACTTCTCTGGTG 17 | 592 |
| 2 | MMR | 2 | 10 | HNF1Bex2F_and_HNF1Bex2R TTTTGGCCTCATGTCTACCC GCCACCTTCCTCATATCTGC 17 | 534 |
| 3 | MMR | 2 | 10 | HNF1bEx3F_and_HNF1bEx3R CATCTCCAGCTCCACATGC GAGGGTTCCTGGGTCTGTG 17 | 472 |
| 4 | MMR | 2 | 10 | HNF1Bex4F_and_HNF1Bex4R actcccaaccaagactgctg GATCCGTGGCAAGAACCA 17 | 415 |

(continued)

**Table 1**
**(continued)**

| *Gene: HNF1B Accession No.: NM_000458.1* | | | | | |
|---|---|---|---|---|---|
| **Exon** | **PCR method** | **Primer concentration (pmol/μl)** | **DNA concentration (ng/μl)** | **Forward and reverse primer sequences (M13 tailed) chromosome number** | **Size (bp)** |
| 5 | MMR | 2 | 10 | HNF1bEx5F_and_HNF1Bex5R cctcgtggcgcttacattc ctggacagccctcattttcc 17 | 535 |
| 6 | MMR | 2 | 10 | HNF1bEx6F_and_HNF1bEx6R TAGTCATGCCAAGGAATCG GAGTTTGAAGGAGACCTACAG 17 | 361 |
| 7 | MMR | 2 | 10 | HNF1bEx7F_and_HNF1bEx7R GGTGACTGGGACATTGAGC ACTTCCGAGAAAGTTCAGACC 17 | 414 |
| 8 | MMR | 2 | 10 | HNF1bEx8F_and_HNF1bEx8R CTCACAGCCAAGCATCCAC TGTCATCCAGTCTCCAGCAA 17 | 631 |
| 9 | MMR | 2 | 10 | HNF1bEx9F_and_HNF1bEx9R TTCAGGATTCAGGTCAGCAAG AGGTCACTGGGCTTTTCCA 17 | 430 |
| *Gene: HNF4A Accession No.: NM_175914.4* | | | | | |
| **Exon** | **PCR method** | **Primer concentration (pmol/μl)** | **DNA concentration (ng/μl)** | **Forward and reverse primer sequences (M13 tailed) chromosome number** | **Size (bp)** |
| P2 + 1D | MMR | 2 | 10 | HNF4aEx1F_and_HNF4aEx1R CCAGGTTGGACTCTCACCTCTC GTGTCCCATGGCCTCCCAAAG 20 | 535 |
| 2 | MMR | 2 | 10 | HNF4aEx2F_and_HNF4aEx2R AGGTGATGGAGTGGGAACAG AGACCTTGGGGCCATGAG 20 | 380 |
| 3 | MMR | 2 | 10 | HNF4aEx3F_and_HNF4aEx3R AGATGAGAGCACTGAGGTTGG GCCTGCCACTGAGTCATAAAG 20 | 309 |
| 4 | MMR | 2 | 10 | HNF4aEx4F_and_HNF4aEx4R GCTCCCACTCCTCATCAGTC CAAACTGGGCCATGTGAAAC 20 | 250 |
| 5 | MMR | 2 | 10 | HNF4aEx5F_and_HNF4aEx5R CCTCCGTTTTTACCCTGAGC CCACGGCTATATCCCAGGT 20 | 435 |
| 6 | MMR | 2 | 10 | HNF4aEx6F_and_HNF4aEx6R CACAGTTCAGGCAGGTAGAGG GCCACCATGTGAATCTCCTT 20 | 333 |

| | | | | | |
|---|---|---|---|---|---|
| 7 | MMR | 2 | 10 | HNF4aEx7F_and_HNF4aEx7R TTGCCAACTTAAAAGCCAAAAC TGGAGAGAGAGTCAGGGATGG 20 | 280 |
| 8 | MMR | 2 (80% MF) | 10 | HNF4aEx8F_and_HNF4aEx8R TTGTTGAGGTCCCTGAATCC CAAGGAGCTGAGGGGTGAG 20 | 467 |
| 9 | MMR | 2 | 10 | HNF4aEx9F_and_HNF4aEx9R TGGTTGATTGGCCACGCCTG ATCCTGGTTCTACCTTCTAG 20 | 377 |
| 10 | MMR | 2 | 10 | HNF4aEx10F_and_HNF4aEx10R TGGGACTCACAGAAGGTTGA CACCAGGTGCTCTCTTAGGG 20 | 434 |

***Gene: INS Accession No.: NM_000207.2***

| Exon | PCR method | Primer concentration (pmol/μl) | DNA concentration (ng/μl) | Forward and reverse primer sequences (M13 tailed) chromosome number | Size (bp) |
|---|---|---|---|---|---|
| 1 | MMR | 2 | 10 | INSex1F_and_INSex1R CTGTGAGCAGGGACAGGTCT GCACAGGTGTTGGTTCACAA 11 | 627 |
| 2 | MMR | 2 | 10 | INSex2F_and_INSex2R ctctgcagcagggaggac gggagctggtcacttttagg 11 | 522 |
| 3 | MMR | 2 | 10 | INSex3F_and_INSex3R CCCTGACTGTGTCCTCCTGT AGAGAGCGTGGAGAGAGCTG 11 | 423 |

***Gene: INSR Accession No.: NM_000208.2***

| Exon | PCR method | Primer concentration (pmol/μl) | DNA concentration (ng/μl) | Forward and reverse primer sequences (M13 tailed) chromosome number | Size (bp) |
|---|---|---|---|---|---|
| 1 | MMR | 2 (80% MF) | 10 | INSRex1F_and_INSRex1R GGGCGTGGAAGAGAAGGAC GGCTCGATTTTGGCTTGG 19 | 294 |
| 2A | MMR | 2 | 10 | INSRex2AF_and_INSRex2AR GCTCTGCCCCTGATCCTTC TGTAGAGGCCGAGTTCCTTG 19 | 381 |
| 2B | MMR | 2 | 10 | INSRex2BF_and_INSRex2BR TCAAAACGAGGCCCGAAG AATGCCACCACCCACTATTC 19 | 583 |
| 3 | MMR | 2 | 10 | INSRex3F_and_INSRex3R TGTTTGGTTGGCTTTCACTG AGTTTTAACAAGCGGCATCG 19 | 541 |

(continued)

**Table 1**
**(continued)**

| *Gene: INSR Accession No.: NM_000208.2* | | | | | |
|---|---|---|---|---|---|
| **Exon** | **PCR method** | **Primer concentration (pmol/μl)** | **DNA concentration (ng/μl)** | **Forward and reverse primer sequences (M13 tailed) chromosome number** | **Size (bp)** |
| 5 | MMR | 2 | 10 | INSRex5F_and_INSRex5R CAACAGACGCAGCCAGTG TTAGCACTCAGGCCATACACAC 19 | 399 |
| 6 | MMR | 2 | 10 | INSRex6F_and_INSRex6R TATGTGCCAAGCAAGTGGAG GGTCCCTCATGCCAAAAAG 19 | 384 |
| 7 | MMR | 2 | 10 | INSRex7F_and_INSRex7R TTCCCCCATTCATACTCAGC TGGAGCACAAACGTAGCAAG 19 | 367 |
| 8 | MMR | 2 | 10 | INSRex8F_and_INSRex8R TCCTTTCTCTTTGGCTGTTCC AAAGCAAGAGGTCTGATTCACATAC 19 | 467 |
| 9 | MMR | 2 | 10 | INSRex9F_and_INSRex9R CATCCTCCCACCAGCTTTC GATAGCTGCTTCCCTAGAGGTG 19 | 322 |
| 10 | MMR | 2 | 10 | INSRex10F_and_INSRex10R ATGTGTGTTCAGCCGCAGAG AAGGGCTCCATTCAGACTCC 19 | 389 |
| 11 | MMR | 2 | 10 | INSRex11F_and_INSRex11R GATTTCTTCCCCTTCCCTTG AAGCATCTGCTCTCCAGCAC 19 | 377 |
| 12 | MMR | 2 | 10 | INSRex12F_and_INSRex12R TAATCCATGTTCCCCATTGC GCACTGCTTAGAGGGTGGAG 19 | 496 |
| 13 | MMR | 2 | 10 | INSRex13F_and_INSRex13R TGTGGGATGAGTTTTAGATGTCC GAGGAAGGAGGTACCAAGTGC 19 | 371 |
| 14 | MMR | 2 | 10 | INSRex14F_and_INSRex14R AAATTCTGCAATTCTCAAAGTCG ATGTCCCACCATGCTCAGTG 19 | 385 |
| 15 | MMR | 2 | 10 | INSRex15F_and_INSRex15R GTGGAAGAGCAGCAGAGAGG CAACTGTTCCCAGCACACC 19 | 285 |
| 16 | MMR | 2 | 10 | INSRex16F_and_INSRex16R AGGATTATGGGGATTCTGCTG GAAGGCAAAGGAAGCTGATG 19 | 249 |

| | | | | | |
|---|---|---|---|---|---|
| 17 | MMR | 2 | 10 | INSRex17F_and_INSRex17R GCATGGGTCCTGGATCAC CTGTGTCCTCTGTCGCTCTG 19 | 467 |
| 18&19 | MMR | 2 | 10 | INSRex18&19F_and_INSRex18&19R ATAGACACCAGGGAGGGAGG AAGACTTAACGGCTCATTATAGACAAC 19 | 546 |
| 20 | MMR | 2 | 10 | INSRex20F_and_INSRex20R TTACTGGATTTGGCCACCAC CTGCCTTCCTTTCCTTGATG 19 | 399 |
| 21 | MMR | 2 | 10 | INSRex21F_and_INSRex21R TTTATGAACTGCAGCATGAATTG GGGCAATACCCTTTCAACG 19 | 593 |
| 22 | MMR | 2 | 10 | INSRex22F_and_INSRex22R ACCATCTCTCAGCACCTCTAGC AGGAAAGCGAAAATGGGAAC 19 | 587 |

***Gene: IPF1 Accession No.: NM_000209.1***

| Exon | PCR method | Primer concentration (pmol/μl) | DNA concentration (ng/μl) | Forward and reverse primer sequences (M13 tailed) chromosome number | Size (bp) |
|---|---|---|---|---|---|
| 1 | MMR | 2 | 10 | IPF1ex1F_and_IPF1ex1R AACGCCACACAGTGCCAAATC TTAGTCCGACCCGGGATAATC 13 | 651 |
| 2A | MMR | 2 | 10 | IPF1ex2AF_and_IPF1ex2AR CGCTGAAATGGGATGCTG CGCTTCTTGTCCTCCTCCTT 13 | 405 |
| 2B | MMR | 2 | 10 | IPF1ex2BF_and_IPF1ex2BR TGAACTTGACCGAGAGACACA CTGAGAGAGCGGGTTTTCC 13 | 500 |

***Gene: KCNJ11 Accession No.: NM_000525.3***

| Exon | PCR method | Primer concentration (pmol/μl) | DNA concentration (ng/μl) | Forward and reverse primer sequences (M13 tailed) chromosome number | Size (bp) |
|---|---|---|---|---|---|
| 1B | MMR | 2 | 10 | KCNJ11ex1BF_and_KCNJ11ex1BR GTGCCCACCGAGAGGACT AGTGGGCACTCCTCAGTCAC 11 | 524 |
| 1C | MMR | 2 | 10 | KCNJ11ex1CF_and_KCNJ11ex1CR CACCAGCATCCACTCCTTCT GTTTCCACCACGCCTTCC 11 | 546 |
| 1D | MMR | 2 | 10 | KCNJ11ex1DF_and_KCNJ11ex1DR CTACCATGTCATTGATGC CCACATGGTCCGTGTGTA 11 | 491 |

(continued)

**Table 1**
**(continued)**

| *Gene: LMNA Accession No.: NM_005572.2* | | | | | |
|---|---|---|---|---|---|
| **Exon** | **PCR method** | **Primer concentration (pmol/μl)** | **DNA concentration (ng/μl)** | **Forward and reverse primer sequences (M13 tailed) chromosome number** | **Size (bp)** |
| 1 | MMR | 2 | 10 | LMNAex1F_and_LMNAex1R CCGAGCAGTCTCTGTCCTTC CCCTCTCACTCCCTTCCTG 1 | 564 |
| 2 | MMR | 2 | 10 | LMNAex2F_and_LMNAex2R CTGGTAATTGCAGGCATAGC GTTAGGTGGGGCCATGGGT 1 | 344 |
| 3 | MMR | 2 | 10 | LMNAex3F_and_LMNAex3R atgtgtgaaggggtgcacag ccagccctactccatgagc 1 | 419 |
| 4 | MMR | 2 | 10 | LMNAex4F_and_LMNAex4R TAAAGTGGGGCTGGTAGTGG TAAGGGTAGGGCTGCCAAG 1 | 380 |
| 5 | MMR | 2 | 10 | LMNAex5F_and_LMNAex5R GGGATCAGGCAGATGGTG ACCCTTCTCTGTGGTTGTGG 1 | 385 |
| 6 | MMR | 2 | 10 | LMNAex6F_and_LMNAex6R CTGGGGAAGCTCTGATTGC CAGAGGACACTGCCAGCAC 1 | 420 |
| 7 | MMR | 2 | 10 | LMNAex7F_and_LMNAex7F gtccctccttccccatactt tctcacagccaaagagtcca 1 | 813 |
| 8 | MMR | 2 | 10 | LMNAex8F_and_LMNAex8R gttgtcaggaagatgaaagataagg cctccccagagtcccaag 1 | 395 |
| 9 | MMR | 2 | 10 | LMNAex9F_and_LMNAex9R ATGGAGATGATCCCTTGCTG tctagaaaggggccctgaat 1 | 420 |
| 10 | MMR | 2 | 10 | LMNAex10F_and_LMNAex10R CAGGCCACAAGAAAAGTTGC GTTCAAGGTATAGGGAGGAG 1 | 388 |
| 11 | MMR | 2 (80% MF) | 10 | LMNAex11F_and_LMNAex11R GGGCACAGAACCACACCTT CAGACAAGAGGGGCAGGA 1 | 610 |
| 12 | MMR | 2 | 10 | LMNAex12F_and_LMNAex12R GGGAGATGCTACCTCCCTTC GGGTTATTTTTCTTTGGCTTCA 1 | 240 |

| Gene: NEUROG3 Accession No.: NM_020999.2 | | | | | |
|---|---|---|---|---|---|
| **Exon** | **PCR method** | **Primer concentration (pmol/μl)** | **DNA concentration (ng/μl)** | **Forward and reverse primer sequences (M13 tailed) chromosome number** | **Size (bp)** |
| 2A | MMR | 2 | 10 | NEUROG3ex2AF_and_NEUROG3ex2AR ctattcttttgcgccggtag cagtgccgagttgaggttg 10 | 499 |
| 2B | MMR | 2 | 10 | NEUROG3ex2BF_and_NEUROG3ex2BR gagttggcactgagcaagc ccctctcccttacccttagc 10 | 475 |
| **Gene: NEUROD1 Accession No.: NM_002500.1** | | | | | |
| **Exon** | **PCR method** | **Primer concentration (pmol/μl)** | **DNA concentration (ng/μl)** | **Forward and reverse primer sequences (M13 tailed) chromosome number** | **Size (bp)** |
| 2A | MMR | 2 | 10 | NeuroD1ex2AF_and_NeuroD1ex2AR CAAGCATTTGTACAGGTTTAG CTCCAGGCGAGCCTTAGTCATC 2 | 443 |
| 2B | MMR | 2 | 10 | NeuroD1ex2BF_and_NeuroD1ex2BR CCTCGAAGCCATGAACGCAG GCTGTCCATGGTACCGTAAG 2 | 619 |
| 2C | MMR | 2 | 10 | NeuroD1ex2CF_and_NeuroD1ex2CR CCTGCAACTCAATCCTCGGAC CTGTAAGCACAGTGGGTTCG 2 | 597 |
| **Gene: NKX2-2 Accession No.: NM_002509.3** | | | | | |
| **Exon** | **PCR method** | **Primer concentration (pmol/μl)** | **DNA concentration (ng/μl)** | **Forward and reverse primer sequences (M13 tailed) chromosome number** | **Size (bp)** |
| 1 | MMR | 2 | 10 | NKX22ex1F_and_ NKX22ex1R CAATAATTAAAGCCAATTcccc CTTCCCCTTTCACTCCCAG 20 | 491 |
| 2A | MMR | 2 | 10 | NKX22ex2AF_and_ NKX22ex2AR CCAGGGTGCTCCGAGTC GTTTGCCGTCCCTGACC 20 | 459 |
| 2B | MMR | 2 | 10 | NKX22ex2BF_and_ NKX22ex2BR CAGCGGTACCTGTCGGC CACCATAAGGACCGAGGC 20 | 460 |

(continued)

**Table 1**
**(continued)**

| *Gene: PPARG Accession No.: NM_015869.4* | | | | | |
|---|---|---|---|---|---|
| **Exon** | **PCR method** | **Primer concentration (pmol/μl)** | **DNA concentration (ng/μl)** | **Forward and reverse primer sequences (M13 tailed) chromosome number** | **Size (bp)** |
| 1 | MMR | 2 | 10 | PPARG_1F_and_PPARG_1R AGTTCACGCCCCTCACAA GACAAACTACAAGAGCAATTTTACC 3 | 534 |
| 2 | MMR | 2 | 10 | PPARG_2F_and_PPARG_2R CTGGGTAAAGGGTGACTTCC TGGGTGAATAAATGAATGGTGA 3 | 597 |
| 3 | MMR | 2 | 10 | PPARG_3F_and_PPARG_3R TTTCTTTTTCTTGCCTTAACTCC CCTTGGAGAAGTCACCTTTTTG 3 | 734 |
| 4 | MMR | 2 | 10 | PPARG_4F_and_PPARG_4R GCAGAGAACATTTAGTTCCAGAGA GCCCAACCACAGAGAGAAAG 3 | 550 |
| 5 | MMR | 2 | 10 | PPARG_5F_and_PPARG_5R TGATGGTCTGTGCTACTTTTGTG TGAAAACACTTCCTGCGTTTC 3 | 585 |
| 6A | MMR | 2 | 10 | PPARG_6AF_and_PPARG_6AR TTGAAGGGAAAGAAGACCAAAA AGGAGGCCAGCATTGTGTAA 3 | 522 |
| 6B | MMR | 2 | 10 | PPARG_6BF_and_PPARG_6BR TGGAGGCTGTGCAGGAGA CCGCAAACCTATGACACTCTTT 3 | 535 |
| 7A | MMR | 2 | 10 | PPARG_7AF_and_PPARG_7AR accttcctccccacctatt GGCAGTGGCTCAGGACTCT 3 | 456 |
| *Gene: PTF1A Accession No.: NM_178161.2* | | | | | |
| **Exon** | **PCR method** | **Primer concentration (pmol/μl)** | **DNA concentration (ng/μl)** | **Forward and reverse primer sequences (M13 tailed) chromosome number** | **Size (bp)** |
| 1A | AG58 | 2 | 10 | PTF1Aex1AF_and_PTF1Aex1AR ctcggacgggccttagaaac tcgcggtagcagtactcgtg 10 | 304 |
| 1B | AG58 | 2 | 10 | PTF1Aex1BF_and_PTF1Aex1BR acgacttcttcaccgaccag gggtaggccaggcacgag 10 | 340 |
| 1C | AG58 | 2 | 10 | PTF1Aex1CF_and_PTF1Aex1CR ggctactgctgcgagacg agcgtgtccaccttggag 10 | 356 |
| 1D | AG58 | 2 | 10 | PTF1Aex1DF_and_PTF1Aex1DR atcaacgacgccttcgag gagtgcccgacccttct 10 | 332 |

| | | | | | |
|---|---|---|---|---|---|
| 2 | AG58 | 2 | 10 | PTF1Aex2F_and_PTF1Aex2R gggacttgaagtgtggagga AAACAGTTGATTGCCATTCG 10 | 492 |
| REG | MMR | 2 | 10 | PTF1AexREGF_and_PTF1AexREGR GATGATTCTTCCCTAGAAGTCTCAG CAAGAAAGTCAAGTGGTGCATG 10 | 488 |

***Gene: RFX6 Accession No.: NM_173560.3***

| Exon | PCR method | Primer concentration (pmol/μl) | DNA concentration (ng/μl) | Forward and reverse primer sequences (M13 tailed) chromosome number | Size (bp) |
|---|---|---|---|---|---|
| 1 | MMR | 2 | 10 | RFX6ex1F_and_RFX6ex1R GCCTGGGCTGTACCTGTG TGTTTGTTCGGGATGCATTA 6 | 495 |
| 2 | MMR | 2 | 10 | RFX6ex2F_and_RFX6ex2R TGCATCCCGAACAAACATAA CCCAAAAAGTTTGAGGAAGAA 6 | 487 |
| 3 | MMR | 2 | 10 | RFX6ex3F_and_RFX6ex3R CATGCTATCTGCCTGACATGA TGAGAAAGTTGAAGGAAAAGGAA 6 | 246 |
| 4 | MMR | 2 | 10 | RFX6ex4F_and_RFX6ex4R GTGGCTTGCATTAGGACCAT TCAATCTTCATGCACAAGAGC 6 | 172 |
| 5 | MMR | 2 | 10 | RFX6ex5F_and_RFX6ex5R TCATCAGGGTTTGCAGTTCT GGTATCATGCATATTTAAAGAAACACA 6 | 249 |
| 6 | MMR | 2 | 10 | RFX6ex6F_and_RFX6ex6R TCCAGCTTATTTCTCTAATCATGG ACATTTGCCAAAGGGAATAA 6 | 237 |
| 7 | MMR | 2 | 10 | RFX6ex7F_and_RFX6ex7R TGGTTTGCAGGATGAAGAAG TACCATGAAATTCCCAGCAA 6 | 300 |
| 8 | MMR | 2 | 10 | RFX6ex8F_and_RFX6ex8R AAAGGCAGTGTTAAAAGGATGC TGAACTCATTAAGAACAGAACATGAA 6 | 201 |
| 9 | MMR | 2 | 10 | RFX6ex9F_and_RFX6ex9R TTTCATGTTCTGTTCTTAATGAGTTC GCTACGTAAAGAAATAAATGGCTCA 6 | 236 |
| 10 | MMR | 2 | 10 | RFX6ex10F_and_RFX6ex10R GCTAGGAATAAAAAGTAGTTGACCA CCAGCAAATACAAAGGGACAA 6 | 369 |
| 11 | MMR | 2 | 10 | RFX6ex11F_and_RFX6ex11R GGCAGATCTAGGCTGTCTGA TTCCTCAATCTGTCCTTCTCA 6 | 300 |

(continued)

**Table 1**
**(continued)**

| *Gene: RFX6 Accession No.: NM_173560.3* | | | | | |
|---|---|---|---|---|---|
| **Exon** | **PCR method** | **Primer concentration (pmol/μl)** | **DNA concentration (ng/μl)** | **Forward and reverse primer sequences (M13 tailed) chromosome number** | **Size (bp)** |
| 12 | MMR | 2 | 10 | RFX6ex12F_and_RFX6ex12R CTCAAGGAACTATTTTTCTGATAGC CAGCTCAAGATGTCAATTTTCTG 6 | 383 |
| 13 | MMR | 2 | 10 | RFX6ex13F_and_RFX6ex13R TCTGTCTTTCCCTTTCATGC GCCTGCCTTATTCGTAGAGC 6 | 297 |
| 14 | MMR | 2 | 10 | RFX6ex14F_and_RFX6ex14R TGCCATCTGTCCATTTGTTAG GACAGGAACTGTGACTGAGGA 6 | 328 |
| 15 | MMR | 2 | 10 | RFX6ex15F_and_RFX6ex15R TCCCCTTTTTACATTTCACACTG GACATGTTTGGAGAAAAACTCTGA 6 | 700 |
| 16 | MMR | 2 | 10 | RFX6ex16F_and_RFX6ex16R TGGGTTTATCTACGAGGAATGTG TGAAGCAACAGGCTTCTCTG 6 | 357 |
| 17A | MMR | 2 | 10 | RFX6ex17AF_and_RFX6ex17AR TGAAGCAAGCTGGAAAACAA AGAGGTGGAACGCAATGTCT 6 | 495 |
| 17B | MMR | 2 | 10 | RFX6ex17BF_and_RFX6ex17BR AGAGGTGGAACGCAATGTCT TGAAGCAAGCTGGAAAACAA 6 | 495 |
| 18 | MMR | 2 | 10 | RFX6ex18F_and_RFX6ex18R TTTTCCTTCCTGAAAGTTCTTTGT TGGAAACATGCTTGCTCAGT 6 | 487 |
| 19 | MMR | 2 | 10 | RFX6ex19F_and_RFX6ex19R TGAGTGGCATTTGCAGAGAA CAGCCACTGCATATTCATTTT 6 | 246 |
| *Gene: SLC19A2 Accession No.: NM_006996.2* | | | | | |
| **Exon** | **PCR method** | **Primer concentration (pmol/μl)** | **DNA concentration (ng/μl)** | **Forward and reverse primer sequences (M13 tailed) chromosome number** | **Size (bp)** |
| 1 | MMR | 2 | 10 | SLC19A2ex1F_and_SLC19A2ex1R gcgtccgctgtgattggtt gagaaaagcgctcgagcc 1 | 606 |

| | | | | | |
|---|---|---|---|---|---|
| 2A | MMR | 2 | 10 | SLC19A2ex2AF_and_SLC19A2ex2AR agatctttgaggtatttgtagg acacaggtaagagagatgaca 1 | 534 |
| 2B | MMR | 2 | 10 | SLC19A2ex2BF_and_SLC19A2ex2BR acagccactgaaattgccta agatctaccaagagggagttt 1 | 529 |
| 3 | MMR | 2 | 10 | SLC19A2ex3F_and_SLC19A2ex3R ttcgccagaggggataaatg cctgctccacttgagtactt 1 | 596 |
| 4 | MMR | 2 | 10 | SLC19A2ex4F_and_SLC19A2ex4R ccctccataatcttgagctatt ttcctcccatttgcctcattt 1 | 476 |
| 5 | MMR | 2 | 10 | SLC19A2ex5F_and_SLC19A2ex5R gttggaaaggcaattgacagt actttacatctgttccctattg 1 | 423 |
| 6 | MMR | 2 | 10 | SLC19A2ex6F_and_SLC19A2ex6R ctcaggcagtcaggctttatt gctgctgtgaagtcaagaaat 1 | 470 |

***Gene: SLC2A2 (GLUT2) Accession No.: NM_000340.1***

| Exon | PCR method | Primer concentration (pmol/μl) | DNA concentration (ng/μl) | Forward and reverse primer sequences (M13 tailed) chromosome number | Size (bp) |
|---|---|---|---|---|---|
| 1 | MMR | 2 | 10 | SLC2A2_Ex1F_and_SLC2A2_Ex1R ctctccttgctcctcctcct aaacagttcttcaattggcaaag 3 | 297 |
| 2 | MMR | 2 | 10 | SLC2A2_Ex2F_and_SLC2A2_EX2R cgatattgaggggaaagaacc gggagtcaaggccaagttatc 3 | 384 |
| 3 | MMR | 2 | 10 | SLC2A2_Ex3F_and_SLC2A2_Ex3R tggccaactgtaaacaaatct aaagctattccacaagaagaaaga 3 | 518 |
| 4 | MMR | 2 | 10 | SLC2A2_Ex4F_and_SLC2A2_Ex4R ccccaactagcttttacagca tgctattgcctttccctctg 3 | 398 |
| 5 | MMR | 2 | 10 | SLC2A2_Ex5F_and_SLC2A2_Ex5R aattcagggaggggctttc gagggacgagatggatgaag 3 | 339 |
| 6 | MMR | 2 | 10 | SLC2A2_Ex6F_and_SLC2A2_Ex6R cttgaaccaaagttgtcagaga catgcaccagtcatataaaagc 3 | 418 |

(continued)

**Table 1**
**(continued)**

| *Gene: SLC2A2 (GLUT2) Accession No.: NM_000340.1* | | | | | |
|---|---|---|---|---|---|
| **Exon** | **PCR method** | **Primer concentration (pmol/μl)** | **DNA concentration (ng/μl)** | **Forward and reverse primer sequences (M13 tailed) chromosome number** | **Size (bp)** |
| 7 | MMR | 2 | 10 | SLC2A2_Ex7F_and_SLC2A2_Ex7R gaatttccaacacccatgct gacccatgatgccaatacct 3 | 432 |
| 8 | MMR | 2 | 10 | SLC2A2_EX8F_and_SLC2A2_Ex8R gcatgccgctatagaaacaa tgcagtggttggcttattca 3 | 400 |
| 9 | MMR | 2 | 10 | SLC2A2_EX9F_and_SLC2A2_EX9R tccccaccttgatctcactc ttatgctgttgctctggcttt 3 | 397 |
| 10 | MMR | 2 | 10 | SLC2A2_EX10F_and_SLC2A2_EX10R aaaagttgtatgccgcctgt agcactccagcaaagaggaa 3 | 436 |
| 11 | MMR | 2 | 10 | SLC2A2_EX11F_and_SLC2A2_EX11R gcattcagcaattggacctg tgacatttctgatgagagcaca 3 | 482 |
| *Gene: STAT3 Accession No.: NM_139276.2* | | | | | |
| **Exon** | **PCR method** | **Primer concentration (pmol/μl)** | **DNA concentration (ng/μl)** | **Forward and reverse primer sequences (M13 tailed) chromosome number** | **Size (bp)** |
| 2 | MMR | 2 | 10 | STAT3_2F_and_STAT3_2R CCCCAGAGCATCTTTATCCC CTCATTTTCCCCATCACCTG 17 | 396 |
| 3 | MMR | 2 | 10 | STAT3_3F_and_STAT3_3R GGGTTATAGCATCAGGTTTGC AAGTATACAGAGCTTTGAGAAAGGG 17 | 432 |
| 4 | MMR | 2 | 10 | STAT3_4F_and_STAT3_4R TAGTAACGACCTCCCCTTCG TCTGTTGGATTCTTTTGGTGG 17 | 512 |
| 5 | MMR | 2 | 10 | STAT3_5F_and_STAT3_5R TTCCCTTCCTCTTGTGATGG CAAGAGAAGGCTCCCTGTTG 17 | 594 |
| 6 | MMR | 2 | 10 | STAT3_6F_and_STAT3_6R AACAGGGAGCCTTCTCTTGG ATGACCAGGCTCCTTTGAGG 17 | 382 |

| | | | | | |
|---|---|---|---|---|---|
| 7 | MMR | 2 | 10 | STAT3_7F_and_STAT3_7R GGAGGTACGGGTCCTCAAAG CAACTCCAGAGCAGGAACTTCT 17 | 967 |
| 8 | MMR | 2 | 10 | STAT3_8F_and_STAT3_8R ATTTCAGCGTCTTGTGGCAG GCTAAATTTGAATATGGAAAAGTCC 17 | 402 |
| 9 | MMR | 2 | 10 | STAT3_9F_and_STAT3_9R TTTTCAGCATCCACCCAAC GGAAAGAGAAGATGGGCTCAC 17 | 510 |
| 10 | MMR | 2 | 10 | STAT3_10F_and_STAT3_10R GGTAATTTAGCATCCTTGTCCC ATGGCAACAAATTTCAACCC 17 | 362 |
| 11 | MMR | 2 | 10 | STAT3_11F_and_STAT3_11R GACAGCTTGGCCTATTTACCTG TGTCCACAAAATGAAGATCTCTG 17 | 295 |
| 12 | MMR | 2 | 10 | STAT3_12F_and_STAT3_12R TGCGCTGATCAACTGTAACTG ATTCCCACATCTCTGCTCCC 17 | 492 |
| 13 | MMR | 2 | 10 | STAT3_13F_and_STAT3_13R ATTCCCACATCTCTGCTCCC TGCGCTGATCAACTGTAACTG 17 | 492 |
| 14 | MMR | 2 | 10 | STAT3_14F_and_STAT3_14R ATGGAAGAATCCAACAACGG GTTCATGTCACTTTGGCCTG 17 | 345 |
| 15 | MMR | 2 | 10 | STAT3_15F_and_STAT3_15R TGCTGCTTAGACTGGTCTCG CCCCTGTACGTAGCCTCTCA 17 | 251 |
| 16 | MMR | 2 | 10 | STAT3_16F_and_STAT3_16R CACTCCTCGCCTAGAGTTGG GTCCTCGCTTGGTGGTG 17 | 449 |
| 17 | MMR | 2 | 10 | STAT3_17F_and_STAT3_17R AACATGCTGACCAACAATCC GCCTTGCTCAGGAAAGAAAC 17 | 397 |
| 18F | MMR | 2 | 10 | STAT3_18F_and_STAT3_18R AAATCCTCAGGCCCGTCTAC CCTTCAAAGATGTGAAAGCTG 17 | 323 |
| 18R | MMR | 2 | 10 | STAT3_18F_and_STAT3_18R CCTTCAAAGATGTGAAAGCTG AAATCCTCAGGCCCGTCTAC 17 | 323 |
| 19 | MMR | 2 | 10 | STAT3_19F_and_STAT3_19R CTGAACTCTTGGTCCAGCG AAAGCCCATGATGTACCTGG 17 | 365 |

(continued)

**Table 1**
**(continued)**

| *Gene: STAT3 Accession No.: NM_139276.2* | | | | | |
|---|---|---|---|---|---|
| **Exon** | **PCR method** | **Primer concentration (pmol/μl)** | **DNA concentration (ng/μl)** | **Forward and reverse primer sequences (M13 tailed) chromosome number** | **Size (bp)** |
| 20 | MMR | 2 | 10 | STAT3_20F_and_STAT3_20R GCTGGCAAGGGCTTCTC AAGCAAACCAATCCTTCAGC 17 | 524 |
| 21 | MMR | 2 | 10 | STAT3_21F_and_STAT3_21R CACTACAATTCTTTCCCATAAGGAG AACAGGGTGTTCAGGGTCTC 17 | 483 |
| 22 | MMR | 2 | 10 | STAT3_22F_and_STAT3_22R TAAATGAGGGCAGACAACCC TCAAACTCTGGTCTCCAACAG 17 | 397 |
| 23 | MMR | 2 | 10 | STAT3_23F_and_STAT3_23R AGCCCCTGGGCTATGTTTAG TCTCTTTTGGAAAGCAAAGCTC 17 | 428 |
| 24 | MMR | 2 | 10 | STAT3_24F_and_STAT3_24R TCCAGGGAGGAGGGTAAATC AGCAGATCACCCACATTCAC 17 | 425 |
| *Gene: ZMPSTE24 Accession No.: NM_005857.2* | | | | | |
| **Exon** | **PCR method** | **Primer concentration (pmol/μl)** | **DNA concentration (ng/μl)** | **Forward and reverse primer sequences (M13 tailed) chromosome number** | **Size (bp)** |
| 1 | MMR | 2 | 10 | ZMPSTE24ex1F_and_ZMPSTE24ex1R TCGGAAAGAACGGATATTGC GACCACAAAGACGAGACTGG 1 | 381 |
| 2 | MMR | 2 | 10 | ZMPSTE24ex2F_and_ZMPSTE24ex2R ATCAAGTGCAATATTTGTGTAGG TCTGGGACTTGTAAGTGTGG 1 | 420 |
| 3 | MMR | 2 | 10 | ZMPSTE24ex3F_and_ZMPSTE24ex3R GATGGGGTCTCAACTCACCT CCTGCCAAGCTAAAAGAAATACC 1 | 373 |
| 4 | MMR | 2 | 10 | ZMPSTE24ex4F_and_ZMPSTE24ex4R GATGATATTTCAGACCTTATGTTATCC ATGATCTTTACCATATCTGTAGTTCC 1 | 432 |

| | | | | | |
|---|---|---|---|---|---|
| 5 | MMR | 2 | 10 | ZMPSTE24ex5F_and_ZMPSTE24ex5R TGCAAGACATTTACCCATTGT TGGTCAGTCAATACTCCTGTGTC 1 | 575 |
| 6 | MMR | 2 | 10 | ZMPSTE24ex6F_and_ZMPSTE24ex6R GGAATACCAGAGCAAGTAAGTTCC TAAAAAGCCAAAAGGTAAACTCC 1 | 471 |
| 7 | MMR | 2 | 10 | ZMPSTE24ex7F_and_ZMPSTE24ex7R actgctggtggtgaattatgtt aaggagccatggttttcatct 1 | 475 |
| 8 | MMR | 2 | 10 | ZMPSTE24ex8F_and_ZMPSTE24ex8R TGTCTCATGTGGAGCAGTGG CAGGTAGCCTGGCTGTGG 1 | 415 |
| 9 | MMR | 2 | 10 | ZMPSTE24ex9F_and_ZMPSTE24ex9R ACTTTATGGATGCTACTGATCC TTGGGCTTGAATTTTTCTGC 1 | 406 |
| 10 | MMR | 2 | 10 | ZMPSTE24ex10F_and_ZMPSTE24ex10R AGGCTCAATTTATAATTTCCTCACC CATCAAGAGCTGGAACATGC 1 | 504 |

### 2.6 Next-Generation Targeted Sequencing

1. 0.65 ml Nonstick hydrophobic tubes (Anachem Cat No. 1110-10).
2. TE (10 mM Tris–HCl, 1 mM EDTA, pH 8.0) (Sigma-Aldrich 93,283—100 ml).
3. AMPure (Beckman Coulter A63881).
4. Ethanol (Sigma-Aldrich E7023—500 ml).
5. $dH_2O$ (Baxter UKF7114).
6. End-repair buffer (New England Biolabs E6050L).
7. 10× dA tailing buffer (New England Biolabs E6053L).
8. Klenow fragments (New England Biolabs E6053L).
9. Next Flex96 DNA barcodes (adapters; BioScientific).
10. Fast-link DNA ligase (Epicentre, Illumina (LK6201H)).
11. 10 mM ATP (Epicentre, Illumina (LK6201H).
12. 5× Herculase buffer (Agilent).
13. Herculase dNTP mix (100 mM) (Agilent).
14. Herculase II polymerase (Agilent).
15. NEXTflex primers (*see* Tables 1–3).
16. SureSelect Hybe #1 (Agilent (5972-3551)).
17. SureSelect Hybe #2 (Agilent (5190-4405)).
18. SureSelect Hybe #3 (Agilent (5190-1980)).
19. SureSelect Hybe #4 (Agilent (5190-4406)).
20. SureSelect Index block #1 (Agilent (5972-3641)).
21. SureSelect Index block #2 (Agilent (5190-1979)).
22. SureSelect Index block #3 (Agilent (5972-3602)).
23. SureSelect RNase block (Agilent (5910-1976)).
24. Library: Custom Agilent SureSelect assay [4].
25. Dynabeads MyOne (Invitrogen (2021-02)).
26. SureSelect binding buffer (Agilent (5972-3554)).
27. SureSelect wash buffer 1 (Agilent (5972-3555)).
28. SureSelect wash buffer 2 (Agilent (5972-3556)).

**Table 2**
**NEXTflex primer sequences**

| | |
|---|---|
| NEXTflex primer forward | AATGATACGGCGACCACCGAGATC TACAC |
| NEXTflex primer reverse | CAAGCAGAAGACGGCATACGAGAT |

**Table 3**
**Nextflex adapter sequences**

| Name/sequence | Name/sequence | Name/sequence | Name/sequence |
|---|---|---|---|
| HT1/AACGTG | HT38/CCGTGA | HT75/ACAGAT | HT17/AAGGTA |
| HT13/AACAAC | HT50/GCCACA | HT87/CCTAAT | HT29/ATTGAG |
| HT25/AGATCG | HT62/TCCGTC | HT4/AGTGGT | HT41/CGACTG |
| HT37/CCGAAG | HT74/ACACGA | HT16/AAGACG | HT53/GCTCGG |
| HT49/GATAGA | HT86/CCGACA | HT28/ATCCTG | HT65/TGGAAC |
| HT61/TATCAG | HT3/ATGCCT | HT40/CGAACT | HT77/AGCACC |
| HT73/AATGTT | HT15/AACGCT | HT52/GCTAAC | HT89/CGACAC |
| HT85/CCATCC | HT27/AGTCAC | HT64/TGAAGA | HT6/ACATTG |
| HT2/AAACAT | HT39/CCTCCT | HT76/AGATGT | HT18/ACACAG |
| HT14/AACCGA | HT51/GCGAGT | HT88/CCTCTA | HT30/CAACCA |
| HT26/AGCAGG | HT63/TCTTCA | HT5/ACCACT | HT42/CGCATA |
| HT54/GGAGAA | HT66/TGGCTT | HT78/AGCCAT | HT90/CGGATT |

### 2.7 Equipment

1. Thermocycler.
2. Agencourt SPRIPlate® magnetic plate.
3. Agencourt 384 Direct Inject Magnet Plate.
4. ABI 3730XL.
5. Illumina HiSeq2500.
6. Bioruptor®.
7. Agilent 2200 TapeStation®™.
8. Vacuum concentrator (SpeedVac).

### 2.8 Methods: Sanger Sequencing

The PCR and sequencing methods detail primers and PCR conditions for Sanger sequencing of all coding regions and intron–exon boundaries for single gene analysis to detect missense, nonsense, frameshift, and splicing mutations. For a list of genes, primer pairs, amplicon sizes, and optimized PCR conditions for each amplicon *see* Table 1.

## 3 Methods

### 3.1 PCR Amplification

A PCR is set up for each of the primer pairs using one of the following conditions (Tables 4 and 5).

**Table 4**
**MegaMix Royal (MMR) 10 μl PCR reaction per sample**

| | Per sample (*n*) (μl) |
|---|---|
| Megamix | 5 |
| Primer mix | 2.5 |
| DNA (10 ng/μl) or $dH_2O$ for the negative control | 2.5 |

**Table 5**
**AmpliTaq Gold (AG) with dNTP mix 2 and mix 3, 25 μl PCR reaction per sample**

| | Per sample (*n*) (μl) |
|---|---|
| $dH_2O$ | 7.9 |
| 10× buffer without $MgCl_2$ | 2.5 |
| $MgCl_2$ | 2.5 |
| dNTPs (*see* mix 2) | 1.0 |
| Deaza-dGTP (*see* mix 3) | 1.25 |
| DMSO | 1.25 |
| Betaine | 5.0 |
| Primer mix | 1 |
| AmpliTaq Gold | 0.1 |
| DNA (10 ng/μl) or $dH_2O$ for the negative control | 2.5 |

### *3.2 PCR Cycling Conditions*

The following (Tables 5–8) outlines the thermocycler programs for using MegaMix Royal and AmpliTaq Gold (*see* **Note 2**).

### *3.3 PCR Product Purification Prior to Sanger Sequencing*

The PCR product is purified prior to sequencing to remove excess primers, primer dimers, unincorporated dNTPs, salts, and other contaminants. There are several commercially available methods for purifying PCR products. We use the Agencourt AMPure XP PCR purification system, a solid-phase paramagnetic bead technology that is highly amenable to automation and high sample numbers. We use the Biomek $NX^P$ (Beckman Coulter) to perform our liquid handling, though other liquid handling workstations are available. To summarize, the PCR products are bound to paramagnetic beads and separated before being washed to remove any contaminants. The purified PCR products are then eluted from the magnetic beads ready for the sequencing reaction.

1. Transfer 5 μl of the PCR products to a clean 384-well plate.
2. Briefly centrifuge the plate so that the PCR product is at the bottom of the well.

**Table 6**
**MegaMix Royal (MMR) PCR cycling conditions**

| Step | Temperature | Time |
|---|---|---|
| Step 1 | 95 °C | 5 min |
| Step 2 | 95 °C | 30 s |
| | 60 °C | 1 min |
| Step 3 (repeat step 2 for 30 cycles) | | |
| Step 4 | 72 °C | 10 min |

**Table 7**
**AmpliTaq Gold (AG60) PCR cycling conditions**

| Step | Temperature | Time |
|---|---|---|
| Step 1 | 95 °C | 12 min |
| Step 2 | 94 °C | 1 min |
| | 60 °C | 1 min |
| | 72 °C | 2 min |
| Step 3 (repeat step 2 for 40 cycles) | | |
| Step 4 | 72 °C | 10 min |

**Table 8**
**AmpliTaq Gold (AG58) PCR cycling conditions**

| Step | Temperature | Time |
|---|---|---|
| Step 1 | 95 °C | 12 min |
| Step 2 | 94 °C | 1 min |
| | 58 °C | 1 min |
| | 72 °C | 2 min |
| Step 3 (repeat step 2 for 40 cycles) | | |
| Step 4 | 72 °C | 10 min |

3. Gently shake the Agencourt AMPure bottle to resuspend the solution so that it appears homogenous and consistent in color.
4. Add 9 μl of the Agencourt AMPure XP magnetic beads to the PCR reaction and mix by pipetting (15 times) so that the color of the mixture appears homogenous.

5. Place the plate onto the magnetic stand for 3–5 min. This step separates the beads containing the bound PCR products from the solution.
6. The beads form a spot on the side of the well. Remove the cleared solution from the plate and discard. This step needs to be performed while the plate is situated on the magnetic stand so that the bead pellet is not disturbed.
7. Dispense 30 μl of 85% ethanol to each well of the plate while placed on the magnetic stand. Incubate for 30 s at room temperature. Remove the ethanol and discard (*see* **Note 3**).
8. Repeat **step 6** (total of two washes).
9. Allow the plate to air dry completely.
10. Add 30 μl of elution buffer ($dH_2O$).
11. Transfer the purified PCR products into a new plate.

### 3.4 Sanger Sequencing Reaction

Prepare a sequencing master mix ($n$ + 5) if there are more than 10 samples. If there are less than 10 samples, make up a sequencing mix of $n$ + 1. We perform unidirectional sequencing (forward direction) and all our primers are M13 tailed so that a universal sequencing master mix can be used. Note: for samples shown to contain a frameshift mutation or if mosaicism is suspected, the reverse sequencing is performed using a revere M13 (M13R) primer so that bidirectional sequence can be analyzed [5].

1. Add the sequencing reaction mix as in Table 9 (4.52 μl) to 2 μl of each PCR sample and run on the thermocycler using the program detailed in Table 10.

### 3.5 Sequencing Reaction Clean-Up

The sequencing reaction clean-up is performed using Agencourt Cleanseq, a SPRI® (solid-phase reversible immobilization) magnetic bead-based sequencing purification system which is amenable to automation. The methodology is performed directly in the thermal cycling plate and requires no centrifugation or filtration. The system efficiently purifies sequencing products to deliver superior quality sequencing data (see manufacturer's instructions for further details).

**Table 9**
**Sequencing reaction**

| | Per sample (*n*) (μl) |
|---|---|
| Water | 2.0 |
| BigDye 5× sequencing buffer | 1.10 |
| M13F primer mix | 1.2 |
| BigDye Terminator v3.1 | 0.22 |

**Table 10**
**Sequencing PCR cycling conditions**

| Step | Temperature | Time |
|---|---|---|
| Step 1 | 96 °C | 10 s |
| Step 2 | 50 °C | 5 s |
| Step 3 | 60 °C | 2 min |
| Step 4 (repeat steps 1–3 for 24 cycles) | | |

1. Gently shake the Agencourt CleanSEQ solution so that it appears homogenous and consistent in color.
2. Add 5 μl of Agencourt CleanSEQ to 7 μl of PCR product.
3. Add 17.14 μl of 85% ethanol to each sample and mix by pipetting seven times until the solution appears homogenous to ensure that the sequencing products bind to the magnetic beads (*see* **Note 4**).
4. Place the sample plate on the magnetic stand for 2–3 min until the solution is clear (*see* **Note 5**).
5. Aspirate the cleared supernatant from the plate and discard. This step must be performed while the plate is situated on the magnetic stand (*see* **Note 6**).
6. Dispense 30 μl of 85% ethanol into each well then pipette mix seven times to wash the beads. Wait for at least 30 s to allow the beads to resettle before continuing to the next step. This step should be performed while the plate is situated on the magnetic stand.
7. Completely remove the ethanol and discard. This step must be performed while the plate is situated on the magnetic stand.
8. Repeat **steps 6** and **7** for a total of two 85% ethanol washes.
9. Let the samples air dry for 10 min at room temperature (the sample plate can be situated on or off the magnet while drying) (*see* **Note 7**).
10. Add 15–30 μl of elution buffer and incubate the plate for 5 min at room temperature to elute (*see* **Note 8**). Do not denature samples prior to loading on capillary sequencers.
11. Load the plate on the detector and use the Agencourt 384 Direct Inject Magnet Plate (*see* **Note 9**).
12. Seal samples and store at 4 °C for up to 24 h prior to loading (*see* **Note 10**).
13. Sequencing is performed on a 3730XL DNA Analyzer (Applied Biosystems).

### 3.6 Targeted Next-Generation Sequencing Using the Agilent SureSelect System

Targeted next-generation sequencing (also called massive parallel sequencing, MPS) is a powerful methodology for the analysis of multiple genes in a single assay. It enables the surveillance of a subset of the genome which contains genes relevant to the phenotype in question. There are many different platforms, chemistries, and enrichment strategies available. We designed a custom Agilent SureSelect exon-capture assay with baits for all the diagnostic monogenic diabetes and hyperinsulinism genes to identify pathogenic mutations located within 50 bp upstream and 10 bp downstream of each exon [4]. Sequencing is performed on an Illumina HiSeq 2500. This methodology will identify the same types of mutations detected by Sanger sequencing as well as large deletions or duplications previously identified by a separate dosage assay.

The majority of the liquid handling in this protocol is amenable to automation. We use the Bravo liquid handling platform which is equipped with a ThermoCube thermoelectric and INHECO temperature control system, used to incubate components at defined temperatures during the procedure, but other systems are available. Samples for the capture library are individually tagged with unique barcodes and then combined into 12-plex pools prior to hybridization. We process 48 samples at a time.

One library is prepared for all samples, which are individually tagged with unique barcodes. The process is described below and is modified from Agilent Technologies SureSelect Automated Library Prep and Capture System protocol.

### 3.7 DNA Quantification

DNA is quantified using the Qubit® dsDNA BR assay kit which is designed for use with the Qubit® 2.0 fluorometer. The assay measures the concentration of double stranded DNA (dsDNA) in the sample. Used according to the manufacturer's specific protocols.

### 3.8 Sample Dilution and Fragmentation Using the Bioruptor® Instrument

1. Label Anachem tubes (1 for each sample).
2. Dilute 1000 ng of DNA from each sample in a final volume of 80 μl TE buffer.

### 3.9 Fragmentation Using the Bioruptor® Instrument

The Bioruptor® uses high-frequency sound waves at potentially damaging noise level, ensure that safety ear protectors are worn at all times.

1. Fill the Bioruptor® water bath with fresh deionized water and allow it to cool to 4 °C.
2. Vortex samples briefly and centrifuge briefly to collect the entire sample at the bottom of the tube.
3. Place 12 samples at a time in the Bioruptor® adapter (*see* **Note 11**).

4. Make sure all the tube hinges face outward and the tubes are "flush" and the adaptor is tightened properly. Refer to the Bioruptor® instrument user's guide for more details.
5. Place the adaptor head in the Bioruptor® and fragment for 54 min.
6. Briefly centrifuge the samples.
7. Transfer each of the samples (80 μl) to a 96-well skirted Eppendorf plate.
8. Repeat **steps 2–8** for all of the samples.
9. Centrifuge the plate briefly to collect the sample at the bottom of the well and seal the plate (*see* **Note 12**).

### 3.10 Purification of Sheared DNA Using the Agencourt AMPure XP System

This system can be used in manual and automated formats. To summarize, samples are cleaned up with 120 μl AMPure beads (1.5 volumes) and eluted in 40 μl $dH_2O$.

1. Allow the AMPure XP beads to equilibrate to room temperature before use and shake well so that the reagent appears homogenous and consistent in color.
2. Add 80 μl of the sheared DNA to each well and mix by pipetting.
3. Add 120 μl of the AMPure XP beads to each well of a Nunc DeepWell plate.
4. Incubate for 5 min at room temperature.
5. Place the plate onto the magnetic stand to separate the beads from the solution for 3 min.
6. Remove the cleared liquid from the solution while the plate is situated on the magnetic stand, being careful not to disturb the separated beads.
7. Add 70% ethanol to each well, enough to cover the beads, while the plate is situated on the magnetic stand and incubate for 30 s at room temperature.
8. Repeat for a total of two washes.
9. Remove the plate from the magnetic stand and add 40 μl of $dH_2O$.
10. Resuspend the beads by pipetting up and down.
11. Incubate for 1 min.
12. Place the plate onto the magnetic stand and transfer the eluate to a fresh plate.

### 3.11 Sample Quality Check Using Agilent 2200 TapeStation®™

A quality control check on D1000 tapes is performed to ensure that each of the samples are fragmented sufficiently. Set up the Agilent 2200 TapeStation®™ according to the manufacturer's instructions.

1. Take out the appropriate number of tapes and allow to equilibrate to room temperature.
2. Pipette 3 μl of loading buffer per sample into 96-well plate or strip tubes.
3. Transfer 1 μl of your sample into the loading buffer and mix carefully by pipetting against the side of the well.
4. If using a plate, use a foil seal to cover the samples. If using strip tubes, use strip caps.
5. Vortex the samples at 2000 rpm for 1 min.
6. Briefly spin down the plate/tubes.
7. Transfer your samples to the TapeStation®™ loading block and start the run according to the Agilent 2200 TapeStation®™ user manual (remove strip caps if using strip tubes).
8. The average sample peak should be 180–250 bp (or the max sample peak should be no higher than 250 bp).
9. If the samples are not fragmented enough, then perform an additional sonication of 15–30 min depending on the fragmentation results. Make sure you dilute the samples (which are AMPure cleaned) with TE buffer to a final volume of 80 μl. If the DNA quantity of a sample is below 350 ng, repeat the sonication with more stock DNA and 54 min of sonication (*see* **Note 12**).

### 3.12 Pre End-Repair Dilutions

1. Dilute 350 ng of the fragmented DNA in $dH_2O$ to 8.75 ng/μl to a final volume of 40 μl in a 96-well skirted Eppendorf plate.

### 3.13 End Repair

Forty microliters diluted fragmented DNA is converted by the NEBNext End Repair Module to blunt ended DNA having 5′ phosphates and 3′ hydroxyl, to a final volume of 50 μl.

1. Make an end-repair master mix on ice (*see* Table 11) and pipette into a plate. Add 40 μl of DNA from the previous step.
2. Incubate the samples for 30 min at 20 °C (*see* **Note 12**).

**Table 11**
**End-repair master mix**

| | **Volume ($n = 1$) (μl)** |
|---|---|
| 10× End-repair buffer | 5.0 |
| End-repair enzyme mix | 2.5 |
| $dH_2O$ | 2.5 |
| Total volume per sample | 10 |

### 3.14 AMPure XP Clean-Up

Samples are cleaned up with 90 μl AMPure XP beads (1.8 volumes) and eluted in 22 μl $dH_2O$

1. Allow the AMPure XP beads to equilibrate to room temperature before use and shake well so that the reagent appears homogenous and consistent in color.
2. Add 90 μl of the AMPure XP beads to each well of a Nunc DeepWell plate.
3. Add the 50 μl sample to each well and mix by pipetting.
4. Incubate for 5 min at room temperature.
5. Place the plate onto the magnetic stand for 3 min to separate the beads from the solution.
6. Remove the cleared liquid from the solution while the plate is situated on the magnetic stand, being careful not to disturb the separated beads.
7. Add 70% ethanol (enough to cover the beads) to each well while the plate is situated on the magnetic stand and incubate for 30 s at room temperature.
8. Repeat for a total of two washes.
9. Remove the plate from the magnetic stand and add 22 μl of $dH_2O$. Resuspend the beads by pipetting.
10. Incubate for 1 min.
11. Place the plate onto the magnetic stand and transfer the elute to a fresh plate (*see* **Note 12**).

### 3.15 A-Tailing

A dAMP is incorporated on the 3′ end of the 21-μl blunt (end-repaired) DNA.

1. Prepare the dA-tailing master mix (Table 12) on ice and mix by vortexing.
2. Pipette 25 μl into each well of a Nunc DeepWell plate.
3. Add 21 μl of each DNA sample to each well and mix by pipetting.
4. Seal the plate with a film lid and incubate at 37 °C for 30 min (*see* **Note 12**).

**Table 12**
**dA tailing master mix**

| | **Volume ($n = 1$) (μl)** |
|---|---|
| 10× Rx buffer | 3 |
| Klenow fragment (without exonuclease activity) | 1.5 |
| $dH_2O$ | 4.5 |
| End-repaired DNA | 21 |
| Total volume | 25 |

### 3.16 AMPure Clean-Up

Samples are cleaned with 54 μl AMPure beads (1.8 volumes) and eluted in 12 μl $dH_2O$

1. Allow the AMPure XP beads to equilibrate to room temperature before use and shake well so that the reagent appears homogenous and consistent in color.
2. Add 54 μl of the AMPure XP beads to each well of a Nunc DeepWell plate.
3. Add 50 μl sample to each well and mix by pipetting and incubate for 5 min at room temperature.
4. Place the plate onto the magnetic stand to separate the beads from the solution for 3 min.
5. Remove the cleared liquid from the solution while the plate is situated on the magnetic stand, being careful not to disturb the separated beads.
6. Add 70% ethanol (enough to cover the beads) to resuspend and mix by pipetting. Incubate for 1 min at room temperature.
7. Repeat for a total of two washes.
8. Remove the plate from the magnetic stand and add 12 μl of $dH_2O$ to elute the samples. Incubate for 2 min.
9. Place the plate onto the magnetic stand for 2 min and transfer the eluate to a fresh plate (*see* **Note 12**).

### 3.17 Adaptor Ligation

Ligation with 3.5 μl paired-end adapter to 12 μl A-tailed DNA.

1. Make up the ligation master mix ($n + 1$, *see* Table 13) on ice and pipette 4.5 μl on ice into each well.
2. Dilute each of the NEXTflex adapters to 6.25 nM.
3. On ice, add 3.5 μl of the diluted NEXTflex adapters per sample (note each adapter is used only once for each sequencing run).
4. On ice, add 12 μl of repaired DNA.
5. Seal the plate with a film and incubate 20 °C for 15 min.

**Table 13**
**Ligation master mix**

| | **Volume ($n = 1$) (μl)** |
|---|---|
| Fast-Link DNA ligase | 1 |
| 10 mM ATP | 1 |
| 10× buffer | 2 |
| Water | 0.5 |
| Total volume | 4.5 |

### 3.18 AMPure Clean-Up

Clean samples with 20 μl AMPure beads (1.0 volumes) and eluted in 42 μl $dH_2O$ (*see* **Note 13**).

1. Allow the AMPure XP beads to equilibrate to room temperature before use and shake well so that the reagent appears homogenous and consistent in color.
2. Add 20 μl of the AMPure XP beads to each well of a Nunc DeepWell plate.
3. Add the 20 μl sample to each well and mix by pipetting and incubate for 5 min at room temperature.
4. Place the plate onto the magnetic stand for 3 min to separate the beads from the solution.
5. Remove the cleared liquid from the solution while the plate is situated on the magnetic stand, being careful not to disturb the separated beads.
6. Add 70% ethanol (enough to cover the beads) and resuspend and mix by pipetting to each well while the plate is situated on the magnetic stand and incubate for 1 min at room temperature.
7. Repeat for a total of two washes.
8. Remove the plate from the magnetic stand and add 42 μl of $dH_2O$ to elute the samples.
9. Incubate for 2 min.
10. Place the plate onto the magnetic stand and allow to separate for 2 min.
11. Transfer the eluate to a fresh plate (*see* **Note 12**).

### 3.19 Pre Hybe PCR

Twenty microliter adapter-ligated DNA is amplified in a final PCR volume of 50 μl.

1. Prepare the PCR master mix (Table 14) and add 30 μl of the PCR master mix to each adapter-ligated DNA sample.
2. Run the program in Table 15 on the thermocycler (*see* **Note 12**).

**Table 14**
**PCR reaction mix**

| | **Volume ($n = 1$) (μl)** |
|---|---|
| 5× Herculase II buffer | 10 |
| NEXTflex primer mix (12.5 μM each primer) | 2.0 |
| dNTP mix (Herculase kit only) | 0.5 |
| Herculase II polymerase | 1.0 |
| PCR-grade water | 16.5 |
| Total volume | 30 |

**Table 15**
**PCR cycling conditions**

| Step | Temperature | Time |
|---|---|---|
| Step 1 | 98 °C | 2 min |
| Step 2 | 98 °C | 30 s |
| Step 3 | 65 °C | 30 s |
| Step 4 | 72 °C | 1 min |
| Step 5 (repeat steps 2–4 for seven cycles) | | |
| Step 6 | 72 °C | 10 min |
| Step 7 | 4 °C | Hold |

### 3.20 AMPure Clean-Up

Samples are cleaned up with 60 μl AMPure beads (1.2 volumes) and eluted in 30 μl $dH_2O$

1. Allow the AMPure XP beads to equilibrate to room temperature before use and shake well so that the reagent appears homogenous and consistent in color.
2. Add 60 μl of the AMPure XP beads to each well of a Nunc DeepWell plate.
3. Add 50 μl sample to each well and mix by pipetting and incubate for 5 min at room temperature.
4. Place the plate onto the magnetic stand to separate the beads from the solution for 3 min.
5. Remove the cleared liquid from the solution while the plate is situated on the magnetic stand, being careful not to disturb the separated beads.
6. Add 70% ethanol (enough to cover the beads) and resuspend and mix by pipetting to each well while the plate is situated on the magnetic stand and incubate for 1 min at room temperature.
7. Repeat for a total of two washes.
8. Remove the plate from the magnetic stand and add 30 μl of $dH_2O$ to elute the samples.
9. Incubate for 2 min.
10. Place the plate onto the magnetic stand and allow to separate for 2 min.
11. Transfer the eluate to a fresh plate (*see* **Note 12**).

### 3.21 TapeStation®™ Quality and Quantity Check

A quality control check on D1000 tapes are performed to ensure adapters have been ligated and there is sufficient sample to continue (see the Agilent 220 TapeStation®™ user manual for the manufacturer's instructions).

1. To analyze results, set the region from 115 to 700 bp (this will exclude any adapter dimer peaks [~135 bp] from the analysis). The average sample peak should be less than 350–400 bp (due to the adapter ligation, products will be longer by about 120 bp) (*see* **Note 14**).

### 3.22 Hybe Pools

Four 12-plex pools each containing 1200 ng total DNA (i.e., 100 ng per sample) are prepared for hybe reactions.

1. Label 4 Anachem tubes (e.g., A–D).
2. Add 12 samples per tube (100 ng per sample) to form a pool of 1200 ng.
3. Mix well on a vortex mixer and spin in a microcentrifuge for 1 min.
4. Using a vacuum concentrator dry the samples until no liquid is left in the tubes (~60 min). A little white pellet may be visible (*see* **Note 12**). We use a SpeedVac, although different instruments are available.
5. If a sample is not completely dehydrated after 60 min, continue dehydration for an additional 5–10 min (*see* **Note 15**).
6. Reconstitute the dehydrated samples in 8.2 μl $dH_2O$ to bring the final concentration up to 147 ng/μl (*see* **Note 16**).

### 3.23 Hybridization

For each pool, prepare one hybridization and capture 3.4 μl pooled DNA (500 ng) hybridized with the Capture library in a final volume of 28 μl. During the following steps, some of the transfers are carried out while tubes remain on the PCR thermocycler. During these steps care should be taken to remove and replace tube lids without disturbing samples. After transfers, lids should be replaced as quickly as possible to minimize loss by evaporation.

From this point onward, one sample refers to one pooled library.

1. Label three rows of strip tubes as follows:
   (a) Row 1: Pools A–D prepped library.
   (b) Row 2: Pools A–D hybridization buffer.
   (c) Row 3: Pools A–D SureSelect capture library.
2. Make up the SureSelect block mix ($n + 1$) as in Table 16 in strip tubes for each pool (5.6 μl) and add the DNA.
3. Place the tubes on a PCR thermocycler and incubate at 95 °C for 5 min and then hold at 65 °C (*see* Table 17).
4. In separate strip tubes, make up the hybridization buffer (one for each pooled sample) (*see* Table 18), and once the PCR block has reached 65 °C from the previous step, place the tubes containing the hybridization buffer on the PCR thermocycler set at 65 °C for 5 min.

**Table 16**
**SureSelect block mix**

| Reagent | Volume ($n = 1$) (μl) |
|---|---|
| SureSelect indexing block #1 | 2.5 |
| SureSelect indexing block #2 | 2.5 |
| SureSelect indexing block #3 | 0.6 |
| Total | 5.6 |

**Table 17**
**PCR thermocycler program**

| Step | Temperature | Time |
|---|---|---|
| Step 1 | 95 °C | 5 min |
| Step 2 | 65 °C | Hold |

**Table 18**
**Hybridization buffer**

| Reagent | Volume ($n = 1$) (μl) |
|---|---|
| SureSelect Hyb#1 | 25 |
| SureSelect Hyb#2 | 1 |
| SureSelect Hyb#3 | 10 |
| SureSelect Hyb#4 | 13 |
| Total | 49 |

**Table 19**
**RNase block dilution**

| Reagent | Volume ($n = 1$) (μl) |
|---|---|
| SureSelect RNase block | 0.5 |
| $dH_2O$ | 4.5 |
| Total | 5 |

5. Dilute the RNase blocker (Tables 19 and 20) and put on ice.
6. The custom library is stored at −80 °C, remove from the freezer, and defrost quickly and gently (i.e., gloved hand).
7. On ice, add 5 μl of the diluted RNase blocker to the labeled tubes.

**Table 20**
**Capture library (for capture size <3.0 Mb)**

| | Volume ($n = 1$) (μl) |
|---|---|
| SureSelect library | 2 |
| RNase block dilution (*see* Table 19) | 5 |
| Total | 7 μl |

8. Add 2 μl of the capture library to the same tubes and put on the thermocycler set at 65 °C for 2 min.
9. Add 13 μl of hybridization buffer (on the 65 °C block) into the capture library RNase tubes.
10. Then add all of the SureSelect block mix and DNA to the capture library tubes and pipette to mix.
11. Close the lids and incubate for 16 h at 65 °C on a thermocycler.

### 3.24 Capture of the Hybridization Library Pools on to Streptavidin-Coated Beads

Clean-up ~28 μl hybridization library pools with streptavidin-coated beads.

1. Vigorously resuspend the Dynabeads MyOne Streptavidin T1 on a vortex mixer.
2. For each hybridization pool, add 50 μl of Dynabeads MyOne Streptavidin T1 to a clean 1.5 ml microfuge tube.

Wash the beads:

1. Add 200 μl of SureSelect binding buffer to each of four tubes.
2. Mix the beads on a vortex mixer for 5 s.
3. Place the tubes into the magnetic stand for 2 min.
4. Remove and discard the supernatant.
5. Repeat **steps 1** through **4** for a total of three washes.
6. Resuspend the beads in 200 μl of SureSelect binding buffer.
7. Transfer the bead mixture to a Nunc DeepWell plate (200 μl per well, four wells in total).
8. Using a multichannel pipette, transfer each of the samples from the hybridization step to the wells of the Nunc plate containing the beads.
9. Mix thoroughly by pipetting and incubate in a vortex mixer for 30 min at room temperature.

### 3.25 Washing the Capture Library

1. Place the tubes into the magnetic stand for 2 min and remove the supernatant.
2. Resuspend the beads in 500 μl of SureSelect wash buffer 2 pre-warmed to 65 °C.

3. Mix on a vortex mixer for 5 s to resuspend the beads.
4. Incubate the samples for 10 min at 65 °C in a heat block. Occasionally mix on a vortex mixer.
5. Briefly centrifuge the tubes so that the sample is at the bottom of the well.
6. Separate the beads by placing the tubes on a magnetic stand and remove all the supernatant.
7. Repeat **steps 2–6** for a total of three washes.
8. Mix the beads in 30 μl of $dH_2O$ on a vortex mixer for 5 s to resuspend the beads. Captured DNA is retained on the streptavidin beads.

### 3.26 Posthybridization PCR

Fifteen microliter captured DNA amplified in a final PCR volume of 50 μl.

1. Make a PCR master mix for $n + 1$ samples according to Table 21.
2. Pipette 35 μl of posthybridization PCR master mix into a strip tube for each of the pools.
3. Add 15 μl of the hybridization DNA (including streptavidin beads) and place on the PCR thermocycler and run the PCR thermocycler program as in Table 22.

### 3.27 AMPure Clean-Up

Samples are cleaned up with 90 μl AMPure beads and eluted in 30 μl $dH_2O$

1. Allow the AMPure XP beads to equilibrate to room temperature before use and shake well so that the reagent appears homogenous and consistent in color.
2. Label four tubes.
3. Transfer the entire PCR product of the labeled tubes.

**Table 21**
**Posthybridization PCR master mix**

| | **Volume ($n = 1$) (μl)** |
|---|---|
| 5× Herculase II buffer | 10 |
| NEXTflex primer mix (12.5 μM each primer) | 2 |
| dNTP mix (Herculase kit only) | 0.5 |
| Herculase II polymerase | 1.0 |
| PCR-grade water | 21.5 |
| Total volume | 35 |

**Table 22**
**PCR thermocycler conditions**

| Step | Temperature | Time |
|---|---|---|
| Step 1 | 98 °C | 2 min |
| Step 2 | 98 °C | 30 s |
| Step 3 | 65 °C | 30 s |
| Step 4 | 72 °C | 1 min |
| Step 5 (repeat steps 2–4 for 16 cycles) | | |
| Step 6 | 72 °C | 10 min |
| Step 7 | 4 °C | Hold |

4. Add 90 μl AMPure XP beads to each of the tubes containing the PCR products and mix by pipetting.
5. Incubate at room temperature for 5 min on the vortex.
6. Transfer the tube to the magnetic stand and separate the beads for 3 min.
7. Remove the supernatant without disturbing the beads.
8. Add 500 μl of 70% ethanol and incubate for 1 min.
9. Remove the ethanol.
10. Add another 500 μl of 70% ethanol and incubate for 1 min.
11. Remove the ethanol.
12. Incubate the samples at 45 °C until all of the ethanol has been removed, little cracks should appear in the bead pellets.
13. Resuspend the beads in 30 μl $dH_2O$ by carefully pipetting up and down.
14. Incubate for 2 min.
15. Transfer the tubes to the magnetic stand and allow the beads to separate for 3 min.
16. Carefully transfer the supernatant to labeled strip tubes.

### *3.28 TapeStation®™ Quality Control*

The concentration of the pooled samples is determined prior to sequencing. Analysis of the samples is performed on HSD1K tape according to the manufacturer's instructions.

1. Measure the concentration of the samples with the Qubit dsDNA BR assay using 1 μl sample.
2. Using the concentration from the Qubit assay, dilute the samples to 1.5 ng/μl using 2 μl samples.
3. Run the diluted samples in triplicate on a HSD1K tape on the Agilent 2200 TapeStation®™.
4. To analyze results, set the region from 150 to 700 bp.

### 3.29 Final Library Pool

Fifty microliter of a 10 nM pool are sequenced on the Illumina 2500HiSeq.

1. Make the final library pool of all the samples in an Anachem tube to appropriate concentration (50 μl at 10 nM) (*see* **Notes 12** and **17**).

### 3.30 TapeStation®™ Quality Check

A final quality check is run on HSD1K tape to ensure the library pool has a concentration of 10 nM.

1. Dilute the sample 1:3 using 2 μl sample.
2. Run the diluted sample in triplicate on a HSD1K tape on the TapeStation®™ according to the manufacturer's instructions.

The samples are now ready to be sequenced. We use the Illumina HiSeq2500 according to standard procedures (*see* **Note 12**).

## 4 Notes

1. All primers are M13 tailed and HPLC purification is recommended.
2. Variations in these programs for particular amplicons are detailed in Table 1.
3. Be sure to remove all of the ethanol from the bottom of the well as it may contain residual contaminants.
4. Volume of ethanol = 1.428 × (5 μl + Sample Volume).
5. The magnetic beads will be pulled to the side of the well.
6. Remove as much of the supernatant possible as it contains excess fluorescent dye and contaminants.
7. Excessive drying can lead to degradation of fluorescent dye.
8. Elution of the sequencing products is rapid. It is not necessary for the beads to go back into solution for complete recovery.
9. If no Agencourt 384 Direct inject magnet plate is available, allow the sample plate to separate on the magnet for 3–5 min until solution is clear. Transfer clear sample into a new plate for loading on the detector. Leave 2–5 μl of liquid behind to prevent transfer of beads into the final plate. Residual beads can interfere with injection, causing late starts or failed injections.
10. If samples are not loaded within 24 h, store at −20 °C.
11. If less than 12 samples, fill the empty spaces with balance containing 80 μl of $dH_2O$.
12. Note, samples can be stored at −20 °C at this point.
13. Note, low AMPure is used to ensure removal of the unligated adapters.

14. If the samples are too strong and the presence of artifacts >900 bp long in the TapeStation®™ trace can be seen, repeat the PCR with fewer cycles. If too weak, repeat with more cycles.
15. This is not DNA, but precipitated salt from the input sample.
16. The samples should be dried for the minimum time possible, excessive drying may result in poor resuspension of DNA.
17. The final volume of the pooled library can be adjusted to the desired concentration. Exact library pool dilutions and processing can vary based on the cell capacity and analysis pipeline being used. Refer to appropriate Illumina guide for instructions.

## References


1. Pearson ER, Flechtner I, Njølstad PR, Malecki MT, Flanagan SE, Larkin B, Ashcroft FM, Klimes I, Codner E, Iotova V, Slingerland AS, Shield J, Robert JJ, Holst JJ, Clark PM, Ellard S, Søvik O, Polak M, Hattersley AT, Neonatal Diabetes International Collaborative Group (2006) Switching from insulin to oral sulfonylureas in patients with diabetes due to Kir6.2 mutations. N Engl J Med 355(5):467–477
2. Shields BM, Hicks S, Shepherd MH, Colclough K, Hattersley AT, Ellard S (2010) Maturity-onset diabetes of the young (MODY): how many cases are we missing? Diabetologia 53(12):2504–2508
3. Flanagan SE, Kapoor RR, Hussain K (2011) Genetic of congenital hyperinsulinemic hypoglycemia. Semin Pediatr Surg 20(1):13–17
4. Ellard S, Lango Allen H, De Franco E, Flanagan SE, Hysenaj G, Colclough K, Houghton JA, Shepherd M, Hattersley AT, Weedon MN, Caswell R (2013) Improved genetic testing for monogenic diabetes using targeted next-generation sequencing. Diabetologia 56 (9):1958–1963
5. Ellard S, Shields B, Tysoe C, Treacy R, Yau S, Mattocks C, Wallace A (2009) Semi-automated unidirectional sequence analysis for mutation screening in a clinical diagnostic setting. Genet Test 13(3):381–386

# Chapter 9

# Isolation and Purification of Rodent Pancreatic Islets of Langerhans

**Jacqueline F. O'Dowd and Claire J. Stocker**

## Abstract

This chapter describes the detailed protocol for the isolation and purification of islets of Langerhans from rodent pancreas using collagenase digestion. The first step of the process is to separate and isolate the insulin-producing islets of Langerhans from the rest of the pancreas. The pancreas is excised from the animal, trimmed of nonpancreatic tissues before being inflated and chopped into small pieces. The connective tissue is then broken down with a collagenase enzyme solution to selectively digest the bulk of the exocrine tissue while leaving the endocrine islets intact and separated from their surrounding non-islet tissue. Once this process is completed, the islets of Langerhans are separated from the remaining mixture by centrifugation and purified by the means of hand picking. Once isolated, the subsequent islets can be used for several varied experimental processes, including transplantation, the study of pathophysiological mechanisms in diabetic conditions, and in the screening of novel therapeutic approaches in pharmacological research.

**Key words** Islets of Langerhans, Insulin, Isolation, Endocrine pancreas, β-cell, Collagenase

## 1 Introduction

The pancreas is a highly vascular retroperitoneal gland located in the abdomen behind the stomach and on the posterior abdominal wall surrounded by the liver and intestine. It is composed of both exocrine and endocrine tissue. Embedded throughout the exocrine glandular tissue, clusters of secretory endocrine cells, called the islets of Langerhans, secrete hormones directly into the bloodstream. Discovered in 1869 by the German pathological anatomist Paul Langerhans, the islets of Langerhans constitute only 1–3% of the total pancreatic volume [1] but fulfill a vital role in glucose homeostasis. The number of islets within a human pancreas can range from 200,000 to almost two million. Each islet itself can range in size from a cluster of a few cells less than 40 μm in diameter to ovoids of 400 μm in diameter [2]. Within the pancreas, islets are not randomly distributed: small islets (160 nm or less, in diameter)

Claire J. Stocker (ed.), *Type 2 Diabetes: Methods and Protocols*, Methods in Molecular Biology, vol. 2076,
https://doi.org/10.1007/978-1-4939-9882-1_9, 

tend to be scattered throughout the exocrine tissue while larger islets, 250 nm or more in diameter, appear to be located near larger ducts and blood vessels [3].

The ability to isolate islets from the pancreas enables investigators to use them in a number of downstream applications [4]. Once isolated, islets of Langerhans can be maintained as viable units for extended periods of time in tissue culture or they can be used in more acute experiments investigating aspects of mechanistic functionality. Isolated islets have long been used for the static and perfusion incubations (to assess hormone release in response to compounds, but recent advances such as RNA interference (RNAi), a powerful and convenient tool for studying gene function, mean that the ability to isolate islets is a useful tool that allows investigators to gather functional information without using cell lines.

Islets are isolated by a modification of the method originally described by Lacy in 1967 using enzymatic digestion with a relatively crude preparation of collagenase [5]. The less fibrous nature of the rodent pancreas, as compared to man, makes the release of islets easier and allows for the preferential use of less purified collagenase preparations in many laboratories. The first step of the process is to remove the pancreas from the animal and trim it of non-pancreatic tissues. The pancreas is then inflated to increase the surface area and the connective tissue digested with collagenase. After digestion is complete, the mixture is centrifuged to separate the islets from non-islet tissue. The pellet is then resuspended in physiological saline. A small sample of the resuspended pellet is then placed on a black petri dish containing more buffer. The black background of the petri dish allows the white islets to be visible under a dissection microscope with an external light source. Islets are then purified by hand picking using a very fine glass pipette. The picking procedure is repeated twice to ensure no carryover of unwanted exocrine tissue debris and to ensure that the islets are of the highest quality and purity. It is very important that the islets being isolated are intact and relatively pure. Contamination of islets with acinar cells when used for functional studies may lead to a high level of proteases that will later influence islet integrity and functionality during incubation. The highest level of purity is required if protein or RNA is to be extracted from the isolated islets as any contamination of the preparation with acinar cells will cause spurious data to be obtained.

With the increasing focus on the need to isolate viable islets and to overcome the berries of islet transplantation, a number of modifications to this low activity collagenase digestion technique have been described including low temperature Percoll centrifugation [6] and sedimentation of islets [7], as well as their embedding in hydrogel post purification [8].

In this chapter, a method for the isolation of islets of Langerhans from the pancreas by collagenase enzymatic digestion and then harvesting by handpicking individual islets is described. Although the process of handpicking islets is both time-consuming and labor-intensive, this method gives islet preparations with the highest purity.

## 2 Materials

### 2.1 Reagents

1. Collagenase (Type XI, Sigma) (*see* **Note 1**).
2. Buffered saline solution: either Gey and Gey or Krebs Ringer buffer supplemented with 1 mM $CaCl_2$, 4 mM glucose and gassed with $CO_2$:$O_2$ (95:5).
   (a) Gey and Gey Buffer—111 mM NaCl, 27 mM $NaHCO_3$, 5 mM KCl, 1 mM $CaCl_2$, $MgCl_2$, 0.3 mM $MgSO_4$, 1.18 mM $Na_2HPO_4$, 0.29 mM $KH_2PO_4$, and 4 mM D-glucose gassed to pH 7.4 by $CO_2$:$O_2$ (95:5).

   A ten times stock solution without KCl, $CaCl_2$, $MgCl_2$, $MgSO_4$, $KH_2PO_4$, and D-glucose can be made and kept for 1 month at room temperature.
3. RPMI-1640 culture medium.

### 2.2 Equipment

1. Sterilized Forceps.
2. Sterilized scissors: One for skin incision and another for removal of pancreas from adjacent tissue and another for chopping the pancreas into pieces.
3. 10-ml syringe.
4. 25-G needle.
5. 15-ml polypropylene tubes.
6. 25-ml glass measuring beaker.
7. 50-ml conical flask with lid.
8. Water bath with shaker.
9. Plastic Pasteur pipette.
10. 90-mm petri-dish painted 'in house' with two layers of black enamel paint to ensure a darkened background to visualize and pick islets against.
11. Dissection microscope with external light source.

### 2.3 Islets Isolation

1. For islets isolated from normal rats (150–180 g) use two animals per isolation or three normal mice (*see* **Note 2**).
2. Just prior to dissection, euthanize the donor rodent by an appropriate technique.

3. On a sterilized area, make a V-incision starting at the genital area, move the bowel to the left side of the open rodent. This will expose the pancreas which is tan in color and can be easily differentiated from the surrounding fat as can the spleen.
4. Using forceps to grasp the spleen, gently push up and back the stomach.
5. Cut the pancreas away from the surrounding fat and where attached at the small intestine.
6. Remove the pancreas from the body and place the pancreas, still attached to the spleen, into 100 ml of Gey and Gey in a Petri dish and cut away from the spleen—any retained fat, lymph nodes, and other non-pancreatic tissues.
7. Inflate the pancreas by inserting a 25-gauge needle attached to a 10-ml syringe into the pancreas and injecting small volumes (1–2 ml at a time) of Gey and Gey solution into all the folds of the tissues so that the pancreas increases in size, thus creating a larger surface area.
8. Place the pancreata into a glass 50-ml beaker and chop using scissors until all the pieces were approximately the same size (1 mm × 1 mm).
9. Transfer the contents to a 15-ml tube and centrifuge for 5 min at 100 × *g*. After centrifugation, remove the supernatant, which contains fat, and transfer the pellet to a 15-ml conical tube.
10. Digest the pancreas with collagenase type XI (1–2 mg/pancreas) in a 1:1 mixture of Gey and Gey solution in order to release islets from exocrine tissue.
11. Place the conical tube in a shaking water bath at 37 °C and shake at 800 oscillations per minute until the solution appears "milky" and most of the pieces of pancreas are digested (approximately 5–10 min—time varies with strain and age of the animal). During this time, take a small amount (approximately 400 μl) in a plastic pipette and examine under a dissecting microscope to confirm whether islets are free from the exocrine tissue. If there are no islets visible continue the shaking by hand and repeat the process (*see* **Note 3**). Normally, a total shaking time of 6–8 min is enough to release the bulk of free islets.
12. Place the contents of the conical flask and stop the digestion by adding 15 ml of cold buffer.
13. Centrifuge at 500 × *g* for 5 min to remove the collagenase in the solution.
14. Aspirate the supernatant and resuspend the pellet in 15 ml of the isolation buffer.

15. Add a sample of the resuspended pellet (1 ml) to a blackened 90-mm Petri dish, add buffer to the top of the Petri dish, and mix with a plastic Pasteur pipette.
16. Using a dissection microscope and an external light source, handpick and count individual islets using a drawn out glass pipette (*see* **Note 4**).
17. Only pick clean and intact islets free of exocrine tissues (*see* **Note 5**).
18. Repeat the picking procedure at least twice.
19. Incubate the islets with isolation buffer in a 37 °C water bath until use. Always use the islets within 30 min to 1 h after isolation.
20. While the yield of islets is variable, approximately 600–1200 islets are obtainable from two Wistar rats and 400 from three mice using this method (*see* **Note 6**).

### 2.4 Islets Culturing

For certain experimental protocols, it may be necessary to culture the isolated islets. When culturing, it is important to handle the islets under aseptic conditions and use sterile tubes and flasks.

1. Wash the islets in more than ten volumes of sterile Gey and Gey solution.
2. Resuspend groups of 200 islets in RPMI-1640 containing 11.1 mM glucose (*see* **Note 7**) and transfer to a six-well cell-culture plate.
3. Incubate the islets in a humidified culture incubator with 5% $CO_2$; 95% air.

## 3 Notes

1. A wide variety of collagenase preparations are available for islet isolation but in our experience Collagenase Type XI from Sigma-Aldrich is best suited for isolations. This crude mixture isolated from *Clostridium histolyticum* contains several enzymes (collagenase, neutral proteases, clostripain, and caseinase) that act together to break down tissue. While collagenase Type XI has one of the highest collagenase activities, not every batch is equivalent, and it is usually appropriate to test small quantities from several different batches before choosing to make a bulk purchase of a particular batch.
2. The age and weight of the animals can influence the numbers of islets of Langerhans obtained. Rats heavier than 180 g often yield fewer islets per pancreas. Although younger animals can give high yields, the islets obtained from these animals should be considered from a 'juvenile' stage of development.

3. If no islets are isolated or isolated islets are not intact, the islets are over-digested. This can be prevented by decreasing the collagenase digestion time or collagenase concentration (*see* Subheading 2.3 **step 10**).
4. Normal bore pipettes draw up too much liquid as islets are picked, so drawn pipettes are preferential. Draw glass pipettes by heating in a Bunsen flame. Once the glass begins to give, pull sharply to yield pipettes with a bore of approximately 1 mm.
5. If most of the islets are not discrete and difficult to isolate (*see* Subheading 2.3 **step 15**), the exocrine tissues are under-digested. In order to overcome this problem, increase the collagenase digestion time (*see* Subheading 2.3 **step 10**) and/or increase the collagenase concentration (*see* Subheading 2.3 **step 10**) and ensure vigorously shaking of the vial to disrupt the pancreas (*see* Subheading 2.3 **step 11**).
6. The yield of islets will vary depending on the age and strain. Diabetic and older animals will have reduced numbers of viable islets. Digestion continues as the handpicking selection proceeds; therefore, speed is important. Islets should be collected within 15–20 min, and the entire isolation completed within 45 min to 1 h of removal of the organ.
7. The culture medium can be altered depending on the experimental conditions required.

## References

1. Hellerstrom C (1984) The life story of the pancreatic β-cell. Diabetologia 26(6):393–400
2. Lifson N, Kramlinger K, Mayrand R, Lender E (1980) Blood flow to the rabbit pancreas with special reference to the islets of Langerhans. Gastroenterology 79(3):466–473
3. Bonner-Weir S, Orci L (1982) New perspectives on the microvasculature of the islet of Langerhans in the rat. Diabetes 31(10):883–889
4. Nolan AL, O'Dowd JF (2009) The measurement of insulin secretion from isolated rodent islets of Langerhans. Methods Mol Biol 560:43–51
5. Lacy P, Kostianovsky M (1967) Method for the isolation of intact islets of Langerhans from the rat pancreas. Diabetes 16(1):35–39
6. Olack B, Finke E, Scharp DW (1987) Low-temperature culture of human islets by the distension method and purified with Ficoll or Percoll gradients. Surgery 102(5):869–879
7. Saliba Y, Fares N (2019) Isolation, purification and culture of mouse pancreatic islets of Langerhans. Methods Mol Biol 1940:255–265
8. Ayenehdeh JM, Niknam B, Hashemi SM, Rahavi H, Rezaei N, Soleimani M, Tajik N (2017) Introducing a new experimental islet transplantation model using a biometric hydrogel and a simple high yield islet isolation technique. Iran Biomed J 21(4):218–227

# Chapter 10

# Characterization of Islet Leukocyte Populations in Human and Murine Islets by Flow Cytometry

**Matthew J. Butcher, Michelle B. Trevino, Yumi Imai, and Elena V. Galkina**

## Abstract

An increasing body of evidence indicates that a local islet immune response is not only limited to type 1 diabetes, but also is associated with islet dysfunction in type 2 diabetes. Recently, the presence of pancreatic $CD68^+$ macrophages within islet tissues was demonstrated by RT-PCR and immunohistochemical methods. However, the precise profile and activation status of intraislet leukocytes, which are present in both murine and human islets, are poorly defined. Here, we describe a detailed flow cytometry protocol designed to analyze both human and murine islets for intraislet leukocytes and leukocyte subsets. This approach permits the simultaneous identification of multiple intraislet leukocyte subsets, as well as their activation statuses. The use of flow cytometry-based approaches will advance the field of islet biology and help to identify unique changes in the immune cell composition that accompanies pathological islet inflammation and dysfunction in type 2 diabetes.

**Key words** Type 2 diabetes, Leukocytes, Human islets, Murine islets, Flow cytometry

## 1 Introduction

Type 2 diabetes results from the combination of insulin resistance and islet dysfunction [1]. It has been well-known that chronic inflammation within peripheral insulin-responsive tissues contributes to insulin resistance [1]. While the exact mechanisms that drive islet dysfunction in type 2 diabetes are incompletely understood, recent evidence suggests that the immune system may be involved [2]. One of the first changes that occurs in response to metabolic stress from excessive nutrition occurs in the peripheral circulation, with a contaminant increase of T helper 1 (Th1) and Th17 cells and a decrease in T regulatory cells (Tregs) [3, 4]. Interestingly, peripheral blood circulating B cells from type 2 diabetic patients also display a proinflammatory phenotype, and notably secrete IL-8 and support contact-dependent T-cell activation [5]. To date, it is unclear whether these systemic alterations also occur within pancreatic islets. Recent studies have examined the

Claire J. Stocker (ed.), *Type 2 Diabetes: Methods and Protocols*, Methods in Molecular Biology, vol. 2076,
https://doi.org/10.1007/978-1-4939-9882-1_10, 

immune cell content of human type 2 diabetic islets and demonstrated an elevated number of $CD68^+$ macrophages in histological samples from type 2 diabetic patients [6, 7]. As type 2 diabetic conditions may affect not only macrophages, but also lymphocytes and likely other types of leukocytes, additional studies are necessary to fully characterize the immune cell composition within islets and to determine their potential impact on intraislet inflammation in type 2 diabetes.

While extensive work on animal models of type 2 and type 1 diabetes have provided valuable insights into islet biology, human islets are known to differ from rodent islets in terms of their morphology [8, 9] and functionality [10], highlighting the importance of studying human islets. Nevertheless, there are some limitations in investigating the human intraislet immune composition and insulin-producing beta cells. The scarcity and difficulty in obtaining human islets are significant barriers for performing large-scale studies using human islets. Additionally, well-established methods of RT-PCR and immunohistochemistry may provide limited information about the cell type, stage of activation, and relative proportions of leukocyte subsets within whole tissues. Flow cytometry-based analyses of secondary lymphoid organs and several other nonlymphoid tissues have provided "high-throughput" data about the overall numbers, subsets, and phenotypes of cells isolated from dissociated tissues through the use of multiple surface antigen markers [11]. Several reports have taken advantage of flow cytometry-based approaches and have characterized endocrine cells in both human and murine islets [12, 13]. There has been targeted characterization of myeloid cell populations in murine islets [14–16]. However, this approach was not used to analyze leukocyte populations in human islets or study other leukocytes in murine islets. Thus, we adapted a flow cytometry protocol to better characterize leukocyte subsets and their activation statuses within human islets [17]. Here, we describe in detail a method for preparing both human and murine islets for flow cytometry. In addition, we provide specific advice on a gating strategy for analyzing all intraislet leukocytes, and we discuss potential issues and workaround solutions for preparing and analyzing islets by flow cytometry.

## 2 Materials

### 2.1 Human Islets

1. Supplemented CMRL-1066 media: CMRL-1066, 10% fetal bovine serum, 1% penicillin–streptomycin.
2. A 100 × 20-mm polystyrene nontreated tissue culture dish.

### 2.2 Murine Islets: Harvest and Preparation for Flow Cytometry

1. Dissection instruments: Hooked nose forceps, scissors, hemostat clamps, 30 gauge syringe.
2. Surgical microscope.
3. 1× Dulbecco's phosphate-buffered saline (PBS) without calcium or magnesium.
4. 12 × 75 mm, 5 ml polystyrene round bottom test tubes (FACS tubes).
5. Collagenase P (Roche).
6. Ficoll PM400.
7. 1× Hank's balanced salt solution (HBSS).

### 2.3 Preparation of Islet and Splenic Cell Suspensions

1. Islet digestion buffer: Trypsin/ethylenediaminetetraacetic acid (EDTA) (0.25% trypsin and 0.2 g/l EDTA) in phosphate-buffered saline.
2. 1× Dulbecco's phosphate-buffered saline (PBS) without calcium or magnesium.
3. 40 and 70 μm nylon cell sieves prewetted with cold PBS.
4. Temperature controlled, table-top centrifuge 5810R.
5. Red blood cell lysis buffer: 8.3 g/l ammonium chloride ($NH_4Cl$), 1 g/l potassium bicarbonate ($KHCO_3$), 0.37 g/l EDTA, pH 7.4.
6. Low-retention pipette tips.

### 2.4 Cell Counting

1. 0.4% Trypan blue solution.
2. Bright-line hemocytometer.
3. Light microscope.

### 2.5 Extracellular Staining

1. Human or mouse Fc blocking antibodies (anti-CD16/CD32).
2. Fc block PBS: 0.25–1.0 μg/ml human or mouse Fc blocking antibodies in PBS.
3. Appropriate extracellular flow cytometry antibodies.
4. Fixable viability dye (optional).
5. Paraformaldehyde (PFA).
6. HPa2, HPi2 antibodies (for endocrine cell staining).

### 2.6 Intracellular Staining

1. Commercial fixation and permeabilization reagents.
2. Appropriate intracellular flow cytometry antibodies.

### 2.7 Sample Acquisition and Analysis

1. Flow cytometer (e.g., a DXP 8-color upgraded BD FACSCalibur).
2. Flow cytometry tubes with cell strainer caps.
3. Flow cytometry data analysis software (such as FlowJo, Kaluza, etc.).

## 3 Method

### 3.1 Human Islets: Care Post-procurement and Preparation for Flow Cytometry (See Note 1)

1. Upon receiving the islets, culture the islets in a 100 × 20-mm polystyrene nontreated tissue culture Petri dish in supplemented CMRL-1066 media overnight (37 °C, 5% $CO_2$) to allow the islets to recover from the shipment. 5000–7000 Islet equivalents (IEQ) of human islets are sufficient for a flow cytometry experiment (*see* **Note 2**).
2. Prepare a 40-μm nylon mesh cell sieve by wetting it with 4 °C PBS in a 35 × 10 mm polystyrene nontreated tissue culture Petri dish, making sure that the entire mesh has been soaked. Using a pipette, gently collect the islets from culture and transfer them to the center of a 40-μm cell strainer placed in a clean 100 × 20-mm polystyrene nontreated tissue culture Petri dish. This will remove cellular debris and disintegrated islets, and only the intact islets will be retained on the cell sieve.
3. Wash the islets retained on the sieve by very gently pipetting cold PBS over the strainer into the dish. Transfer the strainer containing intact islets to a new 35 × 10-mm polystyrene nontreated tissue culture Petri dish containing 1–2 ml of cold PBS. Very gently pipette up and down to suspend the islets off of the sieve and into a 15 ml tube. Repeat by adding 1–2 ml of cold PBS to the strainer to pick up residual islets. Centrifuge (800 × *g*, room temperature, 1 min) and aspirate the excess PBS with a transfer pipette, leaving the islet pellet intact.
4. Resuspend the islets in 0.5 ml PBS by gently pipetting up and down using low-retention pipette tips to minimize islet loss (*see* **Note 3**).
5. Continue the protocol with Subheading 3.2.

### 3.2 Murine Islets: Harvest and Preparation for Flow Cytometry

1. After euthanizing the mouse, open the abdominal cavity, locate and clamp the common bile duct as it enters the duodenum. Inject 1.4 mg/ml collagenase P solution into the common bile duct with a 30-gauge needle until the pancreas appears fully inflated. Transfer to a 15 ml tube containing 1 ml of cold HBSS. Keep on ice before proceeding to the next step as collagenase injections are repeated when multiple pancreata are isolated. Typically, 500–800 islets are used for a single analysis by flow cytometry. This requires combining pancreata from three to five mice.
2. Collect the spleen in order to prepare single-color and positive flow cytometry controls. Place the spleen in a FACS tube with 1–2 ml of PBS and place the tube on ice.
3. Incubate the 15 ml tube containing the pancreas in a 37 °C water bath and mechanically disrupt the pancreatic tissue (*see* **Notes 4** and **5**).

4. Transfer the digested pancreas to a 50-ml tube containing 30 ml HBSS, centrifuge (168 × *g*, 4 °C, 1 min) and wash once more with 30 ml of HBSS.
5. After discarding the supernatant, add 5 ml of 27% Ficoll solution in HBSS to the tissue pellet and vortex to create a homogenous tissue suspension. Carefully layer 3 ml each of 23%, 20%, and 11% Ficoll solution to generate Ficoll density gradient and centrifuge (887 × *g*, 4 °C, 15 min).
6. Transfer the Ficoll supernatant to an opaque Petri dish and carefully handpick the islets using a P10 pipette tip to a 1.5-ml tube containing 1 ml of PBS.
7. Wash islets twice in 1 ml of PBS to remove all the Ficoll by centrifugation at 887 × *g* at 4 °C for 3 min. Suspend the final islet suspension in 100 μl of PBS.
8. Continue the protocol with Subheading 3.3.

### 3.3 Preparation of Islet and Splenic Cell Suspensions

1. Resuspend the islet pellet gently to a final concentration of trypsin (0.05%)/EDTA (0.04 g/l) PBS. Digest the islets briefly at 37 °C for 90 s for human islets and 60 s for mouse islets. Pipette up and down to mechanically loosen the islet structure until it appears that 70–80% of islets are dispersed. When the islets are dispersed, add 1 ml of PBS to dilute the trypsin (*see* **Note 5**).
2. Pass the partially intact islets through a 40-μm nylon mesh cell sieve into a new 35 × 10-mm polystyrene nontreated tissue culture dish, and using the rubber end of a 1-ml syringe plunger, gently rub any partially intact islets into the nylon mesh until all islet clumps disappear to create an islet single-cell suspension. Transfer the dissociated islet cell suspension to a new 1.5-ml tube and wash the suspension with PBS once, aspirate the supernatant, and resuspend the cells in 1 ml of PBS. Place the islet cell suspension on ice.

   Note: If mouse spleens or lymph nodes were collected for single-color and positive flow cytometry controls, resume the protocol at Subheading 3.3, **step 3**. Otherwise, proceed to Subheading 3.4.
3. To create a splenic or lymph node cell suspension, use a 70-μm cell sieve, a small Petri dish, and a syringe plunger to gently disrupt the organ and release leukocytes. Collect the cell suspension from the Petri dish and pellet the cells by centrifugation (400 × *g*, 4 °C, 5 min). Discard the supernatant with a pipette.
4. If a spleen was used to create the cell suspension, add 2 ml of 1× RBC lysis buffer to the suspension and vortex briefly to resuspend the pellet. Incubate the suspension for 5 min at room temperature. Proceed to Subheading 3.3, **step 5**.

If a lymph node was used to create the cell suspension, gently pellet the cells via centrifugation (400 × *g*, 4 °C, 5 min) and resuspend the cells in 1 ml of PBS. Place the suspension on ice and resume the protocol at Subheading 3.4.

5. Wash the suspension twice with PBS and resuspend the pellet in 1 ml of PBS. Place the splenic cell suspension on ice and resume the protocol at Subheading 3.4.

### 3.4 Cell Counts

1. Pipette or gently vortex the cell suspensions to ensure that they are homogenous.
2. Collect a 10- to 20-μl aliquot of each sample and determine the approximate number of viable leukocytes using trypan blue and a hemocytometer or an automated cell counter that is capable of distinguishing between leukocytes and stromal cells.
3. Calculate the approximate number of leukocytes present in the suspension.
4. Centrifuge cells (400 × *g*, 4 °C, 5 min) and decant the supernatant. Resuspend the pellets in an appropriate volume of PBS and transfer approximately $1 \times 10^6$ cells to labeled FACS tubes.

   For a successful flow cytometry experiment, single-color controls, positive and negative splenic/lymph node controls, nonstained islet, isotype islet controls, and experimental islet tubes are necessary (*see* **Notes 6–8** and Fig. 2).
5. Add 1 ml of PBS to each tube and pellet the cells (400 × *g*, 4 °C, 5 min, and aspirate the supernatant). Proceed to Subheading 3.5.

### 3.5 Extracellular Flow Cytometry Staining

1. Resuspend the pelleted cells (Subheading 3.4, **step 5**) in 50 μl of Fc block-PBS (0.25–1.0 μg/ml human or mouse Fc blocking antibodies in 1× PBS).
2. Incubate for 10–15 min at 4 °C to block extracellular Fc receptors and nonspecific antibody recognition. Prepare the extracellular antibody cocktails (50 μl/tube) using appropriate flow cytometry antibodies and Fc block-PBS (*see* **Note 6**).
3. Add 50 μl of the extracellular antibody cocktail to the corresponding FACS tube(s). Gently vortex to mix and incubate the samples for 20–30 min in the dark at 4 °C to stain for extracellular antigens.
4. Add 1 ml PBS to each tube to wash the cells.
5. Gently pellet the cells and decant the supernatant (400 × *g*, 4 °C, 5 min).
6. Repeat **steps 4** and **5**.
7. To additionally stain for intracellular antigens, proceed to Subheading 3.5. Otherwise proceed to Subheading 3.5, **step 8**.

8. Gently resuspend the pelleted cells in 100 μl of 2% paraformaldehyde in PBS. The tubes may be stored at 4 °C in the dark or immediately analyzed on the flow cytometer.

### 3.6 Intracellular Staining

1. Very gently resuspend the pelleted cells (Subheading 3.5, **step 6**) in 100–200 μl of a suitable fixation/permeabilization reagent (i.e., BD Cytofix/Cytoperm), following the manufacturer's instructions for preparation and use (*see* **Note 9**).

   The rest of the protocol assumes that BD Cytofix/Cytoperm reagents were used to fix and permeabilize the cells. If other intracellular staining reagents were used, the intracellular staining protocol should be modified following the manufacturer's instructions.
2. Incubate the samples for 20–30 min at 4 °C in the dark to permeabilize the cells. Intracellular antibody cocktails (100 μl/tube) should be prepared using BD permeabilization/wash solution. The appropriate amount of intracellular antibody to use for one test should be empirically determined (*see* **Note 6**).
3. Add 1 ml of BD permeabilization/wash solution to each tube and pellet the cells by centrifugation (400 × *g*, 4 °C, 5 min). Discard the supernatant.
4. Gently resuspend the samples in 100 μl of the correct intracellular antibody cocktail. Incubate the samples for 20–30 min at 4 °C in the dark to stain for intracellular antigens.
5. Add 1 ml of 1× permeabilization/wash solution to each tube to wash the cells.
6. Gently pellet the cells and decant the supernatant (400 × *g*, 4 °C, 5 min).
7. Repeat **steps 4** and **5**.
8. Gently resuspend the pelleted cells in 100 μl of 2% paraformaldehyde in PBS. The tubes may be stored at 4 °C in the dark or immediately analyzed on the flow cytometer.

### 3.7 Sample Acquisition on the Flow Cytometer

1. Start and set up the flow cytometer and instrument settings according to manufacturer's instructions and in-house protocols. The islet samples should be filtered using a 70-μm cell strainer cap just before the sample acquisition.
2. The splenic unstained and single-color control samples should be used to set and adjust the gain values on the forward (FSC) scatter, side (SSC) scatter, and fluorescent channels. Ideal single-color controls should have a clearly defined positive and negative population. Once the acquisition settings have been finalized, the positive control, negative control, and experimental samples can be acquired.

3. In order to analyze the maximum number of cells in the sample tube, when the sample volume reaches the lower limit of the sample injection port (SIP), the tube can be washed with a small volume of sheath fluid to acquire the rest of the specimen.

### 3.8 Analysis

1. Using an appropriate flow cytometry data analysis program (such as FlowJo), setup and define a compensation matrix using the single-color controls. Once the compensation matrix is complete, apply the matrix to the experimental samples.
2. For islet samples, CD45 should be used to distinguish between endocrine cells and infiltrating leukocytes. In addition, cellular debris and events that are smaller than ~30K on the FSC axis or larger than 250K on the SSC axis may be excluded from the analysis (Fig. 1). Finally, doublets and cellular aggregates should be excluded from the analysis as well, based on FSC/FSC-A (Fig. 1) or FSC/FSC-W parameters. As many as possible cells should be collected. Subsets of single $CD45^+$ $FSC^+$ gated leukocytes can be distinguished using additional markers (Fig. 2).
3. Critically, as islet-infiltrating leukocytes are relatively low in abundance, and islet endocrine cells are highly autofluorescent in comparison to islet leukocytes, nonstained islets, isotype control islets, and fluorescence minus one control islets are necessary to determine the correct placement of the gates (Figs. 1 and 2).
4. If a cell viability dye was used, the experimental islet sample should be compared with a viability dye positive control islet sample to correctly distinguish between live and dead cells.

## 4 Notes

1. We have primarily used human islets obtained through the Integrated Islet Distribution Program (IIDP, http://iidp.coh.org/), which provides human pancreatic islets for research to preapproved investigators. Further information regarding the standard procedures and policies is available online at http://iidp.coh.org/. In our experience, human islets within 3 days of the isolation produce a better quality single-cell suspension in comparison to the suspensions of islets that were isolated 3 or more days prior. Typically, human islets were cultured at the isolation centers for 1–2 days and then shipped overnight in CMRL-1066 medium supplemented with 10% FBS and 1% penicillin–streptomycin at 10–20 °C. Of note, there have been changes in the shipping protocol utilized by the IIDP recently and we have not performed flow cytometry using islets shipped under the new protocol. Human islets with a purity

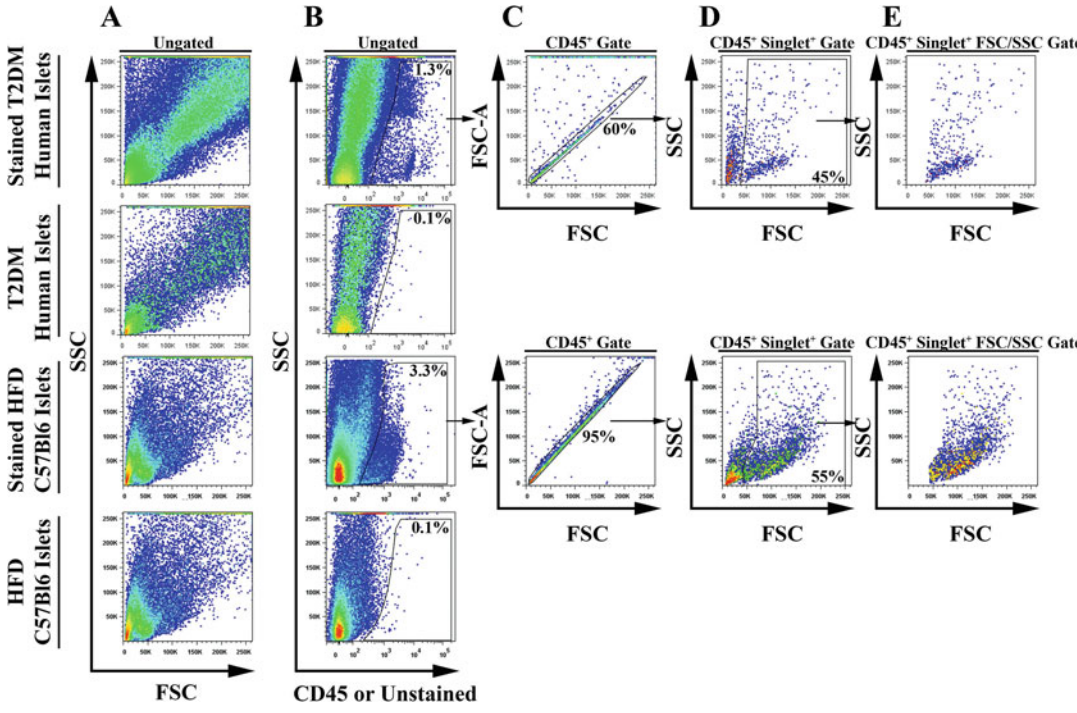


**Fig. 1** Recommended gating scheme for human and murine islet-infiltrating leukocytes. As multiple cell types are present within pancreatic islets, including alpha, beta, delta, PP cells, and leukocytes, the initial forward scatter (FSC) and side scatter (SSC) settings should be set based on a tissue or specimen with clear leukocyte populations, such as peripheral blood leukocytes, splenocytes, or lymphocytes (not shown). As shown in the figure, the initial ungated islet cell forward and side scatter profile will have various cell populations that are dispersed throughout the graph (far left column, **a**). To specifically examine leukocytes within the islet suspension, CD45, the common leukocyte marker, can be used (**b**)—second column first and third rows: CD45 staining, second and fourth rows: nonstained control). As large granular endocrine cells are more autofluorescent than leukocytes, islet CD45 staining should be compared with an islet isotype control for each specimen to place the initial CD45 gate (second column, empty channel). After the CD45 gate has been set, aggregates of cells should be excluded from the analysis using FSC/FSC-A (**c**) or FSC/FSC-W (not shown) plots. Once single $CD45^+$ leukocytes have been gated, a forward versus side scatter should be placed to exclude debris that are under 40K on the FSC axis and any events that are larger than 250K on the side scatter axis ((**d**)—fourth column). Single $CD45^+$ cells ((**e**)—shown in the fifth column) can be used for subsequent leukocyte subset, phenotype, and activation analyses. Note: a cell viability dye can also be used to specifically gate on viable islet-infiltrating leukocytes (not shown). To correctly distinguish between dead cells and viable cells, an appropriate islet-positive control should be used. *HFD* High-fat diet, *CD* Show diet, *T2DM* Type 2 diabetes mellitus, *Non-DM* Nondiabetic, *FSC* Forward scatter, *SSC* Side scatter, and *FSC-A* Forward scatter-area

and viability above 80% were suitable for flow cytometry experiments [17].

2. We typically use 5000–7000 islet equivalents (IEQ) of human islets culture in 5–10 ml of medium for a single flow cytometry assay. Human islets of variable diameters are converted to IEQ based on their diameter following a conversion table [18]. One

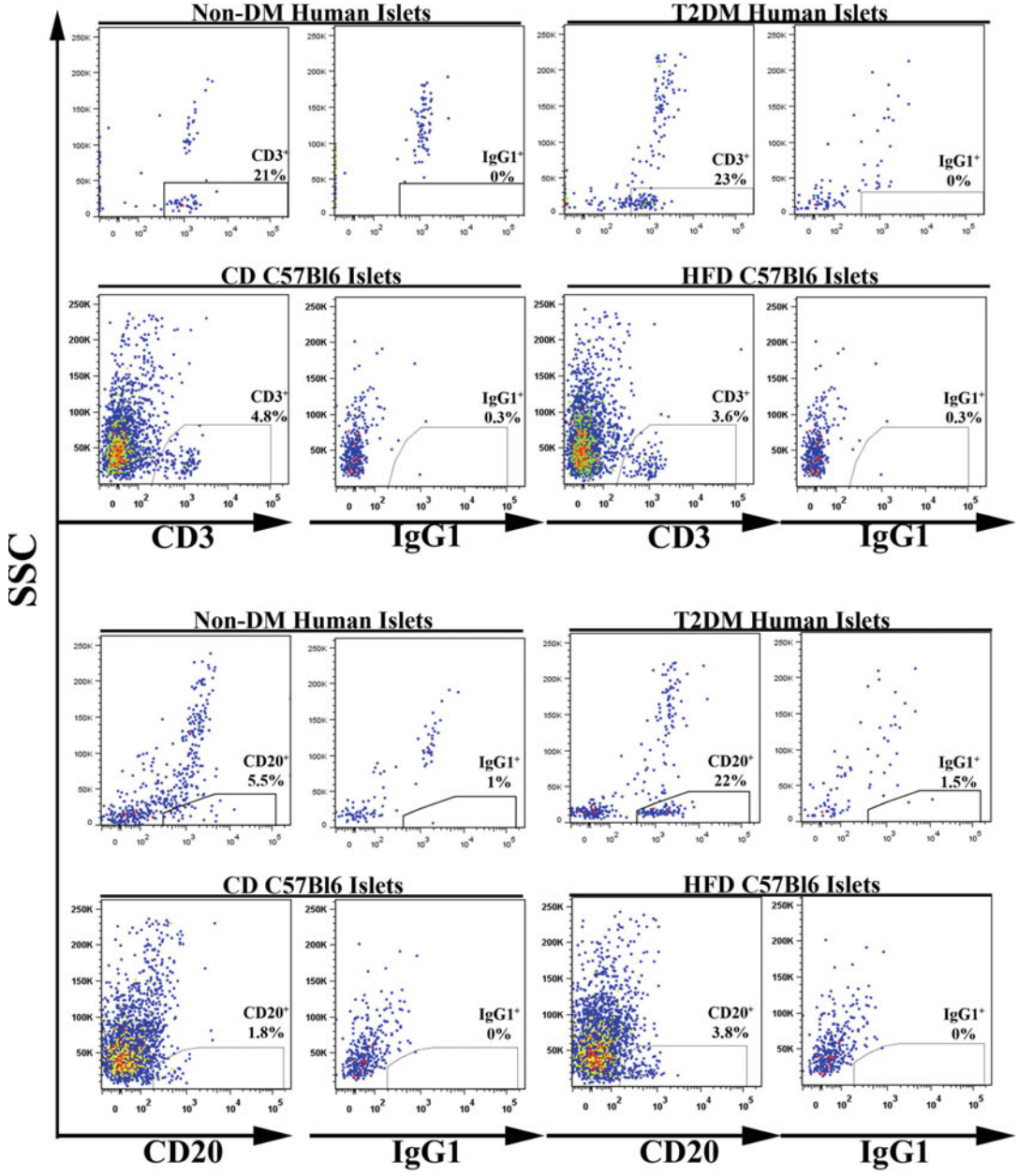


**Fig. 2** Representative $CD3^+$ T-cell and $CD20^+$ B-cell staining within nondiabetic and type 2 diabetic human and murine islets. To examine intraislet $CD3^+$ T-cell and $CD20^+$ B-cell content, single $CD45^+$ islet leukocytes were gated as described in Fig. 1 and analyzed for CD3 (top) and CD20 (bottom) staining. Nondiabetic and type 2 diabetic human islets (first and third rows) and their corresponding isotype controls are shown. In addition, chow diet fed and high-fat western diet fed C57Bl6 islets (second and fourth rows) and their corresponding isotype controls are also shown. Islet isotype controls are useful and recommended for initially placing the gates as nonspecific staining or high autofluorescence can be a confounding factor when analyzing non-lymphoid cell suspensions by flow cytometry

IEQ corresponds to an islet volume equivalent to that of diameter at 150 μm [18].

3. Upon and after trypsinization of the human and mouse islets, we found it ideal to use low-retention pipette tips such as TipOne Repel-Polymer Technology (USA Scientific, Ocala, FL) to reduce islet and cell loss due to islets sticking to the sides of the tips.
4. The optimum incubation time for the collagenase digestion period may differ depending on the enzymatic activity of the collagenase lot preparation and will need to be determined empirically.
5. It is important to avoid overdigesting the pancreatic tissue at this stage. Ideally, the pancreatic tissue should be mechanically disrupted by gently inverting the tube three or four times, or until the entire solution looks homogenous. Overdigestion (both enzymatic and/or mechanical) will break the islets.
6. The recommended flow cytometry test volumes found in commercial technical data sheets are typically standardized to 100 μl test volumes/$1 \times 10^6$ cells/tube. The optimal volume of antibody to use per test (100 μl test volumes/$1 \times 10^6$ cells/tube) should be empirically determined by the experimenter through titration curve experiments. The number of cells and the volume of antibody used in the experiment can be scaled up or down as desired. As islet leukocytes are relatively low in abundance, our group recommends scaling up the number of islet cells used in the experimental panel if enough islets are available. 1–2 $\times$ $10^6$ cells are sufficient to study major leukocyte populations of interest and additional IEQ are recommended to study leukocyte subsets (i.e., T helper cell subsets, B-cell subsets, macrophage subsets, etc.).
7. As islet-infiltrating leukocytes are relatively low in abundance, and islet endocrine cells are comparatively autofluorescent, running positive and negative controls (nonstained samples, isotype, and fluorescence minus one controls) on splenocytes or lymph nodes are recommended, in addition to negative islet controls. A successful flow cytometry experiment should have the following controls:
   (a) Unstained splenic or lymph node cell suspensions.
   (b) Unstained islet cell suspension.
   (c) Single-color controls prepared using splenocytes or lymph nodes. There should be one separate single-color control tube for each fluorophore-conjugated antibody that will be used in the experimental cocktail.
   (d) Fluorescent minus one (FMO) controls prepared using splenocytes or islet cell suspension if enough sample is available.

(e) Separate isotype controls prepared using splenocytes and islet cell suspensions.

Isotype controls should contain all of antibodies present in the experimental cocktail aside from one marker, which is replaced by an equivalent amount of a nonspecific antibody conjugated with the correct fluorophore. For example, if an experimental panel comprised CD45-PerCP, CD20-Pacific Blue, and CD3-APC, an appropriate isotype control panel for CD20 would include CD45-PerCP, the recommended isotype control for the CD20 antibody (e.g., IgG1-Pacific Blue), and CD3-APC.

8. Human and mouse endocrine cells, which are larger and more granular, are autofluorescent in comparison to islet leukocytes. We highly recommend running unstained and isotype controls with portions of the islet cell suspension.
9. Commercial intracellular staining kits typically contain a fixative as well as a mild detergent (e.g., saponin) in order to permeabilize the cells and allow the antibodies to access intracellular antigens. However, the cells become fragile when they are permeabilized. The cells should therefore be carefully handled and resuspended gently throughout the intracellular staining protocol.

## Acknowledgments

We thank the Eastern Virginia Medical School Flow Cytometry core facility for their excellent technical support. The human islets were provided by the Integrated Islet Distribution Program (IIDP). This work was supported by the National Institutes of Health grants RO1-DK090490 (Y.I.), the IIDP pilot program (Y.I.), a BD Biosciences research grant (E.G.), and Eastern Virginia Medical School pilot grant (Y.I. and E.G.).

### References

1. Osborn O, Olefsky JM (2012) The cellular and signaling networks linking the immune system and metabolism in disease. Nat Med 18 (3):363–374
2. Imai Y, Dobrian AD, Morris MA, Nadler JL (2013) Islet inflammation: a unifying target for diabetes treatment? Trends Endocrinol Metab 24(7):351–360
3. Jagannathan-Bogdan M, McDonnell ME, Shin H, Rehman Q, Hasturk H, Apovian CM, Nikolajczyk BS (2011) Elevated proinflammatory cytokine production by a skewed T cell compartment requires monocytes and promotes inflammation in type 2 diabetes. J Immunol 186(2):1162–1172
4. Zeng C, Shi X, Zhang B, Liu H, Zhang L, Ding W, Zhao Y (2012) The imbalance of Th17/Th1/Tregs in patients with type 2 diabetes: relationship with metabolic factors and complications. J Mol Med (Berl) 90 (2):175–186
5. Jagannathan M, McDonnell M, Liang Y, Hasturk H, Hetzel J, Rubin D, Kantarci A, Van Dyke TE, Ganley-Leal LM, Nikolajczyk BS (2010) Toll-like receptors regulate B cell

cytokine production in patients with diabetes. Diabetologia 53(7):1461–1471

6. Ehses JA, Perren A, Eppler E, Ribaux P, Pospisilik JA, Maor-Cahn R, Gueripel X, Ellingsgaard H, Schneider MK, Biollaz G, Fontana A, Reinecke M, Homo-Delarche F, Donath MY (2007) Increased number of islet-associated macrophages in type 2 diabetes. Diabetes 56(9):2356–2370
7. Richardson AJ, Willcox A, Bone AJ, Foulis AK, Morgan NG (2009) Islet-associated macrophages in type 2 diabetes. Diabetologia 51:1686–1688
8. Brissova M, Fowler MJ, Nicholson WE, Chu A, Hirshberg B, Harlan DM, Powers AC (2005) Assessment of human pancreatic islet architecture and composition by laser scanning confocal microscopy. J Histochem Cytochem 53 (9):1087–1097
9. Cabera O, Berman DM, Kenyon NS, Ricordi C, Berggren PO, Caicedo A (2006) The unique cytoarchitecture of human pancreatic islets has implications for islet cell function. Proc Natl Acad Sci U S A 103:2334–2339
10. MacDonald MJ, Longacre MJ, Stoker SW, Kendrick M, Thonpho A, Brown LJ, Hasan NM, Jitrapakdee S, Fukao T, Hanson MS, Fernandez LA, Odorico J (2011) Differences between human and rodent pancreatic islets: low pyruvate carboxylase, ATP citrate lyase, and pyruvate carboxylation and high glucose-stimulated acetoacetate in human pancreatic islets. J Biol Chem 286(21):18383–18396
11. Beare A, Stockinger H, Zola H, Nicholson I (2008) Monoclonal antibodies to human cell surface antigens. Curr Protoc Immunol 4:4A
12. Dorrell C, Abraham SL, Lanxon-Cookson KM, Canaday PS, Streeter PR, Grompe M (2008) Isolation of major pancreatic cell types and long-term culture-initiating cells using novel human surface markers. Stem Cell Res 1 (3):183–194
13. Pechhold K, Zhu X, Harrison VS, Lee J, Chakrabarty S, Koczwara K, Gavrilova O, Harlan DM (2009) Dynamic changes in pancreatic endocrine cell abundance, distribution, and function in antigen-induced and spontaneous autoimmune diabetes. Diabetes 58 (5):1175–1184
14. Nackiewicz D, Dan M, He W, Rosa K, Salmi A, Rutti S, Westwell-Roper C, Cunningham A, Speck M, Shuster-Klein C, Guardiola B, Maedler K, Ehses JA (2014) TLR2/6 and TLR4 activated macrophages contribute to islet inflammation and impair beta cell-insulin gene expression via IL-1 and IL-6. Diabetologia 57:1645–1654
15. Westwell-Roper CY, Ehses JA, Verchere CB (2013) Resident macrophages mediate islet amyloid polypeptide-induced islet IL-1beta production and beta cell dysfunction. Diabetes 63(5):1698–1711
16. Yin N, Xu J, Ginhoux F, Randolph GJ, Merad M, Ding Y, Bromberg JS (2012) Functional specialization of islet dendritic cell subsets. J Immunol 188(10):4921–4930
17. Butcher MJ, Hallinger D, Garcia E, Machida Y, Chakrabarti S, Nadler J, Galkina EV, Imai Y (2014) Association of proinflammatory cytokines and islet resident leucocytes with islet dysfunction in type 2 diabetes. Diabetologia 57(3):491–501
18. Ricordi C (1991) Quantitative and qualitative standards for islet isolation assessment in humans and large mammals. Pancreas 6 (2):242–244

# Chapter 11

# Analysis of Histone Modifications in Rodent Pancreatic Islets by Native Chromatin Immunoprecipitation

**Ionel Sandovici, Lisa M. Nicholas, and Laura P. O'Neill**

## Abstract

The islets of Langerhans are clusters of cells dispersed throughout the pancreas that produce several hormones essential for controlling a variety of metabolic processes, including glucose homeostasis and lipid metabolism. Studying the transcriptional control of pancreatic islet cells has important implications for understanding the mechanisms that control their normal development, as well as the pathogenesis of metabolic diseases such as diabetes. Histones represent the main protein components of the chromatin and undergo diverse covalent modifications that are very important for gene regulation. Here we describe the isolation of pancreatic islets from rodents and subsequently outline the methods used to immunoprecipitate and analyze the native chromatin obtained from these cells.

**Key words** Islets of Langerhans, Histone modifications, Nucleosomes, Native chromatin immunoprecipitation (NChIP), Antibodies

## 1 Introduction

The islets of Langerhans represent the endocrine component of the pancreas and comprise only 1–2% of the volume of the whole organ. They are composed of several types of hormone-secreting cells including alpha cells (glucagon), beta cells (insulin and amylin), delta cells (somatostatin), PP cells (pancreatic polypeptide), and epsilon cells (ghrelin), as well as an intricate network of blood vessels, which enable the direct release of these hormones into the bloodstream. In rodents, endocrine cells are first specified around embryonic day 15.5 (E15.5) and, upon their migration, they form the first islets of Langerhans between E16.5 and birth [1]. In adult rodents beta cells constitute the major endocrine cell type (65–80%) and are generally centrally located in the pancreatic islets, being surrounded by the other cell types.

There are several methods used for isolation of islets of Langerhans from adult rodents. Most of these techniques rely on digestion of the whole pancreas with collagenase injected into the

Claire J. Stocker (ed.), *Type 2 Diabetes: Methods and Protocols*, Methods in Molecular Biology, vol. 2076,
https://doi.org/10.1007/978-1-4939-9882-1_11, 

common bile duct, the splenic vein, or after pancreas fragmentation. This step is then followed by separation of pancreatic islets using gradient density solutions and manual picking of individual pancreatic islets [2–4].

Epigenetic mechanisms, such as DNA modifications and post-translational histone modifications (methylation, acetylation, phosphorylation, ubiquitination) play important roles during the development of the pancreas, as well as in the maintenance of cellular differentiation states and the normal functioning of adult pancreatic endocrine cells [5]. Epigenetic alterations induced by environmental exposures during early development or throughout the lifetime are currently thought to play important roles in pancreatic islets dysfunction and subsequently in the growing incidence of type 2 diabetes [6, 7].

Chromatin immunoprecipitation (ChIP) is a type of immunoprecipitation that is often used for characterization of covalent histone modifications. There are two main types of ChIP: cross-linked ChIP (XChIP), which uses as starting material reversibly cross-linked chromatin sheared by sonication and native ChIP (NChIP), which instead uses chromatin sheared by micrococcal nuclease digestion. NChIP is the method of choice when histone modifications are studied [8, 9]. The major advantage of NChIP over XChIP is antibody specificity. This is because most antibodies used for recognizing specific histone modifications are raised against unfixed, synthetic peptides that bear the target covalent modification. These epitopes can be disrupted or even destroyed by formaldehyde cross-linking, particularly as the cross-links are likely to involve lysine amino groups which are often the sites for many histone modifications. This phenomenon also explains the consistently lower efficiency of XChIP protocols compared to NChIP [8, 9].

In this chapter, we will first describe the isolation of pancreatic islets from adult mice and rats and then outline the NChIP protocol that can be used for analysis of specific posttranslational histone modifications. Characterization of histone modifications in pancreatic islets collected from fetuses or from neonatal rodents requires alternative protocols, such as carrier ChIP [10].

## 2 Materials

Prepare all solutions fresh using nuclease-free water and molecular biology-grade reagents (unless indicated otherwise). Some solutions can be stored for a short time at 4 °C (specified below). Housing, breeding, and killing of rodents should be performed in accordance with the local institutional Scientific Procedures act.

### 2.1 Instruments and Reagents Required for Pancreatic Islets Isolation

1. $CO_2$ gas chamber for euthanasia.
2. Surgical board, dissection microscope, and light source.
3. Dissection scissors, blunt forceps, and metallic clamps.
4. Ethanol.
5. 18 G (gauge), 25 G, 27 G, and 30 G needles.
6. 1 ml, 5 ml, and 10 ml syringes.
7. 15 ml and 50 ml Falcon tubes.
8. Disposable pipettes (5 ml, 10 ml, and 25 ml) and pipette aid.
9. Water bath at 37 °C.
10. Bench-top centrifuge with a swing-out bucket rotor for 50 ml polypropylene tubes and microcentrifuge with cooling system for 1.5 ml tubes.
11. HBSS buffer.
12. Collagenase P (Sigma Aldrich, 11213865001).
13. Histopaque 1119 (Sigma Aldrich, 11191) and Histopaque 1077 (Sigma Aldrich, 10771).
14. Sterile Petri dishes.
15. Liquid $N_2$ and liquid $N_2$ container.

### 2.2 Instruments and Reagents Required for NChIP

1. Magnetic stirrers.
2. Glass dounce homogenizers/disruptors.
3. 15 ml and 50 ml Falcon tubes.
4. Sigmacote (Sigma Aldrich) (for siliconizing Eppendorf and Falcon tubes).
5. Rotating wheels at 4 °C and room temperature.
6. Dialysis tubing (0.5 mm thick, 10 kDa pore width).
7. Disposable pipettes (5 ml, 10 ml, and 25 ml) and pipette aid.
8. 10 μl, 100 μl, and 1000 μl pipettor and filtered tips.
9. Phosphate-buffered saline (PBS).
10. Sodium butyrate (for analyzing histone acetylation only).
11. Phenylmethanesulfonyl fluoride (PMSF).
12. Tween 40.
13. Protease inhibitors cocktail (Sigma Aldrich, 11697498001).
14. Micrococcal nuclease (MNase; 100 units/μl in 10 mM Tris–HCl pH 7.5, 50 mM NaCl, 1 mM EDTA, 50% (v/v) glycerol).
15. Affinity-purified antibodies, ChIP-grade, e.g., rabbit polyclonal anti-H3K27ac, rabbit polyclonal anti-H3K27me3, rabbit polyclonal anti-H3K4me1, rabbit polyclonal anti-

H3K4me3, rabbit polyclonal anti-H3K9me3 (Diagenode is preferred).

16. DiaMag protein A-coated magnetic beads (Diagenode is preferred).
17. Magnetic rack for 1.5 ml Eppendorf tubes.
18. Horizontal electrophoresis system for agarose gels.
19. Gel Doc 2000 gel documentation system (Bio-Rad provides an excellent set of equipment).
20. Agarose.
21. Ethidium bromide solution (20 mg/ml).
22. 100 bp DNA size ladder.
23. NanoDrop spectrophotometer.
24. Other chemicals: $MgCl_2$, $CaCl_2$, Tris, boric acid, EDTA, SDS, sucrose—all molecular grade.

### 2.3 Instruments and Reagents Required for DNA Isolation and Downstream Analysis by Quantitative PCR (qPCR)

1. Proteinase K (Melford Laboratories is preferred).
2. Thermomixer shaker.
3. Phenol:chloroform:isoamyl alcohol 25:24:1 (v:v:v).
4. Chloroform.
5. 2 ml Phase Lock gel tubes.
6. 3 M sodium acetate, pH 5.2.
7. Absolute ethanol.
8. Glycogen solution 20 mg/ml, molecular grade.
9. 10 mM Tris–Cl, pH 7.5.
10. Qubit® 3.0 Fluorometer.
11. Qubit® dsDNA HS assay (Life Technologies is a recommended choice).
12. Locus-specific primers (Sigma Aldrich is an excellent recommended supplier).
13. SYBR-Green master mix.
14. QuantStudio6Flex system (Life Technologies) or equivalent (compatible for SYBR-Green-based quantitative PCR).

## 3 Methods

### 3.1 Isolation of Pancreatic Islets from Adult Mice or Rats (Fig. 1)

1. Prepare fresh collagenase P solution in HBSS (at a concentration of 4 mg/ml) and place on ice (*see* **Note 1**). Prepare 3 ml and 10 ml solution for each adult mouse and rat, respectively.
2. Adult mice or rats should be euthanized using a $CO_2$ chamber following institutionally approved instructions. The rodent is

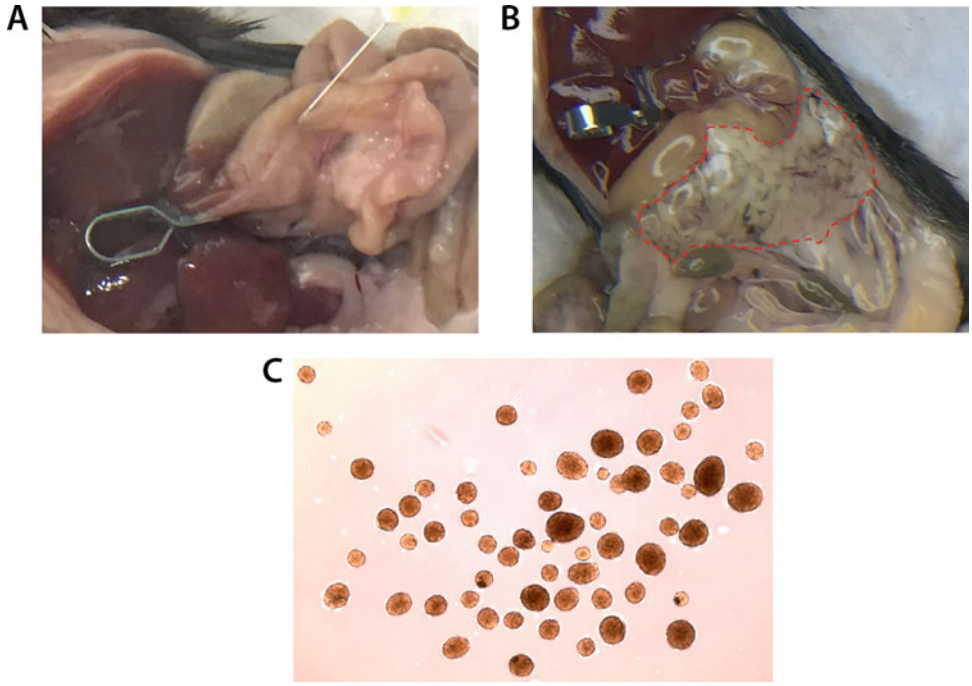


**Fig. 1** Isolation of pancreatic islets from mature mice. (**a**) The metallic clamp is first placed on the common biliary duct near liver, and then the collagenase P solution is slowly injected into the duct under a microscope. (**b**) The red dotted line indicates the fully inflated pancreas at the end of the collagenase injection. (**c**) Isolated mouse pancreatic islets

ready for exsanguination after no response to pinching its foot. Exsanguination is performed by heart puncture using 1 ml syringes fitted with 25 G needles (for mouse) or 5 ml syringes fitted with 18 G needles (for rat).

3. Wet the abdominal fur with 70% ethanol to reduce the chance of hair contamination in the intraperitoneal cavity during subsequent steps. Open the abdomen with a cross-like incision, in order to expose all the organs within the peritoneal cavity. Place the animal with the head toward the surgeon and the tail away. This allows easier clamping of the common bile duct near the liver, using metallic clamps. Additional clamping of the duodenum on each side of the junction with the common biliary duct is optional but desirable, as it avoids leakage of the collagenase solution into the gut.
4. Under the microscope, cannulate the common bile duct immediately downstream the junction between the cystic duct and the left hepatic duct, using a 27 G (rat) or 30 G (mouse) needle. Slowly inject the entire volume of collagenase P solution, until the pancreas is completely inflated (*see* **Note 2**).

5. Using dissection scissors, remove the pancreas, by carefully detaching it from the duodenum, jejunum, the greater curvature of the stomach, and finally the spleen. Then, place the dissected pancreas in a 50-ml Falcon tube containing 1 ml cold HBSS and immediately place on ice.
6. Repeat the above steps for each rodent (we recommend maximum four rodents for one collection), and then place all the Falcon tubes in a water bath prewarmed at 37 °C for 20 min (*see* **Note 3**).
7. After incubation, add 10–15 ml ice-cold HBSS to each Falcon tube to stop the digestion. Place the Falcon tubes in a rack and shake them hard by hand for approximately 1 min to complement the enzymatic digestion of the pancreas with mechanical dissociation of the tissue fragments (the solution should now have the consistency of a pea soup and should be free of large, undigested pancreatic fragments).
8. Place the Falcon tubes in a prechilled centrifuge (4 °C) and spin for 1 min at 200 × *g*. Then, carefully remove and discard the supernatant using a pipette. Wash the pellets with 10 ml ice-cold HBSS, shake the tubes for 1 min, and centrifuge as above (repeat for a total of three washes).
9. After the third wash, resuspend the pellet in 10 ml cold HBSS using a pipette and pass the mixture through a strainer (0.5 mm metallic mesh) into a new 50-ml Falcon tube and wash one more time with HBSS as above.
10. Subsequently resuspend the pellet in 5 ml ice-cold Histopaque 1119 (by pipetting until homogeneous), then carefully layer on top 8 ml ice-cold Histopaque 1077, followed by another 8 ml of ice-cold HBSS (the three layers should not mix).
11. Carefully place the Falcon tubes in the centrifuge and spin at 1065 × *g* and 4 °C for 25 min. At the end of the centrifugation, the islets should be visible as rounded white specs at the interface between the Histopaque 1077 and HBSS layers (*see* **Note 4**).
12. Carefully aspirate the islets and place them on ice in Petri dishes containing HBSS. Under an optic microscope, wash the islets several times with HBSS to remove any traces of Histopaque, as well as to minimize any contamination with small fragments of exocrine pancreas. Then, count the islets, hand pick them with a pipette, and place them in 1.5 ml microcentrifuge tubes (*see* **Note 5**). Pellet the islets by centrifugation for 3 min at 200 × *g* and 4 °C, carefully remove the HBSS, wash three times in ice-cold PBS, snap-freeze the tubes in a liquid $N_2$ container, and store them at −80 °C until used for NChIP.

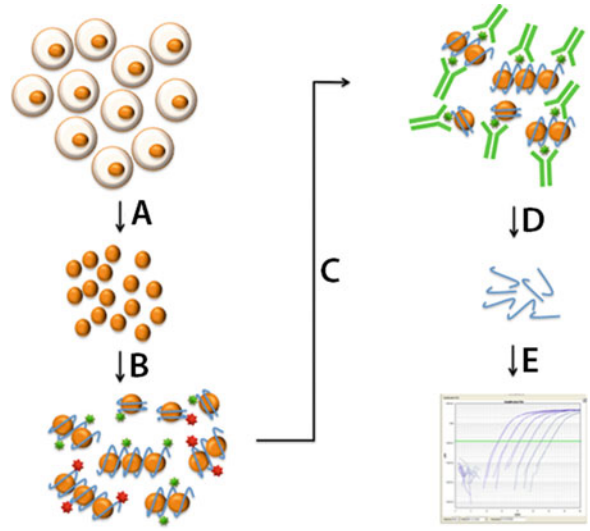


**Fig. 2** Diagram depicting the principle of NChIP. (**a**) Isolation of nuclei. (**b**) Chromatin digestion. (**c**) Immunoprecipitation with an antibody that recognizes a specific chromatin modification (green star). (**d**) DNA purification. (**e**) Analysis by quantitative PCR

### *3.2 Isolation of Chromatin from Pancreatic Islets (Fig. 2)*

1. Isolation of nuclei. Approximately 1000 pancreatic islets snap frozen at collection and stored at −80 °C (i.e., islets collected from ~4 adult mice or 2 rats) are placed in a 7-ml all-glass homogenizer (kept on ice) containing 2.5 ml ice-cold 1× TBS (10 mM Tris–HCl pH 7.5, 150 mM NaCl, 3 mM $CaCl_2$, 2 mM $MgCl_2$, 5 mM Na butyrate pH 8.0) and supplemented with protease inhibitors (1 pellet mini inhibitor per 20 ml) (*see* **Note 6**). Then, add an equal volume of 1.0% v/v Tween 40 in 1× TBS and supplement with PMSF to a final concentration of 0.5 mM (*see* **Note 7**).
2. Incubate on ice for a total of 30 min. After the first 10 min, apply 10 strokes using the loose fitting pestle, then after another 10 min, apply again 10 strokes with the tight fitting pestle (*see* **Note 8**).
3. The cell lysates are then transferred to 15-ml Falcon tubes, which are spun at 10,000 × *g* and 4 °C for 20 min and the supernatants are discarded. The nuclei pellets are then resuspended in 5 ml 25% [w/v] sucrose/1× TBS and the suspension is underlayed with 2.5 ml of 50% [w/v] sucrose/1× TBS. Spin the tubes for 25 min at 14,000 × *g* and 4 °C.
4. Discard the supernatants and wash the nuclei pellets in 5 ml 25% [w/v] sucrose/1× TBS. Centrifuge again the tubes for 25 min at 14,000 × *g* and 4 °C (*see* **Note 9**).
5. Resuspend the nuclei in 0.5 ml digestion buffer (0.32 M sucrose, 4 mM $MgCl_2$, 1 mM $CaCl_2$, 50 mM Tris–HCl,

pH 7.5, 0.1 mM PMSF, 5 mM Na butyrate, and protease inhibitors) in 1.7 ml Eppendorf tubes.

6. A small aliquot of 5 μl nuclei is then mixed with 5 μl digestion buffer supplemented with 0.2% SDS and is then used for checking the amount of chromatin with a NanoDrop spectrophotometer. Tubes are then centrifuged at 10,000 × *g* and 4 °C for 10 min and the nuclei resuspended in digestion buffer at a final concentration of 50 μg/ml (*see* **Note 10**).
7. Digestion of chromatin: The conditions used for chromatin digestion with micrococcal nuclease (MNase) should be determined empirically. We usually obtain good results with 5 min digestion at 37 °C using 5 UI MNase per 50 μg chromatin. These conditions give us a chromatin ladder rich in mono-, di-, tri-, tetra-, and penta-nucleosomes. However, if a more detailed map of histone marks is required, this step can be extended to 7 min, which normally increases the yield of mono- and di-nucleosomes in the final preparation (*see* **Note 11**).
8. At the end of the previous step, the MNase digestion is stopped by adding 0.5 M EDTA solution, to a final concentration of 5 mM, and placing the tubes on ice for 5 min. The tubes are then spun at 8000 × *g* and 4 °C for 5 min. The supernatant is placed in a new eppendorf tube (this is fraction S1 (mostly mono-nucleosomes), which is kept at 4 °C until the next day, when fraction S2 is obtained; the pellet is retained for dialysis.
9. Chromatin dialysis: This step requires special dialysis tubing (0.5 mm thick, 10 kDa pore width). Before use, the tubing is washed twice with distilled water (*see* **Note 12**).
10. The pellet obtained after fraction S1 is resuspended in 500 μl dialysis buffer (0.2 mM EDTA, 1 mM Tris–HCl pH 7.5, 0.2 mM PMSF, 5 mM Na butyrate and protease inhibitors).
11. The above mix is placed in the dialysis tubing and the ends are closed with plastic clamps. The tubing is submerged in 2 l of dialysis buffer and incubated overnight at 4 °C with constant slow stirring using a magnetic stirring bar.
12. The dialysate is placed in 1.7 ml eppendorf tubes and spun at 4 °C and 500 × *g* for 10 min. The supernatant represents fraction S2. The pellets are resuspended in 200 μl dialysis buffer (fraction S3).
13. Assessment of chromatin quality: Small aliquots (18 μl) of chromatin are removed from each fraction (S1, S2, and S3) and each sample is mixed with 2 μl of 1% [w/v] SDS (final concentration 0.1% SDS). After the mixtures are gently flicked and incubated at room temperature for 5 min (which will allow a good separation of the nucleosome DNA fragments from the

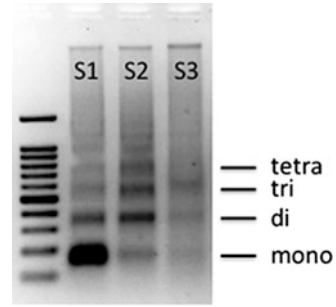


**Fig. 3** Analysis of native chromatin fractions isolated from pancreatic islets using agarose gel electrophoresis. Bands corresponding to chromatin fragments of one nucleosome (mono) to four nucleosomes (tetra) in length are indicated. The sizes of the chromatin fragments are verified against the 100 bp DNA ladder (Hyperladder IV—Bioline) loaded on the right side of the gel

histone proteins), their concentrations are measured with a NanoDrop spectrophotometer (two readings using 1 μl each).

14. The remaining 18 μl of each mixture receives 4 μl of 6× DNA loading buffer, then the samples are loaded onto a standard 1.2% agarose gel without ethidium bromide (*see* **Note 13**). The gel is run at 2–3 V/cm for about 3 h (this low voltage facilitates good separation of the DNA fragments). The gel is then stained with 0.5 μg/ml ethidium bromide and the sizes of the DNA fragments are observed under UV light. Typically, fraction S1 contains mostly mono-nucleosomes, S2 di- to penta-nucleosomes, and S3 mostly large fragments of undigested DNA (Fig. 3).

### 3.3 Chromatin Immunoprecipitation

1. Only fractions S1 and S2 are used for immunoprecipitation, mixed in equal amounts. We obtain good results with as little as 2 μg chromatin per IP (1 μg fraction S1 plus 1 μg fraction S2). Using this amount, we can perform 3–4 IPs/sample. An equal aliquot (2 μg) of chromatin should be stored at 4 °C (to be used as input fraction during qPCR quantification). The IPs are performed in siliconized eppendorf tubes and the total volumes are adjusted to 1 ml, using incubation buffer (5 mM EDTA, 20 mM Tris–HCL pH 7.5, 50 mM NaCl, 0.1 mM PMSF, 20 mM Na butyrate).
2. The amount of antibody required depends on manufacturer's recommendations (depending on the antibody, usually 1–2 μg is required for an IP on the equivalent chromatin isolated from 300,000 pancreatic islet cells). The use of affinity-purified ChIP-grade antibodies is recommended. At least one mock tube (containing an isogenic IgG serum that is not directed against chromatin proteins, for example, rabbit IgG antibody)

should be used in each experiment as negative control for unspecific binding (*see* **Note 14**).

3. Wrap the tubes in parafilm and incubate for 16 h (overnight) in the cold room (4 °C) on a rotator machine, at slow speed (20 rpm).
4. Next morning, 20 μl DiaMag protein A-coated magnetic beads are prepared for each immunoprecipitation (they are recommended when rabbit polyclonal antibodies are used, as well as mouse $IgG_{2a}$, $IgG_{2b}$, and IgA, guinea pig IgG, dog IgG, or pig IgG) (*see* **Note 15**). The beads are washed four times with 1 ml ice-cold incubation buffer (5 mM EDTA, 20 mM Tris–HCL pH 7.5, 50 mM NaCl, 0.1 mM PMSF, 20 mM Na butyrate) in 1.5 ml siliconized eppendorf tubes, using the magnetic rack to recover the beads after each wash. After the fourth wash, resuspend the beads in 20 μl incubation buffer.
5. Using siliconized pipette tips, 20 μl prewashed beads are added to each IP tube (including the mock tube) and the tubes are incubated at 4 °C on the rotator machine (20 rpm) for 4–6 h.
6. The three washing buffers (A, B, and C) are prepared and prechilled. The washing buffers have the same composition, except for increasing concentrations of NaCl: 50 mM Tris–HCl pH 7.5, 10 mM EDTA, 5 mM Na butyrate, 50 mM NaCl (wash A), 50 mM Tris–HCl pH 7.5, 10 mM EDTA, 5 mM Na butyrate, 100 mM NaCl (wash B), 50 mM Tris–HCl pH 7.5, 10 mM EDTA, 5 mM Na butyrate, 150 mM NaCl (wash C).
7. All washes are performed at 4 °C. After the incubation with DiaMag protein A-coated magnetic beads is over, the tubes are briefly spun, then placed on the magnetic rack for 1 min. The supernatants are discarded by aspiration, and the beads are resuspended in 1 ml wash A. Incubate the tubes on the rotating wheel for 5 min, spin the tubes briefly, place them for 1 min on the magnetic rack, and discard the supernatants. Repeat in the same way with washes B and C.
8. After the last supernatant is discarded, resuspend the beads in 500 μl elution buffer (50 mM NaCl, 20 mM Tris–HCl pH 7.5, 20 mM Na butyrate, 0.1 mM PMSF, 5 mM EDTA, and 0.5% SDS). Incubate for 30 min on a rotating wheel at room temperature (this is the bound fraction).

### 3.4 DNA Extraction and Quantification

1. To each bound and mock fraction, add proteinase K (to a final concentration of 20 μg/ml), then incubate the tubes at 55 °C and 800 rpm (on a Thermomixer Comfort shaker or equivalent) for 1–2 h (*see* **Note 16**). The input sample (saved in Subheading 3.3) should also be used at this stage for DNA extraction. After the proteinase K digestion is over, briefly spin the tubes and place them in the magnetic rack for 1 min.

Transfer supernatants to phase lock tubes (eppendorf) and discard the tubes containing the magnetic beads (*see* **Note 16**).

2. Next, perform a phenol–chloroform extraction. First, add an equal volume (500 µl) of phenol:chloroform:isoamyl alcohol 25:24:1 in each tube, vortex for 1 min, and spin (16,000 × *g*) for 10 min in a microcentrifuge. Transfer the aqueous supernatant into a new phase lock tube, add 500 µl chloroform, vortex again for 1 min, and spin for 10 min at 16,000 × *g* (*see* **Note 17**).
3. Finish the DNA extraction with a standard ethanol precipitation (required to reduce the concentration of salts): add 100 µl of 3 M sodium acetate (pH 5.2), 2 µl glycogen solution (20 mg/ml), and 700 µl pure ethanol. Vortex thoroughly and incubate at −20 °C overnight. Next day, centrifuge the samples (16,000 × *g*, 15 min, 4 °C) to precipitate the DNA, aspirate the supernatant, wash the pellets with 1 ml ice-cold 70% ethanol, spin again (16,000 × *g*, 15 min, 4 °C), aspirate the supernatant, and air dry the pellets. At the end, dissolve the DNA from input, bound, and mock tubes in 50 µl of 10 mM Tris–Cl (pH 7.5).
4. Take 5 µl (10%) of each bound, mock, and input DNA and determine the concentrations using the Qubit® 3.0 Fluorometer. First, mix 10 µl of each standard solution provided in the Qubit® dsDNA HS assay kit with 190 µl Qubit® working solution. Vortex the tubes for 2–3 s, incubate at room temperature for 2 min, then read the tubes in the Qubit® Fluorometer. For each sample (bound, mock, or input), mix 2.5 µl DNA with 197.5 µl working solution and perform duplicate readings. All fractions are diluted to the same final concentration (*see* **Note 18**), then the DNA samples are stored at −20 °C until ready to analyze them by qPCR. Alternatively, the bound and input DNA can be used for preparation of libraries and for high-throughput sequencing (NChIP-Seq protocols are described elsewhere [11, 12]).

### 3.5 Analysis by Quantitative PCR (qPCR) and Data Interpretation

1. Design primers suitable for qPCR (80–150 bp) using freely available software such as Primer3. Before the first use, primers should be tested for specificity, using input DNA as template. The optimal annealing temperature (no primer dimers or non-specific PCR products) can be identified using a gradient PCR machine and by melting curve analysis (ideally this should be between 58 °C and 62 °C). Using ten-fold serial dilutions of input DNA, the efficiency of each primer pair can be calculated using the formula $E = 10^{(-1/\text{slope})} - 1$. The optimal primer efficiency is 1; however, primer efficiencies between 0.9 and 1.1 are acceptable. A good primer pair should generate $C_t$ values

around 25 when 1 ng input DNA is used as template. If $C_t$ values are >30, primers should be redesigned.

2. For qPCR analysis of NChIP samples, 1 ng DNA from each fraction is used as template. qPCR measurements can be done with primers designed for the regions of interest and the SYBR Green system. Ratios of bound/input >1 signify local enrichment of the histone mark analyzed, while ratios <1 mean local depletion.

## 4 Notes

1. The type of collagenase used is important for maintaining the integrity of pancreatic islets. Collagenase P, isolated from *Clostridium histolyticum*, has a very high collagenase activity (>1.5 U/mg) and has been functionally tested for the isolation of rodent pancreatic islets.
2. If the integrity of the common biliary duct is compromised during cannulation, the collagenase P solution can also be carefully injected into each lob of the pancreas. However, this may reduce the total number islets isolated per animal.
3. Incubation times may vary between different lots of collagenase and should be tested prior to use in experimental conditions. Incomplete digestion of the pancreas results in reduced yield of pancreatic islets.
4. If fewer islets than expected are observed, resuspend the pellet produced during the previous step and inspect for islets. This can happen if more than one pancreas is used per tube during the gradient centrifugation.
5. Using the protocol described here, we regularly harvest 200–300 islets/adult mouse or 500–800 islets per adult rat.
6. An average rodent islet is estimated to contain approximately 1000–2000 cells [13].
7. It is essential to use 5 mM Na butyrate in all solutions throughout the chromatin isolation steps when using antibodies against acetylated histones, in order to prevent histone deacetylation. PMSF is a serine protease inhibitor with a short half-life in aqueous solutions (110 min at pH = 7 and 35 min at pH = 8). PMSF stock is regularly prepared as 0.1 M solution in isopropanol and stored in aliquots at −20 °C.
8. We found that incubation for 30 min in presence of the detergent and the addition of 10 + 10 pestle strokes lead to efficient lysis of pancreatic islet cells. Excessive extension of this step increases the probability of nuclei bursting and could lead to failure of the chromatin extraction. Efficient release of nuclei is

verified using a phase-contrast microscope (intact cells have the central dark region of the nucleus surrounded by a halo, which is the less dense cytoplasm). At least 80% free nuclei should be obtained for a successful NChIP and additional strokes using the tight-fitting pestle can be applied if required.

9. The gradient sucrose centrifugation leads to very clean nuclei preparations, which are essential for a successful immunoprecipitation. However, when the percentage of free nuclei obtained during the cell lysis is very high, this step can be omitted in order to limit the excessive loss of material.
10. Obtaining a suspension of single nuclei (no visible clumps) in digestion buffer is critical for ensuring even access of the micrococcal nuclease to chromatin in the following step.
11. With a starting amount of ~1000 islets, we usually obtain up to 10 μg chromatin. It is essential to carefully control the conditions for micrococcal nuclease digestion, especially in the initial preparations. Excessive digestion of the chromatin leads to sub-nucleosomal fragments, while underdigestion leads to excess of larger oligonucleosomes, which severely reduces the resolution of the assay.
12. Pieces of 10–20 cm dialysis tubing are first boiled for 10 min in 0.5 l of 2% sodium bicarbonate, then rinsed twice in distilled water, boiled again for 10 min in 1 mM EDTA (pH 8.0), then cooled and stored until use at 4 °C in 1 mM EDTA (pH 8.0). The tubing can be stored in these conditions for several months.
13. Do not place ethidium bromide in the agarose gel or the electrophoresis buffer, because of the presence of SDS.
14. Diagenode offers premium antibodies, which have reached the highest level of validation from extensive in-house validation, in combination with numerous collaborations with epigenetics experts.
15. The binding capacity for DiaMag protein A-coated magnetic beads is approximately 5 μg antibody per 20 μl beads. If the amount of antibody used during immunoprecipitation is higher, the volume of DiaMag protein A-coated magnetic beads should be increased accordingly. As an alternative to magnetic beads, a 50% w/v slurry of Protein A Sepharose (PAS—GE Healthcare) can be used. Add 100 μl of PAS and incubate for a minimum of 2 h at room temperature on a rotating platform. Centrifuge 300 × *g*, 5 min at room temperature, and wash the pellets as described in Subheading 3.3 **steps 6**–7 except with centrifugation after each wash. Elute the bound material using 100 μl 1% SDS/incubation buffer, and incubate for 5 min with gentle agitation. Centrifuge

300 × *g*, 5 min at room temperature, and retain the supernatant (bound).

16. When required, both the DNA and protein can be isolated from the same input and bound samples. Add an equal volume of phenol:chloroform to the input and bound material. Briefly vortex before centrifugation at 300 × *g* for 5 min. Transfer supernatant to a phase lock tube and continue from Subheading 3.4 **step 1** to isolate the DNA. Keep the first phenol:chloroform phase and add 5 μl bovine serum albumin, 1/100th volume 10 M $H_2SO_4$ and 12 volumes of acetone. Following precipitation at −80 °C for 16 h, centrifuge at 300 × *g* for 10 min at 4 °C, and wash the pellet once in acidified acetone (one volume of 100 mM $H_2SO_4$ mixed with six volumes of acetone) and three times in dry acetone. Resuspend the pellet in 50–100 μl TE (10 mM Tris–HCl, 1 mM EDTA), before analysis using either SDS-PAGE or AUT-PAGE.
17. As an alternative to phenol:chloroform and ethanol precipitation for purification of DNA, the Qiaquick purification kit (Qiagen) can be used, following the manufacturer's instructions.
18. The expected yield of DNA depends upon the amount of antibody used and the amount of starting material, as well as the distribution of the histone modification in the genome. For example, the recovery rate in a successful immunoprecipitation with the H3K4me3 antibody is about 10–20% (i.e., 200–400 ng when the starting material is 2 μg chromatin). For less frequent histone modifications such as H3K4me1, the recovery rate could be around 5%. The recovery in the negative control (mock) sample should be less than 1%.

## References

1. Puri S, Hebrok M (2010) Cellular plasticity within the pancreas—lessons learned from development. Dev Cell 18:342–356
2. Carter JD, Dula SB, Corbin KL et al (2009) A practical guide to rodent islet isolation and assessment. Biol Proced Online 11:3–31
3. Ravier MA, Rutter GA (2010) Isolation and culture of mouse pancreatic islets for ex vivo imaging studies with trappable or recombinant fluorescent probes. Methods Mol Biol 633:171–184
4. Li F, Jiang X, Li Y et al (2013) Isolation of mouse islet by collagenase perfusion through the splenic vein. Transplantation 96:e88–e89
5. Sandovici I, Hammerle CM, Ozanne SE et al (2013) Developmental and environmental epigenetic programming of the endocrine pancreas: consequences for type 2 diabetes. Cell Mol Life Sci 70:1575–1595
6. Sandovici I, Smith NH, Nitert MD et al (2011) Maternal diet and aging alter the epigenetic control of a promoter-enhancer interaction at the Hnf4a gene in rat pancreatic islets. Proc Natl Acad Sci U S A 108:5449–5454
7. Haumaitre C (2013) Epigenetic regulation of pancreatic islets. Curr Diab Rep 13:624–632
8. O'Neill LP, Turner BM (2003) Immunoprecipitation of native chromatin: NChIP. Methods 31:76–82
9. Wagschal A, Delaval K, Pannetier M et al (2007) Chromatin immunoprecipitation (ChIP) on unfixed chromatin from cells and

tissues to analyze histone modifications. CSH Protoc 2007:pdb.prot4767

10. O'Neill LP, VerMilyea MD, Turner BM (2006) Epigenetic characterization of the early embryo with a chromatin immunoprecipitation protocol applicable to small cell populations. Nat Genet 38:835–841
11. Cuddapah S, Barski A, Cui K et al (2009) Native chromatin preparation and Illumina/Solexa library construction. Cold Spring Harb Protoc. https://doi.org/10.1101/pdb.prot5237
12. Brind'Amour J, Liu S, Hudson M et al (2015) An ultra-low-input native ChIP-seq protocol for genome-wide profiling of rare cell populations. Nat Commun 2015(6):6033
13. Jo J, Choi MY, Koh DS (2007) Size distribution of mouse Langerhans islets. Biophys J 93:2655–2666

# Chapter 12

# Quantification of Pancreatic Islets: Using Image Analysis Tools

**Parvathy E. Harikumar**

## Abstract

Histological image analysis is becoming an increasingly important tool for research in biological science. They are important in analyzing biological systems on various scales, from structural details to determination of number of cells, its area, localization, and concentration. This chapter focuses on analysis of pancreatic sections stained for insulin and glucagon using a commercially available software.

**Key words** Histology, Pancreas, Immunohistochemistry, Whole-slide image, Image analysis, VisiomorphDP, ImageJ

## 1 Introduction

Histological analysis of tissue sections is very important in clinical research, histopathology, disease diagnosis, and drug discovery. Historically, analysis and evaluation of histological sections was mere qualitative and subjective, and was prone to observer variations. Also, this type of quantification is laborious and time-consuming, as it requires examination of multiple tissue sections from whole-slide images. However, in recent years, the technology has improved so much that digital slide scanners are used for image acquisition, and manual or automated analysis is done using computer-assisted image analysis software for quantitative histomorphometry.

This chapter aims to focus on the analysis of stained histological tissue sections of the pancreas using a commercial image analysis software known as VisiomorphDP. VisiomorphDP software from Visiopharm (Horgholm, Denmark) was used to create a range of specific protocols to perform quantitative image analysis by exploiting spectral and morphological features of pancreatic tissue sections. Image analysis techniques used in the chapter are based on segmentation, whereby the user identifies a feature of interest, and

Claire J. Stocker (ed.), *Type 2 Diabetes: Methods and Protocols*, Methods in Molecular Biology, vol. 2076,
https://doi.org/10.1007/978-1-4939-9882-1_12, 

its constituent pixel values are then used by the software to identify all similar features in an image. Some of the analyses included in this chapter are quantification of total pancreas area, total islet area, alpha and beta cell area, islet number, and size distribution with reference to specific parameters.

Although the method detailed here is specific for analysis with VisiomorphDP, the idea is easily transferrable across different computational image processing systems including imageJ, an open-source image-processing program. This chapter does not discuss the algorithms, its implementation, and image processing techniques in detail as it is beyond the scope. Here, the author presents a general protocol for detecting and quantifying islets and its associated measurable features.

## 2 Materials

### 2.1 Animals

C57/Bl6 mice (Charles River, Manston, UK) were obtained at 5–6 weeks of age. All procedures were conducted in accordance with the UK Government Animals Scientific Procedures Act 1986, and approved by the University of Buckingham Ethical Review Board. The animals were housed in solid-bottomed, sawdust-filled cages with access to tap water and maintained on a standard chow diet fed ad libitum (10% kcal fat, 70% kcal carbohydrates, 20% kcal protein [Beekay Diets, New Brunswick, NJ, USA]). The source of fat in the chow diet was soybean oil. Mice were maintained at a controlled temperature of $23 \pm 1$ °C, on a 12 h light–dark cycle. At 12 weeks of age, mice were killed using carbon dioxide inhalation.

### 2.2 Tissue Preparation & Staining

1. PBS-T: Phosphate buffered saline (PBS) with 0.1% Triton X-100.
2. IMS: Industrial methylated spirit (Hayman Ltd., Essex, UK). IMS can be used instead of molecular grade ethanol.
3. 6% hydrogen peroxide: 30% hydrogen peroxide is diluted with methanol and stored in dark conditions at 4 °C until ready to be used. Use fresh preparations at all times.
4. Acid alcohol: 1% HCl is dissolved in 70% ethanol (v/v).

### 2.3 Suppliers

The following reagents and equipment were purchased from various suppliers: Histology cassettes (VWR International Ltd., UK), automated tissue processor (TP1020, Leica Microsystems, Milton Keynes, UK), Histo-ClearTM II (National Diagnostics, Hessle, UK), paraffin wax (Thermo Scientific, Histoplast, UK), microtome stainless steel blades (Feather S35; pfm medical UK Ltd., Chesire, UK), microscope slides (Starfrost, Fischer Scientific, UK), VECTASHIELD® HardSet™ Mounting medium (Vector Laboratories, Peterborough, UK), insulin and glucagon antibody (Dako,

Denmark), secondary antibodies and blocking serums (Sigma-Aldrich, Poole, UK), ImmPACT DAB and SG peroxidase substrate (SK-4105 and SK-4705;Vector Laboratories, USA), and Aperio Scanscope CS scanner (Aperio, CA, USA).

## 3 Methods

### 3.1 Pancreas Preparation

1. Mice were sacrificed using carbon dioxide inhalation, after which dissection was carried out to obtain pancreas for histology.
2. Excess fat and connective tissues bound to the pancreas were removed using forceps and scissors.
3. Weigh the pancreas and lay each pancreas between two sheets of filter paper to keep the "head" (pancreas bound to duodenum) and "tail" (pancreas bound to spleen) orientation and to maintain the structure of the pancreas.

### 3.2 Fixation and Tissue Processing

1. Individual tissues were placed in histology cassettes and fixed in 10% neutral buffered formalin for 17 h in room temperature (RT) (*see* **Note 1**).
2. Specimens were processed using a semi-enclosed benchtop automated tissue processor. Tissue processing involves dehydration of the samples using graded ethanol (IMS) followed by clearing in Histo-Clear™ II and finally paraffin wax infiltration according to the program listed in Table 1.

### 3.3 Embedding and Sectioning

1. After processing, samples were removed promptly and transferred to metal cassettes before embedding in paraffin wax at 60 °C using a Leica embedding station (model EG1150H) to form paraffin blocks.
2. The blocks were cooled in ice-cold water for few seconds prior to sectioning (*see* **Notes 2** and **3**).
3. Each block was then placed on a Leica microtome (model RM2255) set with a clearance angle of 4° to cut 4 μm sections with stainless steel blades.
4. During sectioning, each pancreas was divided into six different planes that were separated by an interval of 80 μm, and from each plane, 10 serial sections of 4 μm thickness were taken (*see* **Note 4**).
5. Sections were then floated in a 37 °C water bath and were taken using positively charged glass slides.
6. Sections were then initially dried for 10 min on hot plate and then allowed to dry overnight at 35 °C in an oven.
7. The resulting slides can be used for various staining purposes as well as immunohistochemistry.

**Table 1**
**Processing protocol**

| Station | Reagent | Time (min) |
|---|---|---|
| 1 | 50% IMS | 60 |
| 2 | 70% IMS | 30 |
| 3 | 80% IMS | 30 |
| 4 | 90% IMS | 60 |
| 5 | 100% IMS | 60 |
| 6 | 100% IMS | 60 |
| 7 | 100% IMS | 60 |
| 8 | Histo-Clear™ II | 15 |
| 9 | Histo-Clear™ II | 30 |
| 10 | Histo-Clear™ II | 60 |
| 11 | Paraffin wax (60 °C) | 15 |
| 12 | Paraffin wax (60 °C) | 90 |

### 3.4 Rehydration

1. Prior to staining, slides were dewaxed by heating in an oven at 60 °C for 15 min followed by rehydration (*see* **Note 5**).
2. Rehydration involves incubations as follows: Histo-Clear™ II [2 × 2 min], graded IMS [100%, 90%, 70%; each for 1 min], with a final rinse in running tap water.

### 3.5 Hematoxylin and Eosin (H&E)

1. Routine H&E staining was performed according to [1].
2. Briefly, slides were immersed in Harris hematoxylin for 8 min followed by rinsing in water for few seconds.
3. The slides were then immersed for 30 s in acid alcohol (differentiation) followed by 1 min rinsing in water.
4. This was followed by 30 s in 0.1% (w/v) sodium bicarbonate and 5 min rinsing in water.
5. The slides were finally incubated in eosin Y 0.5% (w/v) in acidified 90% ethanol for 3 min before dehydration.
6. Following staining, sections were dehydrated in graded IMS (90% and 100%; 30 s each) and cleared in Histo-Clear™ II (30 s) before mounting in VECTASHIELD® HardSet™ Mounting medium and coverslipping.

### 3.6 Immunohistochemistry (Chromogenic Method)

1. Following dewaxing and rehydration, slides were rinsed in PBS-T.
2. Slides were then immersed in 6% hydrogen peroxide for 10 min to block endogenous peroxidase activity (*see* **Note 6**) before blocking in 5% goat serum in PBS for 20 min.
3. Slides were then incubated with polyclonal anti-glucagon antibody raised in rabbit (1:200) in PBS and 2% goat serum for 90 min at RT followed by rinsing in PBS-T.
4. Subsequently, slides were incubated with a secondary goat anti-rabbit peroxidase conjugated antibody (1:200) with PBS and 2% goat serum for 1 h at RT.
5. After washing in PBS-T, the slides were developed using chromogenic detection method by incubating the slides in ImmPACT DAB peroxidase substrate for 3 min at RT to reveal glucagon (*see* **Note 7**).
6. Following glucagon staining, the slides were rinsed in water for 5 min and subsequently washed in PBS-T for few seconds.
7. The slides were then incubated in 5% rabbit serum in PBS for 20 min.
8. Further to this, the slides were incubated with polyclonal guinea pig anti-swine antibody (1:25 *see* **Note 8**) in PBS and 2% rabbit serum for 30 min at RT followed by rinsing in PBS-T.
9. Subsequently, slides were incubated with rabbit anti-guinea pig antibody conjugated with peroxidase (1:200) in PBS and 2% rabbit serum for 30 min at RT.
10. Insulin was detected by incubating the slides in a different chromogen, ImmPACT SG peroxidase substrate for 4 min at RT (*see* **Note 7**).
11. After immunostaining, slides were counterstained with Nuclear Fast Red for 10 min followed by rinsing in water for 5 min.
12. The slides were then dehydrated, cleared, and mounted as for H&E staining.

### 3.7 Image Capture

1. Whole-slide images of all stained sections were captured with an Aperio Scanscope CS scanner.
2. Images can be captured at any magnification up to 40×. Whole-slide images were scanned at 20× and 40× original magnification.

### 3.8 Image Analysis Software

1. Development of image analysis protocols was a six-step process and an overview is presented in Fig. 1.
2. Once a protocol was created, it could be run on regions of interest (ROIs), an entire image, or a batch of whole-slide

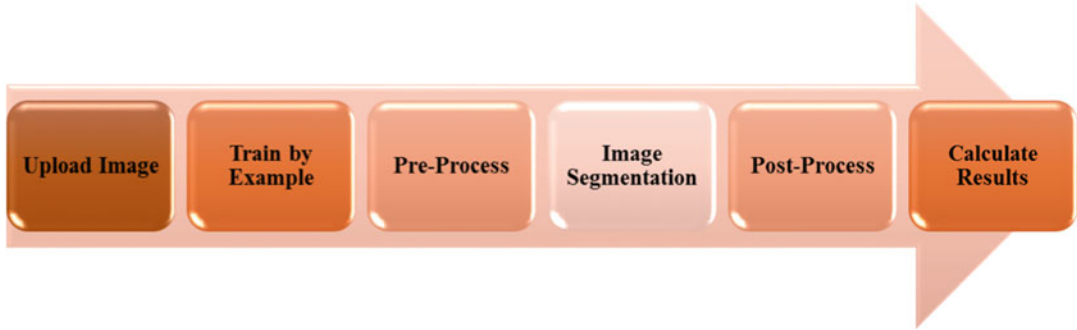


**Fig. 1** Overview of steps involved in developing image analysis protocols. The specific components of each step are described for individual protocols

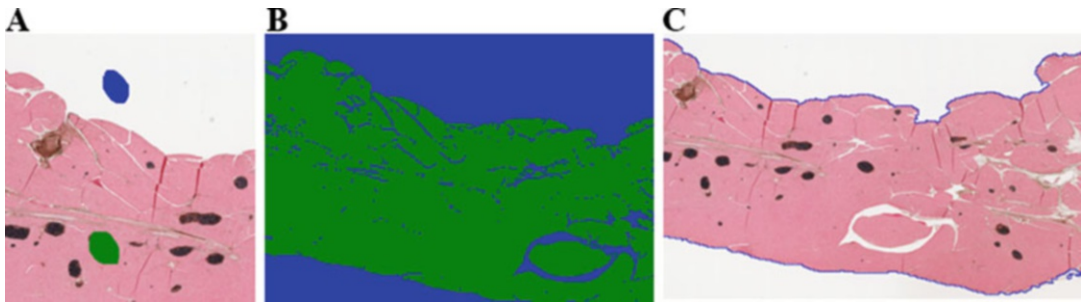


**Fig. 2** Training by example. Panel **A** original image, **B** training image (blue: background, green: pancreas [both identified by user] *see* Table 2) and **C** final segmented image (blue outline: ROI). Original magnification 10× (**A**) and 4× (**B** and **C**)

images. *See* **Note 9** for an important tip before using images for analysis.

3. *Training by Example:* The system was trained to recognize different image features such as exocrine tissue, islets, blood vessels, insulin, and glucagon (Figs. 2a and 3b). These were defined by the operator using a labeling tool to isolate a representative area of the feature to be quantified. The new markup for each object is termed as label and is represented by different colors.
4. *Defining Preprocessing Steps:* The purpose of preprocessing was to allow enhancement of structure of interest by suppressing noise and nonrelevant image components to improve image segmentation. This feature combines information such as spectral (RGB or contrast) or morphological information. For a standard color image, the features are described by red, green, and blue (RGB) pixel values, where each color band has a certain intensity at each given pixel location. If the basic input color band does not provide sufficient robust segmentation results across multiple images, there are other image processing filters available to use as required by the user. For this study,

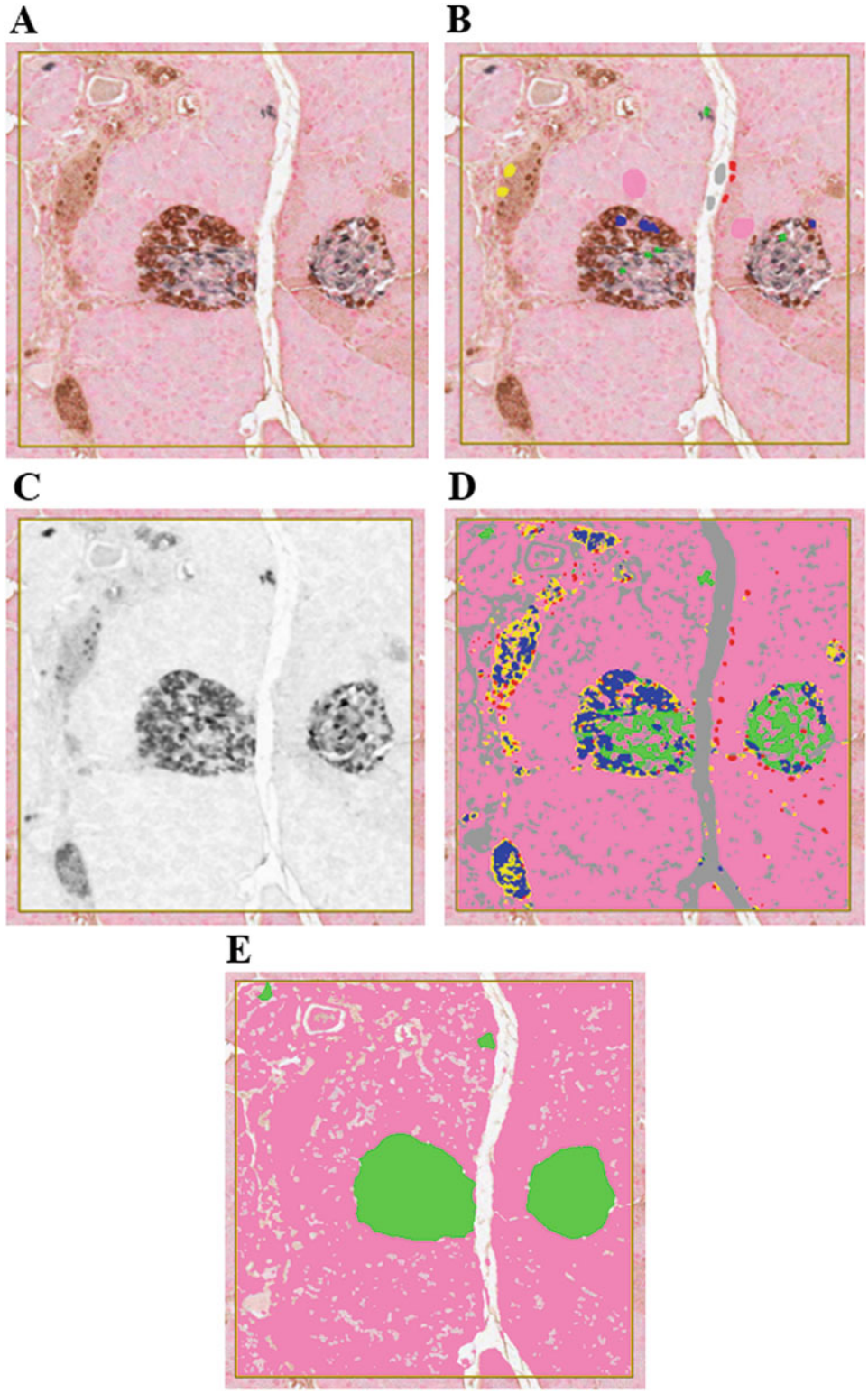


**Fig. 3** Islet detection. Islets are shown in green and exocrine are shown in pink. Panel **A** original image, **B** training by example (*see* Table 3), **C** preprocessed image with median filter, **D** segmented image after Bayesian classification and **E** final image after postprocessing. Image **C** shows the outcome of applying a [9, 9] median filter to an original RGB image. This filter helps to reduce "noise" by smoothing out bright and dark pixels. Original magnification 40×

RGB was insufficient in one case and the use of basic median filter with a kernel size of 9 × 9 to RGB color band enhanced the image by removing noise and preserving the edges. *See* **Note 10** for the list of all preprocessing filters available in VisiomorphDP.

5. *Defining Image Classification Method:* Preprocessed images undergo segmentation where every pixel sharing a defined set of characteristics is segmented to allow quantification. There are many image segmentation methods available, of which thresholding is the most common. A threshold is defined for a given feature and a class is assigned to all pixels with a feature value above or equal to threshold, and remaining pixels are assigned to another class. A Bayesian classifier can be used instead of thresholding for image segmentation under two main reasons. First, colors in specially stained tissues are a mixture, for which thresholding does not allow for accurate segmentation. Moreover, Bayesian classification does not require the user to define an all-inclusive intensity range for an image class as the representative training set defined will attribute all pixels in the image to one of the defined classes. *See* **Note 11** for the list of all classification methods available in VisiomorphDP.
6. *Defining Postprocessing Steps:* Following image segmentation, postprocessing steps can be performed to further refine segmented images based on morphological and contextual information. Postprocessing steps allow incorporation of prior knowledge into the segmentation process, often resulting in better quantitative results. For example, one can fill holes, separate objects, and smooth edges of the feature of interest. Note that these steps create a marked-up image in order that the user can make a visual assessment of the accuracy of segmentation. By repeating the steps above, one may iteratively create an effective algorithm. *See* **Note 12** for the list of all postprocessing operators.
7. *Defining Output:* The final step is the definition of quantification parameters. There are a wide range of output parameters to choose from to measure objects including number, length, area, shape, and intensity. *See* **Note 13** for the list of all outputs available in VisiomorphDP.

### 3.9 Development of Image Analysis Protocols

1. The four protocols developed were for (1) tissue detection; (2) islets detection; and quantification of (3) islet area and (4) alpha and beta cell mass. These protocols were run on micrographs of pancreas sections and each protocol was run one after the other sequentially to get the output of interest.
2. *Tissue Detection (Protocol 1):* As whole-slide images were used for analysis, non-tissue regions were excluded to decrease the

**Table 2**
**Protocol 1 for tissue detection**

| Steps | Chosen parameters |
|---|---|
| Magnification setup | 0.5× |
| Training (labels) | Slide background: blue, tissue: green |
| Preprocess | RGB |
| Classification | Bayesian |
| Postprocess | Close (tissue), fill holes (tissue with tissue), change small (tissue smaller than 6000 $\mu m^2$ to background), outline as ROI (tissue to ROI), change (tissue to clear), change (background to clear) |
| Output | None |

**Table 3**
**Protocol 2 for islet detection**

| Steps | Chosen parameters |
|---|---|
| Magnification setup | 20× |
| Training (labels) | Insulin (green), glucagon (blue), slide background (gray), blood (yellow), tissue (pink), fold (light blue), dark tissue (red) |
| Preprocess | RGB median [9,9] |
| Classification | Bayesian |
| Postprocess | Change (background to clear), change (dark tissue to tissue), change large (blood larger than 100 $\mu m^2$ to tissue), change nearest (blood to insulin), change (blood to tissue), change (fold to tissue), close (glucagon with glucagon, pixel 15), change small (inulin less than 15 $\mu m^2$), change nearest (glucagon close to insulin to insulin), change (glucagon to tissue), fill hole (insulin with insulin), close (insulin with insulin, pixel 70), change small (insulin less than 50 $\mu m^2$ to tissue) |
| Output | None |

time required for analysis. Once protocol 1 was run (Table 2), a ROI was automatically generated to delineate tissue (Fig. 2). The resulting ROI was then analyzed using protocol 2 for islet detection.

3. *Islet Detection (Protocol 2):* This protocol was developed to identify and mask islets from the surrounding tissue (Fig. 3). The steps involved in this protocol are detailed in Table 3.
4. *Quantification of Islets (Protocol 3):* Run this protocol on the image resulting from protocol 2. The aim is get quantitative data from the marked-up image; in this case, number of islets, area of islets, and area of exocrine region (Fig. 4). The steps involved in this protocol are detailed in Table 4.

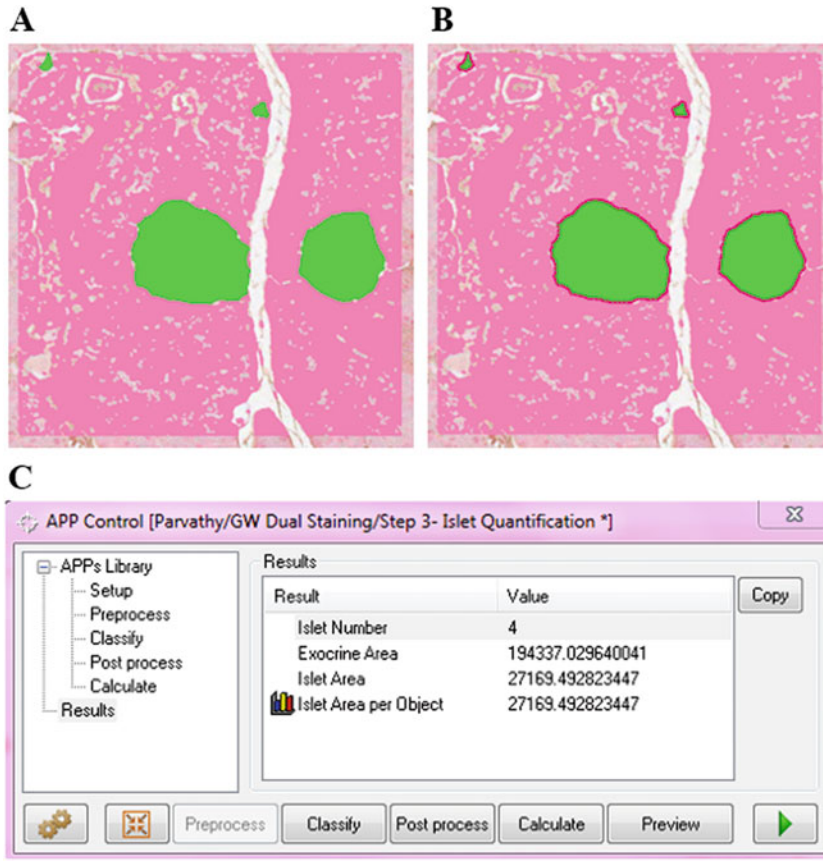


**Fig. 4** Islet quantification. Panels **A** marked-up image (final image from protocol 2), **B** final segmented image with islets (green) marked as ROI (red) and **C** output showing the quantitative data processed from the marked-up image. Output from this analysis includes number of islets, islet area, and exocrine area. Original magnification 40×

**Table 4**
**Protocol 3 for islet quantification**

| Steps | Chosen parameters |
|---|---|
| Magnification setup | 10× |
| Training (labels) | None |
| Preprocess | RGB |
| Classification | None |
| Postprocess | Change (ROI-1 to clear), outline as ROI (insulin to ROI-1) |
| Output | Number of islets, exocrine area, islet area |

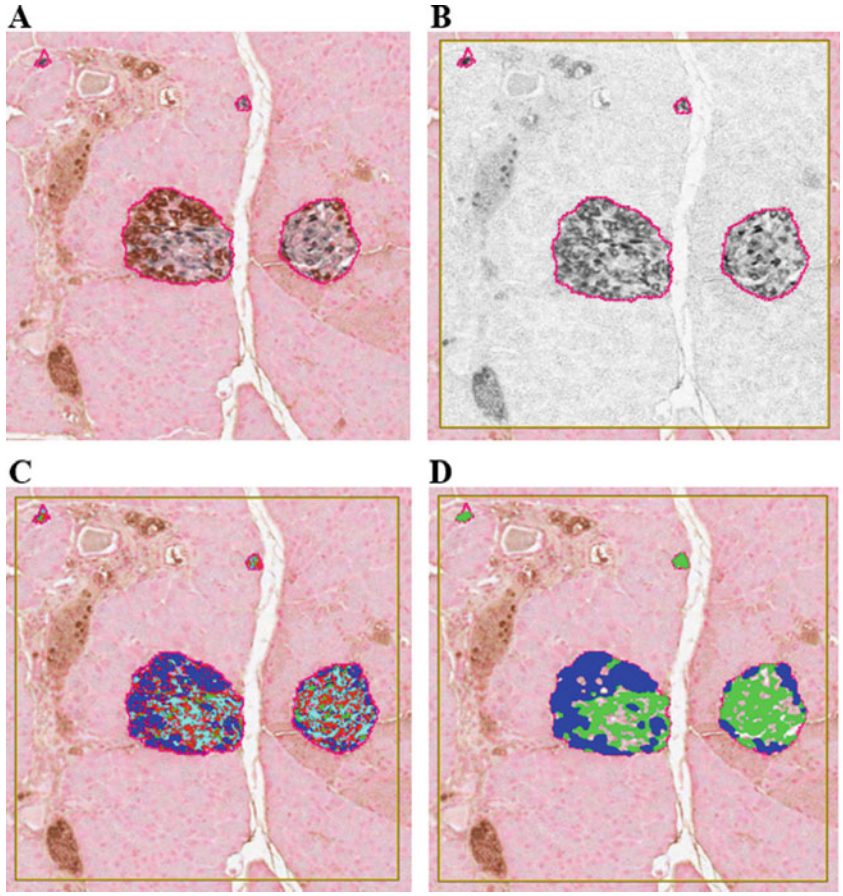


**Fig. 5** Alpha and beta cell area quantification. Panels **A** marked-up image (final image after protocol 3), **B** preprocessed image, **C** image segmented after Bayesian classification and **D** final image after postprocessing showing glucagon-producing alpha cells in blue and insulin-producing beta cells in green. Original magnification 40×

5. *Quantification of Alpha and Beta Cell Area (Protocol 4):* This is the final protocol to be run in order to get additional data such as alpha and beta cell area (Fig. 5). The steps involved in this protocol are detailed in Table 5. Once the data collection is achieved, alpha and beta cell mass can be calculated by using the formula below. Likewise, using islet area calculated, an islet size distribution graph (Fig. 6) can be plotted. Using the information derived from this plot, one can infer information about islet neogenesis.

$$\text{Alpha or beta cell mass} = \frac{\text{Alpha or beta cell area}}{\text{Exocrine area}} \times \text{Pancreas weight}$$

**Table 5**
**Protocol 4 for alpha and beta cell quantification**

| Steps | Chosen parameters |
|---|---|
| Magnification setup | 20× |
| Training (labels) | Insulin (green), glucagon (blue), tissue (pink) |
| Preprocess | RGB |
| Classification | Bayesian |
| Postprocess | Change small (insulin less than 10 $\mu m^2$), change small (glucagon less than 15 $\mu m^2$), close (glucagon with glucagon, pixel 10), close (insulin with insulin, pixel 5), change small (tissue less than 200 $\mu m^2$), change (tissue to clear), change small (insulin less than 20 $\mu m^2$ to clear) |
| Output | Insulin (beta cell) area and glucagon (alpha cell area) |

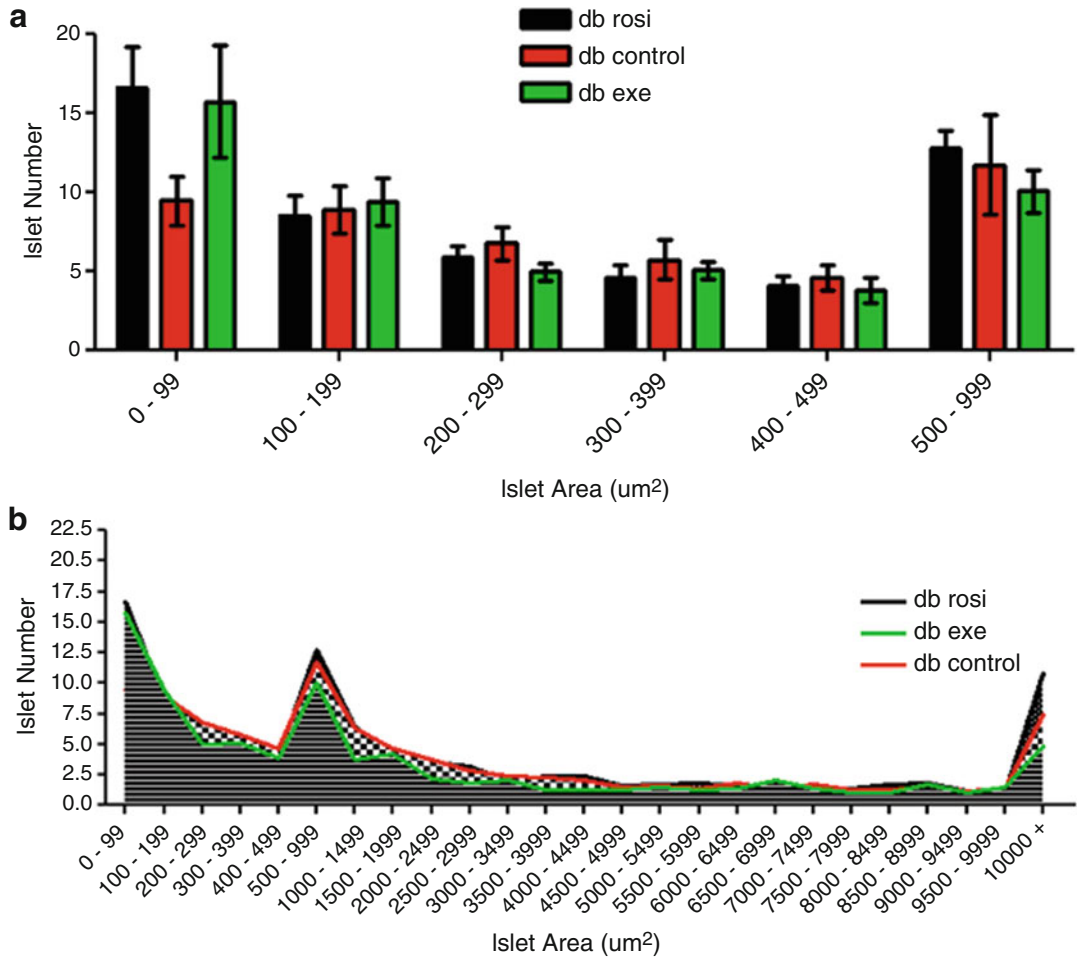


**Fig. 6** Example graphs showing distribution of islets based on its size. Such plots are useful for studies involving drug treatments to show influence of drugs/compounds on islet neogenesis, islet size, and number

## 4 Notes

1. In most histopathology laboratories, 10% NBF, a non-coagulative fixative, is historically the most popular fixative and continues to be the first choice for many pathologists [2]. However, the limitations of 10% NBF include its propensity to mask antigenic sites, degrade certain antigens, promote tissue shrinkage, and reduce nuclear detail [3]. Previous works [4] have shown that performance of 10% NBF across a range of stains indicated that it did not provide optimal fixation for all cutaneous applications. In this study, it was shown that use of alcoholic fixative (895 ml of 95% ethanol and 105 ml 37% formaldehyde) instead of 10% NBF provided consistent results across a range of applications. Thus, it is worth testing which fixative gives better consistent quality sections, as this is an important criterion for automated image analysis.
2. Soaking paraffin blocks in ice-cold water for few seconds is very important for pancreas embedded in paraffin blocks. This helps to get smooth, wrinkle- and fold-free sections.
3. Also, soaking paraffin blocks for 1–2 min in softening reagents sometimes helps to get good-quality sections. The formulation for softening agent is 500 ml of distilled water, 50 ml of glycerol, 5 tablets of PBS, 2.5 ml of methanol, 2.5 ml of Triton X-100, and 5 ml of phenol.
4. The problems associated with producing inconsistent sections can be reduced by changing the microtome blade frequently, cleaning the pressure plates from any wax deposition, and cooling the blocks on tissue paper soaked with ice-cold water.
5. Preheating in an oven ensures consistent dewaxing, as any residual wax greatly impairs subsequent analysis.
6. Endogenous peroxidases may react with chromogenic substrates and contribute to background signals that may compromise subsequent analysis. A solution of 3–6% hydrogen peroxide is commonly used to block such endogenous peroxidases. Also, one can dilute hydrogen peroxide in either methanol, PBS, or distilled water. Methanol is a superior choice in this case as it helps to reduce background signal from peroxidases better than others.
7. Incubation time for DAB and SG chromogen can vary from 2 to 10 min. Ideal time has to be identified through optimization by the user according to the experiment being performed.
8. The guinea pig anti-insulin primary antibody can also be used at a higher dilution such as 1:200. Only use 1:25 dilution if the expression of insulin is known to be decreased, for example, in case of pancreas from diabetic mouse models.

9. One of the key elements in image analysis is the preparation of good-quality sections and subsequently the quality of the image used. Factors like fixation of specimen/biopsy, tissue processing, sectioning, and consistency in staining are all very crucial checkpoints to be assessed in order to get good and accurate results after image analysis. Therefore, it is very critical to take care of these factors as much as possible.
10. *Preprocessing Steps:* Some of the preprocessing filters available in the software are color transformations (such as RGB, HIS [intensity, hue, and saturation], chromaticity, contrast, and color deconvolution), global operations and transformations (such as abs, negate, not, add, subtract, multiply, divide, min, max, square, square root, ln, exponential, and scale), local filter operations (such as mean, median, standard deviation, modus, median unsharp, mean unsharp, normalize by median, and normalize by mean) and polynomial filters (such as gradient, orientation, smoothing, laplace, linear structures, and blob structures). For example, one can use a polynomial local linear filter to enhance the linear structures of interest or use a blob filter to enhance object that has circular shape. Mean and median filters are very useful to reduce "noise" by smoothing out bright and dark pixels. Color deconvolution can be used if the staining contains only hematoxylin and DAB. This hematoxylin–DAB deconvolution allows the user to work in "true stain space" and produces two images of DAB staining and hematoxylin staining.
11. *Classification Methods:* Some of the training by example tools include freehand painting, region growing, ROI, and label tools. The basic classification tool available is thresholding and the advanced tools are K-means clustering, fuzzy K-means clustering, linear Bayesian classification, quadratic Bayesian classification, and automatic background detection.
12. *Postprocessing Steps (Refinement):* Some of the postprocessing categories include change object type (based on object's area, circularity, context [neighboring objects]), special operations (such as enumerate objects), morphological operations (such as fill holes, skeletonize, separate objects, close, conditional erode, and dilate), and ROI operations (such as outline objects as ROIs, create objects from ROIs). For example, close operation can be used to close holes in the object label with a chosen label and fill holes are used to fill the holes in the object label using the fill label. Some of the "change" steps include change (unconditional change of all label objects of one type (label) to another type (replace with), change small (change based on object size), and change nearest (label objects of chosen type (label) are changed to replace with type if they are sufficiently close to a third label type (close to)).

13. *Quantitative Measurement Options (Output):* The outputs are usually in single values or as histograms. While based on segmented image one can quantify object area, object count, perimeter, and interface length, based on original image or feature min/max intensity, mean intensity, standard deviation, median, modus, and entropy can be quantified.

## References


1. Gamble M (2008) The hematoxylins and eosin. In: Theory and practice of histological techniques. Churchill Livingstone Elsevier, London, pp 121–134
2. Grizzle WE (2009) Special symposium: fixation and tissue processing models. Biotech Histochem 84:185–193. https://doi.org/10.3109/10520290903039052
3. Eltoum I, Fredenburgh J, Grizzle WE (2001) Advanced concepts in fixation: effects of fixation on immunohistochemistry, reversibility of fixation and recovery of proteins, nucleic acid, and other molecules from fixed and processed tissues, developmental methods of fixation. J Histotechnol 24:201–210
4. Al-Habian A∗, Harikumar PE∗, Stocker CJ, Langlands K, Selway JL (2014) Histochemical and immunohistochemical evaluation of mouse skin histology: comparison of fixation with neutral buffered formalin and alcoholic formalin. J Histotechnol 37:115–124. https://doi.org/10.1179/2046023614Y.0000000050. (∗ equal contribution)

# Chapter 13

# Measurement of Calcium Signaling in Beta-Cell Lines Using Epifluorescence and Confocal Microscopy

**Joanne L. Selway**

## Abstract

One of the main consequences of glucose action on pancreatic β-cells is the stimulation of $Ca^{2+}$ entry as well as $Ca^{2+}$ release from intracellular compartments. Therefore, one of the cornerstones of any diabetes research laboratory should be the ability to measure changes in intracellular calcium concentrations within pancreatic β-cells. There are a variety of methods available for the measurement of intracellular calcium, from multiple regions of interest (ROIs) within single cells to observe oscillating calcium, to population-based 96-well applications to enable high-throughput screening of the effects of novel agonists. These methods allow calcium signaling to be observed in a single cellular assay to look at oscillations at a cellular level, to view a population response, and to enable high-throughput assays where the mean reflects a single cell response.

**Key words** Calcium, MIN6, Fluorescent microscopy, Beta-cells

## 1 Introduction

One of the main consequences of glucose action on pancreatic β-cells is the stimulation of $Ca^{2+}$ entry and $Ca^{2+}$ release from intracellular compartments. This stimulates an array of different molecular and physiological consequences. One of the major and most important physiological consequences is the stimulation of insulin secretion to ensure a feedback and lowering of peripheral glucose concentrations after a meal. Glucose metabolism and subsequent membrane depolarization of the pancreatic β-cell leads to the activation of voltage-gated calcium channels (VGCCs) and this is believed to mediate $Ca^{2+}$ release from ER stores via calcium-induced calcium release (CICR). This process initiates the fusion of insulin-containing vesicles, already primed at the plasma membrane, to be fused and insulin released into the bloodstream [1]. However, as an important second messenger in intracellular signaling, $Ca^{2+}$ also initiates other signaling cascades. The rise in intracellular $Ca^{2+}$ concentration ($[Ca^{2+}]i$) can activate

Claire J. Stocker (ed.), *Type 2 Diabetes: Methods and Protocols*, Methods in Molecular Biology, vol. 2076,
https://doi.org/10.1007/978-1-4939-9882-1_13, 

additional calcium-sensitive proteins, notably calmodulin, which can initiate changes in gene transcription through the CREB and MAPK pathways [2–4].

Rises in the $[Ca^{2+}]i$ in beta-cells can also be used as a pseudo-marker of any agonist that stimulates insulin secretion or intracellular signaling in beta-cells that permits insulin release, such as secretagogues. In general, high-throughput screening for new compounds involved in the treatment of diabetes, for example, beta-cell proliferation or novel strategies to prevent diabetes-induced pancreatic decline, relies on the activation of transcription factors or growth arrest as a primary readout, but no compound is likely to be validated and taken further in a pharmaceutical development pipeline if it is unable to mediate an improvement in $Ca^{2+}$-mediated insulin secretion [5, 6].

Strategies to measure $[Ca^{2+}]i$ changes in pancreatic beta-cells range from simple fluorescence measurement of one-wavelength with a relatively inexpensive system [4], to fluorescence resonance energy transfer imaging (FRET)-based imaging that can detect subtle changes in the calcium stores of the cells that requires more specialist microscopy equipment [7].

## 2 Materials

Krebs Ringer bicarbonate buffer (KRB): 115 mM NaCl, 5 mM KCl, 10 mM $NaHCO_3$, 2.5 mM $MgCl_2$, 2.5 mM $CaCl_2$, 20 mM HEPES pH 7.4.

Dye loading solution: 1 mg/ml BSA, 1.87 μl/ml 20% pluronic acid (*see* **Note 1**), 2 μM fluorescent dye (Fura-2 AM or Fluo-4-AM), Krebs Ringer buffer, and D1ER-FRET-GFP vector cameleon kindly provided by Professor R Tsien, Department of Pharmacology and Howard Hughes Medical Institute, University of California [8]. This construct is not commercially available, but readers may contact the original laboratory.

## 3 Methods

### 3.1 Cell Culture

1. MIN6 cells, a cell line derived from murine pancreatic β-cells, should be used at approximately 80% confluence between passages 16 and 40.
2. MIN6 cells are grown in DMEM containing 25 mM glucose supplemented with 15% heat-inactivated FCS, 100 μg/ml streptomycin, 100 units/ml neomycin 100 units/ml penicillin sulfate, 40 mM $NaHCO_3$, and 75 μM β-mercaptoethanol, equilibrated with 5% $CO_2$, 95% air at 37 °C.
3. The medium was changed every 2–3 days.

4. When ~80% confluence was reached, cells were washed once in 1× PBS and then placed in 1 ml 0.025% trypsin-EDTA for 2–5 min at 37 °C. Cells are resuspended in DMEM as soon as they start to detach from the plate.
5. MIN6 cells are split 1:3 to 1:4 for maintenance, or as required for experiments (*see* **Notes 2–4**).

### 3.2 $Ca^{2+}$ Imaging Techniques

#### 3.2.1 Epifluorescence Intracellular $Ca^{2+}$ Imaging

1. MIN6 cells are plated on glass coverslips (size dependent on microscopy equipment but typically 25 mm) for approximately 72 h to allow adhesion prior to experimentation (*see* **Note 5**).
2. Initially, cells should be washed three times in KRB to remove DMEM components from the cells by gentle removal of media and then addition and removal of KRB three times to cover the coverslip (*see* **Note 6**).
3. MIN6 cells are then loaded with 2 μM Fura-2-AM by covering the coverslip in dye loading buffer for 1 h at 37 °C. In addition to enabling the fluorescent dye to enter the cells, it starves the cells of glucose and reduce spontaneous oscillations of $Ca^{2+}$.
4. After an hour, wash the cells three times with KRB supplemented with 2 mM glucose by gentle removal of loading solution and then addition and removal of KRB three times, sufficient to cover the coverslip (*see* **Notes 6** and 7).
5. Coverslips can then be mounted on the stage of an inverted microscope (Nikon Diaphot inverted epifluorescence microscope) and left in 200 μl KRB buffer (or a volume sufficient to cover the surface of the coverslip when mounted in a coverslip bath) at room temperature (*see* **Notes 6** and 7).
6. To measure $[Ca^{2+}]i$, the cells must be excited at 340 and 380 nm at 1 s intervals and emissions collected at wavelengths above 520 nm (*see* **Note 8**).
7. A period of recording should occur before agonist stimulation (at least 30 s) to ensure that the cells have a low basal activity (*see* **Note 9**).
8. The agonist of choice (such as glucose) can now be pipetted onto the coverslip in a concentrated form to ensure the final concentration is the required dose. Typically, agonists are applied at 1.4 times the required concentration to the bath directly above the coverslip (*see* **Notes 6,** 7 and **10**).
9. Plot the data by looking at the ratio of 340:380 signal as a pseudo measure of $[Ca^{2+}]i$. The baseline readings should be stable, with a value of 1.

### 3.3 Single-Cell Confocal Intracellular $Ca^{2+}$ Imaging

1. MIN6 cells should be spilt 1:3 onto 25-mm diameter glass coverslips and left for a minimum of 72 h before experimentation (*see* **Note 5**).

2. Before imaging, the coverslips should be washed three times with KRB and left for 30 min at room temperature to ensure $Ca^{2+}$ signaling is at baseline levels (*see* **Note 9**).
3. After 30 min, the KRB should be replaced, via a pipette, with a loading solution containing 2 μM Fluo-4 for further 30 min to load the fluorescence dye (*see* **Note 11**).
4. The cells should be then washed three times with KRB supplemented with 2 mM glucose by gentle removal of loading solution and then addition and removal of KRB, sufficient to cover the coverslip three times (*see* **Notes 6** and **10**).
5. A PERKinElmer UltraVIEW confocal microscope, or equivalent model, is used to measure the $[Ca^{2+}]i$. Cells are excited using the 488 nm laser line and 485 nm excitation filter, and the emitted fluorescence captured at wavelengths >520 nm, with images collected at approximately 2-s intervals.
6. A period of recording should occur before agonist stimulation (at least 30 s) to ensure that the cells have a low basal activity (*see* **Note 10**).
7. An agonist, of choice (such as glucose), can now be pipetted onto the coverslip in a concentrated form to ensure the final concentration is the required dose. Typically, agonists were applied at 1.4× the required concentration directly above the coverslip (*see* **Note 11**).
8. The data is plotted by looking at the 520 emission value divided by the baseline emission prior to stimulation. This ratio provides a pseudo measure of $[Ca^{2+}]i$.

### 3.4 Population Based or High-Throughput Intracellular $Ca^{2+}$ Imaging

1. MIN6 cells should be passaged 1:2 into 96-well plates (200 μl total volume) and left to culture for 48 h.
2. Wells should be washed three times with KRB supplemented with 2 mM glucose by gentle removal of the media and then addition and removal of KRB, sufficient to cover the well, three times (*see* **Notes 6** and **10**) and then placed at room temperature.
3. After 30 min, the KRB is replaced with dye loading solution containing 2 μM Fluo-4.
4. After an additional 30 min, wash the wells three times with KRB supplemented with 2 mM glucose by gentle removal of the media and then addition and removal of KRB, sufficient to cover the well, three times (*see* **Notes 6** and **10**).
5. Cells can then be left with 25% of the total volume of KRB as a starting point (typically this is 200 μl).

6. At least one well of cells that has not been loaded with Fluo-4-AM should be included in all experiments as an autofluorescence control for the data analysis.
7. For stimulation, solutions should be 1.17× higher than required with 75% of the total volume added from the solution plate per well. All measurements must be made at room temperature.
8. The reader required for the population measurement should measure fluorescence at 520 nm every second during the experiment (*see* **Note 12**).

### 3.5 Fluorescence Resonance Energy Transfer Imaging (FRET)-Based Intracellular $Ca^{2+}$ Store Imaging

#### 3.5.1 Lipofectamine Transfection of MIN6 Cells

1. The Lipofectamine 2000 transfection procedure (Invitrogen, Life Technologies, UK) should be utilized as described below.
2. 4 μg D1ER DNA, purified by Qiagen maxi-prep kits, should be added to 225 μl Opti-MEM reduced serum media (Gibco, UK).
3. Simultaneously, 10 μl of Lipofectamine 2000 is added to 225 μl Opti-MEM low serum media. These solutions are incubated for 5 min at room temperature and then are combined by adding the DNA to the Lipofectamine solution (*see* **Notes 2, 3**, and **13**).
4. The solution is mixed gently by flicking, and then left at room temperature for 20 min.
5. The media should be changed on the cells to Opti-MEM and the complexes added to the cells by slowly dripping them from a 1 ml pipette over a min.
6. The complexes should be left on the cells overnight and then the media should be changed to complete media and the cultures left for further 24 h before experimentation (*see* **Note 14**).

#### 3.5.2 FRET-Based Imaging

1. MIN6 cells need to be starved of glucose and serum for at least 1 h in KRB prior to treatment.
2. All experiments must be carried out at room temperature.
3. Images are captured with the 20× objective of an epifluorescence microscope with a CCD camera.
4. The emission ratio imaging of the cameleon is accomplished by using a 436DF20 excitation filter, 450-nm dichroic mirror, and two emission filters (475/40 for enhanced CFP and 535/25 for citrine) controlled by a Lambda 10–2 filter changer.
5. Exposure times are typically 100–1000 ms and images can be collected every 8–20 s for the most optimal results.

6. A period of recording should be taken before agonist stimulation (at least 30 s) to ensure that the cells have a low basal activity (*see* **Note 9**).
7. An agonist of choice (such as glucose) can be pipetted onto the coverslip in a concentrated form to ensure the final concentration is the required dose. Typically, agonists were applied at 1.4× the required concentration directly above the coverslip (*see* **Notes 6** and **10**).
8. Data is plotted by looking at the ratio of emission values which acts as a pseudo measure of $[Ca^{2+}]_{ER}$.

## 4 Notes

1. Make the 20% pluronic acid mix 24 h in advance if possible; if not, warm the mixture to dissolve as it will form an emulsion initially which can be reversed with heat. If you do not warm this solution, it may ultimately reduce the concentration of acid in the loading dye leading to reduced amount of dye being loaded in the cells.
2. Clumping of MIN6 pancreatic beta-cell lines is vital for the survival of the cells and individual cells tend to apoptose. However, clumping of pancreatic beta-cells in the abovementioned assays can lead to low transfection rates and problems with imaging.
   (a) Lipofectamine-mediated transfection of DNA plasmids requires equal access to the membranes of the cells to deposit the coated plasmids into the cells evenly. Clumping of cells prevents the even distribution of plasmid, reducing the transfection efficiency in these cell lines further.
   (b) Clumped cells in the z-plane leads to problems in imaging as signal from other z-positions can sometimes be seen, often known as "bleed through," and thus can interfere with individual cell signals increasing noise. One solution to this is to minimize the laser intensity but this can lead to a compromise on the observation of true signal.
3. To mitigate both of these problems, a balance in plating of the cells is required to ensure cells are only in 2–3 groupings. This can be achieved through the optimization of several different parameters:
   (a) Trypsinization time when plating—regular use of MIN6 cell batches will allow empirical determination of the optimal digestion time required. The optimum time to resuspend the cells in DMEM to quench digestion is when the

majority of cells are slowly sliding down the flask or plate when tilted.

(b) Thorough resuspension in DMEM posttrypsinization allows clumps of cells to be disaggregated appropriately. As a rule of thumb, if the above step is optimal, pipetting up and down through a 10-ml pipette on low speed 10 times will be sufficient. However, the aliquoting of 10 μl of cells and observation under a microscope will demonstrate whether the clumps have been reduced to double or triple cell clumps as required for experimentation.

4. MIN6 cells were used between passages 16 and 40, as higher than this the cells are not as responsive to glucose, meaning that the calcium signals generated by glucose signaling become highly variable.
5. Coating the plates and/or coverslips with poly-D-lysine is an option for retaining cells on the coverslips and the bottom of plates but the coating can interfere with imaging as it has a natural fluorescent property. This interference can be accounted for in the analysis but can increase the noise due to inconsistent coating.
6. MIN6 cells (and other pancreatic beta-cell lines such as rat INS1e cells) can lift from the surface of the plates or coverslips if not treated gently. Gentle treatment involves:
   (a) the use of a bath, rather than perfusion of agonist or stimulant.
   (b) the addition of small volumes slowly onto coverslips.
7. Perfusion rather than bath addition can be used for MIN6 cells in short-scale (<5 min) experiments but the flow rate needs to be minimal with the realization that many of the cells being observed (as well as the individual data points within cells) may be lost.
8. Any fluorescent microscopy with the correct lasers and filters can be utilized for these experiments but here a SpectraMASTER II monochromator has been used (PerkinElmer Life Sciences).
9. A period of recording should occur prior to the addition of any agonist to evoke a $Ca^{2+}$ response. The purpose of this recording is to ensure a stable baseline for recording and as a quality control measure to ensure that the quality of the recoding is satisfactory. If the baseline is not linear or if there is a significant level of activity without agonist, the recording should be rejected. The most common reason for activity is incorrect buffer preparation or flow causing a physical movement of the cells resulting in a $Ca^{2+}$ response.

**Table 1**
**Plate reader parameters to measure fluorescence at 520 nm**

| General settings | | Concentrations/volumes/shaking | |
|---|---|---|---|
| Positioning delay | 0.2 s | *Volume* | |
| No. of kinetic windows | 2 | Start volume | 0 |
| *Kinetic window 1* | | Factor | 1 |
| Measurement start time | 0.00 | *Shaking options* | |
| No. of intervals | *5* | Mode | Orbital |
| No. of flashes per well and interval | 10 | Shaking width | 1 mm |
| Interval time | 1.00 s | Additional shaking | No shaking |
| End of kinetic window 1 | 5 s | *Pump* | |

10. Bath addition of the agonist of choice is the preferred method of addition. When the coverslip is in a bath on the microscope stage, it should be covered with 200 μl of KRB. The agonist of choice should then be added at 1.4X.
11. All $Ca^{2+}$ imaging experiments must be carried out at room temperature as incubation at 37 °C leads to the increased leakage of the fluorescent dye during longer (>20 min) experiments.
12. A plate reader must be set up with the basic parameters given in Table 1 to measure fluorescence at 520 nm.
13. The transfection efficiency of the MIN6 pancreatic beta-cell line is typically low ranging from 20 to 40%, so population FRET imaging (or any imaging requiring a transfection of a plasmid construct without a fluorescent tag) is not advised.
14. After Lipofectamine transfection, cells should be observed at the 8–12 h and 24-h mark to check for cell death. A small proportion of cells may undergo cell death as evidenced by a lack of attachment to the wells or coverslips and a spherical shape but this should not exceed 10% of the treated cells.

## References

1. Mears D (2004) Regulation of insulin secretion in islets of Langerhans by Ca(2+)channels. J Membr Biol 200(2):57–66
2. Arnette D et al (2003) Regulation of ERK1 and ERK2 by glucose and peptide hormones in pancreatic beta cells. J Biol Chem 278 (35):32517–32525
3. Gomez E, Pritchard C, Herbert TP (2002) cAMP-dependent protein kinase and Ca2+ influx through L-type voltage-gated calcium channels mediate Raf-independent activation of extracellular regulated kinase in response to glucagon-like peptide-1 in pancreatic beta-cells. J Biol Chem 277(50):48146–48151
4. Selway J et al (2012) Evidence that Ca2+ within the microdomain of the L-type voltage gated Ca2+ channel activates ERK in MIN6 cells in response to glucagon-like peptide-1. PLoS One 7(3):e33004

5. Hill JA et al (2010) A multi-parameter, high-content, high-throughput screening platform to identify natural compounds that modulate insulin and Pdx1 expression. PLoS One 5(9): e12958
6. Wang W et al (2009) Identification of small-molecule inducers of pancreatic beta-cell expansion. Proc Natl Acad Sci U S A 106 (5):1427–1432
7. Moore CE et al (2011) PERK activation at low glucose concentration is mediated by SERCA pump inhibition and confers preemptive cytoprotection to pancreatic beta-cells. Mol Endocrinol 25(2):315–326
8. Palmer AE et al (2004) Bcl-2-mediated alterations in endoplasmic reticulum Ca2+ analyzed with an improved genetically encoded fluorescent sensor. Proc Natl Acad Sci U S A 101 (50):17404–17409

# Chapter 14

# Nitric Oxide and Redox State Measurements in Pancreatic Beta Cells

**Rodrigo Carlessi, Vinicius Cruzat, Younan Chen, and Philip Newsholme**

## Abstract

The role of oxidative stress in the pathogenesis of type 2 diabetes (T2D), especially pancreatic β-cell dysfunction and death, has become apparent in the last two decades. Peroxidase- and catalase-based antioxidant mechanisms are particularly weak in β-cells and can be easily overwhelmed by excessive production of reactive oxygen and nitrogen species in the course of pathological processes. Recent research has attempted to define in detail the mechanistic aspects of oxidative stress-induced β-cell dysfunction. Here, we describe the procedures for the measurement of various parameters important to assess oxidative stress in pancreatic β-cells. Detailed protocols for determination of nitric oxide (NO) production, the glutathione redox status, and general oxidative status in β-cells are presented in this chapter.

**Key words** Nitric oxide, Glutathione, Oxidative stress, β-cells, Type 2 diabetes mellitus (T2DM)

## 1 Introduction

Reactive oxygen species (ROS) and reactive nitrogen species (RNS) are produced during a number of physiological and pathological processes. The excess production of ROS and RNS, or the inability to effectively scavenge such species, induces oxidative stress in cells. Oxidative stress is involved with various pathological conditions, such as aging, diabetes, inflammation, carcinogenesis, and atherosclerosis [1]. In pancreatic β-cells, glucose catabolism to $CO_2$ and $H_2O$ is essential to generate the enormous amount of energy required to produce and secrete insulin according to demands of growth and energy storage in target tissues. Glucose-stimulated insulin secretion (GSIS) requires glucose metabolism and oxidation in β-cells. Indeed β-cells must satisfy their own energy demands without hampering their ability to drive and regulate insulin exocytosis. Intense oxidative metabolism, combined with the fact that β-cells are associated with relatively low expression levels of some key antioxidant enzymes [2, 3], make β-cells highly susceptible to ROS/RNS-induced damage. In conditions of excessive nutrient

Claire J. Stocker (ed.), *Type 2 Diabetes: Methods and Protocols*, Methods in Molecular Biology, vol. 2076,
https://doi.org/10.1007/978-1-4939-9882-1_14, 

overload (normally associated with type 2 diabetes) the resulting excessive production of ROS and RNS can damage beta cells, leading to loss of insulin secretion and even cell death [4]. In type 1 diabetes (T1D), proinflammatory cytokine-induced β-cell death is known to be partially mediated through excessive ROS/RNS generation [5]. Thus, measurements of reactive species as well as global oxidative stress in β-cells are important to the field of diabetes research. In this chapter, we describe in detail the procedures involved in the measurement of nitric oxide (NO), the glutathione redox state, and general oxidative status in β-cells.

### 1.1 Measurement of Nitric Oxide Free Radical (NO) Release

NO is a free radical that, under physiological conditions, is rapidly oxidized to nitrite ($NO_2^-$) and nitrate ($NO_3^-$). The assay described in this chapter is a modified version of a diazotization reaction that was originally described by Peter Griess [6]. It consists of a simple and well-characterized colorimetric assay for nitrites, with a detection limit around 0.1 μM, adequate to detect nitrites released by beta cells in standard tissue culture conditions.

### 1.2 Glutathione Redox State Measurement

Reduced glutathione (GSH), a tripeptide (g-glutamylcysteinylglycine), is the main free thiol in most living cells and is the most important antioxidant in animal cells. Oxidation of glutathione leads to the formation of glutathione disulfide (GSSG), a process that occurs when GSH reacts with free radicals, protecting cells against oxidative stress. Thus, the ratio GSH/GSSG within cells is often used as an index of intracellular redox status. Inflammation and glucolipotoxicity have been shown to reduce this ratio in β-cells [7, 8]. The protocol detailed here, in order to determine GSH and GSSG, was described by Kolberg et al. [9] and Cruzat et al. [10] adapted from Akerboom, Sies [11].

As described in (Fig. 1), in the presence of GSSG reductase and NADPH, the GSSG resulting from the first reaction (or initially present in the sample), is reduced to GSH, which is then converted back to GSSG and 5-thio-2-nitrobenzoic acid (TNB). As the amount of GSSG reductase is constant and the substrates NADPH and 5,5′-Dithiobis (2-nitrobenzoic acid) (DTNB) are added at saturating concentrations, the velocity of TNB formation is proportional to the initial amount of GSH + GSSH in the sample. The formation of TNB can be assessed using spectrophotometric analysis at 412 nm and gives as estimation of the total amount of glutathione (reduced and oxidized) present in the sample. For the determination of the initial amount of GSSG in the sample, it is necessary to eliminate all GSH before the commencement of the reaction; this is achieved by conjugation with *N*-Ethylmaleimide (NEM). The procedure detailed here describes all the steps necessary to determine total GSH and GSSG levels in β-cell lysates. The amounts of GSH can be calculated by subtracting GSSG values from total glutathione levels.

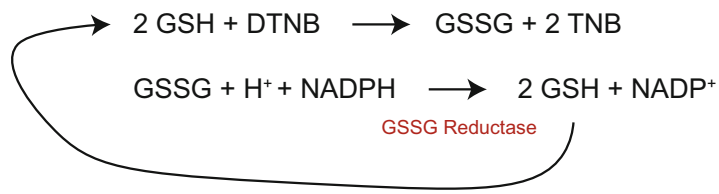


**Fig. 1** Coupled reactions in the DTNB-GSSG reductase recycling assay

### *1.3 General Oxidative Status*

As an alternative to determination of specific ROS or RNE species, general oxidative status can be estimated in living cells. The cell-permeant 2′, 7′-dichlorodihydrofluorescein diacetate (H2DCFDA), also known as dichlorofluorescein diacetate, is commonly used to detect the generation of free radicals in cells. Upon cleavage of the acetate groups by intracellular esterases and subsequent oxidation by ROS and/or RNE, the non-fluorescent H2DCFDA is converted to the highly fluorescent 2′, 7′- dichlorofluorescein (DCF), which can be detected by fluorescence- based methodologies, such as fluorescence spectroscopy, flow cytometry, and confocal microscopy.

In this chapter, we describe in detail a method to estimate total intracellular ROS levels by flow cytometry, using a probe of 5- (and 6-) chloromethyl-2′,7′-dichlorodihydrofluorescein diacetate, acetyl ester (CM-H2DCFDA) (Fig. 2). CM-H2DCFDA is a chloromethyl derivative of H2DCFDA that passively diffuses into cells, where its acetate groups are cleaved by intracellular esterases, and its thiol-reactive chloromethyl group reacts with intracellular glutathione and other thiols. Subsequent oxidation yields a fluorescent adduct that is trapped inside the cell, thus facilitating detection.

## 2 Materials

All chemicals can be purchased from Sigma-Aldrich (St. Louis, MO, USA), unless otherwise stated.

### *2.1 Measurement of Nitric Oxide Free Radical (NO) Release*

1. 0.1% *N*-(1-Naphthyl)ethylenediamine dihydrochloride in water (*see* **Note 1**).
2. 1% Sulfanilamide in 5% phosphoric acid (*see* **Note 2**).
3. 100 mM sodium nitrite in water (*see* **Note 3**).
4. Clear 96-well flat-bottom plate.
5. Plate reader.
6. 1.5 mL disposable polypropylene tubes.
7. Pipettes for ranges 20–200 μL and 200–1000 μL.
8. Disposable 200 and 1000 μL tips.
9. Vortex mixer.

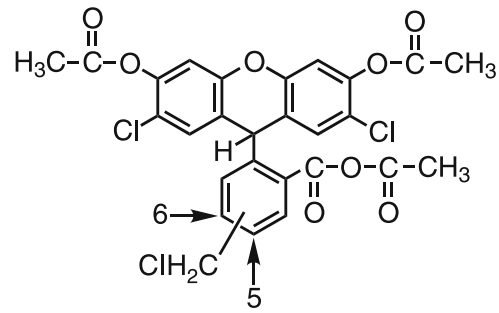


**Fig. 2** 5-(and 6-) chloromethyl-2′,7′-dichlorodihydrofluorescein diacetate, acetyl ester (CM-H2DCFDA, C6827, Life Technology)

10. Centrifuge.
11. Ultrapure or distilled water (*see* **Note 4**).

### 2.2 Glutathione Redox State Measurement

1. 0.2 M *N*-Ethylmaleimide (NEM) in 100% ethanol (740.6 mg/30 mL ethanol).
2. 0.3 M Pipes dissolved in 2 M potassium hydroxide (KOH) (9.07 g/100 mL of 2 M KOH).
3. Ethyl acetate.
4. 5% Meta-phosphoric acid (MPA) (w/v) in water.
5. 1 mg/mL Glutathione reduced (GSH) and oxidized (GSSG) in water.
6. Assay buffer—143 mM Phosphate buffer, pH 7.5 (*see* **Note 7**), containing 6.3 mM EDTA (234.6 mg of ethylenediaminetetraacetic acid (EDTA) in 100 mL of phosphate buffer).
7. 14.1 mM DTNB (5.59 mg of 5,5′-dithiobis-2-nitrobenzoic acid (DTNB) in 1 mL of assay buffer).
8. 1.7 mM NADPH (1.42 mg of NADPH in 1 mL of sodium bicarbonate ($NaHCO_3$) at 5% (w/v) in water).
9. Glutathione Reductase solution—calculate the amount of enzyme solution necessary for the assay (10 μL/sample). Resuspend Glutathione Reductase enzyme suspension (Sigma G3664) to 5 U/mL, and then dilute 1:90 in assay buffer.
10. Clear 96-well plates.
11. Polypropylene microcentrifuge tubes.
12. Microcentrifuge.
13. Vortex.
14. Speed dryer vac.
15. Plate reader.
16. Pipettes for 20–200 μL and 200–1000 μL.
17. Multichannel pipette for 20–200 μL.

### 2.3 General Oxidative Activity

1. 5-(and-6)-chloromethyl-2′,7′-dichlorodihydrofluorescein diacetate, acetyl ester (CM-H2DCFDA), mixed isomers, 50 μg/vial (Life Technologies, NY, USA—C6827).
2. Glucose Oxidase from *Aspergillus niger* (Sigma G7141) (resuspend to 100 U/mL with 0.05 M Sodium Acetate, pH 5.1).
3. Dulbecco's Modified Eagle Medium (DMEM): Phenol red free, and fetal bovine serum (FBS) free.
4. Roswell Park Memorial Institute (RPMI) 1640 media: with 10% fetal bovine serum (FBS).
5. Phosphate-buffered saline (PBS).
6. Trypsin: 0.25% (w/v) in PBS.
7. Dimethyl sulfoxide (DMSO).
8. 6-well cell culture plate.
9. 1.5 mL and 15 mL disposable polypropylene tubes.
10. Flow cytometer.

## 3 Methods

### 3.1 Measurement of Nitric Oxide Free Radical (NO) Release

1. For each assay series, a nitrite standard curve must be prepared for accurate quantitation of $NO_2^-$ levels in experimental samples. Prepare 5 mL of a 100 μM nitrite solution by diluting the 100 mM nitrite stock solution 1 in 1000 in beta cell culture media (such as RPMI, *see* **Note 5**).
2. Label seven 1.5 mL disposable polypropylene tubes with the following concentrations: 100, 50, 25, 12.5, 6.25, 3.125 and 1.56 μM. Pipette 200 μL of tissue culture media to all tubes, labeled from 50 μM downwards, leaving the tube labeled 100 μM empty. Add 400 μL of 100 μM nitrite solution to the tube labeled 100 μM.
3. Perform a serial twofold dilution by pipetting 200 μL from the 100 μM tube into the 50 μM tube. Vortex to mix, then proceed down the serial dilution as shown in (Fig. 3).
4. Designate columns A, B, and C of the 96-well plate for the nitrite standard curve. Pipette 50 μL of each nitrite standard into the wells in rows A–G, starting at A with μM 100 and down to 1.56 μM at G. Into the row H pipette tissue culture media only, which will be the blank.
5. Add 50 μL of each experimental sample to wells in triplicate (*see* **Note 6**).
6. Allow the Sulfanilamide Solution and NED Solution to equilibrate to room temperature.

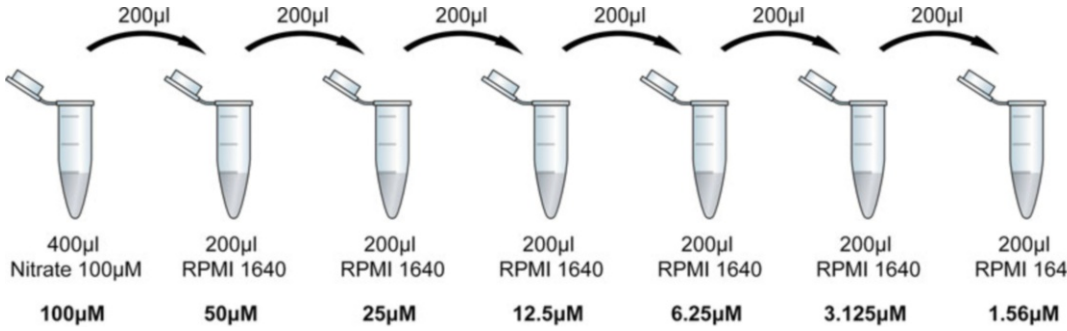


**Fig. 3** Suggested pipetting strategy to prepare the nitrite standard curve

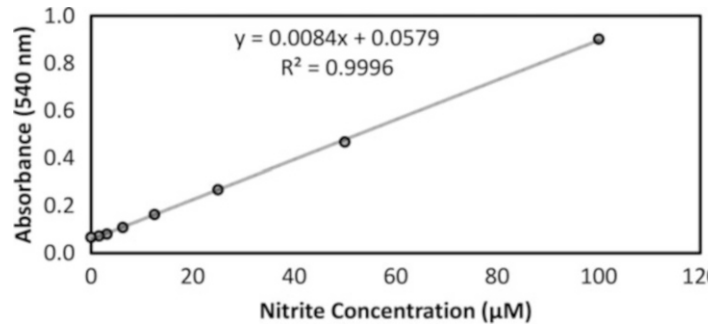


**Fig. 4** Representative nitrite standard curve. Trend line and equation are calculated through linear regression analysis using Microsoft Excel Professional Plus 2013

7. Pipette 50 µL of the Sulfanilamide Solution to all wells containing nitrite standards and experimental samples.
8. Incubate for 5 min at room temperature, protected from the light.
9. Pipette 50 µL of the NED Solution to all wells.
10. Incubate at room temperature for 10 min, protected from the light. The colors start to develop immediately.
11. Measure absorbance within 30 min using a plate reader with a filter between 530–550 nm.
12. Subtract the average absorbance value of the blank wells from all standards and experimental samples wells.
13. Make a standard curve by plotting concentration of the standards on the *X*-axis, and average absorbance of the triplicates measurements on the *Y*-axis. A representative standard curve is shown in (Fig. 4).
14. Determine the average absorbance value of each experimental sample and estimate its concentration by comparison to the nitrite standard curve.

### 3.2 Glutathione Redox State Measurement

1. After treatment, washβ-cells with ice-cold PBS, and then resuspend cell pellet in 5% MPA (150–200 μL of meta-phosphoric acid (MPA) for about $10^7$–$10^8$ cells population or 50–100 μL of MPA for $10^6$–$10^7$ cells) in order to break the cell membranes. Gently homogenize with a pipette, then centrifuge the samples 15,000 × *g* for 5 min at 4 °C and the supernatants (from now on referred to as 'samples') are collected and stored for subsequent analysis (*see* **Note 8)**.
2. Samples designated to measurement of initial GSSG should be conjugated with NEM to eliminate all GSH before commencement of the reaction (**steps 3–6**). Samples designated to total glutathione assay go directly to **step 7**.
3. Using polypropylene microcentrifuge tubes (≤1.5 mL), samples are mixed with NEM and Pipes/KOH (*see* **Note 9)**.
4. Subsequently, samples are centrifuged at max speed for 3 min and supernatants discarded.
5. Pellets are resuspended in 500 μL of ethyl acetate, centrifuged at max speed for 3 min and supernatants discarded. This step is repeated two times more (*see* **Note 10)**.
6. Following the last wash with ethyl acetate, supernatants should be carefully removed with pipette and dried in a SpeedVac machine at room temperature. Finally, samples are resuspended in 50 μL of 5% MPA for determination of GSSG.
7. For the determination of GSH and GSSG, the following components need to be prepared fresh just before the assay: Assay buffer, 14.1 mM DTNB, 1.7 mM NADPH and Glutathione Reductase solution (for details *see* **items 6–9** of Subheading 2.2).
8. A standard curve for GSH and GSSG must be prepared according to Table 1. To start, dilute the stock of 1 mg/mL GSH 1:4 in 5% MPA to get 813.5 μM and 1 mg/mL GSSG 1:2 in 5% MPA to get 816.0 μM.
9. GSH and GSSG assay running in a polystyrene 96-well plate for a final volume of 100 μL. Reagents must be added to the wells of the 96-well plate in the following order (*see* **Note 11)**.
   (a) 10 μL sample in 5% MPA (cold).
   (b) 70 μL of DTNB (37 °C).
   (c) Mix gently (5 s).
   (d) 10 μL NADPH at room temperature.
   (e) Mix gently (5 s) and incubate at 37 °C for 2–3 min.
   (f) Pipette 10 μL of GSSG reductase (it is highly recommended to use a multichannel pipette for fast distribution of GSSG reductase across all wells).

**Table 1**
**Series of dilutions for GSH and GSSG standard curves**

| Dilution | | | GSH (μM) | GSH (μL) | MPA (μL) | GSSG (μM) | GSSG (μL) | MPA (μL) |
|---|---|---|---|---|---|---|---|---|
| 75 μL + | 0 | | 813.5 | – | 0 | 816.0 | – | 0 |
| 25 μL MPA | 3/4 | 1:1 | 610.1 | 75 | 25 | 612.0 | 75 | 25 |
| | 1/2 | | 406.8 | 50 | 50 | 408.0 | 50 | 50 |
| 1:1 | 1/4 | | 203.4 | 50 | 50 | 204.0 | 50 | 50 |
| | 1/8 | 1:1 | 101.7 | 50 | 50 | 102.0 | 50 | 50 |
| 1:1 | 1/16 | | 50.8 | 50 | 50 | 51.0 | 50 | 50 |
| → ZERO = MPA 5% | 0 | 0 | – | 0 | 0 | 0 | | |

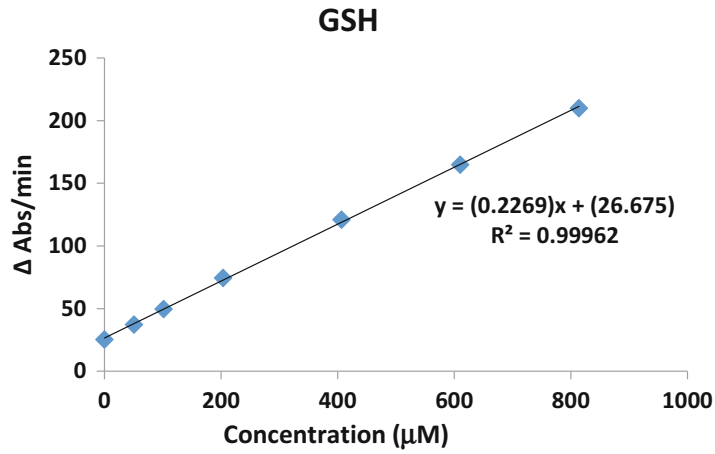


**Fig. 5** Representative GSH standard curve. Trend line and equation are calculated through linear regression analysis using Microsoft Excel Professional Plus 2013

(g) Mix (10 s) and incubate at 37 °C for no more than 2–3 min. Read the absorbance at 415 nm in the plate reader.

10. Calculations: Make a standard curve by plotting concentration of the standards on the *X*-axis, and average absorbance of the replicate measurements on the *Y*-axis. A representative standard curve is shown in (Fig. 5).

11. Using the slope ($m$) generated by the linear portion of the standard curve and the formula $y = mx + b$. Determine average absorbance value of each experimental sample and estimate its concentration by comparison to the standard curve. Importantly, the above calculation will generate the total amount of GSH and GSSG; however, for final concentrations of reduced GSH, the following calculation is required. $\mathbf{[GSH] = GSH_{TOTAL} - 2\,[GSSG]}$.

### 3.3 General Oxidative Activity

1. Seed the β-cells in 6-well plates, $4 \times 10^5$ cells/well, with 1 mL RPMI 1640 (10% FBS). Incubate the plate at 37 °C overnight (*see* **Note 12**).
2. Incubate the cells in the desired experimental conditions.
3. Reconstitute one vial of CM-H2DCFDA (50 μg) as follows: dissolve the lyophilized CM-H2DCFDA with appropriate amount of DMSO to the final concentration of 200 μM (add 432.7 μL of DMSO to one vial of CM-H2DCFDA). Keep it protected from light and on ice until ready to use (*see* **Note 13**).
4. Prepare the working solution of CM-H2DCFDA: dilute the stock CM-H2DCFDA 1:100 (final concentration 2 μM) into phenol red and FBS free DMEM. The total volume of CM-H2DCFDA working solution required is 1 mL per well of 6-well plate. Keep working on ice and protected from light (*see* **Note 14**).
5. Prepare one 15 mL and one 1.5 mL disposable polypropylene tubes for each sample. Warm up the RPMI 1640 (10% FBS) and Trypsin at 37 °C ahead of time.
6. Collect the supernatants of cell culture into individual 15 mL tubes (*see* **Note 15**).
7. Wash the cells with 0.5 mL PBS, then collet the PBS into the same 15 mL tube.
8. Harvest the cells: add 0.25 mL of 0.25% Trypsin, and incubate at 37 °C for 5 min. Stop trypsinization by adding 0.5 mL RPMI (10% FBS). Make sure all the cells are detached by pipetting several times. Collect the cells to the same previous 15 mL tubes.
9. Centrifuge at 500 × *g* for 5 min to precipitate the cells.
10. Wash the cell pellets by resuspending in 5 mL of PBS per tube, and centrifuge again under the same conditions.
11. Discard supernatants and resuspend cells with 1 mL of CM-H2DCFDA working solution. Incubate at 37 °C protected from light for 30 min. Note, the negative control (unstained sample) should be resuspended with 1 mL of phenol red and FBS-free DMEM.

12. Wash the cells with PBS as in **steps 7** and **8** (*see* **Note 16**).
13. Resuspend the cells with 1 mL of DMEM (phenol red and FBS free), and transfer to 1.5 mL tubes. For positive control cells, add 1 U/mL Glucose Oxidase in 1 mL DMEM, and incubate for additional 30 min at 37 °C.
14. Analyze the samples by flow cytometry as follows: (*see* **Note 17**).
15. Set the instrument parameters:
16. CM-H2DCFDA has approximate fluorescence excitation at 492–495 nm and emission at 517–527 nm. Thus, choose channel BL1 with filter range of 515–545 nm (Fluorescein isothiocyanate microscopy (FITC)).
17. Set appropriate gates for the cell population of interest: In the protocol detailed here, we recommend collecting all the cells in the wells, including floating dead cells, and cells in the process of apoptosis. However, the profile of ROS generation is different between living, dead, and apoptotic cells. By forward (FSC) and side (SSC) scatter analysis, it is possible to choose different target populations according to the experimental aims. For instance, if only living cells are wanted, a gate must be set to include only the cell population within typical FSC and SSC values, and exclude dead or apoptotic cells with smaller FSC but larger SSC values (Fig. 6a). Otherwise, a gate can be set to include both populations, and ROS generation analyzed in all cells (Fig. 6b).

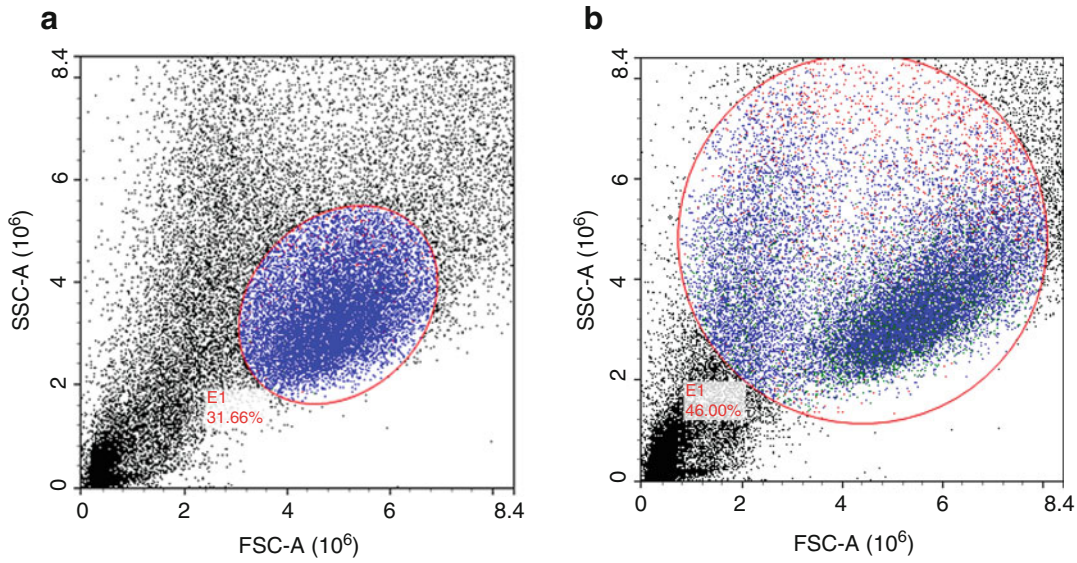


**Fig. 6** FSC/SSC dot plot of palmitate treated BRIN-BD11 cells. (**a**) the gate was drawn to include only living cells. (**b**) the gate was drawn to include both living and dead cells

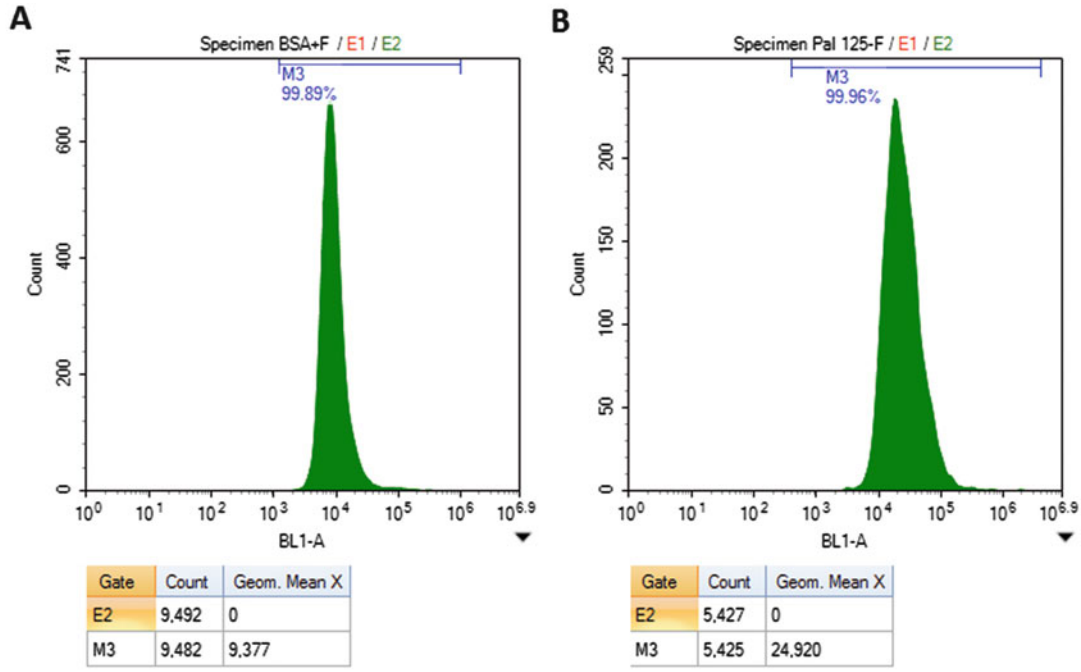


| Gate | Count | Geom. Mean X |
|---|---|---|
| E2 | 9,492 | 0 |
| M3 | 9,482 | 9,377 |

| Gate | Count | Geom. Mean X |
|---|---|---|
| E2 | 5,427 | 0 |
| M3 | 5,425 | 24,920 |

**Fig. 7** Histogram of FITC fluorescence of BRIN-BD11 cells. The *X*-axis indicates fluorescence intensity, and the *Y*-axis indicates cell count. **(a)** cells treated with vehicle (BSA) for 24 h. **(b)** cells treated with 125 μM palmitate for 24 h. Palmitate treatment promoted elevated levels of ROS (Geometric Mean of fluorescence intensity 9377 vs. 24,920 respectively)

18. Data analysis: Collect the data of geometric mean of fluorescence intensity of the gated population (Fig. 7). Geometric mean fluorescence intensity values can be plotted in regular bar plots and an n number of independent samples can be run in order to estimate experimental variability.

## 4 Notes

Measurement of Nitric Oxide Free Radical (NO) Release

1. Prepare a stock solution of 0.1% NED in water by adding 50 mg of NED in 50 mL of water. Store at 4 °C protected from light. Can be stored for at least 6 months.
2. Prepare a stock solution of 1% sulfanilamide in 5% phosphoric acid by adding 500 mg of sulfanilamide in 50 mL of 5% phosphoric acid. Store at 4 °C protected from light. Can be stored for at least 6 months.
3. Prepare a stock solution of 100 mM sodium nitrite in water by adding 69 mg of sodium nitrite in 10 mL of water. Store at 4 °C protected from light. Can be stored for at least 6 months.

4. Distilled water, water which has been treated with a mixed bed ion exchange resin, or ultrapure (17 MW × cm or equivalent) water are considered nitrite-free water and suitable for use. Nitrite-free water should be stored in glass vessels to prevent any possible leaching of $NO_2^-$ compounds from the container.
5. Normally, beta cells are cultured in RPMI 1640 media, supplemented with 10% fetal bovine serum and 100 units/mL penicillin, 0.1 mg/mL streptomycin. Use complete beta cell culture media in order to prepare nitrite standard curve dilution.
6. Experimental samples are the supernatant of beta cells culture media. Beta cells are cultured at the conditions to be tested for NO production and the supernatant of culture media is collected and frozen at −20 °C for subsequent analysis.

Glutathione Redox State Measurement

7. Phosphate buffer 143 mM can be made by mixing 3.1 g of sodium phosphate dibasic heptahydrate ($Na_2HPO_4$ $7H_2O$) and 371.3 mg of sodium phosphate monobasic monohydrate ($NaH_2PO_4 \cdot H_2O$) in 100 mL of distilled water.
8. Samples can be stored at −20 °C for posterior analysis; however, long-term storage is not advised.
9. Samples must be mixed with NEM and Pipes/KOH in the following way. To 50 μL of sample, add 17 μL of NEM and mix with pipette. Then, 10 μL of 2 M Pipes/KOH is added to the wall of the tube at an angle of about 45° without contact with the sample. Once closed, the tube is quickly mixed by vortex.
10. Ethyl acetate washes are necessary in order to remove excess NEM from the samples. This prevents further reactions with GSH molecules that are generated during the GSSG reductase assay recycle.
11. It is recommended to assay all samples and standards in triplicate. In addition, the timing of GSSG reductase activity is crucial for the experimental results. Thus, no more than half of a 96-well plate is recommended for use at any one time.

General Oxidative Status

12. When seeding the cells, in addition to treatment groups, set two wells for both, negative and positive controls. Negative controls are unstained cells (free of probe) to assess autofluorescence from experimental system. A positive control can be

any type definite ROS-inducible interference. For example, 125 μM of palmitate for 24 h can strongly stimulate ROS generation in β-cells, according to our own results. In this protocol, as a positive control, we use glucose oxidase to react with glucose in media to form gluconolactone and $H_2O_2$, and the latter is a strong oxidizing agent for CM-H2DCFDA.

13. Concentrated 200 μM CM-H2DCFDA can be aliquoted, stored, and protected from light at −20 °C. Frozen aliquots must be used within 1 month from reconstitution date.
14. The recommended concentration of the working solution of CM-H2DCFDA is 1–10 μM. In our routine, we use 2 μM.
15. If only living cells are wanted, without the interference of dead and apoptotic cells, discard the supernatant.
16. After treatment with CM-H2DCFDA, protection from light is even more critical since light can induce oxidative reaction.
17. Analyze samples shortly after sample preparation. The fluorescence intensity will decrease with time.

## References


1. Halliwell B (1994) Free radicals, antioxidants, and human disease: curiosity, cause, or consequence? Lancet 344(8924):721–724
2. Tiedge M, Lortz S, Drinkgern J, Lenzen S (1997) Relation between antioxidant enzyme gene expression and antioxidative defense status of insulin-producing cells. Diabetes 46 (11):1733–1742. https://doi.org/10.2337/diabetes.46.11.1733
3. Lenzen S, Drinkgern J, Tiedge M (1996) Low antioxidant enzyme gene expression in pancreatic islets compared with various other mouse tissues. Free Radic Biol Med 20(3):463–466
4. Newsholme P, Cruzat VF, Keane KN, Carlessi R, de Bittencourt PI Jr (2016) Molecular mechanisms of ROS production and oxidative stress in diabetes. Biochem J 473 (24):4527–4550. https://doi.org/10.1042/BCJ20160503C
5. Rabinovitch A, Suarez-Pinzon WL (1998) Cytokines and their roles in pancreatic islet beta-cell destruction and insulin-dependent diabetes mellitus. Biochem Pharmacol 55 (8):1139–1149. https://doi.org/10.1016/S0006-2952(97)00492-9
6. Griess P (1879) Bemerkungen zu der Abhandlung der HH. Weselsky und Benedikt ?Ueber einige Azoverbindungen?? Ber Dtsch Chem Ges 12(1):426–428
7. Krause MS, McClenaghan NH, Flatt PR, de Bittencourt PIH, Murphy C, Newsholme P (2011) L-arginine is essential for pancreatic beta-cell functional integrity, metabolism and defense from inflammatory challenge. J Endocrinol 211(1):87–97. https://doi.org/10.1530/Joe-11-0236
8. Cruzat VF, Keane KN, Scheinpflug AL, Cordeiro R, Soares MJ, Newsholme P (2015) Alanyl-glutamine improves pancreatic beta-cell function following ex vivo inflammatory challenge. J Endocrinol 224(3):261–271. https://doi.org/10.1530/JOE-14-0677
9. Kolberg A, Rosa TG, Puhl MT, Scola G, da Rocha Janner D, Maslinkiewicz A, Lagranha DJ, Heck TG, Curi R, de Bittencourt PI Jr (2006) Low expression of MRP1/GS-X pump ATPase in lymphocytes of Walker 256 tumour-bearing rats is associated with cyclopentenone prostaglandin accumulation and cancer immunodeficiency. Cell Biochem Funct 24(1):23–39. https://doi.org/10.1002/cbf.1290
10. Cruzat VF, Pantaleao LC, Donato J Jr, de Bittencourt PI Jr, Tirapegui J (2014) Oral supplementations with free and dipeptide forms of L-glutamine in endotoxemic mice: effects on muscle glutamine-glutathione axis and heat shock proteins. J Nutr Biochem 25 (3):345–352. https://doi.org/10.1016/j.jnutbio.2013.11.009
11. Akerboom TP, Sies H (1981) Assay of glutathione, glutathione disulfide, and glutathione mixed disulfides in biological samples. Methods Enzymol 77:373–382

# Chapter 15

# Primary Adipocytes as a Model for Insulin Sensitivity

**Mohamed S. Zaibi**

## Abstract

Obesity and its comorbidity insulin resistance lead to the development of chronic metabolic diseases, such as impaired fasted blood glucose and type 2 diabetes. Adipose tissue plays an important role in whole-body glucose homeostasis, particularly in obese individuals; therefore, many in vivo models of type 2 diabetes are obese, such as $Lep^{ob/ob}$ and $Lepr^{db/db}$ mice or ZDF rats. Primary adipocytes therefore represent an attractive in vitro model to study insulin-mediated glucose uptake to investigate the mechanisms of insulin resistance and explore the potential insulin-sensitizing properties of new antidiabetic drugs.

Primary adipocytes are isolated by collagenase digestion of adipose tissue, Glucose transport is evaluated by the measurement of intracellular uptake of a tracer (D-[$U^{14}C$] glucose). The uptake of [U-$^{14}$ C] glucose reflects directly glucose transport.

In this chapter, we will describe the protocol for the isolation of primary rodent adipocytes and the measurement of basal and insulin-stimulated glucose uptake.

**Key words** Primary adipocytes, Collagenase digestion, Insulin sensitivity, Glucose uptake

## 1 Introduction

In the past 20 years, adipose tissue has long been recognized as a site for storage of excess energy derived from food intake; this form of reserve is released during fasting and long-term food deprivation and used as a source of energy [1]. The apparent simplicity of the role of white adipose tissue has been replaced by ever-growing complexity. Indeed, the growth in interest in white adipose tissue has been mainly generated by the increasing concern with obesity-induced insulin resistance and type 2 diabetes and its related complications in public health [2]. Thousands of publications have described the important physiological roles that the adipocytes play in nutrient homeostasis, including appetite, satiety, fatty acid oxidation, and glucose uptake.

Although the exact causes of insulin resistance are yet to be completely understood, the major contributors to insulin resistance are excess weight and physical inactivity. The decrease in insulin sensitivity in target tissues, such adipose tissue is compensated by an

Claire J. Stocker (ed.), *Type 2 Diabetes: Methods and Protocols*, Methods in Molecular Biology, vol. 2076,
https://doi.org/10.1007/978-1-4939-9882-1_15, 

overproduction of insulin from β-cells in the pancreas, which is a fundamental defect that precedes the development of the cluster of abnormalities associated with type 2 diabetes [3–6]. Preventing insulin resistance and/or improving insulin sensitivity appears to be a key factor in the prevention and/or the treatment of type 2 diabetes. Because obesity with or without overt hyperglycemia is associated with insulin resistance [7, 8], and attention has focused on abnormalities in adipose tissue that could lead to decreased insulin sensitivity. Given the important role played by adipocytes in the regulation of systemic energy balance and nutrient homeostasis, it is reasonable to imagine that these cells might be therapeutic targets for metabolic diseases. Primary adipocytes from different adipose tissue depots represent an interesting and relatively simple in vitro model to investigate the underlying mechanisms of insulin resistance, as well as in the research of molecular targets for new insulin sensitizer drugs [9]. Moreover, elucidating such mechanisms will provide new insight into our better understanding of the mechanisms of insulin resistance in vivo.

## 2 Materials

### 2.1 Adipocytes Isolation

1. Forceps.
2. Scissors: one for skin incision, another for removal of fat pads and another to mince the adipose tissue.
3. Krebs-Ringer HEPES (KRH) buffer stock solution (*see* **Note 1**). Make up Krebs/Ringer/HEPES (KRH) buffer in 1liter according to the following.

| | |
|---|---|
| 120 ml NaCl 1 M | (120 mM) |
| 100 ml $NaHCO_3$ 0.1 M | (10 mM) |
| 30 ml HEPES 1 M | (30 mM) |
| 12 ml $MgSO_4$, $7H_2O$ 0.1 M | (1.2 mM) |
| 4.7 ml of KCl 1 M | (4.7 mM) |
| 1.2 ml $KH_2PO_4$ 1 M | (1.2 mM) |

4. Collagenase type II, (*see* **Note 2**).
5. Bovine serum albumin (fraction V).
6. Adenosine.
7. 50 ml polypropylene tubes.
8. 50 ml syringe and tubing.
9. 15 ml polypropylene tubes.

10. Water bath.
11. Stuart SF1 flask shaker, or equivalent.
12. 200–300 μm nylon mesh.
13. Funnel to hold the nylon mesh.
14. 37 °C $CO_2$-incubator.

### 2.2 Glucose Uptake

1. 0.5 ml polyethylene micro centrifuge tubes.
2. Tracer D-[$U^{14}C$] Glucose (ref: NEC042V250UC, PerkinElmer) or equivalent generic with specific activity range 250–360 mCi/mmol and radiochemical purity greater than 97%.
3. Insulin from bovine pancreas.
4. Custom made 37 °C incubator with rotating system and tubes rack holder (Fig. 1).
5. Dinonyl phthalate, (*see* **Note 3**).
6. Refrigerated centrifuge Sanyo Mistral 3000i, or equivalent.
7. −80 °C freezer.
8. Resco guillotine cutter, (Petcetera, UK. Ref: 81243) to cut the tubes http://www.petcetera.co.uk/grooming-preparations-and-tools/nail-care/81243-resco-guillotine-nail-cutter-chrome-small-727.html.
9. 10 ml scintillation vials.

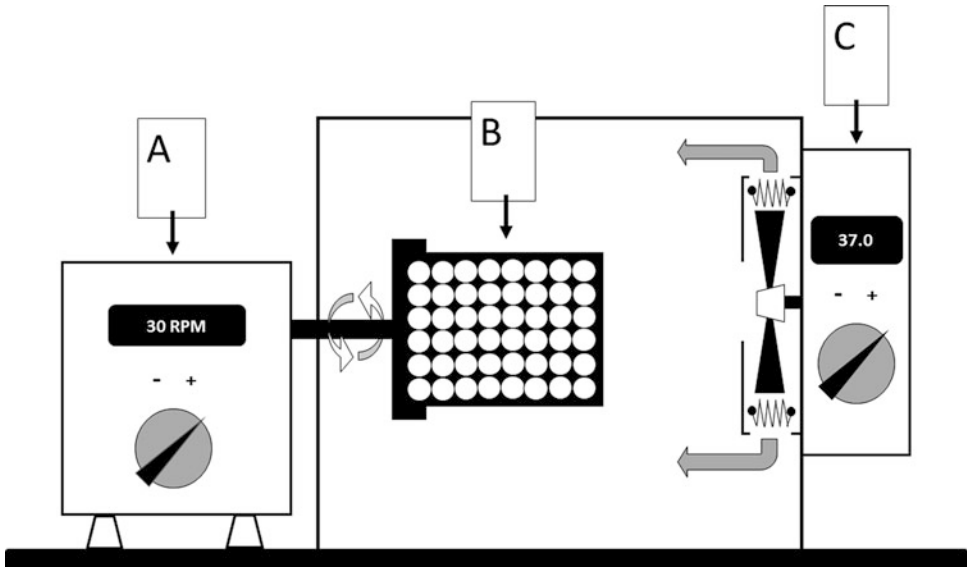


**Fig. 1** 37 °C incubator with rotating system. The 0.5-ml polyethylene microcentrifuge tubes are placed on the rack and incubated at 37 °C for 30 min, under constant rotational movement (30 rpm). Rotating unit (**a**), Clamped rack (**b**), Air flow heating unit (**c**)

10. Vortex mixer.
11. LKB Wallac 1214 RackBeta Liquid Scintillation Counter, or equivalent with a selective window for $^{14}C$.

## 3 Methods

### 3.1 Adipocytes Preparation

Fat cells are prepared from different adipose tissue depots by using the method described previously by Zaibi et al. [10]. Adipose tissue (perigonadal, visceral, or subcutaneous) is minced and digested with collagenase type II in Krebs-Ringer HEPES (KRH) buffer pH 7.4 and 37 °C. Isolated cells are filtered through 250–300 μm nylon mesh, and the floating layer of adipocytes are washed several times with a fresh buffer, then concentrated to 40% of final volume of KRH buffer containing 5% bovine serum albumin (BSA) and 0.3 mM glucose and preincubated for 45 min under 95% $O_2$: 5% $CO_2$.

1. Prepare Prep/Inc. buffers: 500 ml KRH buffer of stock solution containing 1.25 ml $CaCl_2$, 5 g BSA (1%), 0.5 g Glucose.
2. Adjust the pH to 7.4.
3. Split into:
   (a) Preparation buffer 300 ml containing 30 μl of 2 mM adenosine (*see* **Note 4**) to reduce basal lipolysis).
   (b) Incubation buffer 200 ml.
4. Warm both solutions to 37 °C in water bath (*see* **Note 5**).
5. Animals (mice or rats) are euthanized by a method of killing animals that are considered to be acceptable and humane (*see* **Note 6**).
6. Collect the adipose tissue (approximately 5 g) in a 50-ml polypropylene tube containing 30–40 ml of pre-warmed preparation buffer.
7. Weigh the adipose tissue and split into two polypropylene tubes (approximately 2–3 g of adipose tissue/tube), in 6 ml of preparation buffer containing 1.5–2 mg of collagenase/g of adipose tissue.
8. Dice the adipose tissue into small pieces (2–3 mm diameter pieces) is this a note.
9. Incubate at 37 °C in a water bath, under constant shaking (250 cycles/min) until full digestion (approximately 60 min). Gently swirl the tubes every 15 min and check the degree of digestion (*see* **Note 7**).
10. When digestion is complete, adipocytes are separated by filtration through the 200–300 μm nylon mesh and the adipocytes

transferred to a 50-ml polypropylene tube and re-suspended in 40 ml of fresh KRH buffer.

11. Cells are allowed to stand for 2–3 min, and the infranatant is removed by aspiration using a 50-ml syringe (*see* **Note 8**).
12. Wash the floating layer of adipocytes four times by re-suspending the cells in 40 ml of fresh preparation KRH buffer, repeat **step 9**. After each wash, check the purity of the cell suspension (*see* **Note 9**).
13. Wash adipocytes twice with incubation KRH buffer as described previously in **steps 10** and **11**.
14. Transfer the floating layer of adipocytes into 15-ml polypropylene tube.
15. Adipocytes are concentrated to 40% of final volume (e.g., 4 ml of adipocytes in 10 ml of final volume) of incubation KRH buffer, containing 5% BSA and 5.5 mM of glucose, and pre-incubated for 45 min in 95:5% $O_2$:$CO_2$ atmosphere.

### 3.2 Measurement of Glucose Uptake

Glucose transport is measured by the tracer D-[$U^{14}C$] Glucose method. Aliquots of fat cells are incubated at 37 °C for 30 min, with or without insulin in Kreps-Ringer-HEPES buffer containing 5% BSA (fraction V, de Cohn), 0.3 mM glucose and 0.1 μCi/ml of D-[$U^{14}C$] glucose. The reaction is terminated by spinning the cell suspension through dinonyl phthalate. The upper phase which contains fat cells is collected and subjected to liquid scintillation counting. The $^{14}C$-radioactivity associated with the cells directly reflects the glucose uptake by the adipocytes.

1. Add 180 μl to 0.5 ml polyethylene microcentrifuge tubes, of Kreps-Ringer-HEPES buffer containing 5% BSA (fraction V de Cohn), 0.3 mM glucose, and 0.1 μCi/ml of D-[U14C] glucose.
2. Aliquot 20 μl of fat cells (*see* **Note 10**) and add them carefully to each tube.
3. Adipocytes are incubated under gentle rotating movement (30 cycles/min) at 37 °C for 30 min with or without tested compounds (*see* **Note 11**), in the absence or presence of variable concentrations of insulin. *See* example in Fig. 3.
4. After incubation, add 100 μl silicone oil to 400 μl microfuge tubes. Tap to make sure that no air bubbles are present (*see* **Note 12**).
5. Centrifuge the tubes at 3000 × *g* and 4 °C for 15 min.
6. Remove the tubes carefully so as not to disturb the upper phase containing the adipocytes (*see* **Note 13**).
7. Store the tubes overnight in a freezer at −80 °C. At this stage the next steps of the protocol can be delayed (*see* **Note 14**).

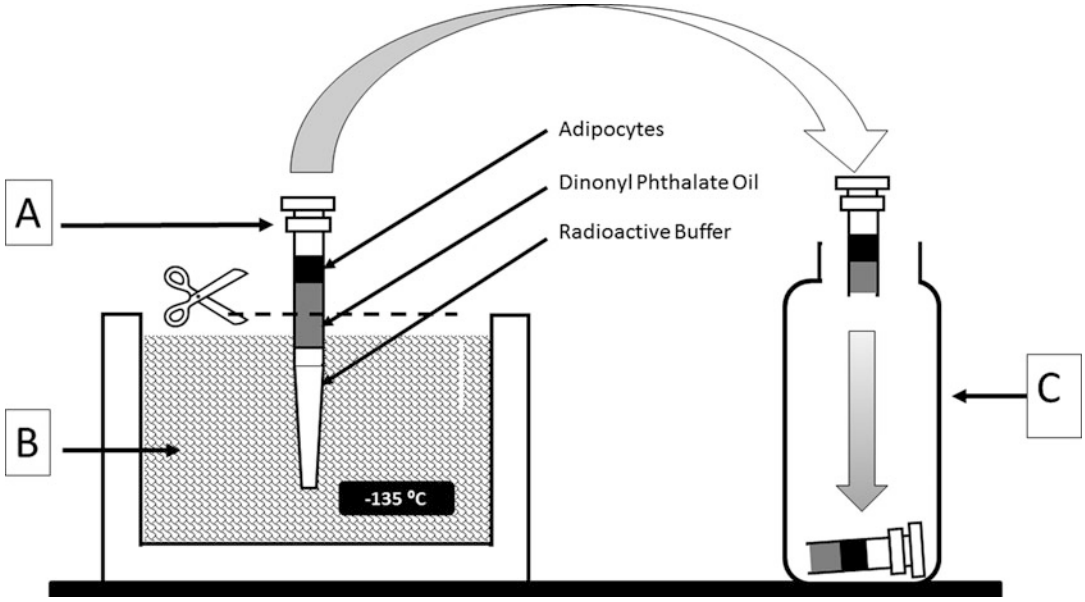


**Fig. 2** Procedure for processing frozen microcentrifuge tubes during the transfer of adipocytes layer into scintillation vials. Frozen microcentrifuge tube (**a**) containing (from top to bottom) radioactive adipocytes, dinonyl phthalate oil and radioactive buffer, container with dry ice (**b**) to maintain the tubes at low temperature, tubes' fraction to be transferred to scintillation vial (**c**)

8. Cut the upper phase which contains adipose cells (Fig. 2), using a small 'Resco guillotine' nail cutter, or a very sharp scissors and transfer it to the scintillation vial (*see* **Note 15**).
9. Add 0.5 ml of distilled water to each vial.
10. To each vial, add 10 ml of scintillation solution Ecosint™ A, or a best equivalent (*see* **Note 16**).
11. Mix each tube for 10–15 s (using the vortex mixer), and leave overnight.
12. Measure samples using the scintillation counter for 300 s.
13. Disintegrations per min (dpm) are recorded and glucose uptake is expressed per mg of total cell protein (*see* **Note 17**).

$$\text{Specific activity (dpm/nmol)} = \frac{\text{Total activity in 180 µl buffer (dpm)}}{\text{Total substrate available in 180 µl buffer (nmol)}}$$

$$\text{Glucose uptake/20 µl of cells (nmol)} = \frac{\left[\text{U}^{14}\text{C}\right] \text{ glucose counts/tube (dpm)}}{\text{Specific activity (dpm/nmol)}}$$

Data are expressed in nmol/mg of total protein measured in 20 µl of adipocytes aliquots.

## 4 Notes

1. Prepare stock solutions 1 M NaCl; 0.1 M $NaHCO_3$; 1 M HEPES; 0.1 M $MgSO_4$, $7H_2O$; 1 M KCl and 1 M $KH_2PO_4$. Make up your KRH buffer stock solution as described in Subheading 2.1, **item 3**; the KRH solutions could be kept at room temperature in the dark.
2. The choice of the type of collagenase is important. Variability exists between lots in the enzyme activity and performance of the type of collagenase used. Collagenase Type II (Sigma) is suitable for adipocytes release. Solutions are typically prepared at 1–2 mg in KRH buffer (3 ml/g of adipose tissue).
3. Dinonyl Phthalate is used to separate adipocytes layer after incubation with KRH buffer containing D-[$U^{14}C$] glucose.
4. The addition of adenosine to the preparation buffer prevents cell breakage and high lipolytic rates during adipose tissue digestion.
5. All the media should be warmed to 37 °C, during the adipose tissue collection, digestion, and for isolated adipocyte incubations and dramatically changing the temperature quickly can shock the cells.
6. There is a Home Office Code of Practice on Humane Killing of Animals linked to Schedule 1 to the Animals (Scientific Procedures) Act 1986**,** which provides the appropriate methods and explains how to ensure that they are carried out competently.
7. The full digestion is achieved when the collagenase solution presents a milky aspect. Collagenase digestion should not be maintained for longer than 60 min, as this reduces adipocytes' viability.
8. The adipocytes are washed by adding gently a fresh media into the tubes, and slowly aspirating the infranatant (below the fat cell layer) using blunt-end needle connected to a syringe.
9. Check the purity of isolated adipocytes suspension, this should have a clear aspect (does not contain stromal vascular fraction, blood cells immune cells, or adipocytes precursors).
10. It is not easy to aliquot a small volume of adipocytes suspension, such as 20 μl, the cells mixture is quiet thick, oily, and sticky; use preferably P200 pipette, and cut the tip to get a volume as exact as possible.
11. The tubes are placed in empty pipette tips rack (the most convenient is P200 rack tips), fixed to the rotating unit by a clamp, and incubated at 37 °C, under a slow rotating movement (30 cycles/min) as described in Fig. 3.

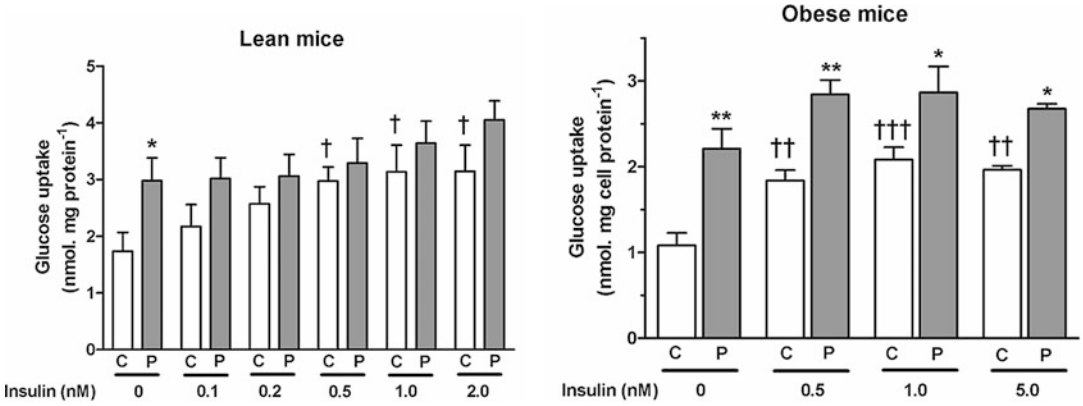


**Fig. 3** Effect of an insulin sensitizer compound (**P**) on glucose uptake in primary adipocytes of female wild-type mice (Lean mice) and insulin-resistant mice model (Obese mice). Adipocytes were treated with insulin, compound **P** (3 μM) alone, or a combination with insulin. $n = 8$ mice per group for all columns. $^{*}p < 0.05$; $^{**}p < 0.01$ for effect of compound P (P) compared to controls at the same concentration of insulin (C). $^{\dagger}p < 0.05$; $^{\dagger\dagger}p < 0.01$; $^{\dagger\dagger\dagger}p < 0.001$ for effect of insulin compared to no insulin at the same concentration of compound P. (Ngala et al. [9])

12. The separation of adipocytes during the centrifugation will not be performed properly if air bubbles are present in the mixture. Make sure that no air bubbles are in the tubes after adding dinonyl phthalate oil.
13. After centrifugation tubes, should be removed and handled very carefully so as not to disturb the adipocytes top layer.
14. At this stage, the microtubes could be stored at −80 °C, the next steps of the experiment could be performed later.
15. Before proceeding with the cells' digestion and measurement of glucose transport in adipocytes, the microtubes should be kept frozen, so as not to disturb the top layer of cells. Take the tubes from −80 °C storage and keep them in dry ice before transferring the top part (containing the cells) to the scintillation vials, the remaining part should go to the *radioactive* waste.
16. Good solvents for liquid scintillation counting are alkylated aromatic organic solvents. The solvent must absorb the energy efficiently, safely, and have low vapor pressure and a high flash point [above 140 °C (nonflammable)]. In case where the scintillation solution Ecosint™ (National Diagnostics) is not available, the Ultima Gold™ cocktails (PerkinElmer Inc.) are an alternative choice for the vast majority of common counting applications.
17. Before incubating adipocytes in KRH buffer containing D-[$U^{14}C$] glucose, keep a few aliquots of 20 μl of cells at −80 °C for the measurement of total protein, using a method based on the Lowry assay (Bio-Rad, Hemel Hempstead, UK).

## References


1. Trayhurn P, Beattie JH (2001) Physiological role of adipose tissue: white adipose tissue as an endocrine and secretory organ. Proc Nutr Soc 60:329–339
2. Bailey CJ (1999) Insulin resistance and antidiabetic drugs. Biochem Pharmacol 58:1511–1520. https://doi.org/10.1016/S0006-2952(99)00191-4
3. Vernon RG, Clegg RA (1985) The metabolism of white adipose tissue in vivo and in vitro. In: Cryer A, Van RLR (eds) New perspectives in adipose tissue: structure, function and development. Butterworths, London, pp 65–86
4. Boden G (2001) Pathogenesis of type 2 diabetes. Insulin resistance. Endocrinol Metab Clin N Am 30:801–815
5. Olefsky JM, Ciaraldi TP, Kolterman OG (1985) Mechanisms of insulin resistance in non-insulin-dependent (type II) diabetes. Am J Med 79:12–22
6. LeRoith D (2002) Beta-cell dysfunction and insulin resistance in type 2 diabetes: role of metabolic and genetic abnormalities. Am J Med 113(Suppl A):3S–11S
7. Ferrannini E (1995) Physiological and metabolic consequences of obesity. Metabolism 44:15–17
8. Walker M (1995) Obesity, insulin resistance, and its link to non-insulin-dependent diabetes mellitus. Metabolism 44:18–20
9. Ngala RA, Zaibi MS, Langlands K, Stocker CJ, Arch JRS, Cawthorne MA (2014) Stimulation of glucose uptake in murine soleus muscle and adipocytes by 5-(4-phenoxybutoxy) psoralen (PAP-1) may be mediated by Kv1.5 rather than Kv1.3. PeerJ 2:e614. https://doi.org/10.7717/peerj.614.
10. Zaibi MS, Stocker CJ, O'Dowd J, Davies A, Bellahcene M, Cawthorne MA, Brown AJ, Smith DM, Arch JR (2010) Roles of GPR41 and GPR43 in leptin secretory responses of murine adipocytes to short chain fatty acids. FEBS Lett 584:2381–2386

# Chapter 16

# Assessing Islet Transplantation Outcome in Mice

**Aileen J. F. King and Chloe L. Rackham**

## Abstract

Islet transplantation is a potential treatment for Type 1 diabetes; however, improvements need to be made before it could become clinically widely available. In preclinical studies, the mouse is often used to model islet transplantation, with most studies aiming to improve transplantation outcome by manipulating the islets prior to transplantation or by treating the recipient mouse. Here, we describe the process of islet transplantation in the mouse, including how one can make the mouse diabetic, isolate donor islets, and transplant the islets into two different sites. Finally, we discuss how to assess the outcome of the transplantation in order to determine whether the experimental intervention has been beneficial.

**Key words** Islet transplantation, Mouse, Islet isolation, Intraportal islet transplantation, Renal subcapsular islet transplantation

## 1 Introduction

Transplantation of islets is a potential treatment for Type 1 diabetes that has clinically been shown to be able to reverse insulin dependence [1]. However, transplantation outcomes in the clinical setting have been disappointing with many patients reverting to insulin dependence [1]. Much effort has been focused upon improving islet transplantations using mouse models. This can involve a variety of strategies and experimental designs. Islets can be manipulated prior to transplantation by encapsulation [2, 3], gene therapy [4, 5] or preculturing with drugs or peptides that may enhance beta cell survival and/or function [6, 7]. Alternatively, the relative importance of particular pathways in islet transplantation outcome can be studied using transgenic [8] or knock-out islets [9]. Islets have been implanted into a variety of sites in the mouse. The most common is the subcapsular site of the kidney, which is chosen for ease of access, ability to easily locate the graft after transplantation and ability to remove the graft by nephrectomy. The intraportal site is the clinically used site and is also used in rodent models although this technique is more invasive and the

Claire J. Stocker (ed.), *Type 2 Diabetes: Methods and Protocols*, Methods in Molecular Biology, vol. 2076,
https://doi.org/10.1007/978-1-4939-9882-1_16, 

graft harder to locate. Two main experimental designs are typically used to demonstrate improved efficacy of an islet graft: minimal mass model or graft survival.

### 1.1 Minimal Mass Models

In minimal mass models, fewer islets are implanted than would be expected to reverse hyperglycemia in all animals [6, 7, 10]. If the intervention has had a positive effect, more animals will become normoglycemic. In mice, implanting between 300 and 500 mouse islets will typically cure all animals. Therefore, the minimal mass chosen is often between 150 and 250 islets which will usually cure around 15–50% of the animals in the control group, depending on site of transplantation, culture period and starting weight of the mice. Due to the large variation in the blood glucose concentrations of mice implanted with a minimal mass number, at least 10–14 mice per group are often required to see an effect.

### 1.2 Graft Survival

Graft survival designs are most useful for allogeneic or xenogeneic transplantations where the intervention intends to prevent or delay immune rejection [2, 5, 11]. In these models, sufficient numbers of islets should be implanted to initially reverse hyperglycemia in all animals. Rising blood glucose concentrations can then be used as an indicator of rejection. In allogeneic mouse models, rejection occurs in control animals around 10–20 days after implantation [2, 5, 11]. Alternatively, the grafts can be harvested at specific time points after implantation to histologically detect rejection by staining immune cell infiltration of the graft [11].

### 1.3 Measurable Outcomes

Prior to transplantation, diabetes can be induced by injection of alloxan [12] or streptozotocin (as described below) [13]. Alternatively, animals developing diabetes spontaneously such as the non-obese diabetic (NOD) or the Akita mouse can be used as islet transplant recipients [14]. Reversal of hyperglycemia is a key outcome of islet transplantation. It is important that blood glucose is measured at the same time every day, preferably first thing in the morning after night feeding, as continuous glucose monitoring in diabetic rodents with an islet graft has shown a substantial diurnal difference in blood glucose concentrations [15]. Although there are no clear guidelines on normoglycemia in mice, our laboratory typically uses a nonfasting blood glucose concentration of less than 11.1 mM on at least three consecutive readings as indicative of normoglycemia. It should be noted that on the day after surgery, the blood glucose concentrations may be artificially low due to leaking of insulin from islets damaged by the transplantation process and reduced appetite in the mouse leading to reduced food intake. It is essential that the weight of the mouse is monitored together with blood glucose concentrations, as it negates any effects on blood glucose due to sickness or reduced appetite. In addition, on an ethical basis, it is undesirable that the mouse loses

considerable weight (>20%). Plasma insulin concentrations can also be measured, but as more blood is needed for those assays, this is not generally measured as frequently as blood glucose concentrations. In cured mice, glucose tolerance tests can be carried out to challenge the grafts further.

### 1.4 Graft Removal

If the islets are implanted below the kidney, a nephrectomy of the graft-bearing kidney can be carried out to demonstrate that the graft is responsible for normoglycemia. After removing the graft, the blood glucose concentrations will rise again if it is indeed the graft that is responsible for maintaining normoglycemia, which helps to rule out endogenous pancreatic beta cell regeneration [2, 10]. In addition, the endogenous pancreas can be analyzed for insulin content or insulin positive cells [16].

#### 1.4.1 Ex Vivo Analysis

Depending on the experimental question, the graft can be histologically analyzed. Usually, the graft remains in situ in the implantation organ. Hormone staining can determine the survival and/or morphology of the islet cells [10], endothelial cell staining can indicate the revascularization process [10], and staining immune cells can indicate the involvement of different cells in rejection [17]. Replication rates of the transplanted islets can be determined by administering 5-bromo-2-deoxyuridine (BrdU) to the rodents prior to killing them, which can then be quantified histologically [18]. Alternatively, Ki-67 staining can detect replicating cells [19].

If more appropriate, the graft can be harvested to measure the insulin content [10], although it should be noted that in diabetic animals, the beta cells will be degranulated so it may not form an accurate basis to determine beta cell mass. There are several steps involved in measuring islet transplantation outcome in mice which will be subdivided into the following sections:

1. Inducing diabetes.
2. Isolation of donor islets.
3. Transplantation of islets (under the renal capsule and intraportally).
4. Posttransplantation monitoring.
5. Graft retrieval.

## 2 Materials

### 2.1 Induction of Diabetes

1. Citrate buffer: Dissolve 0.21 g citric acid in 100 ml saline (0.9% NaCl). Alter the pH to 4.5 and filter through a 0.22 μm filter into a sterile bottle. Store at 4 °C for up to a month or freeze.
2. Streptozotocin solution: Make a 2% streptozotocin solution immediately before injections by dissolving streptozotocin in

citrate buffer (e.g., 5 ml citrate buffer into 100 mg streptozotocin).

3. 1 ml syringes and 27 G needles.

### 2.2 Isolating Islets

1. Suitable cell culture medium for washing the islets (we use Minimum essential medium (MEM)) supplemented with 10% Newborn Calf Serum.
2. Collagenase solution: Collagenase type XI dissolved in serum-free medium (we use MEM) at a concentration of 1 mg/ml. Approximately 2 ml is needed per mouse.
3. Tools for isolating: one large pair of scissors, one large forceps, two small forceps, one small pair of scissors, and one bulldog clamp.
4. Dissecting microscope.
5. 2 ml syringes and 25–30 G needles depending on mouse size.
6. 70% ETOH.
7. Kim wipes.
8. Absorbable paper.
9. Histopaque-1077.
10. Plastic: Sterile 50 ml centrifuge tubes, petri dishes and Eppendorf tubes.
11. Funnel.
12. 10 ml plastic pipettes and autopipettor.
13. 425 micrometer stainless steel mesh.
14. Refrigerated centrifuge with inserts for 50-ml tubes with adjustable settings to allow slow acceleration and brake to be turned off.
15. Phosphate-buffered saline (PBS).
16. Culture medium (RPMI 1640 supplemented with 10% fetal calf serum, 100 U/ml penicillin, and 100 ng/ml streptomycin).

### 2.3 Transplantation of Islets

#### 2.3.1 Renal Subcapsular Islet Transplantation

1. Anesthetic (we use 1–5% isoflurane, 95% oxygen).
2. Analgesic (we use buprenorphine, 30 μg/kg injected subcutaneously).
3. Heating pad.
4. Saline in a syringe to keep kidney moist.
5. Serum-free RPMI 1640 media.
6. Hamilton syringe (500 μl).
7. Razor.
8. Antiseptic skin scrub.

9. 70% alcohol.
10. Centrifuge with 15 ml tube inserts.
11. Tools for operation (per mouse): one scalpel, four small forceps, two small pairs of scissors, drapes, needle holder, suture, 23-G needle and cauterizer.
12. Siliconized PE50 tubing (treated with SigmaCote and gas sterilized).
13. Connector tubing (suitable to connect PE50 tubing to the end of a P200 pipette tip).
14. P200 pipette and tips (+tips cut to fit the end of the Hamilton syringe).

#### *2.3.2 Intraportal Islet Transplantation*

1. Anesthetic (we use 1–5% isoflurane, 95% oxygen).
2. Analgesic (we use buprenorphine, 30 μg/kg injected subcutaneously).
3. Heating pad.
4. Hamilton Syringe (500 μl).
5. Razor.
6. Antiseptic skin scrub.
7. 70% alcohol.
8. 25 G butterfly needle.
9. Tools for operation (per mouse): one scalpel, four small forceps, two small pairs of scissors, alm retractor, Dumont forceps, needle holder, suture, 23 G needle, cauterizer.
10. Drapes.
11. Absorbable hemostatic gelatin sponge (we use Spongostan).
12. Sterile cotton buds.
13. Sterile swabs (we use Topper 8).
14. Sterile saline.
15. Stereo microscope, preferably on an articulated arm.

### *2.4 Posttransplantation Monitoring*

1. Scales.
2. Blood glucose meter and strips.
3. 27 G or 30 G needles.
4. 30% glucose solution.
5. 1 ml syringes and 27 G needles for injection of glucose.
6. Insulin (depending on local ethical guidelines and on advice from a veterinary surgeon).
7. Heparinized glass pipettes with rubber bulb and Eppendorf tubes for collecting blood samples for detection of insulin.

8. Sensitive ELISA to measure insulin in small volume samples (e.g., Mercodia Ultrasensitive Mouse Insulin ELISA).
9. Tools and equipment for operation if graft retrieval by nephrectomy is to be carried out (per mouse): one scalpel, four small forceps, two small pairs of scissors, drapes, needle holder, suture. Anesthetic (e.g., 1–5% isoflurane, 95% oxygen), analgesic (e.g., buprenorphine, 30 μg/kg injected subcutaneously) as advised by veterinarian.
10. Appropriate solution for graft depending on further studies:
    (a) Histology: 4% formalin.
    (b) Graft insulin content: 70% acid alcohol.

## 3 Methods

### 3.1 Inducing Diabetes

We generally induce diabetes 5 days prior to transplantation.

1. Inject the mice immediately after making the streptozotocin solution (*see* **Note 1**).
2. Inject between 150 and 220 mg/kg intraperitoneally into each mouse, depending on mouse strain. For C57Bl/6 mice, use around 180 mg/kg (*see* **Note 2**).
3. Monitor weight and blood glucose of each mouse (*see* **Note 3**).
4. By 5–7 days, the mice should be stably diabetic (blood glucose concentration $> 20$ mM).

### 3.2 Isolating Islets

1. This procedure can be carried out under anesthesia with exsanguination used to kill the mouse at the end of the procedure or alternatively the mouse can be killed prior to the procedure by cervical dislocation.
2. Lay mouse in a supine position and wet the fur with 70% alcohol.
3. Make a large "V" incision in skin and the peritoneum from the pubic region to the front legs to expose liver and intestines.
4. Rotate the mouse with its head toward you; place a lengthways folded Kim wipe on the mouse's chest across the sternum, depress chest and flip back liver on top of tissue using half of the tissue to hold the liver in place to expose posterior-dorsal surface of the liver and the bile duct (*see* **Note 4**).
5. Move the intestines to the right side and gently pull the duodenum distally so the common bile duct can be visualized and is taut.
6. Clamp duodenum at the Vater's ampulla where the common bile duct empties into the duodenum (*see* **Note 5**).

7. Inject 2–2.5 ml of collagenase into the duct to expand the pancreas using a bent (90°) 27 G or 30 G needle and 2 cc syringe (*see* **Note 6**).
8. Detach the duct from the intestine using forceps, and then carefully remove the inflated pancreas. Handle the pancreas as little as possible to avoid leakage of the collagenase.
9. Place the pancreas in a 50 ml conical plastic tube on ice. Up to four pancreata can be added to a single tube prior to incubation/digestion. It should take less than an hour to finish all the mice.
10. Place the tubes containing the pancreata in a 37 °C water bath for 10 min (depending upon the activity of the collagenase).
11. After the incubation, add 25 ml of ice-cold wash medium to stop the reaction.
12. Vigorously shake tube or vortex for 10 s.
13. Centrifuge for 300 G for 1 min and 15 s.
14. Discard the supernatant and resuspend the pellet in 25 ml wash medium (may need to gently shake to resuspend the pellet).
15. Centrifuge for 300 G for 1 min and 15 s.
16. Repeat wash **step** (**14** and **15**) twice.
17. After resuspending the pellet in 25 ml wash buffer, filter the digest through a 425 μm stainless steel mesh into a new 50 ml tube using a funnel. This will remove any undigested tissue.
18. Centrifuge at a higher speed of 340 G for 1 min and 30 s.
19. In one movement, turn the tube upside down to discard the supernatant and with the tube still inverted place on absorbent paper to soak up excess media (the pellet should be as dry as possible). If necessary, you can also remove drops of MEM from tube with a Kim wipe.
20. Resuspend the pellet in 15 ml Histopaque 1077 by vortexing.
21. Carefully, add 10 ml of wash medium by pipetting down the sides of the tube so as not to mix with the Histopaque. There should be a clear interphase between the histopaque and medium.
22. Centrifuge at 1950 RCF for 24 min with slow acceleration and no brake in a refrigerated centrifuge at 10 °C (*see* **Note 7**).
23. Remove islets at the interface using a 10 ml plastic pipette and autopipettor (*see* **Note 8**).
24. Place the islets in a new 50 ml tube and fill up to 50 ml with wash media.
25. Centrifuge at 340 G for 1 min 30 s and remove the supernatant (*see* **Note 9**).

26. Add wash medium up to the 25 ml mark. This in itself will disrupt the pellet so further shaking is not necessary.
27. Repeat this wash step twice.
28. If the islets are contaminated with exocrine tissue, sedimentation stages can be carried out for further purification. If the islets look pure, proceed to **step 30**.
29. Resuspend the islets in 25 ml total media and let them sit for 4 min on ice. Remove the top 10 ml and add 10 ml new media. Repeat four times to further purify the islets.
30. Pellet the islets and resuspend in 10 ml media.
31. Place into petri dish (do not use a coated-tissue culture plate).
32. If islets are to be transplanted immediately, pick them into an Eppendorf tube using a 200 μl pipette and keep on ice or to place in culture follow **steps 33–39**.
33. In a hood, swirl the petri dish, in a circulation motion to coalesce islets in the center. Using the microscope and a 200-μl pipettor, pick the desired number of islets into an Eppendorf tube containing 1 ml of culture medium.
34. Centrifuge using a low speed mini-centrifuge to pellet islets.
35. Wash the islets (resuspend/pellet/remove supernatant) twice with cold sterile PBS.
36. After the last centrifuge, remove the PBS and add 1 ml of culture medium (RPMI 1640 supplemented with 10% fetal calf serum and antibiotics) into the Eppendorf tube with islets.
37. Add 4 ml culture medium into a sterile 60-mm petri dish.
38. Pipette the islets into the petri dish; wash the tube with 1 ml borrowed from the plate to recover all islets.
39. Incubate at 37 °C 5% $CO_2$. A petri dish containing 5 ml media should contain a maximum of 200 islets. Change the media every 48 h.

### *3.3 Transplantation of Islets*

#### *3.3.1 Transplantation of Islets Under the Kidney Capsule*

1. Anesthetize the mouse with isoflurane or another appropriate anesthetic.
2. Shave the fur on the left flank and treat the skin with surgical scrub, followed by 70% alcohol.
3. Administer the analgesic and lay the mouse on a heat pad.
4. Lay drapes over the mouse, with the operation area exposed and check if the mouse is adequately anesthetized (for example, by lack of reaction to a paw pinch).
5. While the mouse is getting anesthetized, prepare the islets. This is ideally carried out by a second person as the islets should be prepared in parallel so they are ready for implantation at the same time as the mouse kidney is externalized.

(a) Allow islets to settle to the bottom of an Eppendorf tube.

(b) Fill the Hamilton syringe with serum-free media and attach a 200-μl pipette tip (the top of which may need to be cut to fit the Hamilton syringe).

(c) Using the plunger, push medium into the tip so that there is no air in the syringe or tip.

(d) Aspirate the islets into the tip and keep vertical to allow to islets to settle, pull up a small amount of air to prevent islet loss from the tip.

(e) Attach the siliconized and sterilized PE50 tubing to the pipette tip using a 0.5 cm piece of larger connecting tubing to fit the bottom of the pipette tip.

(f) Inject the islets about 10 cm into the PE tubing using the plunger.

(g) Fold the PE tubing back on itself just in front of the islet pellet and use a 1 cm piece of connector tubing to hold it in place.

(h) Remove the pipette tip with the PE tubing attached and centrifuge for 2 min at 200 G. The tubing can be kept in place using the cut outer case of a 1-ml syringe within a 15-ml centrifuge tube.

(i) Screw the plunger of the Hamilton Syringe into place.

(j) After the centrifugation, top up the pipette tip with medium so that it can be reattached to the Hamilton syringe without any air bubbles, the islet pellet should be visible just above the connector tubing (Fig. 1).

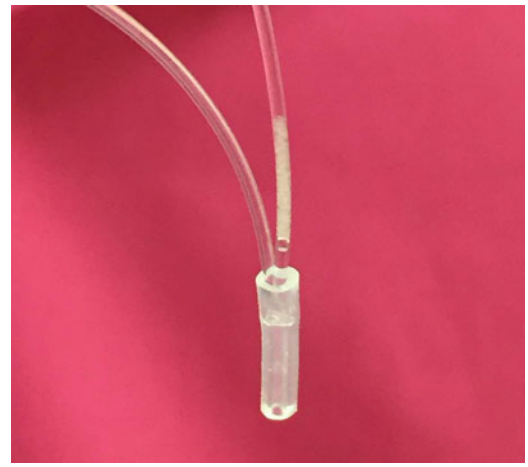

**Fig. 1** Pelleted islets in the PE50 tubing ready for transplantation. To transplant, remove the connector tubing carefully and cut a bevel just in front of the islet pellet

(k) Carefully, remove the connector tubing at the bend of the PE50 tubing, where the islets should have pelleted.

(l) Cut the PE50 tubing close to the islet pellet as a 45° angle.

(m) Turn the plunger so that the islets are at the opening of the PE50 tubing.

6. Using a scalpel, make a 1.5–2 cm incision in the skin and using scissors, cut a 1-cm incision in the peritoneum over the left kidney.
7. Externalize the kidney by gently pressing under each side of the kidney to allow it to pop out.
8. Make an incision in the kidney capsule at the bottom quarter by scoring the capsule surface using a 23-G needle.
9. Keep the capsule moist with sterile saline.
10. Using Dumont forceps, gently lift the kidney capsule and insert the PE tubing containing the islets under the capsule.
11. Push the tubing up into the top quarter of the kidney and using the Hamilton syringe carefully inject the islets into the subcapsular space using the screw function.
12. Once the islets have been injected into the subcapsular space, remove the tubing and cauterize the incision.
13. Pull up on the peritoneum around the kidney so that the kidney falls back into place.
14. Suture the peritoneum and suture the skin.
15. Monitor the recovery of the mouse.

### *3.3.2 Islet Transplantation Intraportally*

1. Anesthetize the mouse with isoflurane or another appropriate anesthetic.
2. Place the mouse in the supine position and shave the abdomen of the mouse and treat the skin with surgical scrub, followed by 70% alcohol.
3. Administer analgesic and lay the mouse on a heat pad with its paws taped down to retain the position of the mouse.
4. Lay drapes over the mouse, with the operation area exposed and check the mouse is adequately anesthetized.
5. In parallel to the operation, the islets should be prepared, ideally by a second person so that they are ready for implantation at the correct time point.

   (a) Fill a Hamilton Syringe with serum-free medium and attach to a butterfly needle (25 G).

   (b) Push the plunger to fill the tubing of the butterfly needle with media.

(c) Aspirate the islets into a Butterfly needle.

(d) Make sure that the islets are a few cm up into the tube before screwing in the plunger.

(e) Keep the tubing vertical to allow the islets to sediment to the bottom of the tube, but keep the needle perpendicular to stop the islets entering the needle until ready for the transplantation.

(f) Immediately prior to the transplantation, screw the syringe carefully until media appears at the needle opening.

6. Using a scalpel, make an approximately 3-cm incision in the skin and then use scissors to make a 3-cm incision in the peritoneum from just above the xiphysternum. Use an alm retractor to open up the abdomen.
7. Place a sterile saline-soaked swab over the right arm of the alm retractor extending over to also cover the skin of the mouse. Use a thin strip of saline-soaked swab (approximately 2 cm) to ensure that the upper lobe of the liver is arranged in the appropriate position so that the portal vein is not blocking access to the portal vein.
8. Using saline-infused cotton buds, carefully move the intestines onto the saline-soaked gauze to expose the intraportal vein. Keep the intestines moist with saline and cover with a saline-soaked swab, which also runs over the tissue next to the portal vein and is pulled slightly downwards to help make the vein taut and helping to place the portal vein in a suitable position for implantation of the islets as seen in Fig. 2.

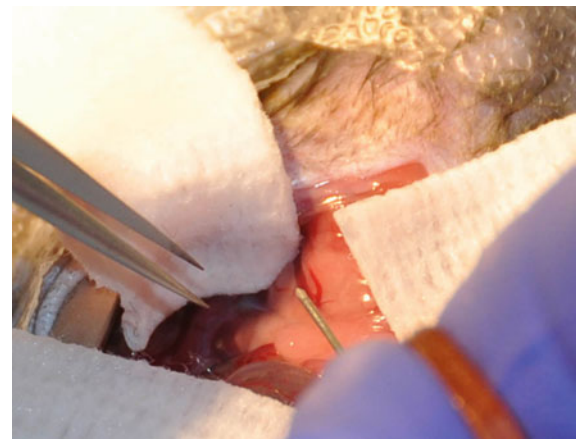

**Fig. 2** The correct position of the portal vein prior to intraportal transplantation. Note the swab to the right is slightly pulling the tissue into the correct position

9. Using fine forceps grip the tissue adjacent (operators left hand side) to the portal vein and cannulate the portal vein.
10. Carefully inject the islets in a volume of approximately 200 μl by using the screw function of the Hamilton Syringe.
11. Prior to removing the needle from the vein, apply spongostan gel foam to the point of needle entry using Dumont forceps to pick up the precut small square of spongostan and ensuring that the foam is placed flat over the vein to prevent excess loss of blood (*see* **Note 10**).
12. Applying some pressure to the Spongostan using a dry cotton bud, remove the needle and hold the Spongostan in place for approximately 2 min.
13. After removing pressure from the Spongostan, observe the vein to check that there is no bleeding.
14. Leaving the Spongostan in place, carefully remove gauze swabs and gently replace the intestines into the peritoneal cavity (using soaked cotton buds).
15. Sew the peritoneum cavity.
16. Sew the skin.
17. Allow the mouse to recover and monitor closely.

### *3.4 Posttransplantation Monitoring*

#### *3.4.1 Blood Glucose Monitoring*

1. Blood glucose concentrations and weight together can indicate glycemic control and should initially (for the first week) be measured daily (*see* **Note 11**).
2. Using a 27-G or 30-G needle, make a small pin prick at the end of the tail.
3. Apply a small amount of pressure to the tail proximal to the pinprick and slide fingers toward the pinprick to form a droplet of blood.
4. Apply the blood drop to a blood glucose meter. Typically, less than 5 μl is required for most meters.
5. If excessive weight loss is evident, insulin can be administered to comply with local ethical requirements.

#### *3.4.2 Intraperitoneal Glucose Tolerance Test*

1. Fast mice for at least 6 h (*see* **Note 12**).
2. Measure blood glucose as described above.
3. Inject 2 g/kg glucose solution in saline (30% glucose) intraperitoneally.
4. Measure blood glucose 15, 30, 60, 90, and 120 min after injection.

#### 3.4.3 Serum Insulin

1. Fasting, nonfasting or glucose-induced plasma insulin concentrations can be measured.
2. Using a 27 G or 25 G needle, prick the end of the tail.
3. Apply pressure to form as large a blood drop as possible and use a heparinized capillary tube to collect blood by capillary action. Use a rubber bulb to inject the collected blood into a 0.5-ml Eppendorf tube on ice.
4. Repeat until the required volume is collected.
5. Centrifuge blood samples within 1 h at 1500 G at 4 °C for 10 min. Aspirate the serum and freeze at −20 °C for later analysis.
6. Insulin can be measured in small serum volumes (5–10 μl) using ELISA.

### 3.5 Graft Retrieval

#### 3.5.1 Nephrectomy to Confirm the Role of the Graft on Glycemia

1. Anesthetize the mouse with isoflurane or another appropriate anesthetic.
2. Shave the fur on the left flank and treat the skin with surgical scrub, followed by 70% ethanol.
3. Administer analgesic.
4. Lay drapes over the mouse, with the operation area exposed and check the mouse is adequately anesthetized.
5. Using a scalpel, make a 1.5–2 cm incision in the skin and using scissors cut a 1-cm incision in the peritoneum over the left kidney.
6. Use scissors to free the kidney from surrounding tissues (being very careful not to cut the renal artery or vein).
7. Externalize the kidney.
8. Clamp the renal artery, renal vein and ureter close to the kidney with a hemostatic clamp.
9. Use a scalpel to cut the kidney free. Place the kidney into appropriate solution for analysis (e.g., formalin for histology or acid alcohol for insulin content detection).
10. Ligate the renal artery, renal vein and ureter by tying two to three times with suture.
11. Remove the hemostatic clamp and monitor whether there is any bleeding (*see* **Note 13**).
12. Suture the peritoneum and suture the skin.
13. Monitor the recovery of the mouse.
14. Measure blood glucose daily until stable hyperglycemia has been reached (at least three consecutive days of blood glucose concentrations greater than 20 mM). The mouse should then be killed and if necessary, the pancreas removed for analysis.

*3.5.2 Graft Retrieval When Confirmation of Hyperglycemia Is Not Required*

1. If confirmation of return to hyperglycemia is not required or not relevant (e.g., in mice that have not become normoglycemic), the graft can be retrieved after the mouse is killed by cervical dislocation.
2. Remove the graft-bearing organ (liver or kidney) as soon as possible after the mouse is killed and place as soon as possible in the appropriate solution for analysis. The pancreas may also be removed for analysis if appropriate.
3. Alternatively, the mouse can be terminally anesthetized and the kidney removed (*see* **Note 14**).

## 4 Notes

1. Make sure that all mice are weighed and marked, with the dose for each mouse calculated, prior to mixing the streptozotocin with the citrate buffer to allow injection as soon as possible after reconstitution (we generally try to inject all mice within 10 min of making the streptozotocin [20]).
2. The dose may need to be adjusted due to variation in the streptozotocin lot and/or mouse strain [20, 21]. As glucose directly competes with streptozotocin, fasting the mice may increase percentage of mice from becoming diabetic.
3. Depending on your local ethical guidelines, mice may require to be treated by insulin (we use 2–3 units daily of Caninsulin) to prevent too much weight loss (more than 15% within 3 days or more than 20% overall). If weight loss exceeds this, mice should be killed. Cages will need to be changed more regularly due to polyuria. In addition, water supply should be checked daily as the mice will drink considerably more than normal. If mice do not become diabetic, they can be re-injected again with streptozotocin (although it is recommended that this is only done once).
4. It is easier to flip the liver back if you clip off the xiphysternum.
5. Clamping should be carried out with precision; if the clamping is not adequate, collagenase will leak into the duodenum. If the clamp is too far down the pancreas, some ducts will be occluded and thus the pancreas will not be fully inflated.
6. The connective tissue around the duct can be gently removed by running the forceps up and down around the duct. This allows the duct to be easily visualized. The forceps can also be placed under the duct to form a support for injection. When getting trained in the technique, it is desirable to initially inject as closely as possible to the liver end of the duct, allowing the entire length of the duct to be recannulated if first attempts are initially not successful.

7. A slow acceleration and no brake on the centrifuge setting prevent the histopaque from mixing with the media during the centrifugation stage.
8. Islets should be collected from the histopaque gradient as soon as the centrifugation has been finished to reduce exposure, as histopaque is toxic to islets.
9. Note that at this stage the pellet is usually not as stable, so rather than just pouring out the supernatant, it is suggested to pipette it out leaving about 5 ml left at the bottom of the tube.
10. Spongostan should be split into half layers before starting the operation to make sure that they are not too thick. A second piece of Spongostan can be applied if the operator is concerned that there may be excess blood loss. It is important that the Spongostan and cotton bud used to apply pressure are dry, allowing optimal absorption.
11. After the first week, blood glucose concentrations can be measured less frequently as the mouse is stable and not showing decline in weight. If the mouse is losing weight and/or is overtly diabetic then they should continue to be monitored daily.
12. Although many laboratories fast mice overnight prior to a glucose tolerance test, it has been suggested that this is too long and induces metabolic stress [22].
13. Before releasing the clamp, keep hold of the suture that was used to ligate the vessels and the ureter. If bleeding is evident on releasing the clamp, reclamp below the suture and repeat the ligation.
14. In diabetic mice, the graft degranulates, making it more transparent and therefore more difficult to identify. If the mouse is terminally anesthetized, the graft can be easily identified while there is still blood circulation. In addition, it is helpful to note the position of the graft at the time of transplantation.

## References


1. Bruni A, Gala-Lopez B, Pepper AR, Abualhassan NS, Shapiro AJ (2014) Islet cell transplantation for the treatment of type 1 diabetes: recent advances and future challenges. Diabetes, Metab Syndr Obes 7:211–223
2. Zhi ZL, Kerby A, King AJ, Jones PM, Pickup JC (2012) Nano-scale encapsulation enhances allograft survival and function of islets transplanted in a mouse model of diabetes. Diabetologia 55:1081–1090
3. Kerby A, Bohman S, Westberg H, Jones P, King A (2012) Immunoisolation of islets in high guluronic acid barium-alginate microcapsules does not improve graft outcome at the subcutaneous site. Artif Organs 36:564–570
4. Estil les E, Tellez N, Escoriza J, Montanya E (2012) Increased beta-cell replication and beta-cell mass regeneration in syngeneically transplanted rat islets overexpressing insulin-like growth factor II. Cell Transplant 21:2119–2129
5. Fernandes JR, Duvivier-Kali VF, Keegan M et al (2004) Transplantation of islets transduced with CTLA4-Ig and TGFbeta using

adenovirus and lentivirus vectors. Transpl Immunol 13:191–200

6. King A, Lock J, Xu G, Bonner-Weir S, Weir GC (2005) Islet transplantation outcomes in mice are better with fresh islets and exendin-4 treatment. Diabetologia 48:2074–2079
7. McCall M, Toso C, Emamaullee J et al (2011) The caspase inhibitor IDN-6556 (PF3491390) improves marginal mass engraftment after islet transplantation in mice. Surgery 150:48–55
8. King AJ, Guo Y, Cai D et al (2013) Sustained NF-kappaB activation and inhibition in beta-cells have minimal effects on function and islet transplant outcomes. PLoS One 8:e77452
9. Toso C, Serre-Beinier V, Emamaullee J et al (2008) The role of macrophage migration inhibitory factor in mouse islet transplantation. Transplantation 86:1361–1369
10. Rackham CL, Chagastelles PC, Nardi NB, Hauge-Evans AC, Jones PM, King AJ (2011) Co-transplantation of mesenchymal stem cells maintains islet organisation and morphology in mice. Diabetologia 54:1127–1135
11. Pawlick R, Gala-Lopez B, Pepper AR, McCall M, Ziff O, Shapiro AM (2014) The combination of anti-NKG2D and CTLA-4 Ig therapy prolongs islet allograft survival in a murine model. Am J Transplant 14:2367–2374
12. Bohman S, Andersson A, King A (2006) No differences in efficacy between noncultured and cultured islets in reducing hyperglycemia in a nonvascularized islet graft model. Diabetes Technol Ther 8:536–545
13. Deeds MC, Anderson JM, Armstrong AS et al (2011) Single dose streptozotocin-induced diabetes: considerations for study design in islet transplantation models. Lab Anim 45:131–140
14. King A, Bowe J (2016) Animal models for diabetes: understanding the pathogenesis and finding new treatments. Biochem Pharmacol 99:1–10
15. King AJ, Austin AL, Nandi M, Bowe JE (2016) Diabetes in rats is cured by islet transplantation... but only during daytime. Cell Transplant 26(1):171–172
16. Mathews CE, Langley SH, Leiter EH (2002) New mouse model to study islet transplantation in insulin-dependent diabetes mellitus. Transplantation 73:1333–1336
17. Hong J, Yeom HJ, Lee E et al (2013) Islet allograft rejection in sensitized mice is refractory to control by combination therapy of immune-modulating agents. Transpl Immunol 28:86–92
18. Krautz C, Wolk S, Steffen A et al (2013) Effects of immunosuppression on alpha and beta cell renewal in transplanted mouse islets. Diabetologia 56:1596–1604
19. Chen X, Zhang X, Chen F, Larson CS, Wang LJ, Kaufman DB (2009) Comparative study of regenerative potential of beta cells from young and aged donor mice using a novel islet transplantation model. Transplantation 88:496–503
20. Leiter EH, Schile A (2013) Genetic and pharmacologic models for type 1 diabetes. Curr Protoc Mouse Biol 3:9–19
21. Sakata N, Yoshimatsu G, Tsuchiya H, Egawa S, Unno M (2012) Animal models of diabetes mellitus for islet transplantation. Exp Diabetes Res 2012:256707
22. McGuinness OP, Ayala JE, Laughlin MR, Wasserman DH (2009) NIH experiment in centralized mouse phenotyping: the Vanderbilt experience and recommendations for evaluating glucose homeostasis in the mouse. Am J Phys Endocrinol Metab 297:E849–E855

# Chapter 17

# Measurement of Insulin Secretion Using Pancreas Perfusion in the Rodent

**Edward T. Wargent**

## Abstract

Under in vivo conditions, the study of physiological and pharmacological functions of an organ is difficult due to whole-body interactions with the organ. Thus, an in vitro technique for the perfusion of isolated pancreata was developed for physiologic and response studies including the investigation of endocrine function and secretory responsiveness under a variety of diabetes-associated conditions. The pancreas is isolated from the connecting spleen, stomach, and duodenum and transferred to a pre-warmed chamber where it is perfused in isolation from all other organs. A detailed description of the isolation of pancreata from rats and mice and the perfusion apparatus is described, as well as the measurement of glucose-stimulated insulin secretion using an in-house-developed radioimmunoassay.

**Key words** Pancreas, Perfusion, Insulin, Radioimmunoassay

## 1 Introduction

In vivo, the study of physiological and pharmacological functions of an organ is difficult due to whole-body interactions with the organ. However, during perfusion, the respective organ is isolated from these interactions and placed under relatively simple experimental conditions, approximating the normal state, thereby facilitating physiological measurements. The pancreas perfusion method is therefore ideally suited for mechanistic studies examining the effects of secretagogues and pharmacological agents.

In contrast to studies looking at secretagogue responses in isolated islet preparations, the isolated whole pancreas perfusion method allows for the study of both endocrine and exocrine tissue function simultaneously as this procedure maintains physiological integrity at both cellular and whole organ levels. There is also a possibility of a control and experimental period of study in the same pancreas preparation. Such control in other in vitro settings requires multiple incubations. Factors affecting insulin secretion are of great importance in the study of type 2 diabetes, and the

Claire J. Stocker (ed.), *Type 2 Diabetes: Methods and Protocols*, Methods in Molecular Biology, vol. 2076,
https://doi.org/10.1007/978-1-4939-9882-1_17, 

isolated pancreas is an invaluable technique of studying insulin secretion from the whole pancreas. The perfused pancreas can also be used to evaluate the effects of drugs and secretagogues that effect pancreatic function. For example, amylin, a protein secreted by the pancreas and a major constituent of islet amyloid deposits in patients with type 2 diabetes, while having no effect on glucose-stimulated insulin secretion, significantly inhibits arginine-stimulated insulin secretion.

The rodent is anesthetized by an appropriate means and both a lateral and midline incision made to expose the stomach, intestines, and mesenteric blood vessels. The pancreas is carefully separated from the overlaying colon, spleen, and connective tissues. The jejunum and its blood supply are ligated so that this distal section can then be removed. All other attachments of the pancreas to the descending colon are then ligated and cut, as are the splenic vessels. Once the mesenteric artery and celiac axis have been identified, the stomach is moved aside and the exposed esophagus and gastric artery are also ligated. The pancreas is isolated from the stomach following ligation of the duodenum and the vascular connections on the posterior wall exposed, which can then be ligated subsequently. By careful dissection, the aorta can be exposed, cleared from the inferior vena cava between the renal artery and superior mesenteric artery, and ligated. Loose ligatures are placed around the hepatic portal vein where it leaves the pancreas for the liver. Once the celiac and mesenteric branches have been identified along the aorta, the aorta can be freed from the vena cava to the ligature below the renal artery. Loose ligatures are positioned around the aorta just below the diaphragm preserving the origin of the celiac artery, which holds the inlet cannula, while the outlet cannula is placed in the portal vein. Once the abdominal aortic ligature is tightened, the pancreatic circulation can be completely isolated by tightening the ligature around the lower vena cava and perfusion can commence.

Based on the original apparatus used by [1], perfusate is pumped from a reservoir by means of a peristaltic pump, into an enclosed organ perfusion chamber, and enters the pancreatic circulation through the celiac arterial cannula. The pancreas is kept moist with normal saline and perfused using a modified Krebs-Ringer bicarbonate-buffered solution containing glucose and bovine serum albumin. The production of insulin by the preparation reflects its responsiveness to glucose and other secretagogues and can be collected by means of perfusate via the portal vein.

This methodology has been applied to a range of investigations studying pancreatic function with relation to diabetes covering physiological functionality in response to endogenous compounds such as nutrients (e.g., glucose-induced insulin, somatostatin, and orexin-A secretion) or the effects of fatty acids or hormones (e.g., amylin, GLP-1, and orexin-A) on the stimulation of insulin release,

the inhibition of glucagon secretion or the leptin inhibition of basal insulin release [2–5]. The prediabetic state or diabetic state may be investigated using rodent models such as the Zucker fatty (*fa/fa*) or Zucker diabetic fatty (ZDF) rats. Furthermore, the isolated perfused pancreas is also a useful method for investigating potential therapeutic candidates, most notably those designed to enhance insulin secretion, such as the GLP-1 receptor antagonists [6].

This chapter describes in detail the ex vivo perfusion technique for the rodent pancreas and has been updated from the previous edition to include specific materials and methods required for both rats and mice (although it should be noted that because of the complexities of scale the technique in mice has a higher variability and generally requires a higher number of perfusions per group than rat studies). When regarding the 3Rs, it is therefore preferable to preform studies in rats when possible. It presents a detailed description of the perfusion technique, a study of some of the functions of the preparation and an observation of the pancreatic response to glucose as an example of secretagogue stimulation of insulin secretion. The development of sensitive radioimmunoassays of biological fluids has enabled the quantitative measurement of hormone secretion using pancreas perfusion techniques. This chapter will also describe the important salient features and optimization stages required to develop an in house radioimmunoassay for use with this methodology.

## 2 Materials

### 2.1 Pancreas Excision

1. Anesthetic and analgesic regime capable of maintaining a level of anesthesia suitable for major surgery for 40 min, for example, isoflurane (*see* **Note 1**).
2. Blunt-nosed straight-dissecting scissors 14–15 cm (FST, cat # 14000-14) (*see* **Note 2**).
3. Standard pattern forceps 14–15 cm (FST cat # 11000-14).
4. Blunt-nosed curved-dissecting scissors 14–15 cm (FST cat # 14003-14).
5. Straight hemostat 14 cm (FST cat# 13004-14).
6. Saline: 0.9% $NaCl_{(aq)}$.
7. Black-cotton thread cut into approximately 10 cm lengths.
8. Pair of curved-eye dressing forceps 10 cm (FST cat # 11051-10).
9. Blunt-nosed straight dissecting scissors 10 cm (FST cat # 14078-10).
10. Cotton buds.
11. Pair of serrefines 35 mm (FST cat # 18051-35).

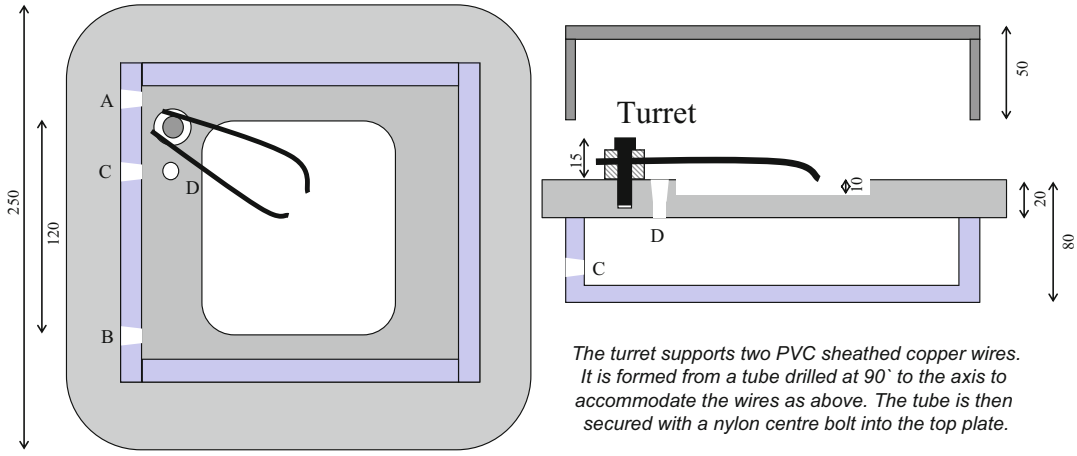


**Fig. 1** Perfusion tank setup. The sheathed copper wires are attached to the two cannulae that are connected to the celiac artery and hepatic portal vein. The pancreas is housed in the central pool surrounded by perfusion buffer. (**a**) inlet and (**b**) outlet for heated water keeps the central pool at 38 °C. (**c**) inlet and (**d**) outlet for tubing transporting the perfusate travels through the heated water re-heating it to perfusion temperature. All dimensions are expressed in millimeters

12. Sharp straight spring scissors 10 cm (FST cat # 15024-10).
13. Polyethylene tubing with a bore of 0.5 mm, wall 25 mm (800/100/160, Scientific Laboratory Supplies, Nottingham, UK, cat # TUB3660).
14. 2.5-ml syringe and needle.

### *2.2 Pancreas Perfusion*

1. Perfusion tank (*see* Fig. 1).
2. 20-ml glass scintillation vials and silicon caps.
3. Water bath.
4. Silicone tubing (Scientific Laboratory Supplies, Nottingham, UK).
5. Three-way male lock stopcocks (Cole-Palmer, Illinois, USA).
6. Water heater/pump.
7. Peristaltic pump.
8. Manometer.
9. Sample collector.
10. Electronic thermometer.
11. Oxygen: carbon dioxide (95:5) cylinder.
12. Perfusion buffer: (5.7 mM KCl, 1.5 mM $KH_2PO_4$, 113 mM NaCl, 1.2 mM $MgSO_4$, 2.3 mM calcium gluconate, 25 mM $NaHCO_3$, 3% (w/v) dextran T40, 1% human albumin, pH 7.4). The buffer should be filtered and oxygenated steadily for 30 min before adjusting the pH to 7.4.

13. Glucose.
14. Arginine.
15. Millex HA 0.45 μm filter, (Millipore, Massachusetts, USA).

### 2.3 Insulin Radioimmunoassay

1. Polystyrene round-base test tubes capable of holding 2 ml (e.g., 64 × 11 mm) (*see* **Note 3**).
2. Gamma counter, for example, PerkinElmer (Waltham, MA, USA).
3. [$^{125}$I]-insulin (diluted 10,000 cpm per 100-μl assay buffer).
4. Rat insulin standard.
5. Rat insulin antiserum.
6. Secondary antiserum (type determined by the species used to generate the insulin antisera).
7. 15% polyethylene glycol, MW 8000 (PEG-8000): This separates bound from unbound antigen by precipitating the antibody–antigen complex (*see* **Note 4).**
8. Assay buffer: (50 mM $NaH_2PO_4$, 150 mM NaCl, 0.5% BSA (RIA grade), 15 mM $NaN_3$, pH 7.4). Sera and PEG should be prepared in this buffer while standards should be prepared in the perfusion buffer.

## 3 Methods

The purpose of this surgical procedure is to create an enclosed system containing an intact pancreas with one inlet (the celiac artery) and one outlet (the hepatic portal vein) for perfusion, with all other blood vessels ligated to prevent leakage. For ease of operation, rat stomach and spleen are excised with the pancreas but are then excluded from the perfusion system by ligation of the connecting blood vessels. With smaller rodents, the appropriate vessels are ligated to isolate the pancreas but remain attached and the whole body placed in the perfusion chamber. Prior to excision, the pancreas is perfused with saline and perfusion buffer to flush out the blood so that clots do not form which would compromise the system. An anticoagulant such as heparin may be introduced into the blood system after laparotomy to achieve this but may require a greater number of perfusions to achieve a similar quality of data (probably due to the effects of heparin on ATP-associated signaling). This perfusion method is preferred unless the procedure is taking longer than 30 min or is performed on smaller rodents such as mice (*see* **Note 5**).

### 3.1 Pancreas Excision

1. Anesthetize the rat with an aesthetic regimen capable of providing a degree of surgical anesthesia and analgesia for 40 min (*see* **Note 1**).

2. During the surgical period, keep the rat warm by means of a heated pad or heated operating table.
3. Perform a laparotomy using blunt-nosed dissecting scissors (14–15 cm is the optimal length for most users). First make an incision in the skin large enough for the same scissors to be inserted between the skin and abdominal wall and then using the scissors tease apart the skin from the abdominal wall so that the skin can be cut from pubis to sternum along the mid-central line. Separate the skin and abdominal wall down the sides (a curved pair of scissors of similar size would be suited to this task) and cut the skin laterally, avoiding blood vessels as much as possible. Lift the abdominal wall with forceps and cut along the mid-central line between the pubis and xyphoid process being careful not to nick the organs below. Cut down each side of the abdominal wall after having occluded the blood vessels with the use of an hemostat (cauterizing works equally well).
4. Place pieces of saline-soaked tissue paper immediately to the left of the subject and place the intestines carefully on top of these. Pour saline over the organs of the abdomen and repeat periodically to prevent the organs from drying. At this point, an anticoagulant such as heparin may be utilized by means of injection via the inferior vena cava.
5. Doubly ligate the descending colon and cut between the ligatures.
6. Use the upper ligature to raise the colon and cut the fascia underneath up to the transverse colon.
7. Tease away the top layer of fascia connecting the intestines and pancreas using a blunt tool being careful not to damage the pancreas (fingers are ideal for this task).
8. The bottom layer of fascia contains jejunal blood vessels that will need to be ligated. First, remove the fascia between the vessels and ligate the vessels to the right of the transverse colon and then those of the mesenteric radix.
9. Ligate the duodenum adjacent to the ligature on the mesenteric radix and cut the intestines below the ligatures (*see* **Note 6**). The lower intestines can now be discarded.
10. Tease apart the fascia linking the pancreas, stomach, and spleen and cut the vessels connecting the stomach and spleen after double ligation.
11. Remove the fascia connecting the stomach, liver, and esophagus to expose the esophagus and esophageal artery. Doubly ligate these and cut.
12. Isolate the pancreas from the stomach by ligating the duodenum adjacent to the pylorus.

13. Remove the fat from around the descending aorta between the diaphragm and aortic bifurcation so that the aorta, caudal vena cava, and any branching vessels are clearly exposed (*see* **Note 7**).
14. Using blunt-ended forceps, separate the entire exposed length of the aorta from the body wall as well as the initial centimeter of the celiac, superior mesenteric, and renal arteries (*see* **Note 8**).
15. Separate a section of aorta from the vena cava between the renal and iliac arteries using blunt-ended forceps (*see* **Note 9**).
16. Lift the liver to the right and clear the hepatic portal vein of any connective tissue. Place an untied ligature around the vein and replace the liver exposing the celiac trunk.
17. Place untied ligatures around the aorta superior to the celiac artery, inferior to the superior mesenteric artery, and between the renal and iliac arteries. Leave several millimeters between the celiac artery and the ligature for ease of manipulation of the inlet cannula and also to avoid risk of cutting the celiac when severing the aorta.
18. Place untied ligatures around the celiac, mesenteric, and renal arteries (*see* **Note 10**).
19. Place a serrefine (*see* **Note 11**) across the aorta immediately inferior to the renal arteries and another at the aortic bifurcation. Using spring scissors make a cut into the aorta halfway between the serrefines.
20. Insert a cannula for connection to a saline-containing syringe into the aorta up to the superior serrefine and secure by tying the ligature. For rats, the cannula should be polyethylene tubing (as described in materials and methods) tapered for easy insertion. Smaller rodents require a needle—rounded so it can be inserted into the aorta. With experience, a 25-G needle is possible, especially, in rodents with a lean body weight over 30 g. A smaller gauge needle, for example, 27 G, may be necessary for smaller animals or when learning the technique, but increases the risk of leaks.
21. Remove the superior serrefine and tie the ligatures around the renal and mesenteric arteries.
22. Tie the uppermost ligature around the aorta and immediately perfuse the system with 2.5-ml saline over a period of about 20–30 s. Replace the saline syringe with one containing the perfusion buffer and perfuse with 2.5 ml over 20–30 s. Immediately, tie the remaining aortic ligature followed by the hepatic portal ligature. Tie the latter ligature as close to the liver as possible.
23. Cut the hepatic portal vein on the liver side of the ligature and cut the aorta on the celiac trunk side of both the top two ligatures. Lift out the section of abdominal organs, cutting

any remaining underlying connective tissue and transfer to the perfusion tank (*see* **Note 12**).

24. Dispose of the rest of the carcass by an appropriate means.

### 3.2 Ex Vivo Preparation for Pancreas Perfusion

1. Locate the ligature around the celiac artery and hepatic portal vein, lift and replace in the center of the tank with the two blood vessels exposed.
2. Maneuver the inlet cannula next to the celiac trunk so that it is as almost horizontal. Holding the opening of the aorta adjacent to the celiac artery, but on the opposite wall, slip the cannula into the celiac trunk so that the cannula enters the celiac artery via the aorta. Secure in place by tying the ligature around the celiac artery and the cannula. The celiac artery cannula can be fashioned from a blunted 23-G needle for rats (or no smaller than 25 G). Celiac cannulas for smaller rodents should already be in place at the surgery stage and now connected to the inlet tubing.
3. Maneuver the outlet cannula vertically next to the hepatic portal vein. The outlet cannula should have an outside diameter of 2–3 mm for rats and 5–6 mm for mice. Glass capillary tubes with the end tapered and melted work well for rats—just make sure the insertion angle is as horizontal as possible to avoid the cannula slipping off. A blunted 25-G or 23-G needle works well for mice. Lift the vein by the ligature and make an incision into the vein as close to the ligature as possible (*see* **Note 13**). Holding the thread of the ligature in one hand and the lip of the aperture in the vein with forceps, slide the cannula into the vein by almost a centimeter. Tape the ligature threads to the cannula holder so the vein does not slip off and secure a ligature around both the vein and cannula (*see* **Note 14**).
4. Perfuse the pancreas at a rate of 2 ml per gram pancreas weight per minute until the perfusate begins to flow out and then perfuse at 2 ml per gram pancreas weight per minute for 20 min to flush out any secretagogues released into the system during the set-up period (*see* **Note 15**).

### 3.3 Pancreas Perfusion

1. Set the perfusion equipment up as shown in Fig. 2. The temperature of the water bath and water heater/pump must maintain the perfusion buffer and perfusion tank temperature at 38 °C. Check the perfusion tank temperature prior to surgery and monitor throughout the experiment (*see* **Note 16**).
2. Glucose is required in the perfusion buffer to maintain the integrity of the pancreas. The perfusion system can detect an increase in insulin secretion at 4.4-mM glucose. 2.8-mM glucose is used to maintain a basal level of insulin secretion and pancreas function. 5.6-mM glucose represents the normal level

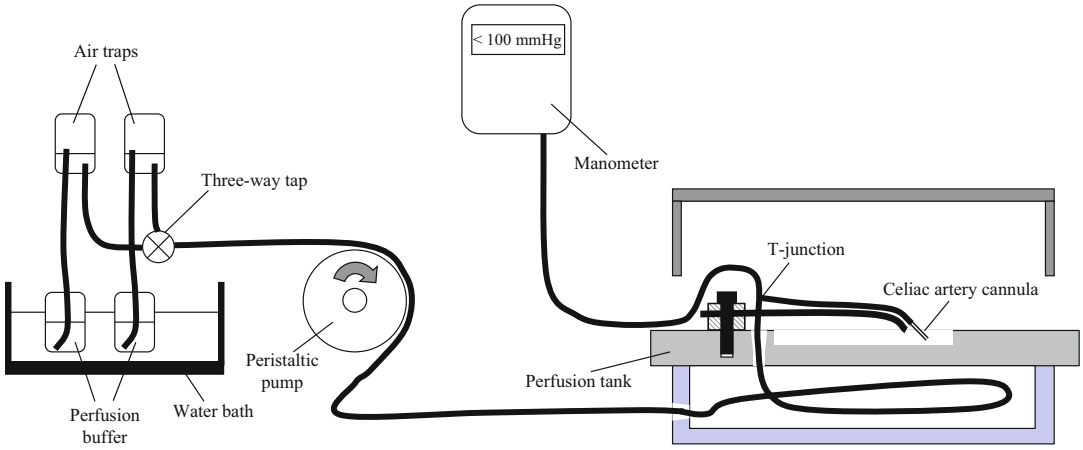


**Fig. 2** Perfusion apparatus. The perfusion buffers are heated in a water bath and connected to air traps. Tubing connects the air traps to a tap, the number and type depending upon the number of different perfusates to be analyzed. The system powered by a peristaltic pump; immediately after which the perfusion tank is connected. A T-junction separates the perfusate into two tubes. One is attached to the cannula inserted into the celiac artery and the other connected to a manometer

of glucose exposure to the pancreas in a free-fed state. Diabetes is defined when glucose appears in the urine and occurs when blood concentrations rise above 11 mM. Concentrations higher than this are important to include when looking at the diabetic state.

3. Arginine stimulates insulin secretion by a mechanism independent from that induced by glucose. Use 20 mM to demonstrate integrity of the system when investigating mechanisms where glucose-induced insulin secretion may be impaired.
4. The sample collector should be set to collect samples over a 1-min period for most experiments. While the perfusion is in progress, samples already collected can be aliquoted in triplicate into tubes ready for radioimmunoassay.
5. Avoid designing perfusions exceeding 100 min in length, though this will not include the initial 20-min "flush-out" period.
6. Check the pH of the perfusion buffer at the end of the perfusion as pH 7.4 is outside the optimal buffering capacity of bicarbonate buffers (pH 5.1–7.1).
7. Monitor the pressure in the perfusion system continuously with the manometer. A pressure rise above 100 mmHg is indicative of a blockage in the pancreas resulting in swelling followed by leakage. Should this occur, the perfusion should be terminated and the collected perfusate discarded.

### 3.4 Insulin Radioimmunoassay

In a radioimmunoassay, a fixed concentration of labeled tracer antigen is incubated with a constant amount of specific antiserum such that the concentration of antigen binding is limiting. If unlabeled antigen is added, there is competition between labeled tracer and unlabeled antigen, so that the amount of tracer bound to the antibody will decrease as the concentration of unlabeled antigen increases. This can be measured after separating antibody bound from free tracer and counting the bound fraction, the free fraction or both.

Interassay controls are included in each assay system. These samples should be of identical composition to the material being assayed, from the same species and medium. These are used to validate the assay and to measure the variation within and between assays. The number of these required should be determined statistically during the method evaluation. The interassay drift must be determined from assay tubes containing identical amounts of reagents (sample, primary antibody, tracer, and secondary antibody). Duplicate sample pools should be placed at the beginning and end of the assay to determine if drift is a problem.

#### 3.4.1 Setting Up An In-House Radioimmunoassay

1. Determine the primary antibody dilution required. Set up three tubes each for total counts (T), non-specific binding (NSB), and at each dilution of primary antibody binding ($B_0$, a range of 1000- to 1,000,000 fold is usually ample, (*see* **Note 17**). Proceed with Subheading 3.4.2 from **step 3**. Plot the data as % (($B_o$-NSB)/(T-NSB)) versus primary antibody dilution factor ($\log_{10}$ scale) using a sigmoidal curve fit (Fig. 3). The primary antibody dilution required corresponds to 30% (($B_o$-NSB)/(T-NSB)) (*see* **Note 18**).
2. Determine the secondary antibody titer by setting up three tubes each for total counts, non-specific binding, and each dilution of secondary antibody. Proceed with Subheading 3.4.2. Plot the data as % (($B_o$-NSB)/(T-NSB)) vs. secondary antibody dilution factor ($\log_{10}$ scale) using a sigmoidal curve fit (Fig. 4). The secondary antibody dilution required is the lowest that gives maximal precipitation (*see* **Note 19**).
3. Validate the assay with a serial dilution of perfusate containing insulin. Either concentrate the perfusate or add enough rat insulin to make a 10 nM solution and serially dilute for a range from 1 pM to 10 nM. Perform Subheading 3.4.2 from **step 3** and compare the range to the standard curve. Express the concentrations relative to the top concentration or stock solution to ascertain whether the regression curves are vertically parallel. If the dilution curves are parallel then the assay is valid to analyze insulin secretion (Fig. 5).

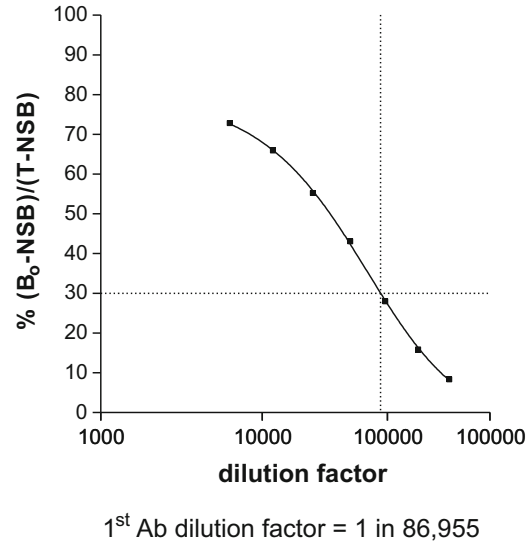


**Fig. 3** Primary antibody titer test. The primary antibody will bind to the hormone of interest as well as the labeled tracer and standard. The bound fraction of the assay is that part of the labeled and unlabeled antigen specifically bound to the primary antibody and counted in the gamma counter. The primary antibody titer test is a preliminary radioimmunoassay to determine what concentration of primary antibody should be used. The amounts of tracer and secondary antibody remain constant between groups of NSB's and 100% tubes, while only the primary antibody concentration in the Total tubes varies. Typically, three totals, three NSBs, and three 100%s for each concentration of primary antibody are tested. The concentration selected depends on the sensitivity desired in the assay. The least primary antibody used, the lower the standard curve doses can be reliable. In this example, the final dilution of primary antisera corresponds to the dilution of the original stock that precipitates 30% of hot antigen added to the tubes (minus non-specific precipitation). Here this corresponds to a final dilution of 1:86,955 of the original stock solution. Note that the primary incubation contains 100 μl of the standard/sample, 100 μl of label and 100 μl of the primary antibody so in this example the primary antibody would be diluted 1:28,985 dilution (final dilution 1:86,955)

*3.4.2 Radioimmunoassay Protocol*

1. Generate radioimmunoassay standard curves from nine concentrations in quadruplicate. Ensure three standards fall on the steep part of the curve, and three standards at or near both the top and the bottom of the curve. When analyzing insulin secretions, from the pancreas perfusion, use the following concentrations: 0.02, 0.05, 0.1, 0.2, 0.5, 1, 2, 5, and 10 nM (*see* Fig. 6). Add 100 μl of standard to the appropriate tubes.
2. In addition to the samples and standards include total counts (T), non-specific binding (NSB), maximum binding ($B_0$), and variance determinants (*see* **Note 20**). Set up at least twenty variance tubes, ten at the start and end of the assay. Set up all other three groups in quadruplicate.

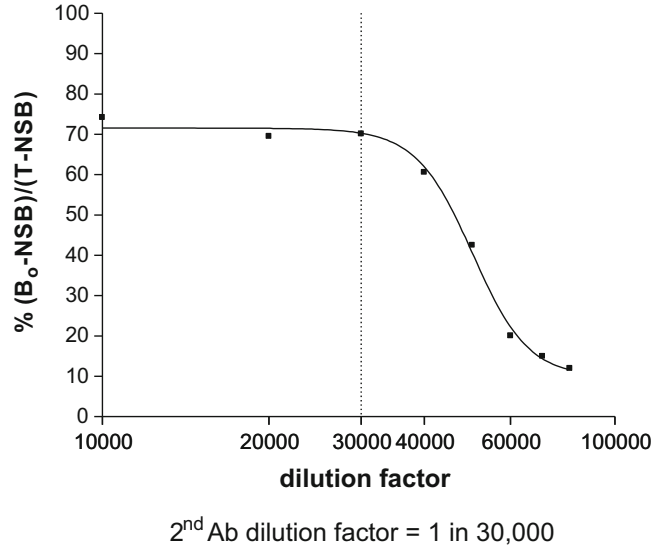


**Fig. 4** Secondary antibody titer test. The secondary antibody binds to the primary antibody/antigen complex (bound fraction) and after centrifugation, is precipitated. After the free supernatant is decanted, the assay tube and precipitate are counted in the gamma counter. A secondary antibody titer test is a preliminary radioimmunoassay to determine what concentration of secondary antibody maximally precipitates the bound fraction of the primary antibody/antigen complex. In this test, the amount of tracer and primary antibody remain constant while only the secondary antibody concentration varies. Typically, there are three total count tubes, and for each different amount of secondary antibody, three NSBs and three 100% tubes. In this example, the final dilution of secondary antisera corresponding to the lowest concentration that will still maximally precipitate the label is 1:30,000 would be used

3. Add 100 μl [$^{125}$I]-insulin solution to all tubes and mix by vortexing.
4. Add 100 μl of primary antisera to all tubes except T and NSB (add 100 μl assay buffer to these) and mix thoroughly (*see* **Note 21**).
5. Cover and incubate at 4 °C for 24 h.
6. Add 100 μl of secondary antisera and incubate for 2 to 24 h.
7. Add 100 μl of PEG solution (*see* **Note 22**).
8. Add 1 ml distilled water at 4 °C to each tube, mix and leave for 10 min.
9. Centrifuge all tubes for 10 min at 3000 × *g*.
10. Remove the supernatant and count each tube for a minimum of 1 min with a gamma counter (*see* Fig. 7).

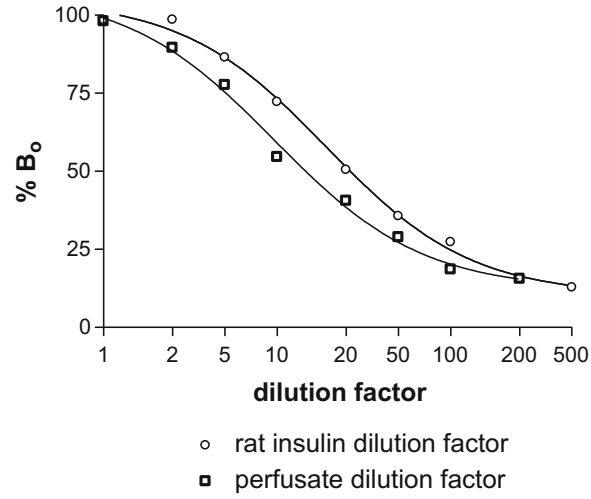


**Fig. 5** The parallelism test. The parallelism test is performed to validate the assay or sample material. A serial dilution of a pooled sample is compared to varying standard curve doses within the same assay. Lines of equal slope demonstrate no significant proportional analytical error within these ranges. This allows the assay of unknown samples with the confidence that the dose estimate per/ml will not have a significant error. This is important when unknowns are run in the same assay at different volumes

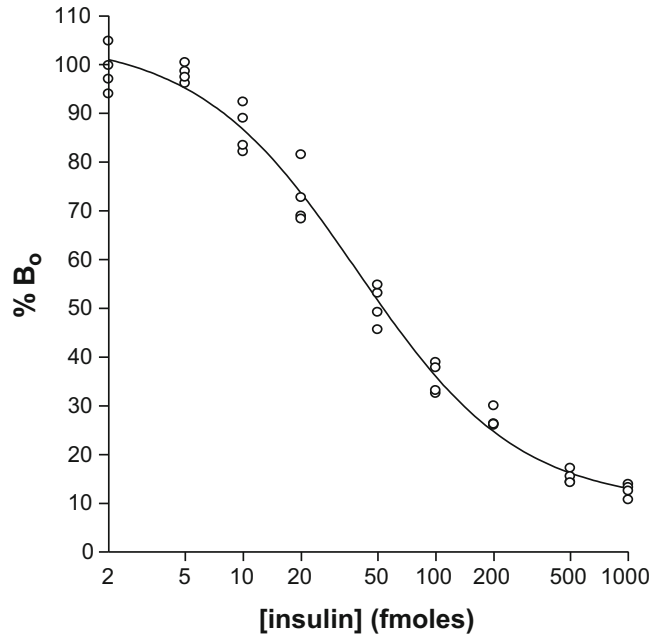


**Fig. 6** Standard curve for the insulin radioimmunoassay. A calibration or standard curve is set up with increasing amounts of known antigen, and from this curve, the amount of antigen in the unknown samples can be calculated. The four basic necessities for a radioimmunoassay are an antiserum to the compound to be measured, the availability of a radioactively labeled form of the compound, a method whereby antibody-bound tracer can be separated from unbound tracer, and a standard unlabeled material. Each circle represents a single data point and a sigmoidal regression line generated

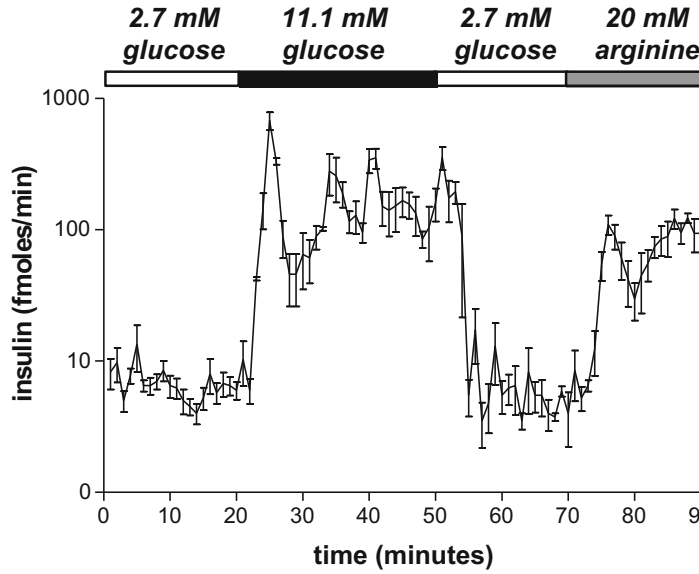


**Fig. 7** Example of a typical insulin secretion profile from perfused pancreata of Wistar rats ($n = 6$). Basal insulin secretion was measured with 2.7 mmol/l glucose in the pefusate and secretagogue-stimulated insulin secretion was measured with 11.1 mmol/l glucose or 20 mmol/l arginine in the perfusate

## 4 Notes

1. Isoflurane is suitable for all rodents and is preferable to injectable anesthetics because of the degree of control it allows and lack of respiratory problems. The fentanyl/fluanisone and midazolam combination described is usually an acceptable injectable regime due to low strain variability in duration of anesthesia. The duration of anesthesia of 40 min described in the text is conservative—the procedure typically lasts 20–30 min.
2. All surgical tools described may be obtained from Fine Science Tools and the catalogue numbers are listed (website www.finescience.com).
3. Borosilicate tubes should be used for radioimmunoassays where peptides stick to tubes made from polystyrene or polypropylene, for example, GLP-1. Borosilicate tubes should also be used if the pellet formation is inadequate.
4. Some commercial products are a combination of secondary antibody and precipitating agent, making this step quicker and easier. If a commercial secondary antibody/precipitator mix is used, then follow the manufacturer's instructions.
5. For rodents smaller than rats, it is advisable to use the anticoagulant method to prevent clotting rather than pre-perfusion

via the aorta. Also, the perfusion should be performed in situ with the whole animal in the perfusion tank rather than excising the isolated pancreas.

6. A double ligature is preferable here, as an incomplete ligation at this site is the most common cause of leakage during the perfusion stage.
7. The left gastric and iliac arteries are easily disrupted and so the area must be cleared with care. Cotton buds are useful in exposing this area, but the entire length of these arteries need not be exposed as long as the coeliac trunk is cleared of fat and connective tissue.
8. The right renal artery may prove difficult to access, if so this ligation may be missed, but it will minimally affect the initial perfusion step. In some strains of rat, the left and right renal arteries arise from the same junction of the aorta and may be ligated together.
9. The connective tissue between the aorta and vena cava may be difficult to remove but do not be tempted to use sharp implements as the vena cava is easily disrupted. Should the vena cava be pierced quickly clamp both the aorta and vena cava where the aorta would be clamped in **step 17**, remove traces of blood, and proceed as rapidly as possible to the initial perfusion step. In this way, blood clots in the pancreas may possibly be avoided.
10. Ensure that all loose ends of all untied ligatures are untangled and easily identified as minimal delay is optimal to prevent clots occurring in the pancreas.
11. A serrefine is a small spring forceps used to close an artery during surgery.
12. The section of excised organs will include the pancreas, spleen, stomach, and part of the intestines, although only the pancreas will be perfused in this system.
13. A small volume of blood will have drawn back into the portal vein due to the lack of valves in the hepatic portal system. This actually aids the insertion of the cannula, as when the internal solution is translucent, the hole in the vein can be difficult to locate.
14. The tape is unnecessary if there is a second person available to tie the ligature around the portal vein and cannula while the operator is holding it in place.
15. Pancreatic blood flow in rodents is approximately 2 ml per gram pancreas weight per minute. As pancreata are not isolated in this technique, they cannot be weighed as part of the procedure. If estimates of pancreas weights are not available, use flow rates of 2 and 4 $ml \cdot min^{-1}$ for rats and 0.25 and 0.5 $ml \cdot min^{-1}$

for mice. Perfusate collected during this period may be used to help validate and assess the variability of the secretagogue assays.

16. Setting up the perfusion equipment in a temperature-controlled room helps to achieve a consistent perfusion tank temperature with little or no adjustment of water bath and water heater/pump temperature.
17. This dilution represents the final dilution, that is, after the label and cold/blank solution has been added.
18. The lower the concentration of primary antisera used, the higher the sensitivity of the assay and the more reliable the lower end of the standard curve. A primary antibody dilution giving 30% of maximum amount of label precipitated is usually ideal.
19. When performing the primary antibody titer test for the first time an excess of secondary antisera may be used. When the secondary antibody titer test has been carried out the primary test should be repeated with the newly calculated secondary antibody dilution. The manufacturer of the secondary antibody will recommend a workable dilution factor. This value should be the middle point dilution in the second antibody titer test.
20. The total counts (T) are used to confirm that the label is in excess to the antibody (% $B_0$/T should be about 30%). This can also be used to estimate gamma counter efficiency (% cpm/dpm). Non-specific binding (NSB) tubes contain no primary antibody and represent the proportion of non-bound label precipitated. This amount should be subtracted from all other values before any further calculations. It represents 0% binding. Maximum binding ($B_0$) tubes contain no added cold insulin and effectively all binding sites are occupied by hot insulin. These tubes should have the highest counts (apart from T tubes) and represent 100% binding. All standards and samples are expressed as a percentage of this value. Intraassay and interassay variances are determined using the same stock of insulin for all assays used in the experiment (this has to be at an insulin concentration not used to generate the standard curve). Intraassay variance is expressed as a % standard deviation of variance tubes/mean of variance tubes and should be less than 10%. Interassay variance is expressed as a % standard deviation of the mean of intraassay means/mean of intraassay means and should be less than 15%.
21. Incubating with primary antisera before addition of the label saturates the binding sites with cold antigen. A shortened incubation time following addition of the hot antigen prevents equilibrium being achieved and results in a more sensitive

radioimmunoassay. If a lack of sensitivity is seen try incubating with primary antisera for 12 h prior to the 8–12 h incubation with hot antigen.

22. A final concentration of 3% PEG has been found to give the greatest percentage of specific binding and the lowest percentage of nonspecific binding in double-antibody radioimmunoassays [7].

## References


1. Sussman KE, Vaughan GD, Timmer RF (1966) An *in vitro* method for studying insulin secretion in the perfused isolated rat pancreas. Metabolism 15:466–476
2. Emilsson V, Liu YL, Cawthorne MA, Morton NM, Davenport M (1997) Expression of the functional leptin receptor mRNA in pancreatic islets and direct inhibitory action of leptin on insulin secretion. Diabetes 46:313–316
3. de Heer J, Rasmussen C, Coy DH, Holst JJ (2008) Glucagon-like peptide-1, but not glucose-dependent insulinotropic peptide, inhibits glucagon secretion via somatostatin (receptor subtype 2) in the perfused rat pancreas. Diabetologia 51:2263–2270
4. Göncz E, Strowski MZ, Grötzinger C, Nowak KW, Kaczmarek P, Sassek M, Mergler S, El-Zayat BF, Theodoropoulou M, Stalla GK, Wiedenmann B, Plöckinger U (2008) Orexin-A inhibits glucagon secretion and gene expression through a Foxo1-dependent pathway. Endocrinology 149:1618–1626
5. Egido EM, Hernández R, Marco J, Silvestre RA (2008) Effect of obestatin on insulin, glucagon and somatostatin secretion in the perfused rat pancreas. Regul Pept 152:61–66
6. Tseng C-C, Zhang X-Y, Wolfe MM (1999) Effect of GIP and GLP-1 antagonists on insulin release in the rat. Am J Physiol Endocrinol Metab 276:E1049–E1054
7. Eisenman JR, Chew BP (1983) Polyethylene Glycol in conjunction with a secondary antibody for 24 hour radioimmunoassay of bovine prolactin and growth hormone. J Dairy Science 66:1174–1179

# INDEX



Claire J. Stocker (ed.), *Type 2 Diabetes: Methods and Protocols*, Methods in Molecular Biology, vol. 2076,
https://doi.org/10.1007/978-1-4939-9882-1, 

## N



## O



## P



## Q



## R



## S



## T



## V



## W